ASSESSMENT AND ANALYSIS OF QUEENSLAND CLAY BEHAVIOUR

Thesis submitted by

Briony Rachelle RANKINE BEng(Hons)

in March 2007

for the degree of Doctor of Philosophy
in the School of Engineering
James Cook University

STATEMENT OF ACCESS

I, the undersigned author of this work, understand that James Cook University will make this thesis available for use within the University Library and, via the Australian Digital Theses network, for use elsewhere.

I understand that, as an unpublished work, a thesis has significant protection and the Copyright Act and I do not wish to place any further restriction on access to this work.

Signature

1/3/07
Date

STATEMENT OF SOURCES

DECLARATION

I declare that this thesis is my own work and has not been submitted in any form for another degree or diploma at any university or other institution of tertiary education. Information derived from the published or unpublished work of others has been acknowledged in the text and a list of references is given.

_____ 1/3/07

Signature Date

ELECTRONIC COPY

I, the undersigned, the author of this work, declare that the electronic copy of this thesis provided to the James Cook University Library, is an accurate copy of the print thesis submitted, within the limits of the technology available.

_____ 1/3/07

Signature Date

Acknowledgements

The author wishes to thank:

My family – Dad, Mum, [redacted]. Thank you for believing in me, and encouraging me to follow my dreams. Your support, as always, has been amazing.

Assoc. Prof. Nagaratnam Sivakugan – My supervisor and my friend – Thanks for everything.

My co-supervisors, Professor Buddhima Indraratna and Mr. Vasantha Wijeyakulasuriya – Your assistance has been greatly appreciated.

And last, but not least, the Engineering Technical Staff (Warren O'Donnell, Stuart Petersen, Curt Arrowsmith and Don Braddick)

This work is dedicated to my wonderful family

Abstract

Within the past few decades, increased population and infrastructure development has necessitated the reclamation and development of previously undesirable sites for civil engineering works. In Australia, significant development has taken place along the Eastern coastal belt. This region is lined with saturated clays of significant depths (15 m to 20 m) which are typically characterized by high compressibility, low bearing capacity, and high lateral displacement upon loading.

The most common and economically viable technique for soil improvement of these foundations is the use prefabricated vertical drains (PVD) in conjunction with preloading. This method accelerates the consolidation process by shortening the drainage path of the soil in the radial direction, and has been used in a number of large projects including the Muar Plains Trial Embankments, Changi East Reclamation Project and the 2nd International Bangkok Airport. Nevertheless, there are very limited case studies of soft clay projects in Australia.

General theory of soil behaviour is well established based on the broad classifications of granular and cohesive soils. . However, due to the innumerable environmental and physical processes a soil may be exposed to during its formation, there is natural variance in soil properties. Thus, a holistic approach is advocated for geotechnical calculations at any site. The design methods should be used together with field observations, as well as data obtained from in situ and laboratory testing.

When examining the deformation behaviour of clays, engineers are interested not only in the consolidation and compressibility characteristics of a soil, but also the index properties of it. The index properties of a soil describe certain critical stages in soil behaviour, and also the consistency of a soil.

Within this dissertation, the index properties of soils from a number of different sites around Queensland have been tested within the laboratory, and analysed statistically. Beta distributions have been Further to this characterization, the inherent variation introduced solely as a result of the manual nature of testing these properties, has been examined and quantified. Covariance between index properties has been examined, and equations specific to Queensland soils produced to describe it.

Laboratory testing and examination of the consolidation and compressibility characteristics specific to Queensland clays have also been undertaken, and are correlated to the measured index properties.

Commonly, settlement calculations for a given embankment loading are considered in three stages – immediate settlement, consolidation settlement and secondary compression. Generally, the consolidation phase contributes the most significant portion of settlement in clays. Calculations for this phase undertaken by using the assumptions of average coefficient of volume compressibility, m_v, and also instantaneous loading. However, both assumptions are incorrect, and can lead to gross miscalculation of the settlement magnitude. A new method of analytically determining the settlement of a foundation taking into account the stress dependence of m_v, and also the loading sequence of an embankment has been formulated and is described herein.

Furthermore, the dependence of the coefficient of volume compressibility (m_v) on the overconsolidation ratio, and consistency of a soil has been examined and an empirical correlation developed to describe it.

The coefficient of secondary compression (C_α) was also examined in the same manner. While no definitive trend was established to describe the influence of consistency on this parameter, it was found that smaller C_α values should be expected for increased overconsolidation ratios.

This dissertation also presents the case study of an embankment constructed in South East Queensland. This case study has been numerically modelled using the finite difference package FLAC. This embankment was comprised of three different sections. The first two embankment sections were installed with vertical drains at spacings of 1 m

and 2 m respectively and the third, was the control case, and was left free of ground improvement.

Lastly, lateral displacements which develop in soft clay foundations during and after the construction are a major source of concern for engineers due to their detrimental effect on the behaviour of adjacent structures and amenities. A method of predicting the short term lateral displacements induced through embankment loading has been developed. The dependence of these displacements on soil properties, embankment geometry and also distance from the embankment toe are also examined

List of Publications

CONFERENCES

Rankine, B.R., Sivakugan, N. and Messer, T. (2004). **"Anisotropy of consolidation parameters in artificially sedimented clays,"** *Proceedings of the 9th Australian and New Zealand Conference on Geomechanics*, Auckland, 1, 717-723

Rankine, B., Sivakugan, N. and Wijeyakulasuriya, V. (2005). **"Observed and predicted behaviour of clay foundation response under the Sunshine Motorway Trial Embankment,"** *Proceedings of the 16th International Conference on Soil Mechanics and Geotechnical Engineering*, Osaka, Vol. 2, 951-954.

Contents

List of Figures

List of Tables

CHAPTER 1

INTRODUCTION

"Unfortunately, soils are made by nature and not by man, and the products of nature are always complex… As soon as we pass from steel and concrete to earth, the omnipotence of theory ceases to exist. Natural soil is never uniform. Its properties change from point to point while our knowledge of its properties are limited to those few spots at which the samples have been collected. "

Karl Terzaghi
Conference Address, 19th June, 1936

1.1 General

The general theory of soil behaviour is well established based on the broad classifications of clays, silts, sands and gravels. However, as Terzaghi states in the quote above and published by Goodman in 1998, the unique feature of soil, unlike any other engineering material, is that it comes engineered by nature, and its properties are site specific due to the innumerable environmental and physical processes to which it is exposed during its formation. There is a natural variance in soil properties that is unavoidable, and thus, for geotechnical calculations at any site, a holistic approach should be adopted, and involve not only design methods and field observations, but also localised knowledge of the area.

In terms of infrastructure development upon clay deposits, the deformation behaviour of the clay becomes the main concern. Engineers interested in examining such behaviour are

interested not only in the consolidation and compressibility characteristics of the soil, but also the index properties, which describe certain critical stages of soil behaviour, and also indicate the soil consistency.

In the past few decades, rapid increases in Australia's population have necessitated both building and infrastructure development upon what were previously regarded as undesirable construction sites. Among these sites are the soft clay deposits which line much of the Eastern coastal belt. These saturated clays are typically characterized by high compressibility, low bearing capacity, and high lateral displacement upon loading.

Such poor ground conditions make traditional forms of construction expensive. Hence, in order to stabilise these soils, and avoid differential settlements, it is critical that the engineering properties of these soils be improved prior to any sort of construction being carried out. Both the strength and compressibility of clays can be improved by reducing the void volume within the soil mass. Such reduction can be achieved through the dewatering of saturated soils.

The most common and economically viable technique for soil improvement of these foundations utilises prefabricated vertical drains (PVD) in conjunction with preloading. This method accelerates the consolidation process by shortening the drainage path of the soil in the radial direction, and has been used in a number of large projects including the Muar Plains Trial Embankments in Malaysia (Indraratna et al., 1997), Changi East Reclamation Project in Singapore (Choa et al., 2001) and 2nd International Bangkok Airport in Thailand (Bergado et al., 1993). Nevertheless, there are very limited case studies published which deal with soft clay projects in Australia.

1.2 Objectives and Scope of Research

The main objective of this study was to investigate, assess and analyse Queensland clays.

Extensive oedometer testing was conducted upon undisturbed clay samples for four different sites within Queensland. The laboratory results from these soil samples were then used to characterise the consolidation, compressibility and consistency properties of the sites from which they were taken. Beta distributions were determined to describe the overall variance of results measured for selected parameters.

There are two main components to overall variation – the inherent property variation, and the variation which is induced through the testing methods. Due to their highly manual nature, index property tests are more highly susceptible to the latter component than many other soil testing methods. Variation of index property results were examined and quantified to establish a minimum expectant variation[◊]. The results used to establish this level of variance were drawn from NATA proficiency testing undertaken on identical soil samples. Covariance between index properties was also examined, and equations specific to Queensland soils produced to describe it.

The method by which the coefficient of volume compressibility (m_v) of a soil is assessed was also examined. Current practice for calculating the total consolidation settlement involves the assumptions of an average m_v, and also instantaneous loading. However, both of these assumptions are incorrect, and can lead to gross miscalculation with regards to settlement magnitude. A new method of analytically determining the settlement of a foundation taking into account the stress dependence of m_v, and also the loading sequence of an embankment has been formulated and is described.

Furthermore, the case study of a trial embankment constructed in South East Queensland has been presented. The behaviour of this embankment was modelled using *FLAC*, and the effectiveness of vertical drain installation with surcharge loading evaluated using the model.

[◊] Test methods will always introduce some level of variation into the results measured. The minimum measure is the minimum expectant variation.

Lastly, a method of predicting the short term lateral displacements induced through embankment loading has been developed. The dependence of these displacements on soil properties, embankment geometry and also distance from the embankment toe has been examined. It should be noted that, the solutions herein have been developed under the assumption of elastic soil foundations, and rigid embankment loading.

1.3 Relevance of the Research

Due to the financial constraints many projects face, empirical relationships are often used in preliminary design studies to predict values for parameters related to the deformation behaviour of a structure. These estimates are then used to further discern the suitability of a site for construction and to assess what further geotechnical testing should be undertaken on the site. Thus, poor parameter prediction due to the use of unsuitable relationships can lead to significant penalties in the construction cost of a project, and also time delays. Results from the extensive laboratory testing undertaken within this study have been compiled into a geotechnical database for Queensland clays.

The interrelationships between the geotechnical properties of these clays were examined thoroughly and established correlations for clays in other parts of the world were also evaluated with respect to their accuracy in predicting the parametric values of these clays. Where appropriate, empirical correlations specific to the data collected were also ascertained.

The geotechnical data both tested, and collected, was then summarised with respect to each source. Such collation provides localised data which may be used for any further developments within these regions.

By computing beta distributions to describe the variation measured for each parameter, the probability of a parameter falling between a certain range may be estimated, and used further in risk analysis.

Development of a functional numerical modelling tool, based on known geotechnical properties, will allow for the prediction of deformation behaviour below embankment loading with and without ground improvement, and can be used to describe how the behaviour is affected by these vertical drains.

And lastly, the lateral displacements which develop in soft clay foundations during and after the construction are also a major source of concern for engineers due to their detrimental effect on the behaviour of adjacent structures and amenities. Producing a method by which the short term lateral displacements can be estimated will provide the framework for further analysis with regards to the horizontal spreading during consolidation.

1.4 Organisation of Thesis

This chapter introduced the research problem, objectives and scope of the research. It also describes the relevance of such research to the engineering discipline.

The following Chapter 2 gives a brief overview of theories associated with the present research, which has not been addressed within any of the other subsequent chapters. It reviews both the finite difference program employed and the constitutive models selected for the numerical modelling components of this dissertation. The salient aspects of consolidation modelling within *FLAC* are discussed. The history and development of vertical drain theory, and the various factors involved in multi-drain analysis are also considered within this chapter.

Chapter 3 describes a statistical analysis completed upon data published by the testing authority, NATA. These figures were collected as part of proficiency testing by the agency, and have been used to quantify the levels of variance for index properties, due solely to the testing methods. Probability distribution functions formulated to describe

these variances are also presented. Finally, this chapter evaluates a well known empirical correlation relating linear shrinkage to the plasticity index of the soil, and discusses the results.

A holistic approach should be used for any design study, and attention should be paid not only to the design process but also local knowledge of the area. Chapter 4 covers the geotechnical characterization of clays at four sites within the Queensland region, by presenting the results of laboratory testing undertaken within this research. Individual analyses have been undertaken for compressibility and consolidation characteristics of both normally and over consolidated clay parameters on each of the sites, and the overall trends which were apparent are discussed. Established correlations of these geotechnical parameters have been assessed, and the relationships which most accurately relate to Queensland clays have been identified. Probability distribution functions are presented for selected parameters. An analytical study on the derivation and selection of representative m_v values identified flaws in present practice, and also detailed the importance of stress increment reduction from the conventional load increment ratio.

Chapter 5 reviews the development and verification of a finite difference model for the embankment loading of soft clay foundations. This model was based on the case study of a fully instrumented trial embankment in South East Queensland, and was programmed using the finite difference code *FLAC*. Field behaviour was simulated using a fully coupled consolidation model, and the Modified Cam Clay theory was adopted for all clay layers, except for the compacted surface crust and the sand layer, which were modelled according to the Mohr-Coulomb theory. Predictions of the excess pore pressure and both vertical and lateral displacements are made and compared with field observations to assess the effectiveness of prefabricated vertical drains in these types of soils.

The development of a series of equations and design charts useful in determining the location and magnitude of short term lateral soil displacement as a result of embankment loading is discussed within Chapter 6. These equations and charts not only describe the displacement profile at the embankment toe, but also at various distances away from it.

Predictions from the FLAC model previously verified in Chapter 5 have been used for verification purposes within this chapter.

And finally, Chapter 7 provides a summary and conclusions of the research and some recommendations for future research.

CHAPTER 2

LITERATURE REVIEW

2.1 General

The following chapter presents an outline of important concepts associated with the present work which have not been addressed subsequently in the following chapters. It gives a brief overview of FLAC (***F***ast ***L***agrangian ***A***nalysis of ***C***ontinua) and discusses salient aspects of constitutive models used for various parts of this dissertation. Vertical drain history and development is considered within the latter half of the chapter, and the method of converting a vertical drain system into equivalent drain walls for plane strain modelling also investigated. This method was used for the numerical model described in Chapter 5.

2.2 Review of *FLAC*

FLAC is a 2-dimensional finite difference program used to model soil and rock behaviour in geotechnical and mining engineering. Originally developed by Itasca Consulting Group, this program represents materials as 'zones'. These zones combine to form a grid, which the user may mould or adjust to fit the geometry of the shape being modelled. Each zone in the grid behaves according to a user prescribed constitutive model, and may yield and undergo plastic flow.

In large strain mode, the grid may deform, and move with the material being modelled. Due to the explicit Lagrangian calculation scheme used in *FLAC*, combined with the mixed discretization zone allocation technique enables large deformations to be modelled accurately and because no large matrices are formed, large 2-dimensional calculations may be undertaken without excessive memory requirements (ITASCA, 2005).

FLAC 5.0, the latest version, and the one used for simulations detailed within this chapter, may be menu-driven or command-driven. The menu-driven mode operates using a graphic user interface with point-and-click access for all operations. The command-driven mode is more difficult than the menu-driven mode, and requires knowledge of *FLAC*'s own built-in programming language.

This language, known as *FISH* (***FLAC*ish**), allows a user to implement special programming requirements such as the definition of new variables, functions and/or constitutive models. Furthermore, *FISH* allows looping and conditional if-statements which are available in most other programming languages (e.g. FORTRAN, BASIC). It is this operating language, *FISH*, and its ability to allow users to tailor analyses to their own specific needs and wants, that enhances FLAC's usefulness in the field of civil and mining engineering.

The process through which FLAC solves a program is known as time-marching or time-stepping. This solution method adjusts the values of each node in the mesh through a series of cycles or steps based on the selected constitutive model and the equilibrium equation.

FLAC provides a number of constitutive models for implementation, including elastic, Mohr-Coulomb, Drucker-Prager, Modified Cam-Clay, ubiquitous joint, double yield, strain-softening and Hoek-Brown. An overview of the three models – elastic, Mohr Coulomb and Modified Cam Clay – used within this dissertation, and derivation of their critical parameters from in-situ values, are given in Section 2.3. Groundwater flow and consolidation (full coupled) models are also available in FLAC.

2.3 Overview of Constitutive Models

To predict the behaviour of an engineering structure accurately, it is necessary to use an appropriate constitutive model, which represents the stress-strain response of the material.

In 1994, Professor Michael Duncan reviewed almost 2000 papers related to geotechnical applications of constitutive models or finite element modelling. With such extensive amounts of constitutive models abounding geotechnical journals and conference proceedings around the world, the choice of model is to some extent a matter of mathematical aesthetics and subjective judgement. However, there are some models which have been so widely published used, that they are generally available in all numerical analysis programs and are intended for application to geotechnical problems: isotropic elasticity; elastic-perfectly plastic Mohr Coulomb; and Cam Clay (Wood, 2004).

Wroth and Houlsby (1985) suggest that in order for a constitutive model to be useful in solving engineering problems, it should be simple and reflect the physical behaviour of the soil. Duncan (1994) further stated that for constitutive models to be practical, it should be possible to obtain the model parameters in a simple manner from conventional soil tests.

Modelling within this dissertation utilised all three of these constitutive models suggested by Wood (2004), albeit the application of Cam Clay theory was using the modified form (Roscoe and Burland, 1968). A brief summary of these three models are given in Sections 2.3.1, 2.3.2 and 2.3.3. For brevity, the summaries of Section 2.3.2 and 2.3.3 do not detail the flow rule or yield functions for either of the models.

2.3.1 Linear Elastic Isotropic Model

This model is characterised by reversible deformations upon unloading, and is based on the generalised Hooke's law. Based on the form proposed by Robert Hooke in 1676, it relates the stresses and strains on three dimensional bodies instead of a spring. However, the general idea behind both forms is essentially the same – that strains are linear functions of stresses. Furthermore, these stress-strain relations are path-independent, and therefore, the loading modulus and unloading modulus are the same for the model.

There are five elastic constants. Of these, four relate the stresses to strains, and the fifth – Poisson's ratio – relates one extensional strain to another. However, these parameters are not independent, and subsequently, only two of these five constants need be known to fully describe the elastic behaviour. The other three can be worked out through simple algebraic relationships. There is one unique situation in which only one elastic constant can be used to describe the behaviour. This case occurs for the undrained response of a saturated soil (Davis and Selvadurai, 1996).

The two most familiar elastic constants, and those used for describing the elastic behaviour studied in Chapter 6, are Young' Modulus (E) and Poisson's ratio (ν). Both of these constants may be established through the interpretation of a drained triaxial test.

Two further parameters are commonly established from E and ν – that of the bulk modulus and the shear modulus of a soil. The bulk modulus, K, measures the response in pressure due to a change in relative volume, of a soil, and may be calculated from Young's Modulus and Poisson's ratio using Equation 2.1. The shear modulus, G, relates the response in shear strain to changes in shear stress (see Equation 2.2). It is recommended that these two parameters be used in FLAC modelling, in preference to E and ν.

$$K = \frac{E}{3(1-2\nu)} \qquad \text{(Eqn. 2.1)}$$

$$G = \frac{E}{2(1+\nu)} \qquad \text{(Eqn. 2.2)}$$

Devices other than the triaxial machine, such as oedometers, can be used to establish the elastic properties of E, ν, G and K, but often these tests result in composite quantities which can only be interpreted through the assumption of another one of the quantities (usually ν).

2.3.2 Mohr Coulomb Model

The classical Mohr Coulomb model is an elastic-perfect plastic model and is suitable for the modelling of sandy soils and overconsolidated clays. In elastic-perfectly plastic models, there is a region of stress space that can be reached elastically, without any irrecoverable deformations. However, once the boundary of this elastic region is reached, the soil will yield (or fail) at a constant stress (Wood, 2004). This boundary is known as the yield surface.

As the name implies, this model is based on the Mohr Coulomb failure criterion. The yield surface (or failure envelope) is shown graphically in Figure 2.1, and can be described using Equation 2.3, where τ_f is the strength of the soil, σ is the applied normal stress, and ϕ and c are the strength parameters of friction angle and cohesion respectively.

$$\tau_f = \sigma \tan\phi + c \qquad \text{(Eqn. 2.3)}$$

It may be described using five parameters – Young's modulus (E), Poisson's ratio (ν), cohesion (c) and friction angle (ϕ) and dilation angle (ψ). However, as was the case with the elastic model, ITASCA (2002) recommends the bulk and shear moduli be used in lieu of E and ν. Both cohesion and friction angle can be measured through triaxial testing.

2.3.3 Modified Cam-Clay Model

The original Cam Clay model was first presented in literature by Roscoe and Schofield in 1963. However, this model was found to be deficient in some aspects, namely the shape of the yield locus, and the predicted value of K_0 (the coefficient of earth pressure at rest).

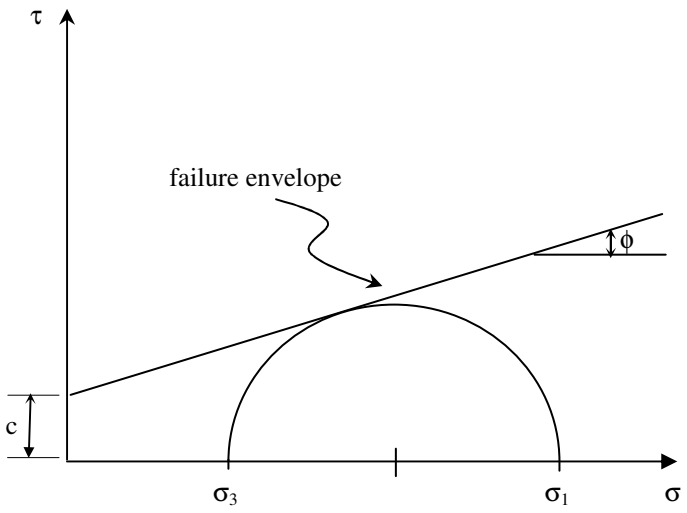

Figure 2.1 Mohr Coulomb failure criterion as defined in $\tau - \sigma$ space

Roscoe and Burland (1968) introduced the modified Cam Clay model to address these problems. It is now more widely used in practice than the original Cam Clay model (Wood, 1990). The following section briefly outlines the basics of this model. For a more detailed discussion, refer to Roscoe and Burland (1968) and Wood (1990).

This type of model should be used to represent materials when the influence of volume change on bulk property and resistance to shear needs to be taken into consideration, such as in soft clays (ITASCA, 2002). Indeed, some of the most successful applications of this type of model have been to problems which involve geotechnical constructions.

Modified Cam Clay is an elasto-plastic model, is based on the critical state concept, and can be described by five main parameters - λ, κ, M, ν and G. Critical state condition is sometimes referred to as the condition in which the samples at large deformations tend to reach a unique state, wherein all samples fail at the same strength (q), the same mean effective stress (p') and the same void ratio (e). Further deformation of the sample is possible only by shear distortion (Redana, 1999).

The critical state parameters of p (effective pressure) and q (deviator stress) describe the state of soil during triaxial testing and are defined by Equations 2.4 and 2.5 (where σ_1' represents the effective axial stress and σ_3' represents the effective confining stress).

$$p' = \frac{\sigma_1' + 2\sigma_3'}{3} \qquad \text{(Eqn. 2.4)}$$

$$q = \sigma_1' - \sigma_3' \qquad \text{(Eqn. 2.5)}$$

The failure surface, or critical state line in q-p' space, is a straight line that passes through the origin. It is described by the parameter M in Equation 2.6, and is shown in Figure 2.2. By combining the critical state line equation into the Mohr Circle plot, M can further be related to the angle of friction (ϕ) for the soil in triaxial compression (see Equation 2.7).

$$q = Mp' \qquad \text{(Eqn. 2.6)}$$

$$M = \frac{6\sin\phi'}{3 - \sin\phi'} \qquad \text{(Eqn. 2.7)}$$

The yield locus for the modified Cam Clay model is elliptical in shape and is given by Equation 2.8. Within this equation, p_c' is the value of p' where the ellipse intersects the p' axis, and corresponds to the preconsolidation pressure of the samples. .

$$q + M^2 p'^2 = M^2 p' p_c' \qquad \text{(Eqn. 2.8)}$$

This yield locus is further shown diagrammatically alongside the yield locus for the original Cam Clay model in Figure 2.3.

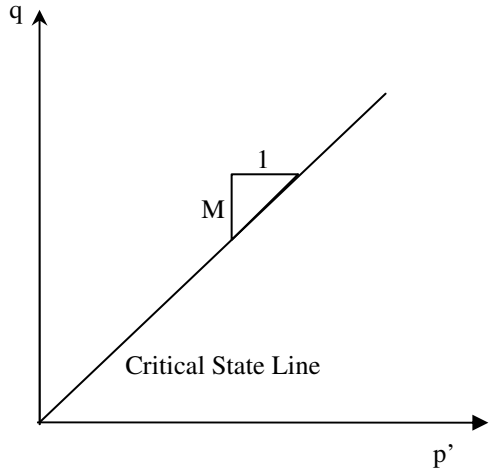

Figure 2.2 Critical State Line based on q-p' Plot

Within critical state theory, the virgin compression and recompression lines are assumed to be straight lines in plots of ln p' against void ratio, e, or specific volume, v. The slopes are denoted by λ and κ respectively. These parameters obtained quite simply by using the following equations, and properties derived from a standard oedometer test.

$$\lambda = \frac{C_c}{2.303} \qquad \text{(Eqn. 2.9)}$$

$$\kappa = \frac{C_r}{2.303} \qquad \text{(Eqn. 2.10)}$$

In the v-ln p' plot, if Γ is used to represent the value of specific volume when $p'=1$ (or ln $p'=0$) (i.e. $\Gamma = e_{cs} + 1$ where e_{cs} = void ratio on the critical state line at $p'=1$), then the equation of the critical state line is given by:

$$V = \Gamma - \lambda(\ln p') \qquad \text{(Eqn. 2.11)}$$

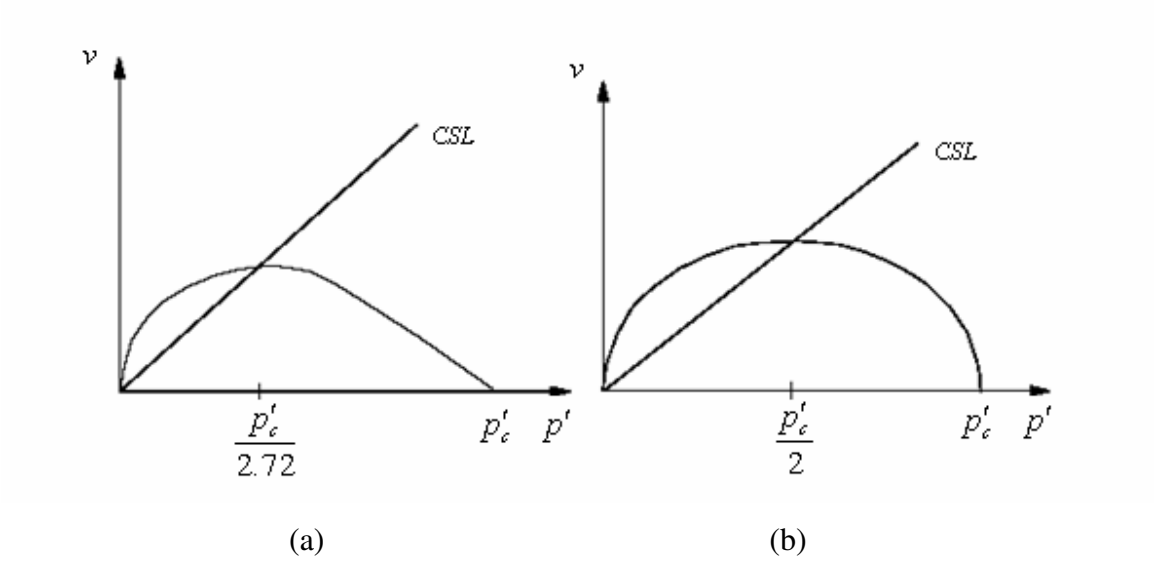

Figure 2.3 Yield loci of (a) Cam Clay and (b) Modified Cam Clay

Overall, the crucial idea of critical state theory is the concept that soil, and other granular materials, if continuously distorted until they flow as a frictional fluid, will come into a well defined critical state determined by Equations 2.6 and 2.11 (Schofield and Wroth, 1968).

Thus, the initial void ratio can be estimated at any depth below the ground level once p_A', q, and p_c' are known (see Figure 2.4). The intersection between the recompression line, and the critical state line is denoted as point A and is positioned at p_A, e_A. The dependence of these coordinates on one another may be simplified to Equation 2.12, where $p_A = \frac{p_c}{2}$ for modified Cam Clay, and $p_A = \frac{p_c}{2.718}$ for the original Cam Clay model.

$$e_A = e_{cs} - \lambda \ln \ p_A \qquad \text{(Eqn. 2.12)}$$

Point P is described by the initial void ratio, e, and the effective mean normal stress, p', for the sample. Thus, the recompression (or swelling) line passing through the initial stress state at P, may be described using Equation 2.13.

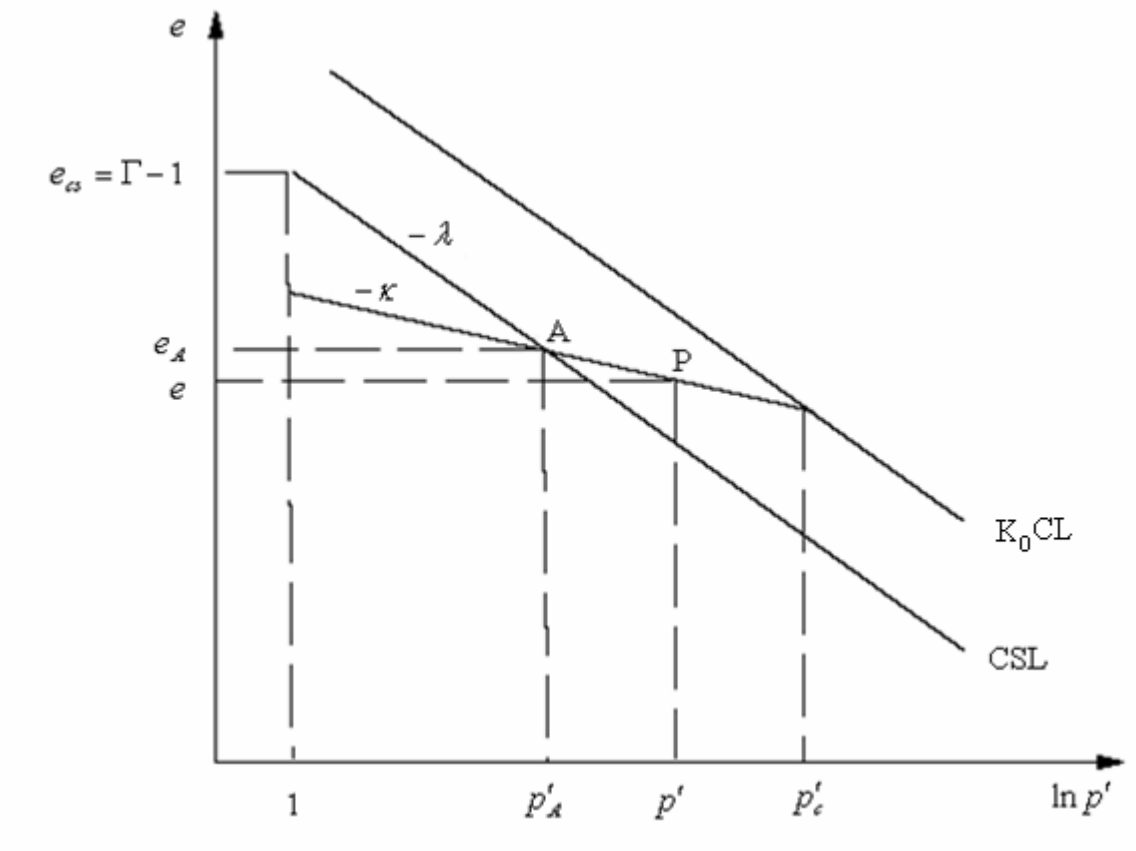

Figure 2.4 Positioning of e_{cs} on e vs ln p' plot

$$e - e_A = \kappa\left(\ln\ p' - \ln\ p_A'\right) \qquad \text{(Eqn. 2.13)}$$

Finally, the stable state boundary surface for Modified Cam Clay models may be expressed as Equation 2.14. The stress ratio, η, in this equation is equal to $\frac{q}{p'}$.

$$V_K = \Gamma + (\lambda - \kappa)\left\{\ln(2) - \ln\left(1 + (\eta / M)^2\right)\right\} \qquad \text{(Eqn. 2.14)}$$

More detailed descriptions, including descriptions of the flow rules associated with the Modified Cam Clay model may be found in elsewhere in literature (Roscoe and Burland, 1968; Atkinson and Bransby, 1978; Britto and Gunn, 1987; Balasubramaniam, 2002)

2.4 Consolidation Modelling in *FLAC*

Consolidation modelling within *FLAC* is a difficult process. Various modelling methods exist to implement full coupling into a program. These approaches and their main calculation commands are outlined in Table 2.1. Selection of the appropriate approach is based on three main factors (Itasca 2002):

1. The ratio between simulation time scale (t_s) and characteristic time (t_c) of the diffusion process
2. The nature of the imposed perturbation (fluid or mechanical) to the coupled process, and
3. The ratio of fluid to soil matrix stiffness (R_k)

A certain level of uncoupling can be performed for some situations to simplify the analysis and speed up calculation time. With respect to consolidation, procedures 5 or 6 shown in Table 2.1 are usually adopted.

The characteristic time (t_c) for the full consolidation response of a soil is given by the Equation 2.15 below, where L = the average flow path length, and c = coefficient of consolidation for the soil. This coefficient is further specified by Equation 2.16 where

k_{FLAC} = *FLAC* Permeability (m^2/Pa.s), n = porosity, K_w = fluid bulk modulus (Pa), K = soil bulk modulus, and G = soil shear modulus.

$$t_c = \frac{L^2}{c_v} \qquad \text{(Eqn. 2.15)}$$

$$c_v = \frac{k_{FLAC}}{\left[\frac{n}{K_w} + \frac{1}{(K + \frac{4}{3}G)}\right]} \qquad \text{(Eqn. 2.16)}$$

The fluid equations and boundary conditions defined within *FLAC* are expressed in terms of a pressure rather than head, although the latter is more common in geotechnical engineering. As a result, *FLAC* uses quite a different 'permeability' throughout (Sivakugan, 2006). Geotechnical permeability and *FLAC* permeability are related through Equation 2.17. In this equation, k_{FLAC} has units of $m^2/Pa.s$, while geotechnical permeability (k) is in m/s, and the unit weight of water, γ_w, in N/m^3.

$$k_{FLAC} = \frac{k}{\gamma_w} \qquad \text{(Eqn. 2.17)}$$

By default, *FLAC* will do a coupled flow and mechanical calculation if the grid is configured for groundwater flow, and both the permeability and fluid bulk modulus are set to realistic values. This default coupling will alternate one fluid step to one mechanical step.

Considering the time scales associated with the mechanical and consolidation processes (mechanical is almost instantaneous, whereas consolidation occurs over days, months or years), this default coupling will lead to inaccurate modelling if left unchanged.

Table 2.1 Recommended Procedure to Select a Modelling Approach for a Fully Coupled Analysis *(Source: ITASCA Consulting Group, 2002)*

Time Scale	**Imposed Process Perturbation**	**Fluid vs. Solid Stiffness**	**Modelling Approach and Main Calculation Commands**	**Adjusted Fluid Bulk Modulus, K_w^a**
$t_s >>> t_c$ (steady state analysis)	Mechanical or Pore pressure	Any R_k	Effective Stress (1) with no fluid flow or	No fluid
			Effective Stress (2) CONFIG gw SET flow off SET mech on	K_w^a=0.0
$t_s <<< t_c$ (undrained analysis)	Mechanical or pore pressure	Any R_k	Pore Pressure Generation (3) CONFIG gw SET flow off SET mech on	Realistic value for K_w^a
t_s in the range of t_c	Pore Pressure	Any R_k	Uncoupled Flow-Mechanical (4) CONFIG gw	
			Step 1. SET flow on SET mech off	$K_w^a = \dfrac{n}{\left[\dfrac{n}{K_w} + \dfrac{1}{(K + \frac{4}{3}G)}\right]}$
			Step 2. SET flow off SET mech on	K_w^a=0.0
t_s in the range of t_c	Mechanical	Any R_k	Coupled Flow-Mechanical (5) CONFIG gw SET flow on SET mech on	Adjust K_w^a so that $R_k \leq 20$
		$R_k >>> 1$	Coupled Fast Flow (6) CONFIG gw SET flow on SET mech on SET fastflow on	Realistic value for K_w^a

The process of controlling the number of fluid and mechanical steps may be done manually using the *SET nmech* and *SET ngw* commands. However, it is recommended that the alternative *SOLVE auto on age* = command be given.

By applying this command, the fluid and mechanical sub steps are adjusted automatically to keep the unbalanced force ratio below a preset value, and continue computing until the age[†] parameter is reached. Unbalanced force ratio is specified using the *SET sratio* command. In the absence of a specificied unbalanced force ratio, FLAC adopts a default value of 1 x 10^{-3} for this parameter (Itasca, 2002).

Deformation and strength properties of the soil should be assigned using 'drained' values. *FLAC* will internally calculate the undrained volumetric deformation and strength properties of the soil depending on the pore pressure present.

For the case of highly deformable soils (such as soft clays), it may be impractical to use the real value of fluid modulus for water (i.e. 2 x 10^9 Pa), as it will lead to the calculation timestep being extremely small. The timestep can be increased by reducing the fluid modulus, but the wrong choice can lead to an inaccurate representation of the consolidation rate and time. In order to gauge whether or not the fluid modulus can be decreased, the ratio of stiffness (R_k) of the fluid to stiffness of the matrix is calculated.

$$R_k = \frac{n}{K_w\left(K + 4/3\, G\right)} \qquad \text{(Eqn. 2.18)}$$

If R_k is large, then the matrix diffusivity will be the controlling factor for solution time. The use of fast flow logic is recommended in this case. However, if the standard method of solution is selected, then in order to increase the timestep without affecting the true diffusivity significantly, it is not computationally necessary to use a value of

[†] The 'age' specified using this command should be the real time (in seconds) for which the consolidation is being computed (NOT the computer time)

K_w that is larger than roughly 20 times $n/(K+4/3G)$. The fluid stiffness should never be made higher than the physical value of the fluid (Itasca, 2002).

2.5 Vertical Drains

2.5.1 General

In locations with poor ground conditions, traditional forms of construction are likely to be quite expensive. Thus, an economical alternative of improving the engineering properties of the soil is sought prior to any building taking place.

One of the most popular methods of ground improvement is the use of vertical drains in combination with preloading. The introduction of a grid of vertical drains into a soil reduces the distance water has to travel through the natural soil, thereby facilitating horizontal flow. This limits the excess pore water pressure generated during and after construction, and increases the rate of settlement. In doing so, they also accelerate the consolidation process, and the primary settlement of a soil is achieved more quickly.

2.5.2 History of Vertical Drains

Vertical drains have been used in some capacity since the 1920's (Bo et al., 2003). Their first introduction was in the form of sand drains. However, due to poor understanding in regards to the behaviour of the sand drains, frequent foundation failures (due to the full load being placed too quickly) were still occurring in the 1940's (Aboshi, 1992). Compaction of the soil during installation was thought to be the solution. Although no effect of densification was expected in clayey soils, these sand columns behaved as granular piles in soft ground, thereby carrying a greater load and functioning as vertical drains at the same time (Jamiolkowski et al., 1983).

It was around this time, that Kjellman (1948) introduced the first prototype of a prefabricated vertical drain made entirely out of cardboard. Subsequently, there have

been several different types of prefabricated vertical drains developed including Geodrain (Sweden), Alidrain (England) and Mebradrain (Netherlands).

2.5.3 Basic Characteristics and Installation of Vertical Drain Systems

All prefabricated vertical drains (otherwise known as PVD) basically consist of a plastic core with longitudinal channel wick functioning as a drain, and a filter which protects the core. This filter is a sleeve of paper or fibrous material.

The installation of PVD is done by a driven or vibratory closed-end mandrel. Figure 2.5 shows the typical shape of a mandrel and prefabricated vertical drain. Compared to sand drains, PVD have much smaller dimensions (see Table 2.2). Consequently, during installation, the degree of soil disturbance (or smear) caused by the size of mandrel is lower.

At the tip of the mandrel is a detachable shoe or anchor made of a small piece of metal. The purpose of this anchor is to prevent soil from entering the mandrel during penetration, and to also keep the drain at the desired depth during mandrel withdrawal. In some cases, this shoe is a piece of the drain itself (Holtz et al., 1991).

Conventional theory of consolidation with vertical drains is based on the assumption of drains with circular cross section. Most prefabricated vertical drains are band shaped, and thus, the rectangular shape has to be converted into an equivalent cylindrical shape prior to any calculations being undertaken. Hansbo (1979) suggests that both band shaped and cylindrically shaped vertical drains produce the same degree of consolidation provided that their equivalent diameters are the same.

Equivalency is calculated as a function of the width (a) and thickness (b) of the drain, and implies that radial capacity of both the band shaped and the equivalent diameter (d_w) drain are identical. Equating the perimeters, d_w is given by:

$$d_w = \frac{2(a+b)}{\pi} \qquad \text{(Eqn. 2.19)}$$

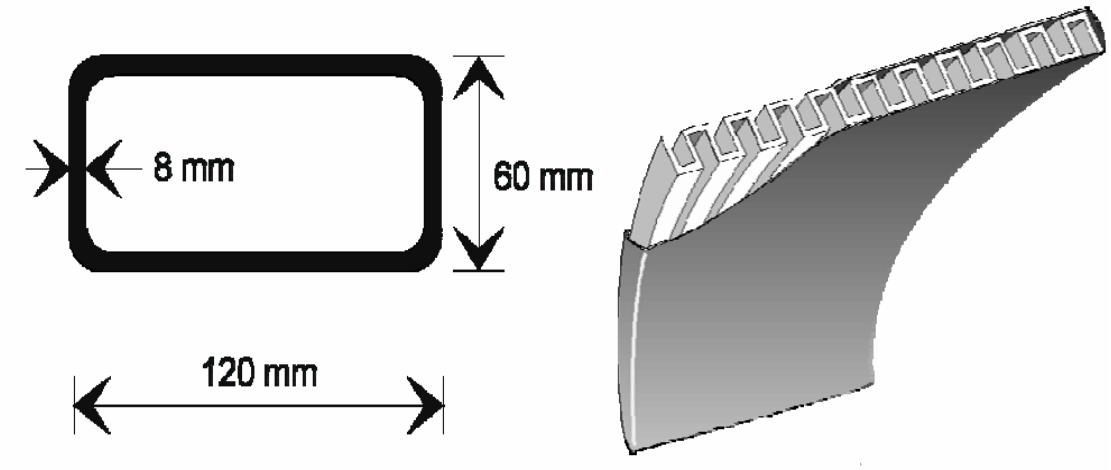

Figure 2.5 Typical mandrel and shape of a prefabricated drain (Mebradrain)

Table 2.2 Types of Vertical Drains (after Holtz et al., 1991)

Drain Type	Installation Method	Drain Diameter (m)	Typical Spacing (m)	Maximum Length (m)
Sand drain	Driven or vibratory closed-end mandrel (displacement type)	0.15 – 0.6	1 – 5	≤ 30
	Hollow stem continuous flight auger (low displacement)	0.3 – 0.5	2 – 5	≤ 35
	Jetted (non-displacement)	0.2 – 0.3	2 – 5	≤ 30
Prefabricated sand drains ("sandwicks")	Driven or vibratory closed-end mandrel; flight auger; rotary wash boring (displacement or non-displacement)	0.06 – 0.15	1.2 – 4	≤ 30
Prefabricated band-shaped drains	Driven or vibratory closed-end mandrel; (displacement or low displacement)	0.05 – 0.1*	1.2 – 3.5	≤ 60

* equivalent diameter

2.5.4 Smear Zone

Vertical drain installation by means of driven or vibratory mandrels causes significant disturbance and remoulding in the soil, especially in those immediately adjacent to the casing. This region of disturbance is known as the smear zone, and was described by Barron (1948) when he stated that the remoulding of soil next to the casing would result in a zone of reduced permeability adjacent to the drain periphery. Such reduced permeability creates additional resistance to pore water pressure dissipation, and thus retards the rate of consolidation. It must, therefore, be accounted for when considering vertical drains.

Analyses by Barron (1948) and Hansbo (1979, 1981) included the effect of smear by dividing the soil cylinder dewatered by the drain into two regions. The first was the smear zone, and was located directly along the drain. The second was the undisturbed or intact zone, situated outside the smear zone and extended to the boundary of the drain influence zone (discussed in Section 2.5.6).

A further three zone hypothesis was suggested by Onoue et al. (1991) following extensive laboratory testing by Ting et al. (1990). This hypothesis was defined by a plastic smear zone in the immediate vicinity of the drain where remoulding was high, a second plastic zone where the permeability was only reduced moderately, and a third, undisturbed zone. However, due to the complexity of the permeability variation in the radial direction, implementation of this three zone approach into vertical drain analyses becomes very difficult. Indraratna and Redana (2000) advocate that for practical purposes, the two zone approach is generally sufficient.

The degree of disturbance caused is dependent on the installation procedure, size and shape of the mandrel and the soil structure.

Akagi (1977, 1981) observed that when a closed end mandrel is driven into saturated clay, the clay will suffer large excess pore water pressure associated with ground heave and lateral displacement. Bergado et al. (1991) also affirmed that the strength

and coefficient of consolidation for the surrounding soil can then decrease considerably with the larger size of mandrel.

Many relationships have been proposed to describe the relationship between the diameter of smear and the equivalent diameter of the mandrel. Jamiolkowski and Lancellotta (1981) propose that:

$$d_s = (2.5 \ to \ 3) d_m \qquad \text{(Eqn. 2.20)}$$

where d_s = smear diameter, and d_m = equivalent mandrel diameter (diameter of a circle with an area equal to the cross section of the mandrel). Hansbo (1981), however, suggests that the diameter of smear is slightly less, and simply two times the equivalent mandrel diameter. Based on laboratory testing, Indraratna and Redana (1998) estimate the ratio of d_s/d_m to be in the vicinity of four to five.

Within the smear zone, the ratio of horizontal to vertical permeability (k_h/k_v) should be assumed as unity (Hansbo, 1981; Bergado et al. 1991). Studies by Indraratna and Redana (1998) were in agreement with these previous studies, and found that the coefficient of horizontal permeability becomes smaller towards the drain, but the coefficient of vertical permeability remains virtually unchanged.

2.5.5 Influence Zones of Drains

Vertical drains are commonly installed in one of two grid arrangements - triangular or square (see Figure 2.6). The equivalent radius of the influence zone for each drain (R) is a function of this grid arrangement and also the drain spacing (S), and is given by:

$$R = 0.546 * S \text{ (for drains installed in a square pattern)} \qquad \text{(Eqn. 2.21)}$$

$$R = 0.525 * S \text{ (for drains installed in a triangular pattern)} \qquad \text{(Eqn. 2.22)}$$

While the square pattern of drains is easier to lay out and control during installation in the field, a triangular pattern is usually preferred since it provides more uniform consolidation between the drains (Holtz et al., 1991).

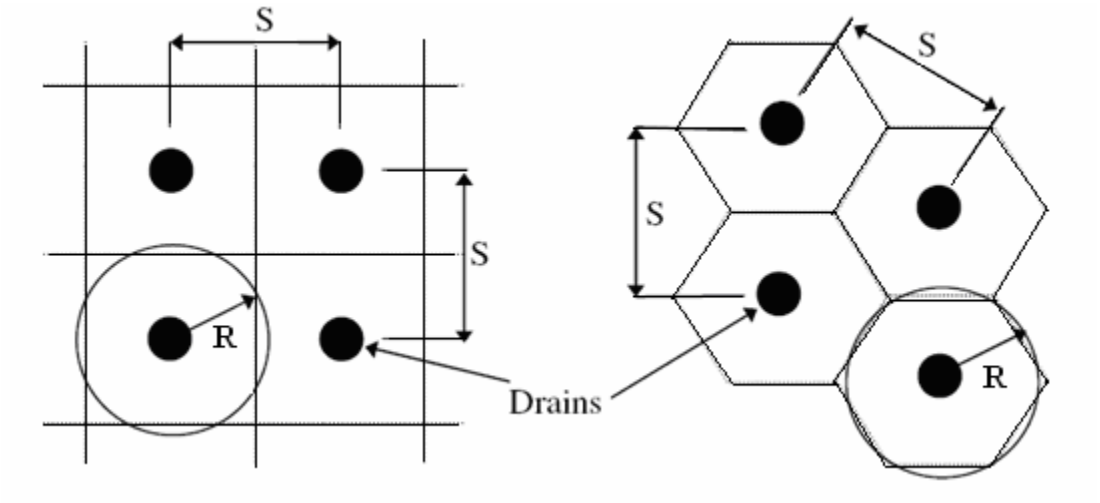

(a) (b)

Figure 2.6 Influence Zones of (a) Square and (b) Triangular Grid Arrangement

2.5.6 Discharge Capacity and Well Resistance

The performance of a vertical drain can be measured in terms of its ability to release excess pore water pressure in the soil and discharge water. Therefore, the higher the discharge capacity of vertical drains, the better the performance of them.

Once water has entered the drain, there are a number of factors which can still affect the flow in the drain itself. The discharge capacity (or well resistance factor) is a function of the following factors (Bergado et al., 1996; Chu et al., 2004):

- Volume of the core or the drain channel
- Lateral earth pressure acting on the drains
- Bending and folding of the drain due to large settlements
- Clogging of the drain due to infiltration of fine soil particles through the filter
- Biological and Chemical degradation
- Hydraulic gradient

Holtz et al. (1988), however, suggests that as long as the working discharge capacity of PVD exceeds approximately 150 m^3/year after installation, then the effect on consolidation due to well resistance may not be significant.

2.5.7 Vertical Drain Modelling Procedure

The geometry and response of PVD are 3-dimensional, and their behaviour is generally investigated using axisymmetric unit cell theory (Barron, 1948; Yoshikuni & Nakanodo, 1974; Hansbo, 1981) which is represented in terms of a single drain surrounded by a cylindrical soil tributary.

However, when considering embankment loading, unit cell analysis is only acceptable under the embankment centreline where the lateral displacements are zero. Elsewhere, especially toward the embankment toe, single drain analysis cannot provide accurate predictions because of lateral yield and heave (Indraratna et al. 1997).

In such multi-drain analyses, true three dimensional analysis are impractical and take exceptionally long times to solve. For the purpose of computational efficiency, the analyses of most of these systems can be conducted using an equivalent plane strain model. Various researchers, including Bergado et al. (1994, 1997), Chai et al.(1995) and Indraratna and Redana (1998, 2000), have used such plane strain solutions in the analysis of field data.

Conversion to equivalent plane strain is achieved by transforming the vertical drain system into a set of equivalent drain walls (see Figure 2.7), which can be achieved through geometric and/or permeability matching (Redana, 1999). .

The method proposed by Indraratna & Redana (1997) converted the vertical drain system into an equivalent drain well by adjusting the coefficient of permeability of the soil, and assuming the plane strain cell to have a width of 2B. The derivation of this method, as explained by Redana (1999), has been reproduced and is shown below.

The drain half width, b_w, and smear zone half width, b_s, equate identically to the axisymmetric radii of r_w, and r_s, respectively. Indraratna & Redana (1997) further showed that the degree of consolidation at a depth, z, in plane strain condition can be represented by:

$$U_{hp} = 1 - \frac{\bar{u}}{u_0} = 1 - \exp\left(\frac{-8T_{hp}}{\mu_p}\right) \qquad \text{(Eqn. 2.23)}$$

where $\bar{u}_0$ is the initial pore pressure, $\bar{u}$ is the pore pressure at time *t* (average values), T_{hp} is time factor in plane strain, and μ_p is given by Equation 2.24, where k_{hp} and k_{hp}' are the undisturbed horizontal and corresponding smear zone permeabilities, respectively.

$$\mu_p = \left[\alpha + \beta\frac{k_{hp}}{k_{hp}'} + \theta\left(2lz - z^2\right)\right] \qquad \text{(Eqn. 2.24)}$$

By ignoring higher order terms, the geometric parameters of α and β, and the flow term of θ, are given by:

$$\alpha = \frac{2}{3} - \frac{2b_s}{B}\left(1 - \frac{b_s}{B} + \frac{b_s^2}{3B^2}\right) \qquad \text{(Eqn. 2.25)}$$

$$\beta = \frac{1}{B^2}\left(b_s - b_w\right)^2 + \frac{b_s}{3B^3}\left(3b_w^2 - b_s^2\right) \qquad \text{(Eqn. 2.26)}$$

$$\theta = \frac{2k_{hp}^2}{k_{hp}' B q_z}\left(1 - \frac{b_w}{B}\right) \qquad \text{(Eqn. 2.27)}$$

where q_z is the equivalent plane strain discharge capacity of the drain, and dimensions B, b_s and b_w are defined as in Figure 2.7.

At a given stress level, to maintain the same degree of consolidation at each time step, the average degree of consolidation for both axisymmetric $\left(\bar{U}_{\mathrm{h}}\right)$ and equivalent plain strain $\left(\bar{U}_{\mathrm{hp}}\right)$ conditions are made equal. Thus,

$$\bar{U}_{h} = \bar{U}_{hp}. \qquad \text{(Eqn. 2.28)}$$

For axisymmetric flow involving vertical drains, the original Hansbo (1981) theory stated that the average degree of consolidation $\bar{U}_{\mathrm{h}}$ on a horizontal plane at a depth z and at time t may be predicted from:

$$\bar{U}_{\mathrm{h}} = 1 - \exp\left(-\frac{8T_{\mathrm{h}}}{\mu}\right) \qquad \text{(Eqn. 2.29)}$$

where T_{h} is the time factor, and μ is a reduction factor to account for smear and well resistance.

When considering the effects of both well resistance and smear effects, μ is given by Equation 2.30.

$$\mu = \ln\left(\frac{n}{s}\right) + \left(\frac{k_{\mathrm{h}}}{k'_{\mathrm{h}}}\right)\ln(s) - 0.75 + \pi\left(2lz - z^2\right)\frac{k_{\mathrm{h}}}{q_{\mathrm{w}}} \qquad \text{(Eqn. 2.30)}$$

In the above, $n = R/r_{\mathrm{w}}$, where R is the radius of the influence zone of the drain and r_{w} is the radius of the drain; $s = r_{\mathrm{s}}/r_{\mathrm{w}}$, where r_{s} is the radius of the smear; l is the length of the drain having one-way drainage or half this value for two-way drainage; z is the depth of the drain under consideration; q_{w} is the discharge capacity of the drain; and k_{h} and k'_{h} are the coefficients of horizontal permeability outside and inside the smeared zone, respectively.

This reduction factor condenses to Equation 2.31 when only considering well resistance (Bo et al., 2000).

$$\mu = \ln(n) - 0.75 + \pi z(2l - z)\frac{k_h}{q_w} \qquad \text{(Eqn. 2.31)}$$

where n = drain spacing ratio (= r_e/r_w); z = depth; l = longest drainage path along vertical drain (equal to half the drain length for 'open end' drains, or the entire length for 'closed-end' drains; q_w = well discharge capacity (= $A_w k_w$); A_w = cross sectional area of the drain; k_h = coefficient of permeability for horizontal flow; and k_w = permeability of drain.

Now, by combining Equations 2.24 and 2.28 with Hansbo (1981) theory (Equation 2.29), the time factor ratio can be derived:

$$\frac{T_{hp}}{T_h} = \frac{k_{hp}}{k_h}\frac{R^2}{B^2} = \frac{\mu_p}{\mu} \qquad \text{(Eqn. 2.32)}$$

If the radius of the axisymmetric influence zone of a single drain (R) were taken to be the same as the half-width (B) in plain strain, the relationship between k_{hp} and k'_{hp} is given by:

$$k_{hp} = \frac{k_h\left[\alpha + \beta\frac{k_{hp}}{k'_{hp}} + \theta\left(2lz - z^2\right)\right]}{\left[\ln\left(\frac{n}{s}\right) + \left(\frac{k_h}{k'_h}\right)\ln(s) - 0.75 + \pi\left(2lz - z^2\right)\frac{k_h}{q_w}\right]} \qquad \text{(Eqn. 2.33)}$$

If the effect of well resistance is ignored ($q_w \to \infty$), all l and z terms from Equation 2.33 are neglected. The ratio of plane strain permeability in the smear zone to the undisturbed permeability can be expressed as Equation 2.34.

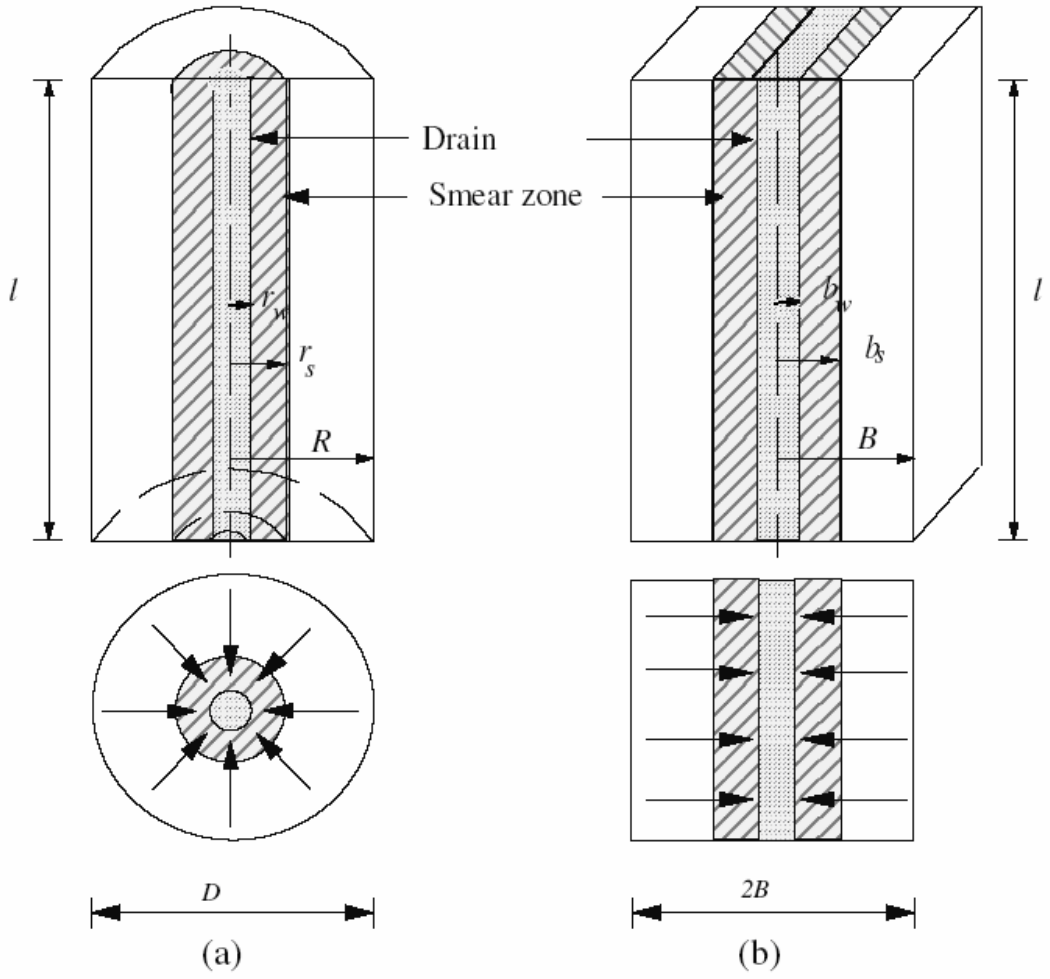

Figure 2.7 Conversion of an (a) Axisymmetric Unit Cell into (b) Plane Strain Condition

$$\frac{k'_{hp}}{k_{hp}} = \frac{\beta}{\frac{k_{hp}}{k_h}\left[\ln\left(\frac{n}{s}\right) + \left(\frac{k_h}{k'_h}\right)\ln(s) - 0.75\right] - \alpha} \qquad \text{(Eqn. 2.34)}$$

If both the smear and well resistance are ignored, then the simplified ratio of plane strain to axisymmetric horizontal permeability k_h is represented by:

$$\frac{k_{hp}}{k_h} = \frac{0.67}{\left[\ln(n) - 0.75\right]} \qquad \text{(Eqn. 2.35)}$$

Well resistance can be derived independently, and the equivalent discharge capacity be calculated using the relation proposed by Hird et al. (1992):

$$q_z = \frac{2}{\pi B} q_w \qquad \text{(Eqn. 2.36)}$$

CHAPTER 3

LABORATORY INDUCED VARIATION IN ATTERBERG LIMIT TESTING

3.1 Introduction

Whilst the general engineering behaviour of a coarse grained soil is governed by grain size distribution, the behaviour of a fine grained soil is governed mainly by the presence of water in the voids of the soil. The Atterberg Limits of a soil, namely liquid limit, plastic limit, plasticity index and shrinkage limit, are the borderline water contents between critical stages in soil behaviour (Holtz & Kovacs, 1981). In particular, the liquid limit of a soil as an index property has wide applicability in geotechnical engineering, and has been used alone, and also in conjunction with other index properties to provide many useful engineering correlations (Prakash & Sridharan, 2002).

The common methods for determining these indices are detailed by the Australian Standards AS1289.3.1.1, AS1289.3.2.1 and AS1289.3.3.1 respectively. However, additional testing methods, approved by the National Association of Testing Authorities (NATA), may also be used for their estimation, such as those detailed by road testing authorities such as the Queensland Department of Main Roads etc.

Liquid limit may be determined using one of two devices – the Casagrande percussion liquid limit apparatus or the fall cone apparatus. The first was developed by A. Casagrande (1932), and shown in Figure 3.1(a), defines the liquid limit as the water content at which a groove cut into the soil will close over a distance of 12.5mm following 25 blows. Due to the difficulty in achieving this in a single test, generally about four tests are undertaken at different water contents (to correspond to different

terminal blow counts), and a line of best fit drawn to determine the water content which corresponds to the 25 blows.

Figure 3.1(b) displays the second apparatus developed by Hansbo (1957). This device defines liquid limit as the water content at which a standard cone (weight = 79.5 grams, apex angle = 30 degrees) will penetrate a distance of 20 mm in five seconds, when allowed to drop from a position of point contact with the soil surface. Again, as with the percussion cup method, it is difficult to achieve the liquid limit from a single test, and thus, four or five tests are generally completed, with liquid limit determined from a line of best fit between these points.

The plastic limit is somewhat more manual, and is defined as the water content at which a thread crumbles when rolled out to a diameter of 3 mm. These crumbled threads should be 3 to 10 mm long.

The shrinkage limit is identified as the boundary between the brittle-solid state and semi-solid states of a soil, and is the water content below which a further loss in moisture will not cause volume decrease of a soil. Conventional testing for shrinkage limit is outlined in AS1289.3.4.1 and involves the measurement of mean longitudinal shrinkage of a clay sample when placed into a brass mould.

Although these tests appear quite simple, they require some practice to get consistent and reliable results, with even highly experienced technicians displaying some differences in their results. Empirical correlations based on these properties are often subject to low regression coefficients due to the variability in the measurements. The variability exhibited in these results is very often the sum of variations from a number of different sources. These sources may include the inherent variance of properties throughout a soil mass, as well as laboratory induced variance. Distinction between these two components in the statistical analysis of geotechnical properties is rarely acknowledged, and total variance is quite often incorrectly reported as the inherent variance.

(a)

(b)

Figure 3.1 Photographs of the Alternative Liquid Limit Devices

(a) Casagrandes Liquid Limit Device (b) Fall Cone Device

With the exception of proficiency testing undertaken by agencies such as NATA, reporting into this area of laboratory induced variation/error is scarce. NATA, the National Association of Testing Authorities, undertakes such tests from time to time to assess the performance of all of its accredited laboratories on their Atterberg Limit determination. The data collected by NATA through such an exercise in June/July 1984 and November, 1989 are analysed in this chapter, in an attempt to quantify the laboratory induced variation in Atterberg Limit determination.

Samples were distributed to each of the participants in the proficiency test program. These samples consisted of a black soil, red clay, sand/loam and river gravel for the 1984 test program, and two unidentified clays and three loam samples for 1989 testing. In this chapter, samples from the 1984 test program have been identified as Samples A through to D, while 1989 clay and loam samples have been identified as E through to I. It should be noted that these sample codes have been applied for ease of reference, and do not correspond to the codes given by NATA (1984, 1989) for the soils. Descriptions of the soils are detailed in Table 3.1.

A statistical analysis has been undertaken on data published subsequent to these proficiency tests (NATA 1984, 1989), and used to quantify the levels of variance that engineers should expect for the index properties of liquid limit, plastic limit and linear shrinkage due solely to testing methods. Furthermore, probability distributions functions have been formulated to describe these variances. Lastly, a well known empirical correlation relating linear shrinkage to the plasticity index of a soil has also been evaluated with respect to the proficiency test programs soil results.

3.2 Testing and Reporting Methods

The main aim of these programs was to assess the level of proficiency of laboratories for the testing of Atterberg Limits. Bulk samples were taken from natural soil deposits known to be somewhat uniform in property. These samples were then air dried, mixed and split into sub samples using a riffle box. To ensure low variability between sub samples, a set of preliminary tests were undertaken on random samples from each different soil.

Table 3.1 Sample Classifications and Data Source

Sample ID	Type of Soil	Data Source
A	Black Soil	NATA (1984)
B	Red Clay	NATA (1984)
C	Loam/Sand	NATA (1984)
D	River Gravel	NATA (1984)
E	Clay	NATA (1989)
F	Clay	NATA (1989)
G	Loam/Sand	NATA (1989)
H	Loam/Sand	NATA (1989)
I	Loam/Sand	NATA (1989)

Program participants were supplied four samples of soils to be tested and asked to abide by a set of clearly outlined instructions. A results sheet was also supplied to the participants to complete to ensure that the data submitted from all laboratories were described in a same format, and that all additional information was included. Examples of the instruction and results sheets included for each participant are shown in Appendix A.

The final report produced by NATA at the completion of these programs contained the following information (NATA, 1984, 1989):

- Summary Statistics (no. of results, mean, standard deviation, variance, coefficient of variation, standard error, range of values)
- Graphical displays (frequency histogram, Youden diagram, box plots)
- Laboratory summary reports (detailing the sample ID, and the accuracy of the laboratory determined parameter in comparison to the consensus mean i.e. within 1 standard deviations etc.)
- Sample preparation and homogeneity testing information

- Limited comments from NATA technical advisers comments
- A copy of the instructions to participants and results sheet from each participant

It should be noted that all statistical analyses completed by NATA upon this data assumed a normal distribution. As shown subsequently by the results of the chi-square tests, this assumption was acceptable in most cases. However, it is the author's opinion that representations of any geotechnical parameters should adopt a beta distribution for probability distribution function formulation, and state the chi-square level beside it. The reasons for this alternate representation are outlined in Section 3.3.4 and are in accordance with similar suggestions by Harr (1977).

3.3 Statistical Methods

3.3.1 General

Virtually all real world processes are subject to variability. The conventional deterministic approach is to ignore the variability of soils and to use some 'average' property and assume a homogenous material with this property for design purposes. The variability taken into account is invariably through personal judgement (Lee et. al., 1983).

Duncan (2000) proposed the more systematic method of adopting what he terms the 'three sigma rule'. This rule suggests that the values for a given soil property be considered within the range of 3 standard deviations above and below the mean. This rule of thumb originally used the normal distribution as a basis; however, it can be applied to any distribution (Harr, 1977).

The following section outlines a brief overview of the concepts and methods of statistical analysis that is used to present, describe and understand this variability described by NATA (1984, 1989) data.

3.3.2 Standardised Z-Score

In statistics, raw data is commonly standardised by converting it into what is known as a Z-score. This score is a dimensionless quantity derived by subtracting the population mean from the raw data score, and then dividing the difference by the population standard deviation (see Equation3.1). This score may be positive or negative, the sign simply indicating whether it is above (positive) or below (negative) the mean.

$$Z = \frac{X - \mu}{\sigma} \qquad \text{(Eqn. 3.1)}$$

Although an indication of the range within which Z-scores lay (< 1 standard deviation, 1 - 2 standard deviations, > 2 standard deviations) were published in NATA (1984, 1989) reports, no actual scores were detailed.

Values for these 'standardised scores' have been calculated, and ordered plots for each total set of Z-scores are included in the Appendices B (Liquid Limit), C (Plastic Limit), D (Plasticity Index) and E (Linear Shrinkage). It should be noted that all laboratories included will have a Z-score. However, this Z-score may appear blank on the ordered plots for laboratories that measured the parameter value most accurately (i.e. measured values equivalent or very close to the mean).

A vertical gridline has been placed on each graph to indicate the median of the population. Horizontal gridlines have been placed at 1 standard deviation through to 4 standard deviations away from the mean. No laboratory numbers have been included with any of these plots for anonymity purposes. The range over which raw data was recorded is displayed in terms of standard deviations.

3.3.3 Youden Plots

When comparing different test methods, the issue of their reproducibility should be addressed as it essentially limits the amount of agreement that is possible for it. That

is, if the reproducibility of a test method is poor, then it is difficult for an operator to achieve similar results for similar samples. Consequently, it is more likely that large variation will occur between measurements and correlation between these results will be mediocre.

The common method of investigating the reproducibility of laboratory test methods is to take measurements on two different duplicate samples, and see how the results from such tests relate to each other. Results are often displayed in terms of a Youden plot (Youden, 1959). To construct this sort of plot, the results from the two duplicate samples are plotted on opposing axes, and median lines are drawn perpendicular from each axis. A reference line is then plotted through the intersection point of these two median lines, and a rectangle constructed to indicate the extent of 2 standard deviations from the median on both axes. For the case in which both axes have used the same scale, this reference line plots at 45 degrees.

This plot is helpful in separating the systematic error from random error in results analysis. If points plot along the reference line, the method under consideration can generally be assumed to be free of systematic errors. Random error can be evaluated by examining the scatter of the points. If the data points are tightly grouped, the random error of the method is minimal. If they are widely spread, the random error is large. A brief overview of the plot will also be able to identify outliers, as the results which sit outside the standard deviation rectangle.

3.3.4 Probability Distribution Functions

Where a significant scatter is observed between measurements of a parameter, it is helpful to have an equation to express the characteristics of the randomness. Such equations are known as probability distributions (or probability models). They may be used in engineering calculations to not only work out the most probable value of a parameter, but also in reliability analyses.

Lumb (1966) suggested that a number of material parameters used in geotechnical engineering appeared to follow a normal distribution. This hypothesis was

corroborated by studies conducted by Schultze (1972) on a number of different types of soils.

Technically, however, as stated clearly by Harr (1977), this is physically impossible for any material parameter, as such a distribution requires observable quantities to be purely symmetrical about the mean, and to also take on both negative and positive values. Harr (1977) went on further to suggest that a beta distribution is better suited to describing the observed characteristics of material parameters, and should be adopted as common practice.

In reality, all three parties are somewhat correct. It is clear that negative values of any material parameter are impossible, and thus the characteristics of any material parameter are unable to follow a normal distribution perse. Material properties may, however, exhibit normality in their distributions (as shown for Atterberg Limits later within this Chapter). Thus, it is suggested, that in calculating the distribution of material parameters, the beta distribution method be employed, and the degree of normality for the distribution be detailed with it. This way, any person interpreting such research is given an indication of the degree to which the population follows the normal distribution, and will also be able to infer the degree to which an assumption of normality will affect the results.

Approximation using a beta distribution dictates that the measurements be always positive, and that the ranges be of a reasonably limited extent. An empirical method by which a probability distribution function may be produced is detailed by Harr (1977) is summarised below.

For the range [a,b], beta probability distribution functions are defined by Equation 3.2:

$$f(x) = \frac{(b-a)^{-1-\alpha-\beta}}{\mathrm{B}(\alpha+1,\beta+1)}(x-a)^{\alpha}(b-x)^{\beta} \qquad \text{(Eqn. 3.2)}$$

where $a \leq x \leq b$, and $\beta > -1$, $\alpha > -1$, and $B(\alpha+1, \beta+1)$ is obtained using Harr's gamma function table shown in Appendix F (Harr, 1977) and the following relationship,

$$B(\alpha+1, \beta+1) = \frac{\Gamma(\alpha+1)\Gamma(\beta+1)}{\Gamma(\alpha+\beta+2)} \qquad \text{(Eqn. 3.3)}$$

Values of $\Gamma(x)$, given in Table F1 are within the range $1 \leq x \leq 2$. The relationship which may be used to reduce the evaluation of the gamma function for values of x greater than 2, to within the range of $1 \leq x \leq 2$ is given by Equation 3.4.

$$\Gamma(x+k+1) = x(x+1)(x+2)....(x+k)\Gamma(x) \qquad \{\text{for k=0, 1, 2…}) \qquad \text{(Eqn. 3.4)}$$

To illustrate this procedure further, we consider the evaluation of $\Gamma(3.5)$. Here, x + k + 1 =3.5. Now, to reduce the argument to $1 < x < 2$, k must equal 1, and x must equal 1.5.

$\Gamma(1.5) = 0.8862$ (from the gamma function table shown in Appendix F)

Hence,

$\Gamma(3.5) = (x)(x+1)\,\Gamma(a)$
$= (1.5)(2.5)(0.8862)$
$= 3.3$

The shape parameters, α and β, cited in Equations 3.2 and 3.3 are functions of two standardised variables – X and Y. These standardised variables are calculated from the mean (μ) and standard deviation (σ) of the measured results, as well as the maximum and minimum limits set by the range [a, b]. Harr (1977) defines these standardised terms using Equations 3.5 and 3.6. The shape factors, α and β, are obtained for data ranging from a to b using Equations 3.7 and 3.8.

$$X = \frac{\mu - a}{b - a} \qquad \text{(Eqn. 3.5)}$$

$$Y = \left(\frac{\sigma(x)}{b - a} \right)^2 \qquad \text{(Eqn. 3.6)}$$

$$\alpha = \frac{X^2}{Y^2}(1 - X) - (1 + X) \qquad \text{(Eqn. 3.7)}$$

$$\beta = \frac{\alpha + 1}{X} - (\alpha + 2) \qquad \text{(Eqn. 3.8)}$$

The range limits for the function are generally assumed to be equivalent to three times the standard deviation on either side of the measured mean. This ensures a 99.7% confidence that the variable being measured will fall between these two values.

The distribution curve is also sometimes described in terms coefficients of skewness (β_1) and kurtosis (β_2). The first of these coefficients, β_1, describes the asymmetry of a curve around its mean, while the latter of the two coefficients, β_2, describes the relative peakedness for the curve compared with the normal distribution. For a beta distribution, these parameters are defined by Equations 3.9 and 3.10. For comparison purposes, the coefficient of kurtosis for a normal distribution is equivalent to 3, while a uniform distribution has a value of 1.8.

$$\beta_1 = \frac{2(\beta - \alpha)}{(\alpha + \beta + 4)} \sqrt{\frac{\alpha + \beta + 3}{(\alpha + 1)(\beta + 1)}} \qquad \text{(Eqn. 3.9)}$$

$$\beta_2 = \frac{3(\alpha + \beta + 3)\left(2(\alpha + \beta + 2)^2 + (\alpha + 1)(\beta + 1)(\alpha + \beta - 4)\right)}{(\alpha + 1)(\beta + 1)(\alpha + \beta + 4)(\alpha + \beta + 5)} \qquad \text{(Eqn. 3.10)}$$

It is important to realise that beta functions do not represent probabilities themselves. It is rather integration of the beta function to find the area between two points that yields the probability of the measured parameter falling within the range selected.

3.3.5 Chi-Square Test

To determine whether observed frequencies of occurrence in a set of samples are drawn from a prescribed probability distribution, a statistical procedure called chi-square test (also known as 'goodness of fit' test) is used (Harr, 1977). A testing statistic, D (given by Equation 3.11), is computed using the observed (O_i) and expected (e_i) frequencies within specific intervals, and then compared to previously published χ_α^2 values for the expected distribution at a specified significance level. Table 3.2 details the critical χ_α^2 values for up to 15 degrees of freedom.

In this situation, the degrees of freedom are given as the number of groups of data (also referred to as 'bins' in statistical analyses) minus 1. If D < χ_α^2, then it can be concluded that the samples are drawn from the assumed distribution. If it is greater than the χ_α^2 value, the sample parameter does not follow the expected distribution.

$$D = \sum_{i=1}^{N} \frac{(O_i - e_i)^2}{e_i} \qquad \text{(Eqn. 3.11)}$$

Normally, to describe something as 'significant' indicates that whatever is under consideration carries a high degree of importance. For this reason, the terms of 'statistical significance' and in turn 'significance level' are commonly misinterpreted. In statistics, to define something as 'statistically significant' indicates that it is probably true (and not due to chance). It does not necessarily convey any level of importance.

'Significance level' indicates the confidence interval of a hypothesis. Though, unlike normal intervals which indicate, for example, a 95% confidence interval as 0.95, the significance level (also known as the alpha level) is indicated by the 1.0 minus the probability in decimals. So, a significance level that corresponds to a 95% confidence interval will be represented as 0.05. Thus, smaller values of significance level are better as they indicate higher levels of confidence.

Table 3.2 Chi-Square (χ_{α}^{2}) Critical Values

Degrees of Freedom	Probabilities		
	P=0.05	***P=0.01***	***P=0.001***
1	3.84	6.64	10.83
2	5.99	9.21	13.82
3	7.82	11.35	16.27
4	9.49	13.28	18.47
5	11.07	15.09	20.52
6	12.59	16.81	22.46
7	14.07	18.48	24.32
8	15.51	20.09	26.13
9	16.92	21.67	27.88
10	18.31	23.21	29.59
11	19.68	24.73	31.26
12	21.03	26.22	32.91
13	22.36	27.69	34.53
14	23.69	29.14	36.12
15	25	30.58	37.7

Significance levels are selected individually by the statistician, depending of course, on the confidence level required. However, the most common significance level chosen is 0.05.

Due to the substantial number of laboratories test data for each sample, and also for ease of calculation, the results from each of the parameters were divided into 5 groups for each sample. The boundaries of these groups were elected to sit at values corresponding to the mean minus 3σ, 2σ, 1σ, and the mean plus 1σ, 2σ and 3σ respectively. In assigning the groups in such a way, the degrees of freedom for each parameter was determined as 4.

3.4 Results and Discussions

3.4.1 General

The proficiency tests analysed within this chapter incorporated a wide variety of soils and also test methods. The classification of samples, along with a description of the soil type, and also the data source are shown previously in Table 3.1.

Statistical summaries, included in each relevant section, detail the number of samples, mean, median, standard deviation and coefficient of variation for each of the soils.

Casagrande's (1943) chart of liquid limit-plasticity index representation is currently used by engineers for the geotecnical identification of soils. Gutierrez (2006) examines the mathematical error introduced into statistical analyisis by using spurious variables. Such variables are 'new' parameters created by a linear combination of other basic ones. He cites plasticity index as one such variable, and suggests that expression of any relationship between liquid limit and plasticity should be in terms of liquid limit and plastic limit, rather than liquid limit and plasticity index. For this reason, the positioning of all of the tested samples have been plotted both on the original Casagrande's PI-LL chart, and also the Gutierrez (2006) PL-LL chart (Figures 3.2 and 3.3 respectively).

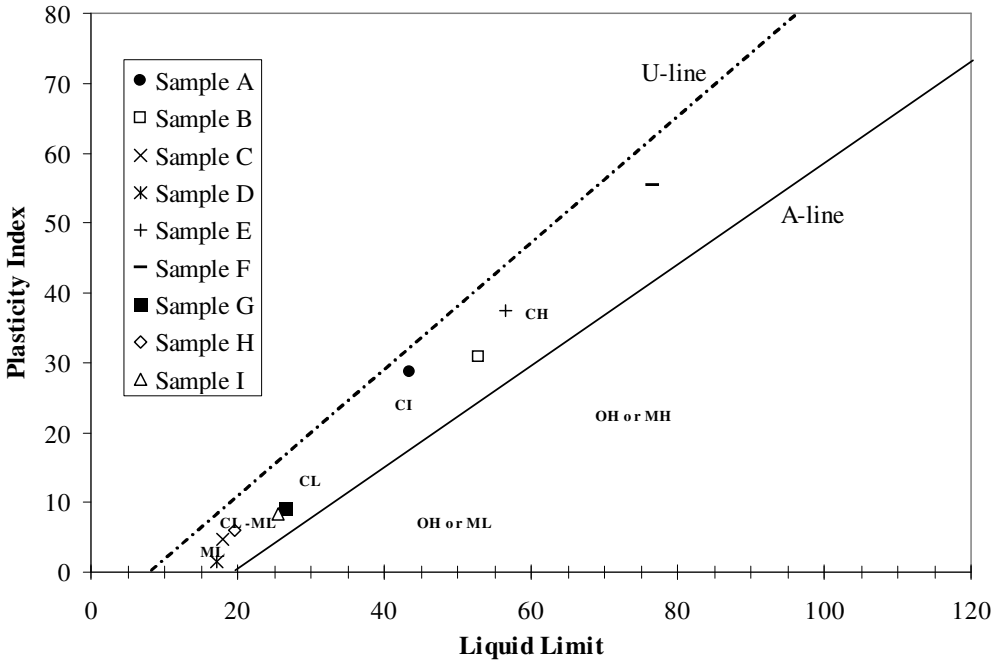

Figure 3.2 NATA Sample Positioning on Casagrande's Plasticity Chart

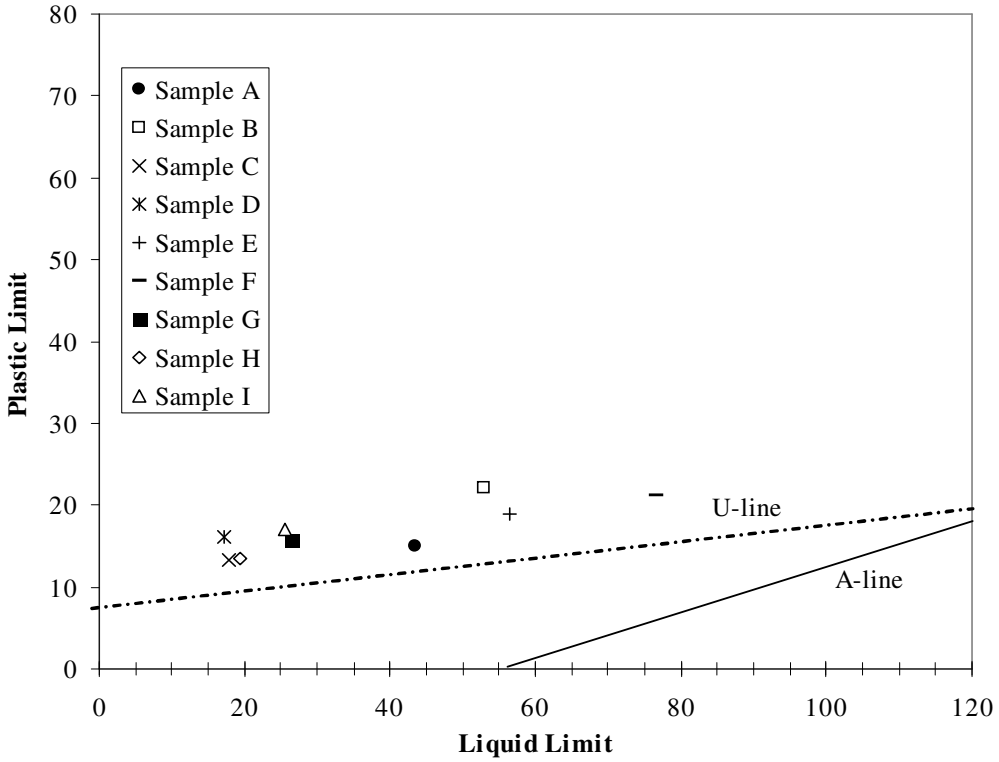

Figure 3.3 NATA Sample Positioning on Amended Casagrande's Plasticity Chart (Gutierrez, 2006)

The beta distribution functions formulated from the raw NATA data indicated a distribution close to normal for many of the soil parameters. Standard normal distributions display a coefficient of kurtosis equivalent to 3, and are symmetrical around the mean. While most of the distributions displayed coefficients of skewness equivalent to zero, their coefficients of kurtosis were less than the standard normal curve, measuring approximately 2.45.

Due to this difference, and the fact that many parametric statistics are based upon the assumption of normality (how well a distribution is approximated by a normal distribution), a chi square test was undertaken on each set of raw data. The results of these 'goodness of fit' tests are displayed in their corresponding sections below.

The distribution functions for each liquid limit, plastic limit, plasticity index and linear shrinkage are all shown simultaneously for each of the respective soils in Figures 3.4 to 3.12. As expected, the plasticity index curves plot between plastic and liquid limits for all clay samples, and to the left of the plastic limit curve for loam/sand samples. All further plots (Ordered z-score plots, Youden plots and histograms) have been included in Appendix B through to E.

3.4.2 Liquid Limit

Intuitively, one can assume that a sandy loamy soil will have a lower liquid limit than a clayey soil by virtue of the amount of fines content within the soil. However, to accurately arrange soils in order of ascending / descending liquid limit, one must further examine the basic statistical descriptors of each of the soils. Due to the similarity of test method between all participants, these descriptors were able to be established using the entire data population.

Table 3.3 presents a summary of some of the basic statistical values calculated from measured liquid limit data of each of the soils tested during the proficiency tests.

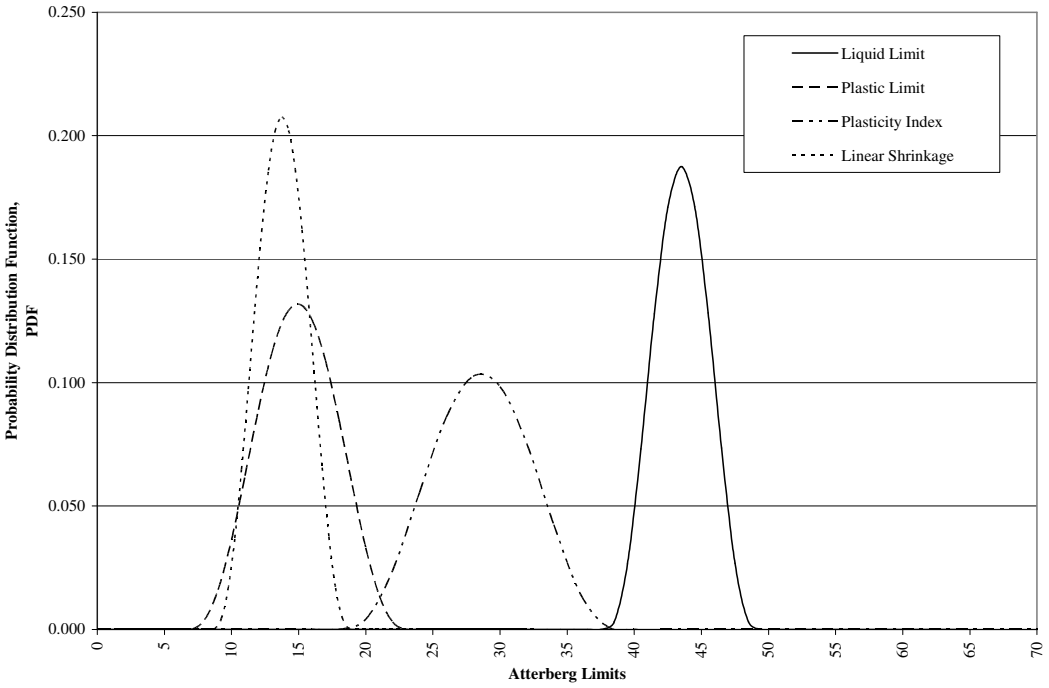

Figure 3.4 Probability Distribution Functions of Index Properties for Sample A

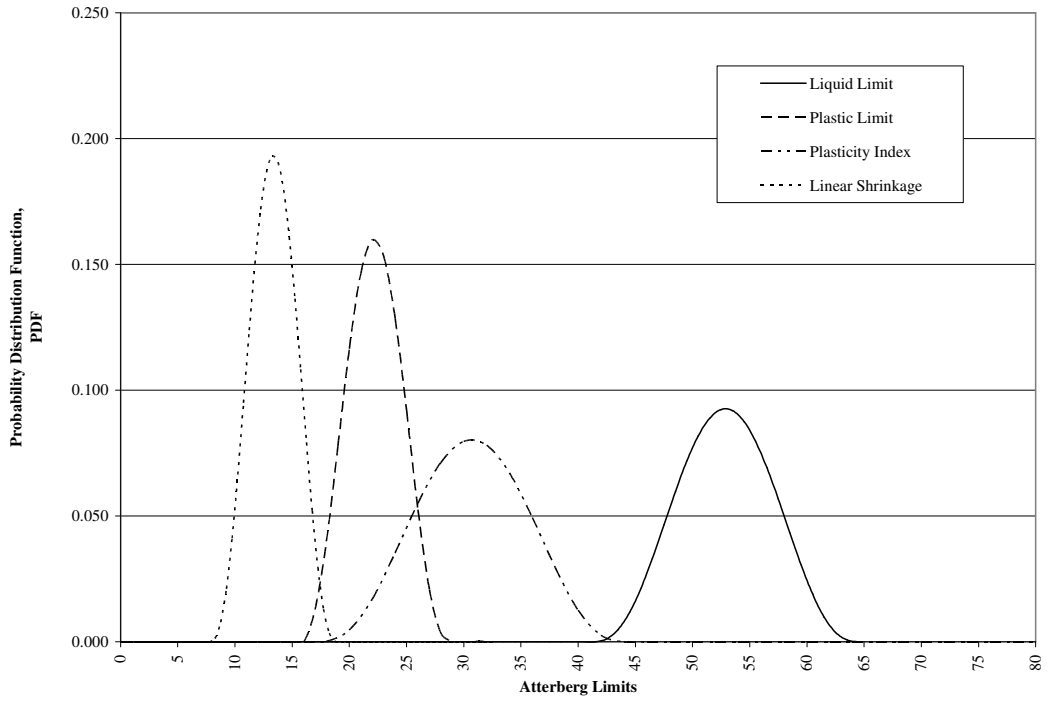

Figure 3.5 Probability Distribution Functions of Index Properties for Sample B

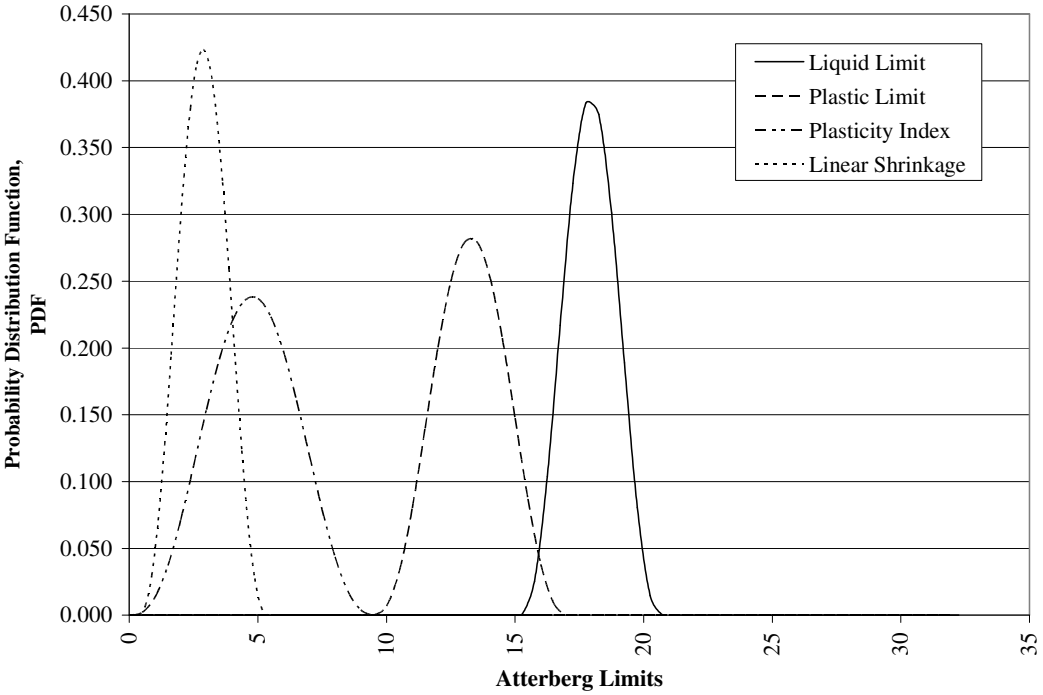

Figure 3.6 Probability Distribution Functions of Index Properties for Sample C

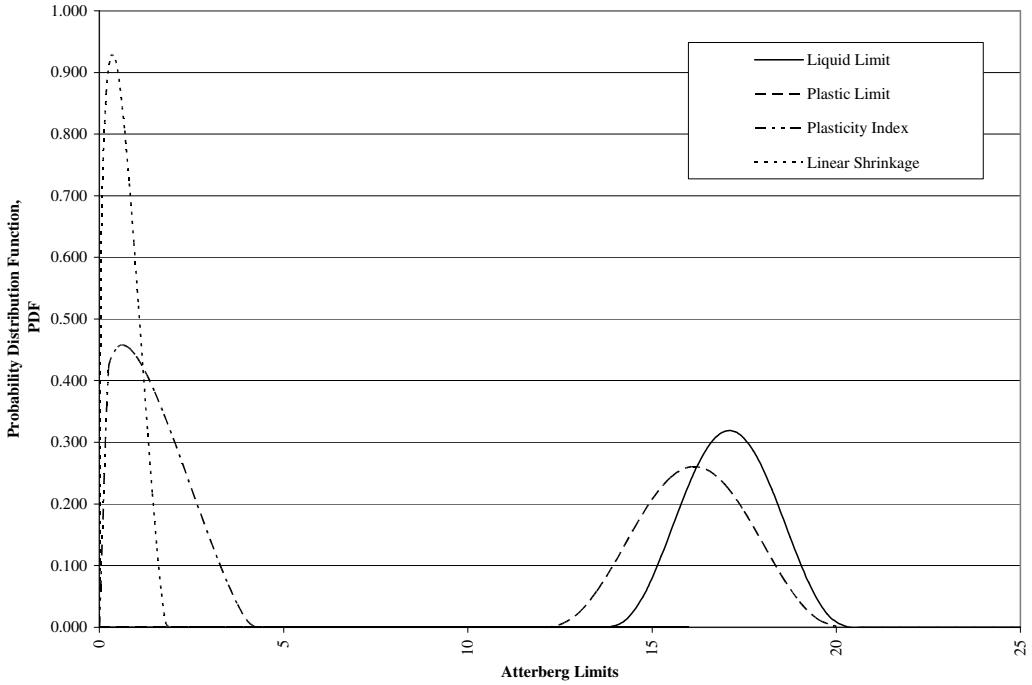

Figure 3.7 Probability Distribution Functions of Index Properties for Sample D

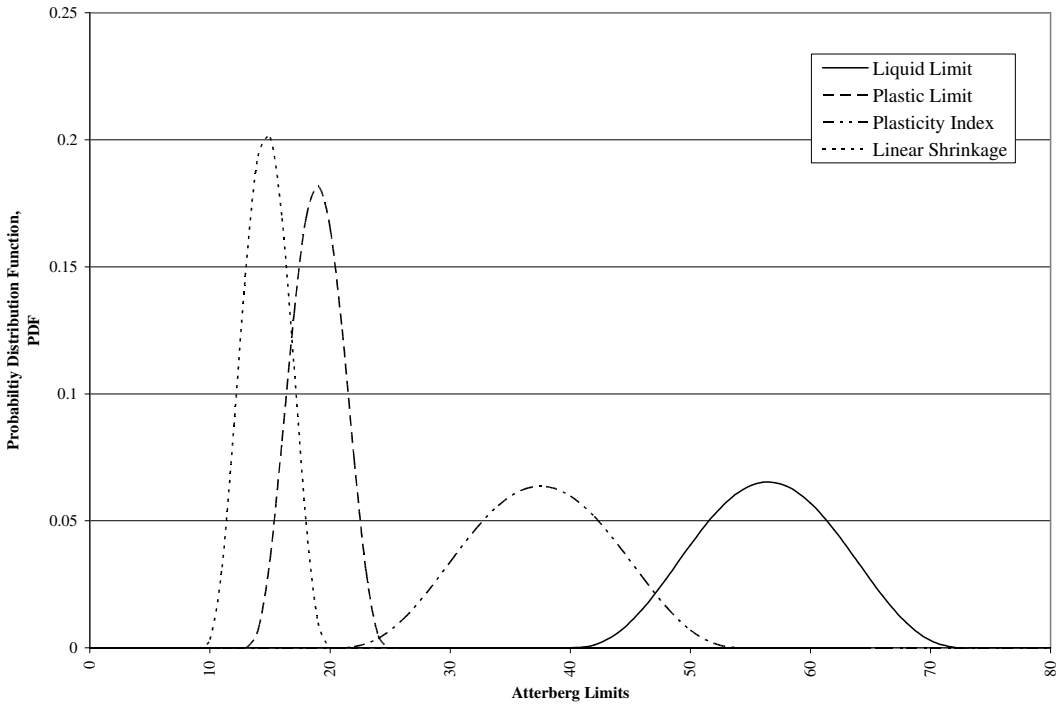

Figure 3.8 Probability Distribution Functions of Index Properties for Sample E

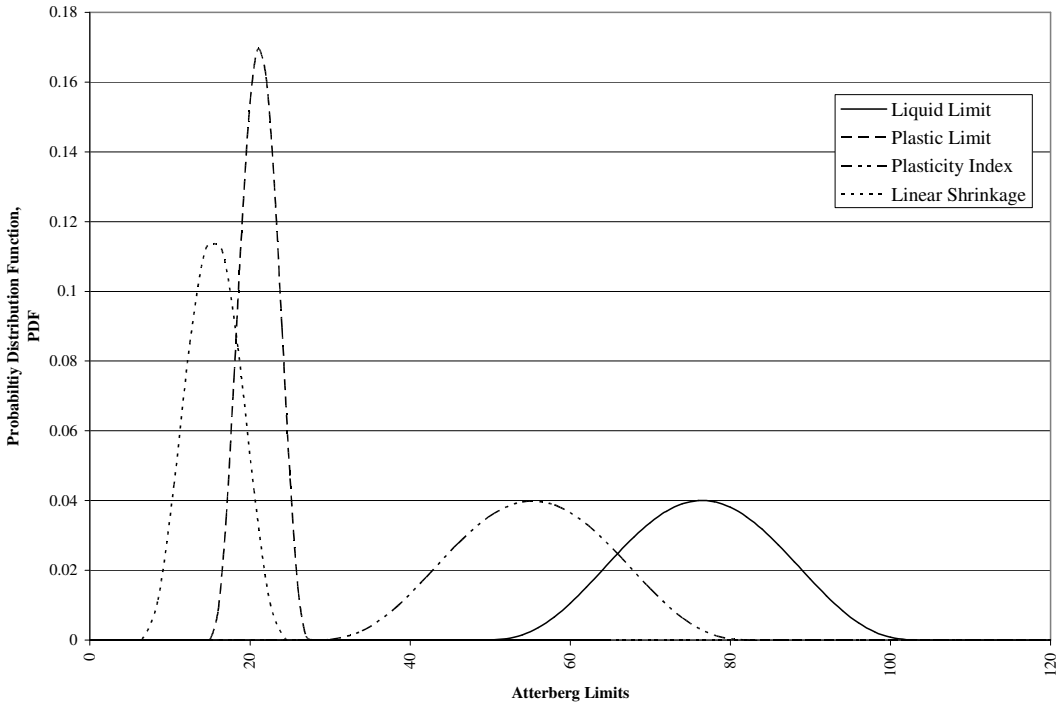

Figure 3.9 Probability Distribution Functions of Index Properties for Sample F

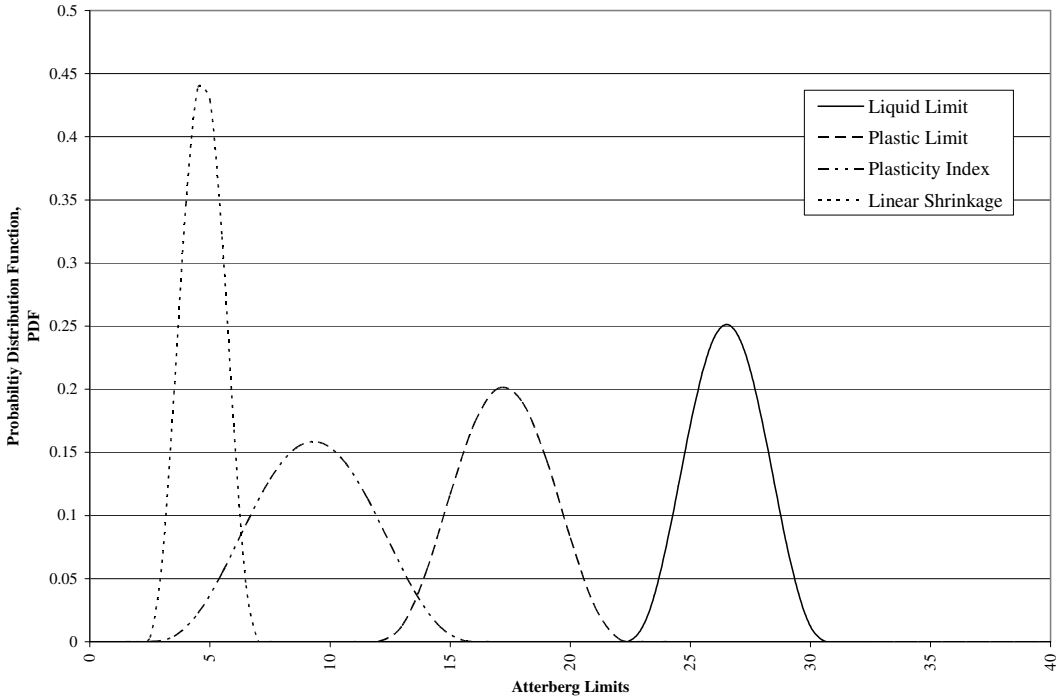

Figure 3.10 Probability Distribution Functions of Index Properties for Sample G

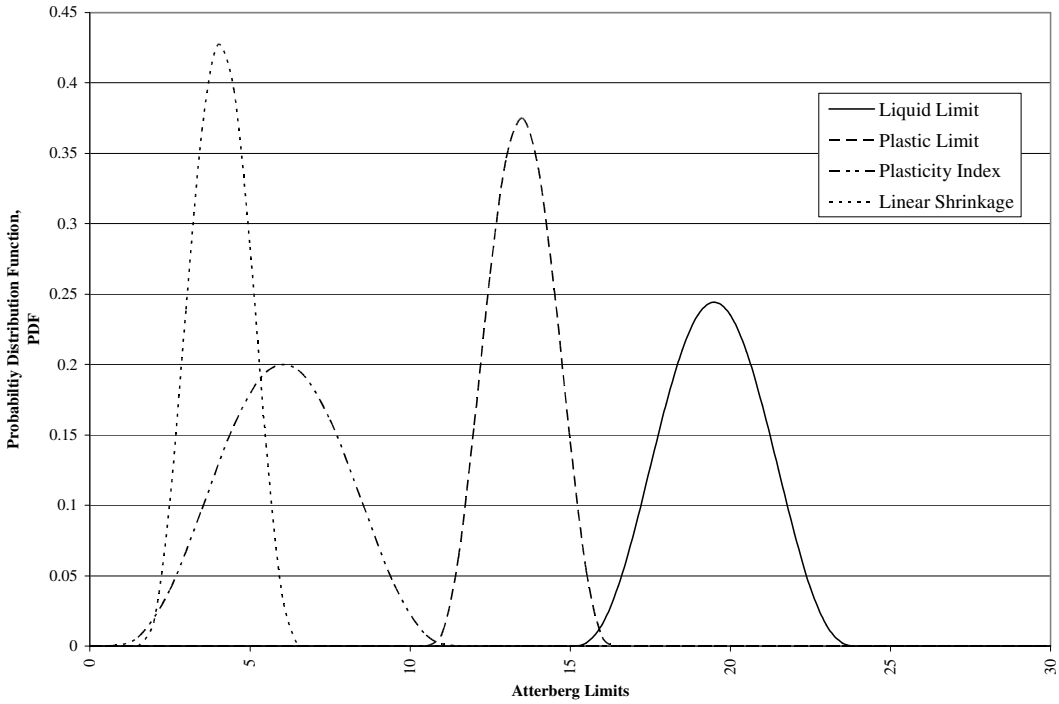

Figure 3.11 Probability Distribution Functions of Index Properties for Sample H

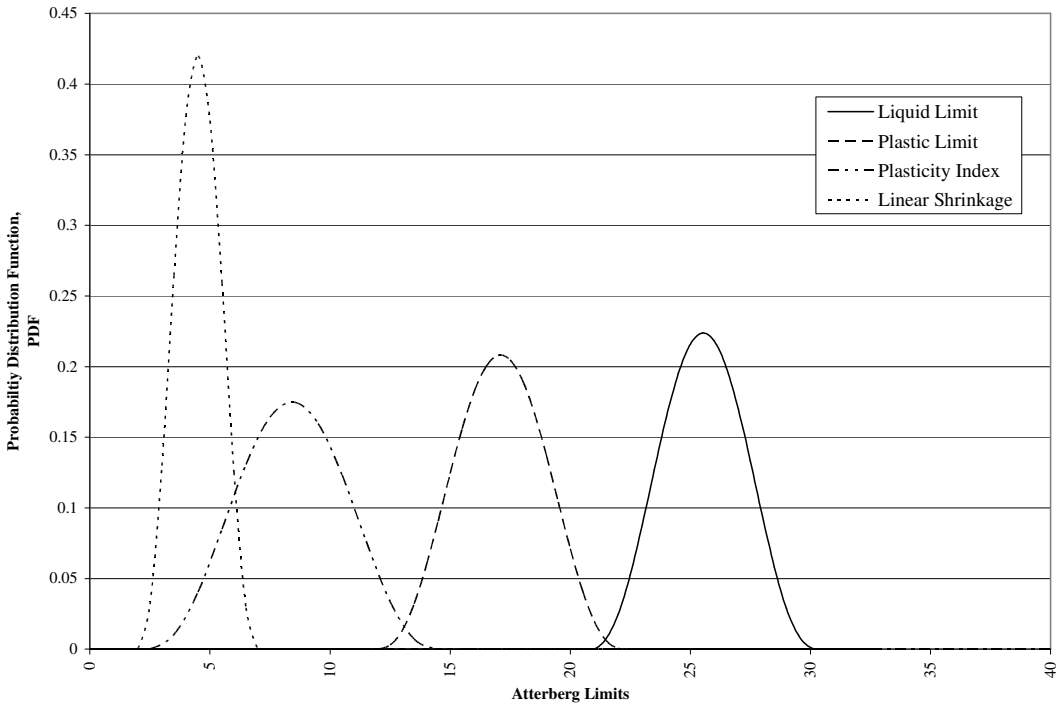

Figure 3.12 Probability Distribution Functions of Index Properties for Sample I

Table 3.3 Statistical Summary of Liquid Limit Results for NATA Samples

Sample ID	Number of Samples	Mean	Median	Standard Deviation	Coefficient of Variation (%)
A	141	43.5	43.8	1.9	4.4
B	141	52.9	52.5	4.0	7.5
C	134	17.9	18.0	0.9	5.3
D	32	17.1	17.2	1.1	6.7
E	220	56.5	56.0	5.6	10.0
F	25	76.5	77.0	9.2	12.0
G	166	26.5	26.5	1.5	5.5
H	53	19.5	19.5	1.5	7.7
I	25	25.5	26.0	1.6	6.4

While most of the samples produced comparable coefficients for standard deviation (and therefore variance), three of the samples – Sample B, Samples E and F - produced significantly higher values. These three samples also recorded highest liquid limit values.

The mean of a sample can be greatly influenced by outliers in the population, therefore, when examining the variation produced at different liquid limits, it is perhaps more correct to examine the median, which will give a better estimate of the central tendency of the data.

The coefficient of variation can also be misleading at low mean values, where the effects of changes in the standard deviation are amplified. For this reason, the variance or standard deviation of each sample will be used to examine any sort of dispersion between the measurements.

An interesting trend is apparent in Figure 3.13 which plots the standard deviation produced by each sample with respect to the median liquid limit of the sample. The soils with high liquid limits appear to produce higher variance, and it is suggested that in situations where limited data is available to establish otherwise, a minimum standard deviation in the order of 10% of the liquid limit should be assumed.

However, it is stressed that this value of standard deviation will only account for the variation produced through testing method, and will not take into account, the inherent soil variability.

Plots of the z-scores, included in Appendix B, give a further appreciation of how the proficiency of liquid limit testing differed between the laboratories. For well behaved bell shaped data, 68% of the data will fall within 1 standard deviation (i.e. have a z-score of less than or equal to 1). Ninety five percent will fall between 2 standard deviations, and 99% between three standard deviations from the mean. From the results (see Figures B.1 to B.3), it is reasonable to assume that the liquid limit data recorded for the range of soils tested are indeed well behaved statistically.

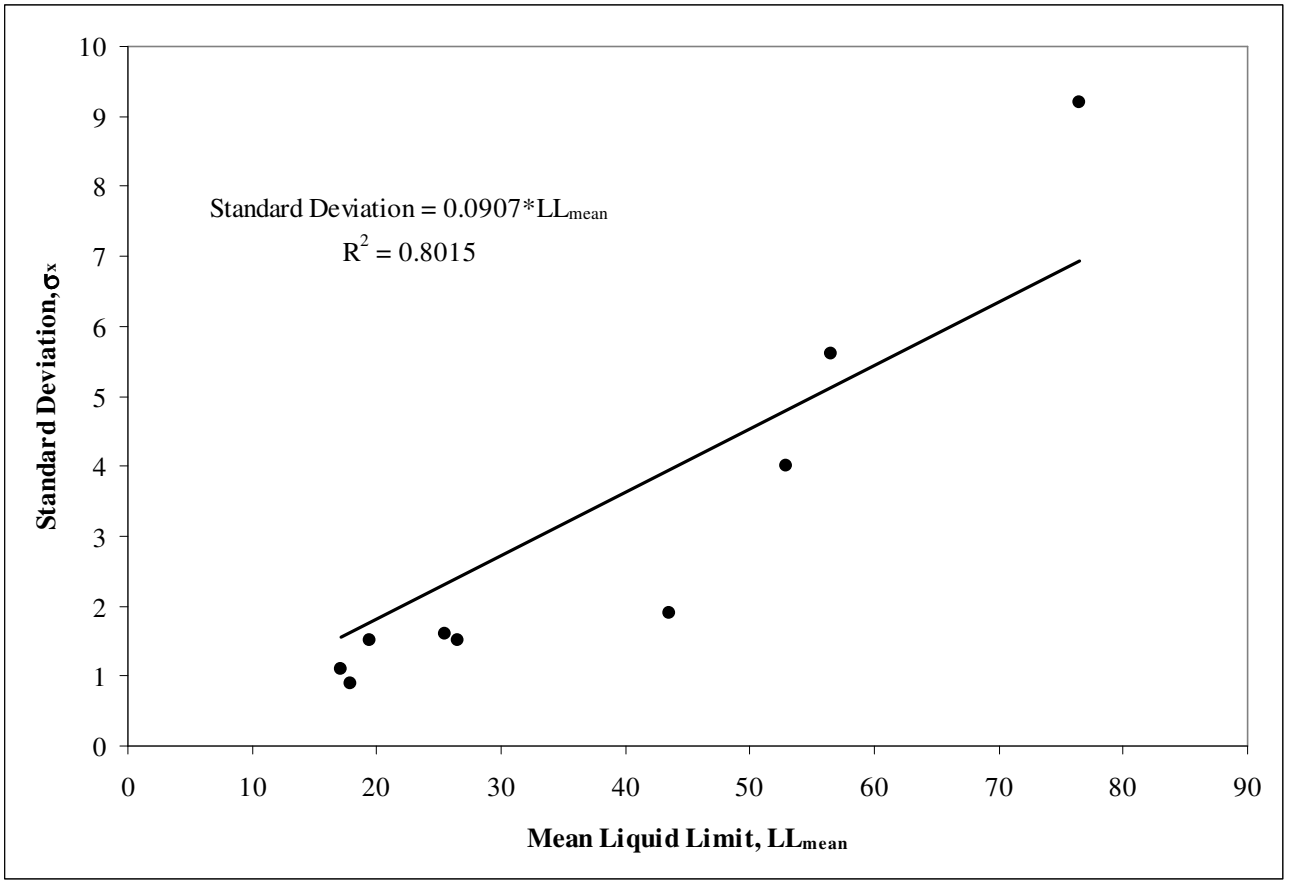

Figure 3.13 Plot showing Mean Liquid Limit versus Standard Deviation produced through Laboratory Testing

While the grooving tool (see Figure 3.1(a)) used in testing was identified by participants in the 1984 testing, the 1989 testing did not differentiate the data in such a method, and for this reason, no further analysis with respect to grooving tool can be carried out for Samples E, F, G, H or I.

As shown, the participants displayed a high degree of accuracy, with the majority of the above 80% of the samples tested recording liquid limits within 2 standard deviations of the total population mean for all samples except one. The percentage of data lying within 1, 2 and 3 standard deviations of the mean have been detailed according to grooving tool for Samples A to D in Tables 3.4 and 3.5.

It is evident from these values, that liquid limit measurements produced using Casagrande's grooving tool are slightly more consistent than those produced using the ASTM grooving tool. Holtz & Kovacs (1981) suggest that inconsistencies using this tool are due to the fact that it does not allow for any control of the height of the groove.

Plots of the duplicate (or split) sample results are also shown in Figures B.4 to B.8 (see Appendix B). These plots indicate that while the liquid limit method was highly repeatable on all soils, Casagrande's grooving tool showed a slight bias to overestimate the liquid limit of Samples A and C, while ASTM grooving tool showed a slight tendency to underestimate the liquid limit of these soils (see Figures B.4 and B.5). These samples were a black soil, and a loam respectively.

Histograms of the relative frequency data for each soil are also shown in Figures B.9 through to B.17 of Appendix B. The beta probability distribution functions developed for each of these liquid limit data sets are described by Equations 3.12 to 3.20.

Sample A: $f(x) = 5.072 \times 10^{-6}(x - 37.717)^3(49.288 - x)^3$ (Eqn. 3.12)

Sample B: $f(x) = 3.296 \times 10^{-8}(x - 41.007)^3(67.766 - x)^3$ (Eqn. 3.13)

Sample C: $f(x) = 7.519 \times 10^{-4}(x - 15.107)^3(20.733 - x)^3$ (Eqn. 3.14)

Sample D: $f(x) = 1.902 \times 10^{-4}(x - 13.650)^3(20.544 - x)^3$ (Eqn. 3.15)

Sample E: $f(x) = 2.845 \times 10^{-9}(x - 39.604)^3(73.318 - x)^3$ (Eqn. 3.16)

Sample F: $f(x) = 9.266 \times 10^{-11}(x - 48.986)^3(103.974 - x)^3$ (Eqn. 3.17)

Sample G: $f(x) = 3.567 \times 10^{-5}(x - 22.134)^3(30.891 - x)^3$ (Eqn. 3.18)

Sample H: $f(x) = 2.923 \times 10^{-5}(x - 14.986)^3(23.995 - x)^3$ (Eqn. 3.19)

Sample I: $f(x) = 1.585 \times 10^{-5}(x - 20.623)^3(30.457 - x)^3$ (Eqn. 3.20)

Due to the similarity in distribution shape, a general expression (Eqn. 3.21) for the variation in liquid limit due to laboratory testing was formulated. The range values of minimum (*a*) and maximum (*b*) were replaced with mean plus or minus 3 standard deviations respectively. The shape factors of alpha and beta were equal to 3.

Substituting $\alpha = \beta = 3$ into Equation 3.2, the general expression for the probability density function of liquid limit can be written as:

$$f(x) = \frac{(b-a)^{-7}}{0.0071}(X-a)^3(b-X)^3 \qquad \text{(Eqn. 3.21)}$$

where $a = \mu - 3\sigma$ and $b = \mu + 3\sigma$

To assess whether normality can safely be assumed for this parameter, chi-square (otherwise known as 'goodness of fit') tests were undertaken. These results are shown in Table 3.6. All D values fall below the χ_α^2 value of 9.49 (obtained from Table 3.2), and thus can be viewed as normal variates.

Table 3.4 Percentage of Laboratory Results with Standard Deviation Ranges for Casagrande's grooving tool of the Casagrandes Percussion Cup Device

Sample ID	Total No. of Labs	Percentage within 1 standard deviation (%)	Percentage within 2 standard deviation (%)	Percentage within 3 standard deviations (%)
Sample A	75	73	97	100
Sample B	73	62	97	100
Sample C	95	77	97	99
Sample D	25	84	92	100

Table 3.5 Percentage of Laboratory Results with Standard Deviation Ranges for ASTM grooving tool of the Casagrandes Percussion Cup Device

Sample ID	Total No. of Labs	Percentage within 1 standard deviation (%)	Percentage within 2 standard deviation (%)	Percentage within 3 standard deviations (%)
Sample A	52	69	96	98
Sample B	54	65	96	98
Sample C	19	63	84	95
Sample D	4	75	75	100

3.4.3 Plastic Limit

The plastic limit for each soil sample was determined using the same method by all participants. As compiled with respect to liquid limit, a summary of the basic statistical descriptors are shown in Table 3.7. From this table, according to median values, the samples, in order of ascending plastic limit are: Sample C, Sample H, Sample A, Sample D, Sample I, Sample G, Sample E, Sample F and finally, Sample G.

Unlike liquid limit, where the difference in minimum and maximum values was 59.8, plastic limits are all relatively close in magnitude, with a range of only 8.5. Thus trends observed should be treated cautiously until further investigation encompassing a larger range of values is undertaken.

As with liquid limit, the magnitude of standard deviation appears to increase with increasing plasticity limit. This trend is displayed in Figure 3.14. Again, as with liquid limit, in situations of limited data, a minimum standard deviation of 10% for the plastic limit can be employed to account for the variation due to testing.

With respect to plastic limit, most of the samples test produced low coefficients of variation (in the order of approximately 10% or below). The exception to this was Sample A, the black soil, which produced a coefficient of variation of 18.6%. Sample G produced the lowest coefficient of variation (5.2%).

Intuitively, due to its manual nature, plastic limit testing is understood to be a less precise testing method than those methods employed for liquid limit. This hypothesis is supported by the spread shown in the Youden plots of plastic limit (given by Figures C.4 through to C.8 in Appendix C).

Table 3.6 Results of Chi Square Test for Liquid Limit

Sample ID	D	$X_{0.05}^2$
Sample A	2.391	9.49
Sample B	4.414	9.49
Sample C	0.997	9.49
Sample D	8.174	9.49
Sample E	1.142	9.49
Sample F	1.021	9.49
Sample G	2.801	9.49
Sample H	4.674	9.49
Sample I	1.544	9.49

Table 3.7 Statistical Summary of Plastic Limit Results for NATA Samples

Sample ID	Number of Samples	Mean	Median	Standard Deviation	Coefficient of Variation (%)
A	141	14.9	14.3	2.8	18.6
B	141	22.2	21.8	2.3	10.3
C	130	13.3	13.2	1.3	9.8
D	43	16.1	16.1	1.4	8.7
E	220	18.9	19.0	2.2	10.7
F	25	21.2	21.0	2.2	10.2
G	166	15.8	17.0	0.9	5.2
H	54	13.5	13.5	1.0	7.3
I	25	17.1	16.5	1.8	10.3

With the exception of Sample G and I, very little bias is shown for this testing method. Sample G, a sand/loam, shows a systematic bias to underestimate plastic limit, while Sample I, another sand/loam, displays a systematic bias to overestimate the plastic limit.

Ordered z-score plots of the measured plastic limits are also given in Appendix C (Figures C.1 through to C.3). These graphs show that the proficiency of laboratories in testing this parameter is quite high with the majority of samples tested recording within 2 standard deviations of the mean. Outliers were observable for Samples A, B, D, E and G. However, in below three outliers were recorded in all cases.

Probability distribution functions have been developed for the plastic limits of each sample. These are described by Equations 3.22 to 3.30. Histograms of the raw data from which these distributions were formulated are shown in Appendix C. Furthermore, chi square test results on this raw data are shown in Table 3.8. From this table, it is apparent that with the exception of Sample G, the plastic limit of each of the soils can be treated as normal variates.

Sample A: $f(x) = 3.894 \times 10^{-7}(x - 6.578)^3(23.274 - x)^3$ (Eqn. 3.22)

Sample B: $f(x) = 1.531 \times 10^{-6}(x - 15.311)^3(29.041 - x)^3$ (Eqn. 3.23)

Sample C: $f(x) = 8.088 \times 10^{-5}(x - 9.385)^3(17.176 - x)^3$ (Eqn. 3.24)

Sample D: $f(x) = 4.604 \times 10^{-5}(x - 11.923)^3(20.366 - x)^3$ (Eqn. 3.25)

Sample E: $f(x) = 3.685 \times 10^{-6}(x - 12.879)^3(24.990 - x)^3$ (Eqn. 3.26)

Sample F: $f(x) = 2.302 \times 10^{-6}(x - 14.683)^3(27.637 - x)^3$ (Eqn. 3.27)

Sample G: $f(x) = 1.127 \times 10^{-3}(x - 13.087)^3(18.433 - x)^3$ (Eqn. 3.28)

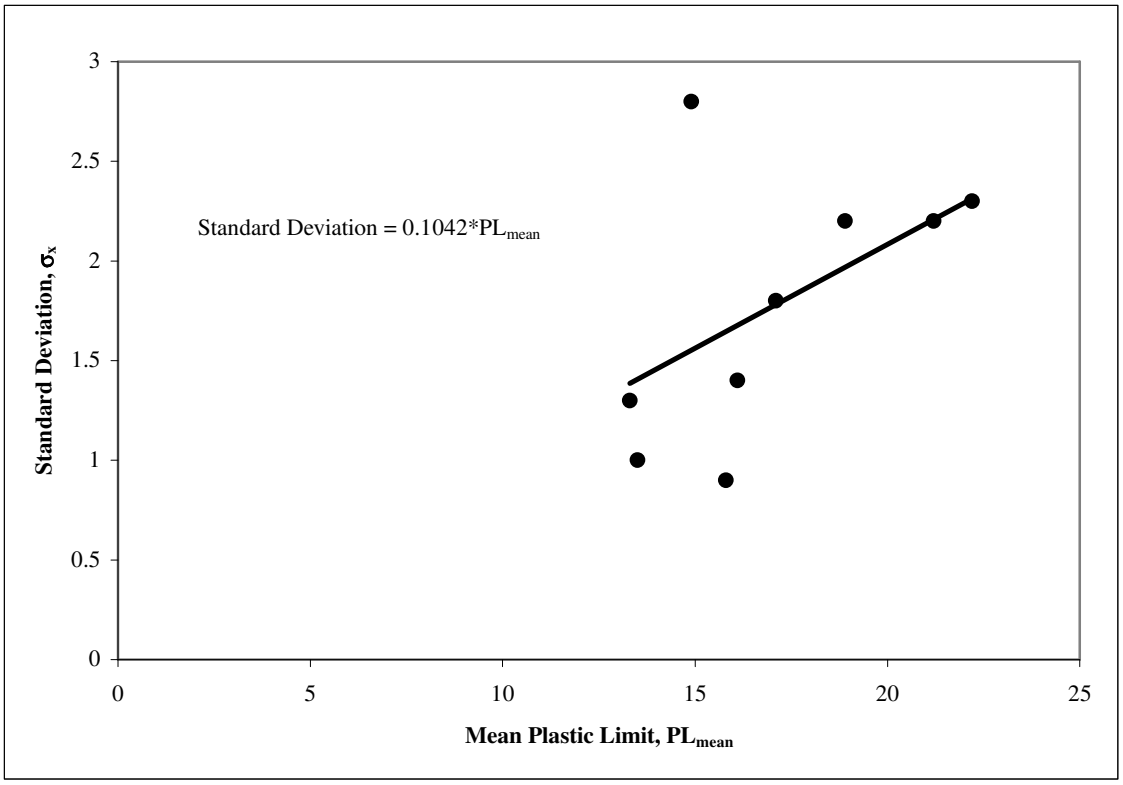

Figure 3.14 Plot showing Mean Plastic Limit versus Standard Deviation produced through Laboratory Testing

Table 3.8 Results of Chi Square Test for Plastic Limit

Sample ID	D	$X_{0.05}^2$
Sample A	4.97	9.49
Sample B	2.89	9.49
Sample C	2.72	9.49
Sample D	6.80	9.49
Sample E	3.19	9.49
Sample F	4.57	9.49
Sample G	13.30	9.49
Sample H	1.78	9.49
Sample I	3.68	9.49

Sample H: $f(x) = 5.873 \times 10^{-4}(x - 10.538)^3(16.407 - x)^3$ (Eqn. 3.29)

Sample I: $f(x) = 9.547 \times 10^{-6}(x - 11.814)^3(22.386 - x)^3$ (Eqn. 3.30)

The general expression (Eqn. 3.21) developed for the probability density function of liquid limit holds for plastic limit also. As stipulated previously, in the absence of testing to suggest otherwise, standard deviations for the plastic limit testing can be assumed as 10% of the actual plastic limit value.

3.4.4 Plasticity Index

Summary statistics for plasticity index are presented in Table 3.9. All of these values have been calculated from the raw data. The mean values are comparable to those derived by subtracting the mean of plastic limit from the mean liquid limit. However, it will not be exactly equivalent to this difference in mean values. The reason for this being that the value of plasticity index for each sample has been calculated as the mean of the values calculated for each split sample, instead of the difference between the mean liquid and plastic limits previously calculated. The order of samples in terms of plasticity follows that which was observed for liquid limit. In ascending order, these are: Sample D, C, H, I, G, A, B, E and finally, Sample F.

A plot of standard deviation versus median plasticity index is also presented in Figure 3.15. Not surprisingly, a linear trend is observable. However, the standard deviation produced can be assumed as approximately 15% of the mean plasticity index value, rather than 10% as observed in both liquid and plastic limits.

The remaining samples (Samples B, C, E, F, G, H, and I) produced values less than 9.49. Thus, due to this majority, it can be considered that plasticity index follows a normal distribution the majority of the time. The chi-square values in Table 3.10 affirm this.

Table 3.9 Statistical Summary of Plasticity Index Results for NATA Samples

Sample ID	Number of Samples	Mean	Median	Standard Deviation	Coefficient of Variation (%)
A	141	28.6	29.3	3.5	12.4
B	141	30.7	30.5	4.6	14.9
C	127	4.8	4.8	1.6	33.8
D	18	1.4	1.3	0.9	64.4
E	220	37.5	37.5	5.8	15.4
F	25	55.3	56.5	9.2	16.6
G	166	9.3	9.3	2.3	24.9
H	53	6.0	6.0	1.8	30.3
I	25	8.4	8.3	2.1	24.9

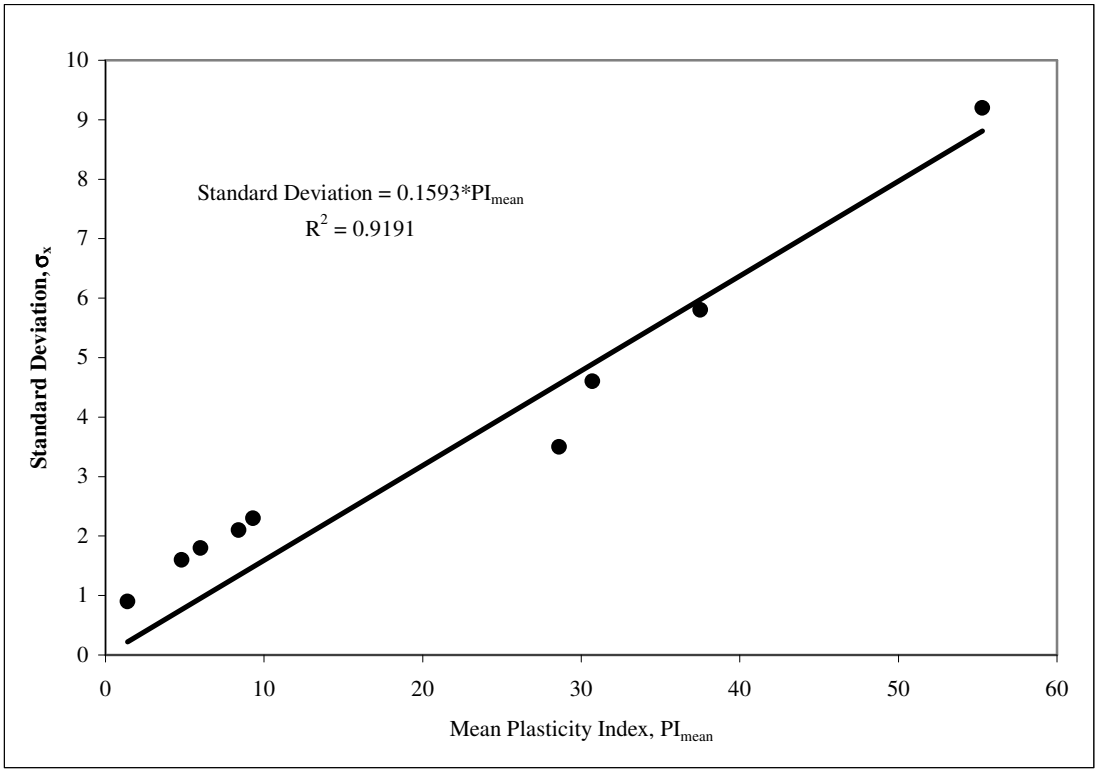

Figure 3.15 Plot showing Mean Plasticity Index versus Standard Deviation produced through Laboratory Testing

Youden plots were not generated with respect to plasticity index. The reason for this was that these plots are, as previously discussed, used for representing the repeatability and precision of testing methods. Plasticity index itself is not a directly measurable quantity. Rather, it has to be calculated from two other totally independent variables. Its 'repeatability' and precision will improve with increase with improvements in either of these variables.

The Z-score plots have been used to identify outliers in the plasticity index data. As can be seen in Figures D.1 to D.3 of Appendix D, Samples A, B, E and H all recorded values outside the three standard deviation limit. Only one measurement from the soil data was present for Samples B, E and H, while two outliers were present for Sample A.

Distribution functions developed for the plasticity indices of each sample are given by Equations 3.31 to 3.39 below. Their associated histograms are displayed in Figures D.4 to D.12 (Appendix D).

Sample A: $f(x) = 7.198 \times 10^{-8} (x - 17.985)^3 (39.235 - x)^3$ (Eqn. 3.31)

Sample B: $f(x) = 1.213 \times 10^{-8} (x - 17.002)^3 (44.407 - x)^3$ (Eqn. 3.32)

Sample C: $f(x) = 2.240 \times 10^{-5} (x)^{2.919} (9.659 - x)^{2.969}$ (Eqn. 3.33)

Sample D: $f(x) = 8.570 \times 10^{-2} (x)^{0.247} (4.187 - x)^{1.141}$ (Eqn. 3.34)

Sample E: $f(x) = 2.380 \times 10^{-9} (x - 20.235)^3 (54.820 - x)^3$ (Eqn. 3.35)

Sample F: $f(x) = 8.995 \times 10^{-11} (x - 27.709)^3 (82.931 - x)^3$ (Eqn. 3.36)

Sample G: $f(x) = 1.421 \times 10^{-6} (x - 2.362)^3 (16.240 - x)^3$ (Eqn. 3.37)

Table 3.10 Results of Chi Square Test for Plasticity Index

Sample ID	D	$X_{0.05}^2$
Sample A	11.49	9.49
Sample B	5.77	9.49
Sample C	7.87	9.49
Sample D	Not Applicable	9.49
Sample E	1.14	9.49
Sample F	1.02	9.49
Sample G	2.80	9.49
Sample H	4.67	9.49
Sample I	1.54	9.49

Sample H: $f(x) = 7.297 \times 10^{-6} (x - 0.545)^3(11.530 - x)^3$ (Eqn. 3.38)

Sample I: $f(x) = 2.827 \times 10^{-6} (x - 2.121)^3(14.699 - x)^3$ (Eqn. 3.39)

While the majority of soils followed the general expression derived previously (Equation 3.21), two out of the eight soils did not. These soils – Sample C and D – were both loams. Extreme caution is advised if such a general expression is to be applied to the plasticity index of these types of soils. While such an assumption would yield negligible difference if applied to Sample C, the results yielded for Sample D would vary significantly from those obtained using Equation 3.33.

3.4.5 Linear Shrinkage

The final index property examined within this chapter is linear shrinkage. Summary statistics for this parameter are outlined in Table 3.11. In order of ascending linear shrinkage, the soils are: Sample D, C, H, I, G, B, A, E and finally F. Predictably, the sand/loams recorded the least linear shrinkage, while the clay soils recorded higher levels of shrinkage.

Linear shrinkage data recorded during the 1984 program identified the mould lengths used alongside their corresponding result, however, 1989 data did not. Consequently, comparisons of the differences (if any) that exist between both mould lengths can only be made with respect to Samples A to D.

Duplicate sample results for the linear shrinkage data have been plotted and are presented in Figures E.4 to E.8 (Appendix E). These plots indicate that while the linear shrinkage method was highly repeatable on all soils, mould 1 (length = 100 mm – 200 mm) showed a slight bias to overestimate the linear shrinkage of the clay samples (Sample A and B), while mould 2 (length > 200 mm) displayed a tendency of underestimating the linear shrinkage limit of clay soils. No distinguishable bias was observed for the sand/loam soils of Sample C and D.

Table 3.11 Statistical Summary of Linear Shrinkage Results for NATA Samples

Sample ID	Number of Samples	Mean	Median	Standard Deviation	Coefficient of Variation (%)
A	137	13.8	14.0	1.8	12.9
B	137	13.4	13.3	1.9	14.2
C	134	2.9	2.8	0.9	30.2
D	100	0.6	0.6	0.4	61.6
E	218	14.7	14.8	1.8	12.3
F	25	15.5	15.5	3.2	20.5
G	164	4.7	4.8	0.8	17.4
H	54	3.6	3.5	0.9	23.9
I	25	4.5	4.3	0.9	19.5

Z-score plots are also included in Appendix E (Figures E.1 to E.3). As shown, the majority of laboratory results measured within 2 standard deviations of the mean linear shrinkage value. The 1984 data was further divided according to mould length, as shown in Tables 3.12 and 3.13.

These results were calculated using the mean and standard deviation established for the entire data set, so the more precise method could be determined. By examining these tables, it can be seen that consistently higher percentages of laboratories measured within two standard deviations using mould lengths greater than 200 mm. However, the difference in percentages was less than 2 percent, and therefore, can be assumed as minimal.

Probability distribution functions developed for the linear shrinkage of each sample are described in Equations 3.40 to 3.48. Their associated histograms are shown in Figures E.9 through to E.17 (Appendix E).

Table 3.12 Percentage of Laboratory Results with Standard Deviation Ranges for Mould 1 (Length = 100 - 200 mm)

Sample ID	Total No. of Labs	Percentage within 1 standard deviation (%)	Percentage within 2 standard deviation (%)	Percentage within 3 standard deviations (%)
Sample A	55	76.4	94.5	100
Sample B	56	67.9	94.6	96.4
Sample C	53	62.3	96.3	98.1
Sample D	36	61.1	94.4	100

Table 3.13 Percentage of Laboratory Results with Standard Deviation Ranges for Mould 2 (Length > 200 mm)

Sample ID	Total No. of Labs	Percentage within 1 standard deviation (%)	Percentage within 2 standard deviation (%)	Percentage within 3 standard deviations (%)
Sample A	78	69.2	96.2	100
Sample B	77	77.9	96.1	100
Sample C	Not Applicable			
Sample D	61	77.0	98.4	98.4

Sample A: $f(x) = 9.340 \times 10^{-6}(x - 8.452)^3(19.056 - x)^3$ (Eqn. 3.40)

Sample B: $f(x) = 5.682 \times 10^{-6}(x - 7.671)^3(19.056 - x)^3$ (Eqn. 3.41)

Sample C: $f(x) = 1.374 \times 10^{-3}(x - 0.266)^3(5.464 - x)^3$ (Eqn. 3.42)

Sample D: $f(x) = 7.392 \times 10^{-1}(x)^{0.36}(1.845 - x)^{1.512}$ (Eqn. 3.43)

Sample E: $f(x) = 8.011 \times 10^{-6}(x - 9.261)^3(20.101 - x)^3$ (Eqn. 3.44)

Sample F: $f(x) = 1.583 \times 10^{-7}(x - 5.967)^3(24.953 - x)^3$ (Eqn. 3.45)

Sample G: $f(x) = 2.053 \times 10^{-3}(x - 2.249)^3(7.157 - x)^3$ (Eqn. 3.46)

Sample H: $f(x) = 1.492 \times 10^{-3}(x - 1.010)^3(6.147 - x)^3$ (Eqn. 3.47)

Sample I: $f(x) = 1.297 \times 10^{-3}(x - 1.870)^3(7.110 - x)^3$ (Eqn. 3.48)

With the exception of Sample D, all linear shrinkage distribution functions can be generalised using Equation 3.21.

The 'goodness of fit' result for each of the linear shrinkage data sets is shown in Table 3.14. With the exception of Samples D and G, all linear shrinkage followed a normal type distribution. As was the case with the plasticity index of Sample D, the presence of structural zeroes rendered the chi-square test not applicable to this data set.

3.5 Correlations involving Index Properties

In the statistical sense, correlation refers to the departure of two random variables, $\hat{X}$ and $\hat{Y}$, from independence. One of the coefficients used to indicate correlation is the Pearson product-moment correlation (PPMC) coefficient, denoted by $P_{x,y}$. This factor

is calculated by dividing the covariance of the random variables, $\hat{X}$ and $\hat{Y}$, by the product of their standard deviations, σ_x and σ_y. It may also be expressed in terms of expected values (μ_x, μ_Y) (given in Equation 3.49).

$$\rho_{X,Y} = \frac{\text{cov}(\hat{X},\hat{Y})}{\sigma_X \sigma_Y} = \frac{E((\hat{X}-\mu_X)(\hat{Y}-\mu_Y))}{\sigma_X \sigma_Y} \qquad \text{(Eqn. 3.49)}$$

Table 3.15 shows a correlation matrix developed to describe the strength of relationships between each of the index properties. It can be seen clearly, that the plasticity index is linked quite strongly to both liquid limit and linear shrinkage. It is not surprising that plasticity index correlated highly with liquid limit, as it is derived from it.

Commonly, the empirical relation plasticity index (PI) = 2.13*linear shrinkage (LS) is assumed to describe the interrelationship between these variables. To assess the accuracy of this assumption, correlations specific to each soil were established. Only results within a 1 standard deviation range of the mean were considered with respect to the correlations. Table 3.16 outlines the ratio of plasticity index to linear shrinkage for each soil.

No overall trend was apparent for estimating the plasticity index / linear shrinkage ratio. However, it was observed that for medium to high liquid limits (greater than 40%), this ratio was approximately equivalent to 0.05 times the liquid limit.

3.6 Conclusions

The above chapter outlined a statistical analysis of the variation induced through laboratory testing of Atterberg Limits. In addition to developing beta distributions specific to each of the soils tested, a general expression that may be used to describe the distribution function of laboratory induced variation for any soil was also developed as (where the minimum and maximum range limits, *a* and *b*, have been assumed as $\mu - 3\sigma$ and $\mu + 3\sigma$ respectively):

Table 3.14 Results of Chi Square Test for Linear Shrinkage

Sample ID	D	$X_{0.05}^2$
Sample A	1.23	9.49
Sample B	3.60	9.49
Sample C	5.34	9.49
Sample D	Not Applicable	
Sample E	5.02	9.49
Sample F	5.05	9.49
Sample G	8.32	9.49
Sample H	4.60	9.49
Sample I	4.01	9.49

Table 3.15 Correlation Matrix between Index Properties

	LL	PL	PI	LS
LL	1.000	0.867	0.996	0.967
PL	0.867	1.000	0.824	0.853
PI	0.996	0.824	1.000	0.961
LS	0.967	0.853	0.961	1.000

Table 3.16 Coefficients relating Plasticity Index to Linear Shrinkage for All Samples

Sample ID	Plasticity Index / Linear Shrinkage Ratio
Sample A	2.11
Sample B	2.33
Sample C	1.78
Sample D	2.72
Sample E	2.56
Sample F	3.70
Sample G	2.03
Sample H	2.86
Sample I	1.95

$$f(x) = \frac{(6\sigma)^{-7}}{0.0071}(X-(\mu-3\sigma))^3((\mu+3\sigma)-X)^3$$

Furthermore, it has outlined values of standard deviation and coefficients of variation for a variety of soils. Such values are critical to design calculations carried out in preliminary studies. Coefficients of variation for liquid limits fall within 10% for most cases, while those of plastic limits reach as much as 19%, confirming that the current method of determining plastic limit is more prone to variation than the method of establishing liquid limit. This inference is not surprising due to the highly manual nature of plastic limit testing.

However, caution should be taken when applying this expression, and indeed avoidance should be exercised in the case where mean liquid limit and plastic limit for a sample are similar.

Typical standard deviations for index properties can be assumed in the order of 10% of the median value for both liquid and plastic limits, and 15% of the median value for plasticity index.

With a few minor exceptions, index properties were determined to behave like normal variates. This was also found in analysis by Lumb (1966) and Schultze (1972).

Further works are suggested to undertake similar statistical analyses on other remaining geotechnical testing methods. Producing probability distribution functions to describe the variation and the probability of certain levels occurring would provide an invaluable tool for risk-benefit analysis.

CHAPTER 4

CHARACTERISATION OF QUEENSLAND NATURAL CLAYS

4.1 Introduction

The substantial population growth that has been experienced by urban centres along the East Coast of Australia in recent years has necessitated a further reclamation of previously undesirable sites for infrastructure development. Much of this coastal region contains very soft clays (estuarine or marine) that have poor geotechnical properties such as low bearing capacity and high compressibility. These clays line the coast of Queensland, and can extend to depths of 15-20 m in some cases.

Soils are produced through the weathering process and thus their composition and behaviour may be affected by innumerable different environmental factors. Considerable scatter, therefore, is understandable, and to a large degree expected, within the measurement of any specific parameter. Frequently, prior to civil engineering works being commenced, a preliminary design study will be undertaken upon the site. Due to the financial constraints of many projects, the scope of the site investigation for the evaluation of parameters to be used in this design study is limited. Should the project be adopted following this preliminary study, unrealistic quantification of these design values may lead to significant economic penalties, and in some cases, serviceability issues later in the project. Thus, a prior knowledge of the region and soil characteristics is an invaluable tool for any geotechnical engineer.

Test data reported within this Chapter has been obtained from four sources. The first three of these sources were results collected from laboratory testing on natural clay samples from three separate construction projects. These construction projects were

located in Cairns, Brisbane and the Sunshine Coast respectively. The fourth source of data for this analysis was obtained from previously published data (Davis, 1999) and was gathered from North Queensland (NQ) sites between Cairns and Townsville.

Individual analysis of parameters for each site, as well as an overall evaluation of the trends apparent for Queensland soils with respect to the parameter under consideration, is included within this chapter. An examination and assessment of various geotechnical correlations in light of the data has also been undertaken to identify which relationships most accurately characterise the geotechnical properties of Queensland clays. Additionally, where permissible, relationships specific to these clays and their prediction have been developed.

Parameters in geotechnical analysis usually refer to an average of the particular continuum property over a specified area. Such an assumption introduces inherent uncertainty into any calculations due to the heterogeneity of soil properties. A model of probability distribution to describe the variability in a system or process is therefore desirable.

Beta distribution functions have been developed for Atterberg limits and natural water content. Functions were calculated individually for all samples from Site B, Site C and Davis (1999) data. Following this, the compressibility parameters are discussed. Due to the large number of samples being analysed within this chapter, data relating to each parameter are collated and shown in Appendices G to J.

4.2 Sampling Method

Natural clays were sampled from their respective sites using the methods and preparation outlined in AS1289.1.3.1 (SAI Global, 1999). This standard describes the preparation and sampling methods that should be adopted to obtain undisturbed samples in the field.

Samples from two of the sites – Sites A and B – were tested by the author at James Cook University. Site C samples and samples referred to by Davis (1999) data were

tested by the Material and Geotechnical Services Branch of the Department of Main Roads. Additional tests completed on samples taken from Site B by two independent consultants were also made available for inclusion in this analysis.

The majority of samples from each of the sites were obtained in the vertical direction using U50 (dia. = 50 mm) tubes. However, a small number of horizontal specimens were also obtained from Sites A and C. In order to avoid sample disturbance, these specimens were not cut from the vertically extruded sample, but actually sampled by pushing the U50 tube into a vertical face in the soil.

4.3 Testing Methods

In studies of this nature, it is imperative that data being analysed come from samples that have been tested under similar conditions. Utmost care was taken to ensure that results considered adhered to this standard.

Classification procedures used to test samples from Sites A and B were conducted in accordance with the standard procedures specified in the Australian Standards and Lambe (1951). Each of the relevant standards is identified within the sections below. All other data samples were tested for classification data according to the Queensland Materials Testing Manuals published by the Department of Main Roads. These too, have been identified within the appropriate sections below.

Oedometer testing undertaken on Site A and external testing on Site B samples were conducted in accordance to the method outlined in AS1289.6.6.1. (SAI Global, 1998). Site C consolidation tests were conducted in accordance with the Queensland Materials Testing Manual Q183 (Queensland Department of Main Roads, 1978).

Oedometer tests conducted by James Cook University for Site B (Samples JCU2_L2, JCU3_L2, JCU4_L3, JCU5_L4, JCU6_L4 and JCU7_L4) followed the standard approach of AS1289.6.6.1 (SAI Global, 1998) for loading stages up to approximately 400 kPa. Subsequently, each specimen was unloaded to a pressure of 42 kPa and left to stand for 36 hours. By leaving the specimen to stand for this period of time, it

allowed the specimen to assume an overconsolidation ratio of approximately 9.5 (= 400 / 42). Following this, the specimen was reloaded to reach OCRs of approximately 7.5, 5, 3.5, 2.5 and 2, also leaving 36 hours between each load increment, to allow the specimen to adopt the 'new' OCR before the next test could begin. The relationship between selected consolidation parameters and overconsolidation ratio has been investigated within this chapter.

4.4 Site Soil Profiles

The total number of samples analysed for each site is shown in Table 4.1. The first site was located approximately 20 km north of Cairns. Specimens from this site were taken from the soft clays immediately adjacent to a small tributary of an estuary creek which lined the site, and were obtained just below the ground surface level. A backhoe was used to cut vertical and horizontal faces into the clay, and U50 tubes were pressed into it in the vertical and horizontal directions. All samples were taken within 30cm of each other to try and ensure similarity between the samples. For this reason, a profile of the site could not be established, and site specific relationships were not developed. Instead, results were used to evaluate the anisotropic relationship between the consolidation parameters at the site.

Site B was situated 13 km northeast of Brisbane. The six specimens sampled from this site were obtained from the same borehole at different depths. The U50 tubes used to collect the samples were 400mm in length, and thus, sample depths were actually recorded as a range. The values of sample depths recorded in Table 4.2 are the middle points of each tubes range. Testing upon this site was used primarily to quantify the relationship between overconsolidation ratio and the compressibility and consolidation parameters of the clay.

Additional consolidation and compressibility results were also obtained for this site from two independent consultants. Using these results, the bore logs and results from the laboratory testing at James Cook University, a soil profile was determined for Site B. This profile is assumed to consist of five layers and is illustrated in Figure 4.2. Due to the high level of organic and shell matter within the U50 tube of Sample JCU1_L1,

no representative oedometer samples were able to be cut without a large degree of disturbance being initiated. Consequently, no oedometer testing was undertaken on Sample JCU1_L1. This sample was, however, tested for water content, density and specific gravity. The density and specific gravity values measured were higher than values obtained for the clay below it. Water content values, on the other hand, were similar.

Qualitative assessment of the soil stiffness by touch also reinforced the belief that the material in Sample JCU1_L1 should not be considered the same material as the underlying clays, and that due to this apparent stiffness, should be regarded as weathered crust material.

Lastly, Site C was located on the Sunshine Coast, approximately 135km north of Brisbane. The test results from this site were supplied by Main Roads (Queensland Department of Main Roads, 1991) for analysis. They have been used to help examine the compressibility and consolidation characteristics of Queensland clays. The soil profile determined for this site also comprised of five layers. As with Site B, the uppermost layer of this soil was found to be weathered crust. Below this layer, three further clay layers were present, and beneath them, a sand layer. A sketch of this profile is shown in Figure 4.2

The soil profiles of sites tested by Davis (1999) were not available. However, a typical soil profile for the North Queensland Region was published alongside this data. This profile is shown in Figure 4.3

4.5 Probability Distribution Functions

Probability distribution functions (or probability models), and Harr's (1977) empirical method by which they can be produced has been outlined previously in Chapter 3. These functions may be used in engineering calculations to not only work out the most probable value of a parameter, but also in reliability analyses. Distribution functions are derived for a number of the parameters analysed in this dissertation, and displayed accordingly.

Table 4.1 Total Number of Clay Samples from each Natural Clay Site*

Site ID	Total Number of Samples
Site A	4
Site B	26
Site C	212

Table 4.2 Sample Depths for Specimens taken at Site B

Sample ID	Depth Below Ground Level (m)
JCU1_L1	1.2
JCU2_L2	2.7
JCU3_L2	5.7
JCU4_L3	13.2
JCU5_L4	17.7
JCU6_L4	20.7
JCU7_L4	23.7

* Not all samples were tested for consistency and consolidation characteristics. Therefore, when analysing the results, only samples in which all parameters under consideration were available were used. All others were ignored.

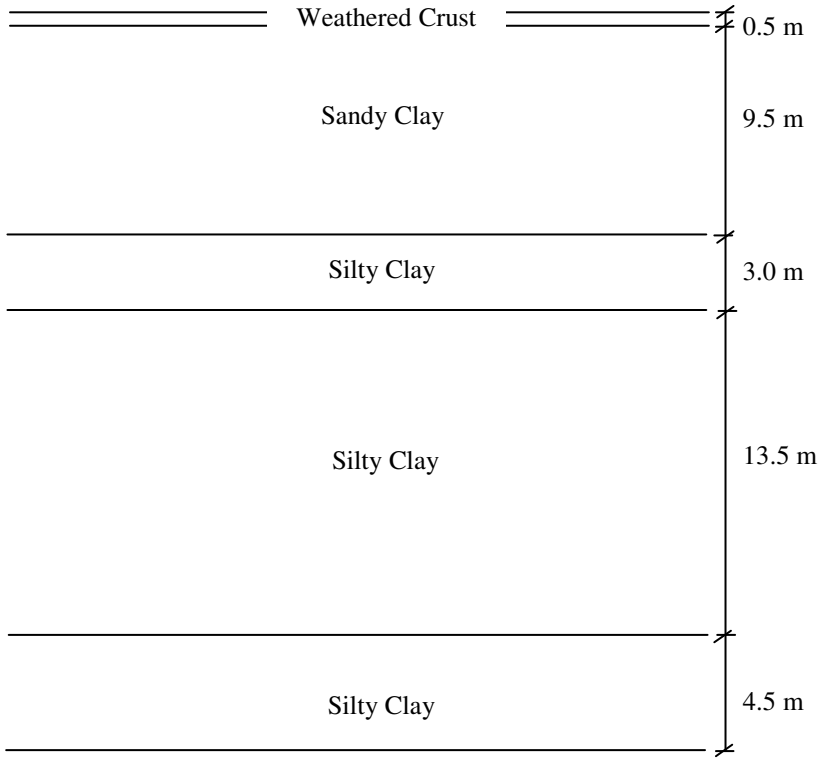

Figure 4.1 Typical Soil Profile of Site B (Brisbane)

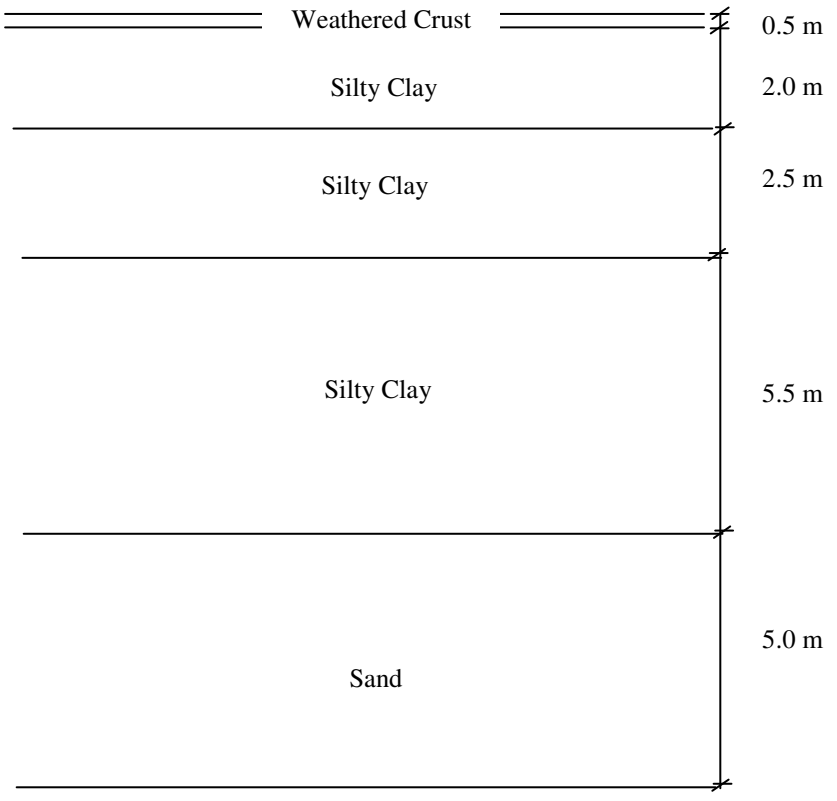

Figure 4.2 Typical Soil Profile of Site C (Sunshine Coast)

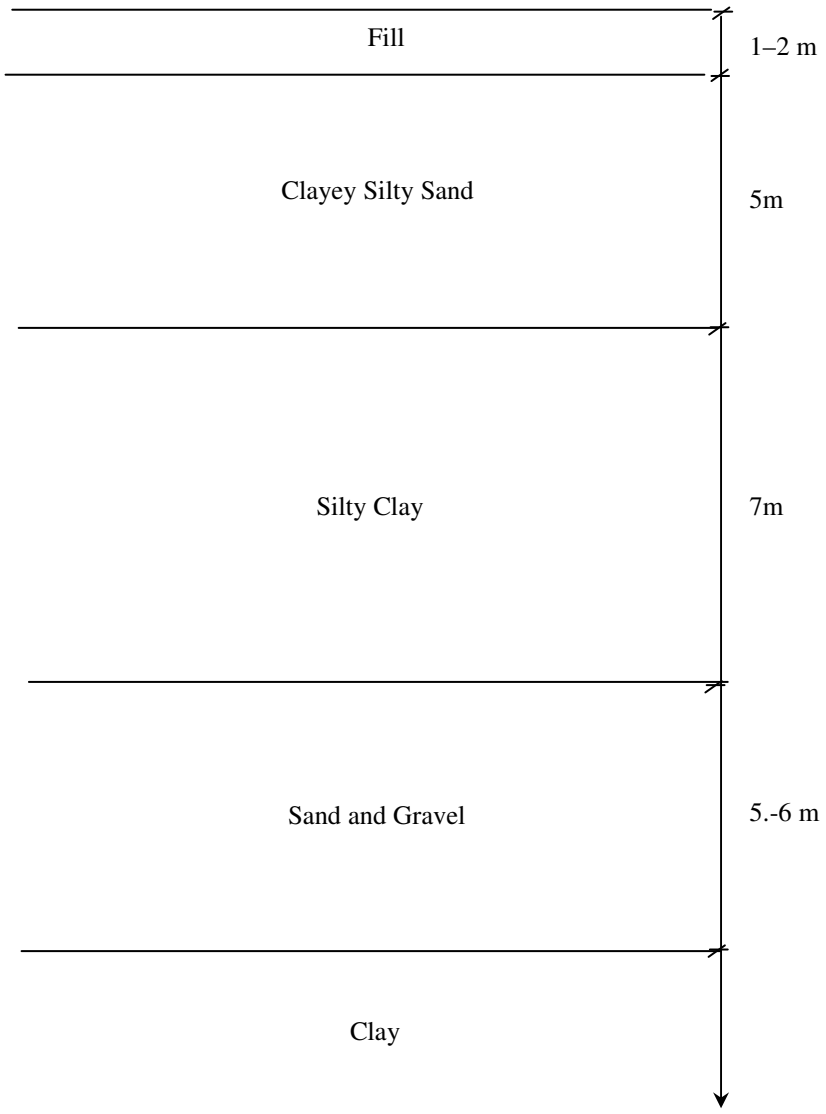

Figure 4.3 Typical North Queensland Soil Profile for Additional Test Data (Davis, 1999)

The three sigma rule was adopted for the minimum and maximum values of each distribution. This rule – as discussed previously in Section 3.3.4 – assumes minimum and maximum values for the distribution lie 3 standard deviations below and above the mean respectively.

Uncertainty exists as to the accuracy of these functions with respect to Site B and also the Davis (1999) data. Measured values from Site B were limited, while the Davis (1999) data was collected from various sites around North Queensland. The proximity of these sites is unknown, and thus, inherent spatial variability has been introduced into the dataset.

4.6 Consistency Limits

First described by A. Atterberg (1911) in the early 1900's, methods to test the consistency limits were standardised by Casagrande (1932, 1958). The techniques adopted to quantify liquid limit (LL), plastic limit (PL) and plasticity index (PI) for Sites A and B are fully detailed in the Australian Standards AS1289.3.1.1 (SAI Global, 1995), AS1289.3.2.1 (SAI Global, 1995) and AS1289.3.3.1 (SAI Global, 1995) respectively. Liquid limit, plastic limit and plasticity index for Site C were completed by the Department of Main Roads according to the Queensland Materials Testing Manuals (1987, 1988).

An additional index used in describing the state of a clay is the liquidity index. This parameter describes the relative consistency of the sample.

$$LI = \frac{w - PL}{PI} \qquad \text{(Eqn. 4.1)}$$

The water content selected for use in Equation 4.1 depends on which form of liquidity index one wants to investigate. For instance, the deposition liquidity index, or liquidity index at placement, will utilise the water content of the slurry which 'deposits' the soil into its current location, whereas, the in-situ liquidity index will use the natural water content in its present condition. The liquidity index referred to

within this chapter is in-situ liquidity index. The influence of deposition liquidity index is reviewed later within this dissertaion.

4.6.1 Site A

The relative variation between Atterberg Limits measured for the samples taken from this site is minimal. Average values for the site were 74.4 for liquid limit and 23.6 for plasticity limit. Thus, the average plasticity index for Site A samples was 50.1. Liquidity index for the soil averaged 0.73. Budhu (2000) qualitatively describes soils according to this parameter, and LI = 0.73 is described as plastic soil of intermediate strength. Similarity between parameters measured for this site was expected due to the close proximity within which the samples were taken.

4.6.2 Site B

Liquid limits for Site B ranged between 30.0 and 74.4, with a mean value of 50.7, while plastic limits varied between the relatively close range of 19.3 and 30.3, with a mean value of 25.2. Coefficients of variation for these two parameters were 14.0% and 38.0% respectively. Mean value for plasticity index of the site was, therefore, was equivalent to 25.5 (the difference between the mean values of liquid and plastic limits).

Equations 4.2, 4.3 and 4.4 specify the probability distribution functions derived for consistency limits at this site. They are also shown diagrammatically in Figures 4.4 through to 4.6. Coefficients of skewness and kurtosis are detailed on the figures.

$$\textbf{\textit{Liquid Limit:}}\ f(x) = 7.030 \times 10^{-12}\, x^{2.29}\,(107.85 - x)^{2.704} \qquad \text{(Eqn. 4.2)}$$

$$\textbf{\textit{Plastic Limit:}}\ f(x) = 6.463 \times 10^{-8}\,(x - 14.501)^{3}\,(36.062 - x)^{3} \qquad \text{(Eqn. 4.3)}$$

$$\textbf{\textit{Plasticity Index:}}\ f(x) = 1.614 \times 10^{-4} \times^{0.002} (80.428 - x)^{1.165} \qquad \text{(Eqn. 4.4)}$$

As evidenced by these figures, the liquid and plastic limit beta distribution functions produced slightly skewed bell shaped curves, indicating maximum probability around

the established mean for the Site B data. The plasticity index, however, produced a triangular distribution curve, which indicates the maximum probability occurs at the minimum value for this distribution function. The mean of this distribution will be located approximately $1/3^{rd}$ of the distance between the minimum and maximum range values respectively.

The mean liquidity index for this site was 0.65. A standard deviation of 0.33 and coefficient of variation of 50.0% were also calculated for the sample population. As explained in Section 4.6.2, a liquidity index of this amount indicates a plastic soil of intermediate strength (Budhu, 2000).

4.6.3 Site C

Like the data analysed for Site B, beta distribution curves were fitted to the data obtained for the Atterberg Limits measured for Site C. Measurements from the 100 samples tested for this source indicated a mean liquid limit of 59.4, and the standard deviation was 19.3. Negative measures of Atterberg limits are not possible, and therefore all minimum range limits for their probability distribution function calculations were set to zero. The maximum boundary for the liquid limit range of Site C samples was set at 117.2. This distance is equivalent to three standard deviations from the mean and ensures a confidence interval of 99.7%.

Using these values and the equations outlined in Chapter 2, the beta distribution function of liquid limit for Site C was determined as Equation 4.5. This probability distribution function is shown graphically in Figure 4.7.

$$\textbf{\textit{Liquid Limit:}}\ f(x) = 5.044 \times 10^{-13} (x - 1.5)^3 (117.2 - x)^3 \qquad \text{(Eqn. 4.5)}$$

With respect to the plastic limit of these samples, the mean and standard deviation of the sample population are 26.6 and 7.8 respectively. The range limits of *a* and *b* are defined as 3.2 and 50.1. Using the method outlined previously, the beta distribution function calculated for the plastic limits is given by Equation 4.6,

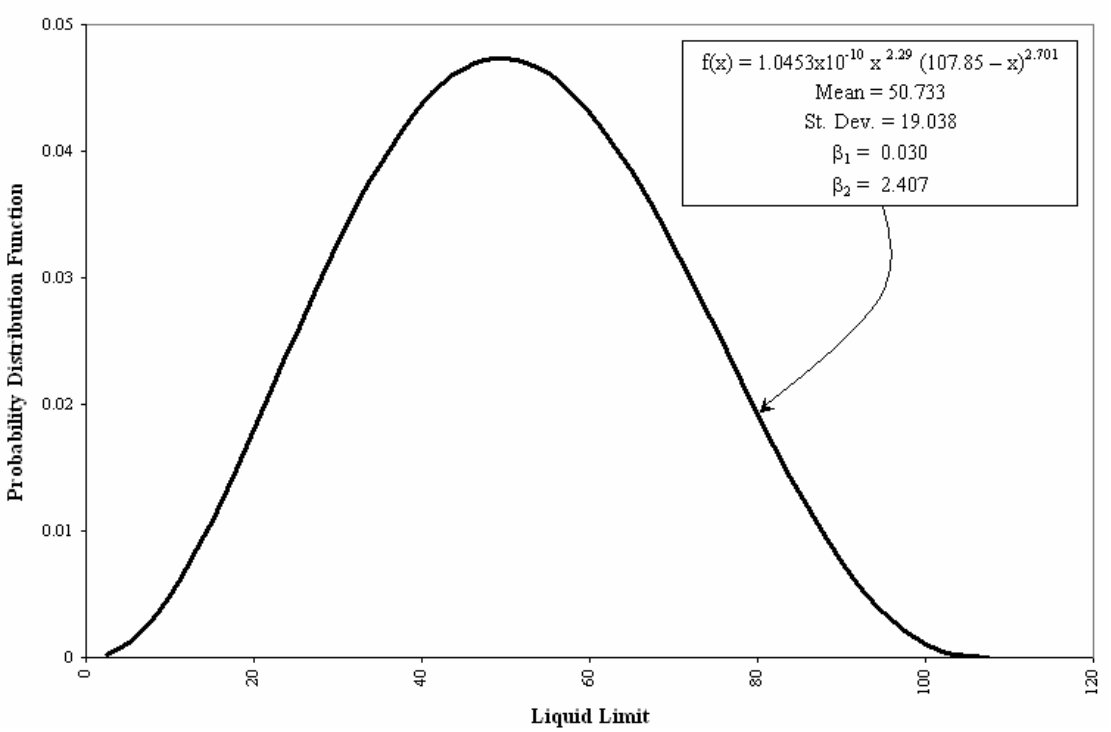

Figure 4.4 Probability Distribution Function of Site B Liquid Limits

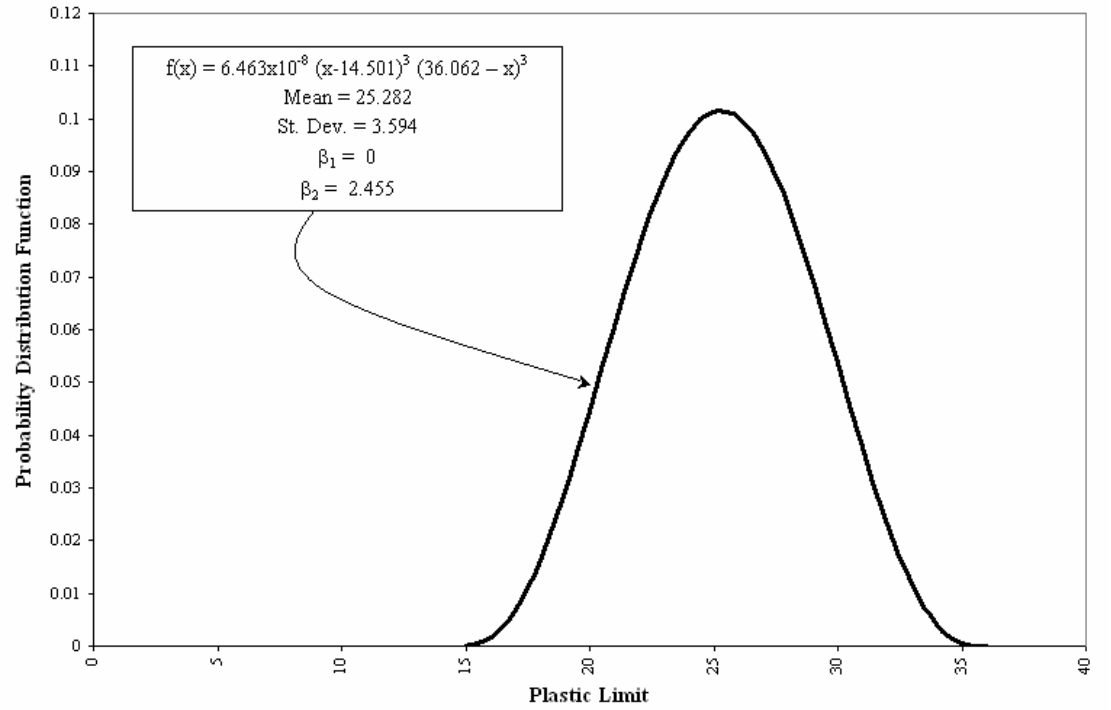

Figure 4.5 Probability Distribution Function of Site B Plastic Limits

Plastic Limit: $f(x) = 2.847 \times 10^{-10} (x - 3.6)^3 (50.0 - x)^3$ (Eqn. 4.6)

The mean and standard deviation of plasticity indices recorded for the Site C results were 32.8 and 14.7 respectively. The maximum range limit for the distribution is assigned three standard deviations from the mean. Thus, the minimum range limit for the distribution was set to zero. The beta distribution for this function is:

Plasticity Index: $f(x) = 2.905 \times 10^{-8} x^{1.441} (76.7 - x)^{2.271}$ (Eqn. 4.7)

Figures 4.8 and 4.9 further illustrate Equations 4.6 and 4.7 graphically for their corresponding indices within the Site C results. As shown, these distributions were all bell shaped. Both liquid and plastic limit distributions were perfectly symmetrical around their mean values, whereas, the plasticity index distribution was slightly skewed positively to the right ($\beta_1 = 0.091$).

Mean liquidity index for this site was 1.55. Such a high value indicates that the soil is of low strength, and will deform significantly. It also indicates that the soil is highly sensitive, and that a certain degree of disturbance will be unavoidable for soil samples taken from this site.

4.6.4 Davis (1999) Data

The mean liquid limit calculated for this data set was 60.5. The standard deviation and coefficient of variation of these results were approximately 13.0 and 0.21 respectively.

Plastic limits, however, measured a mean value of 30.91, and a standard deviation of 6.086. Coefficient of variation for the samples was again of the same order, and was calculated to be 0.20.

A little more scatter was observable between the plasticity index values for these results, with coefficient of variation for the population totalling 0.28. The mean and standard deviation values were 29.6 and 8.5 respectively.

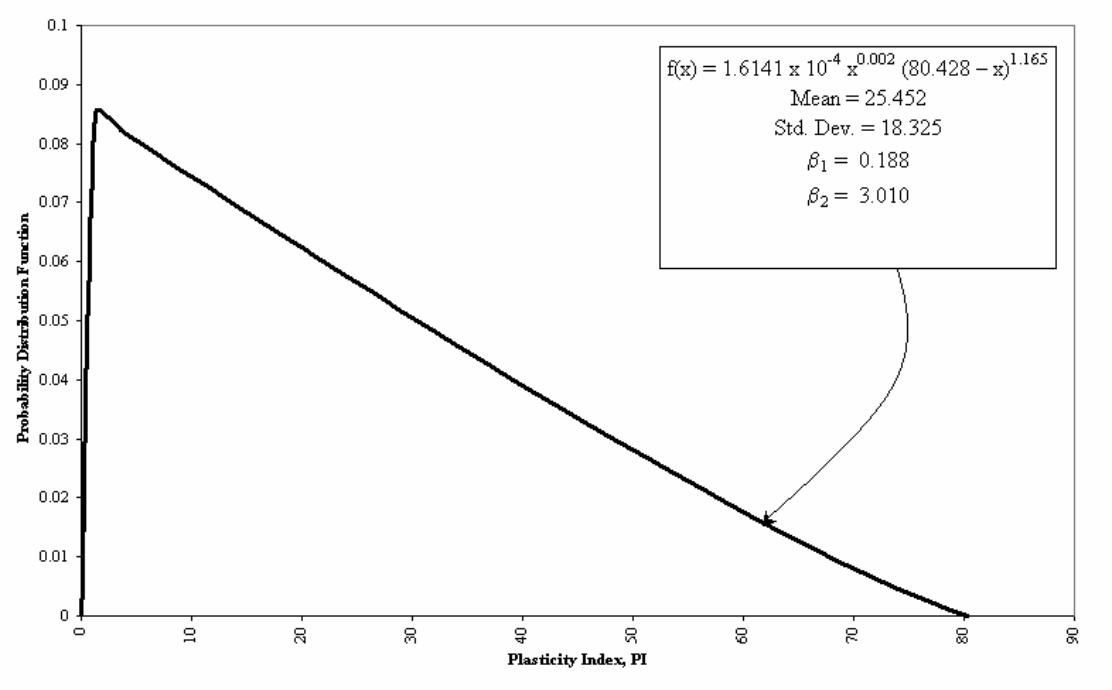

Figure 4.6 Probability Distribution Function of Site B Plasticity Indices

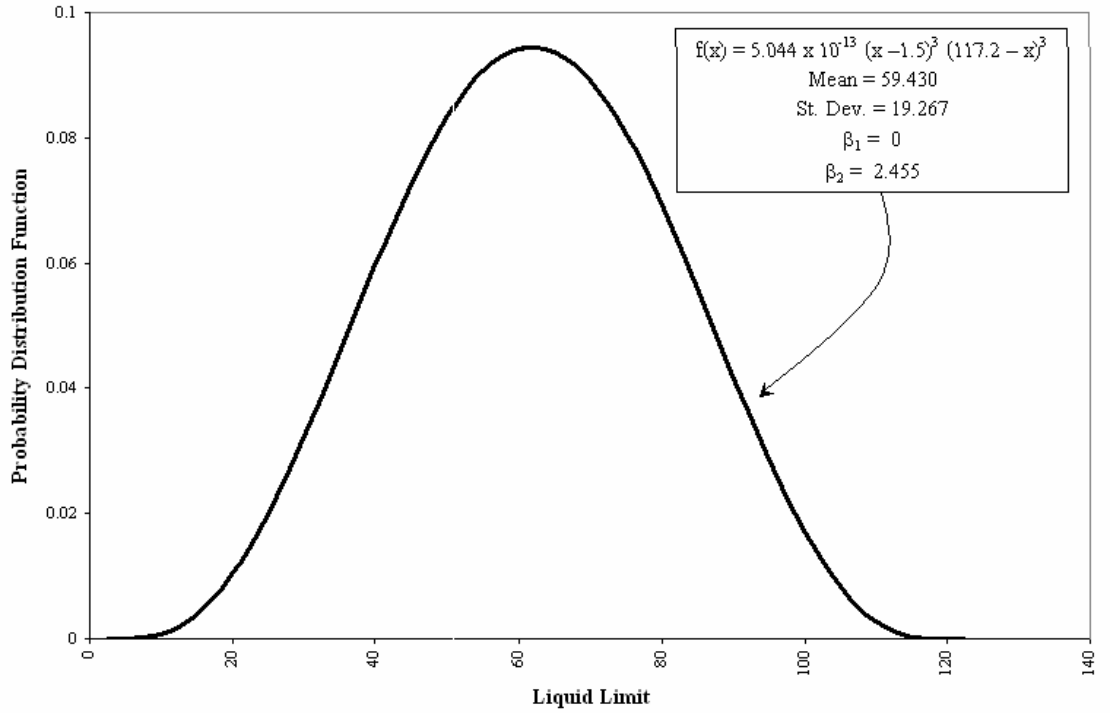

Figure 4.7 Probability Distribution Function of Site C Liquid Limits

As was done with Sites B and C, a beta distribution function was calculated for all three of these parameters. These functions are defined in Equations 4.8 to 4.10, and also plotted graphically in Figures 4.10 to 4.12.

$$\textbf{\textit{Liquid Limit:}}\ f(x) = 8.169 \times 10^{-12} (x - 21.603)^3 (99.329 - x)^3 \qquad \text{(Eqn. 4.8)}$$

$$\textbf{\textit{Plastic Limit:}}\ f(x) = 1.618 \times 10^{-9} (x - 12.648)^3 (49.162 - x)^3 \qquad \text{(Eqn. 4.9)}$$

$$\textbf{\textit{Plasticity Index:}}\ f(x) = 1.601 \times 10^{-10} (x - 4.156)^3 (54.966 - x)^3 \qquad \text{(Eqn. 4.10)}$$

Interestingly, the coefficient of skewness and kurtosis for all three parameters were identical. These values were 0 and 2.455 respectively, indicating that all three distributions were symmetrical, and were slightly less peaked than a normally distributed data sample.

Liquidity indices for this data set averaged a mean value of 1.42. Again, such a high value indicates sensitive soil. However, due to the large standard deviation and coefficient of variation calculated for this data (1.66 and 1.17 respectively), the reliability of this average value is questionable.

4.6.5 Overall Trends

From the beta distribution curves detailed above in Section 4.6, it can be seen that, with the exception of plasticity index for Site B, index properties followed a bell shape. This bell shape slightly skewed right for Site B liquid limits and Site C plasticity index, but was perfectly symmetrical for the remaining index properties. A significantly larger amount of samples were available for analysis for Site C, with respect to all other sites, and thus, it is hypothesised that more testing for soils at both of these sites would have eventually also yielded symmetrical distributions around the mean. It is hypothesised the aberration in distribution shape by Site B plasticity index is due to low plasticity of the site. As shown in Chapter 2, clays of low plasticity tend to produce triangular distributions with respect to plasticity index due to negative values for this parameter being impossible.

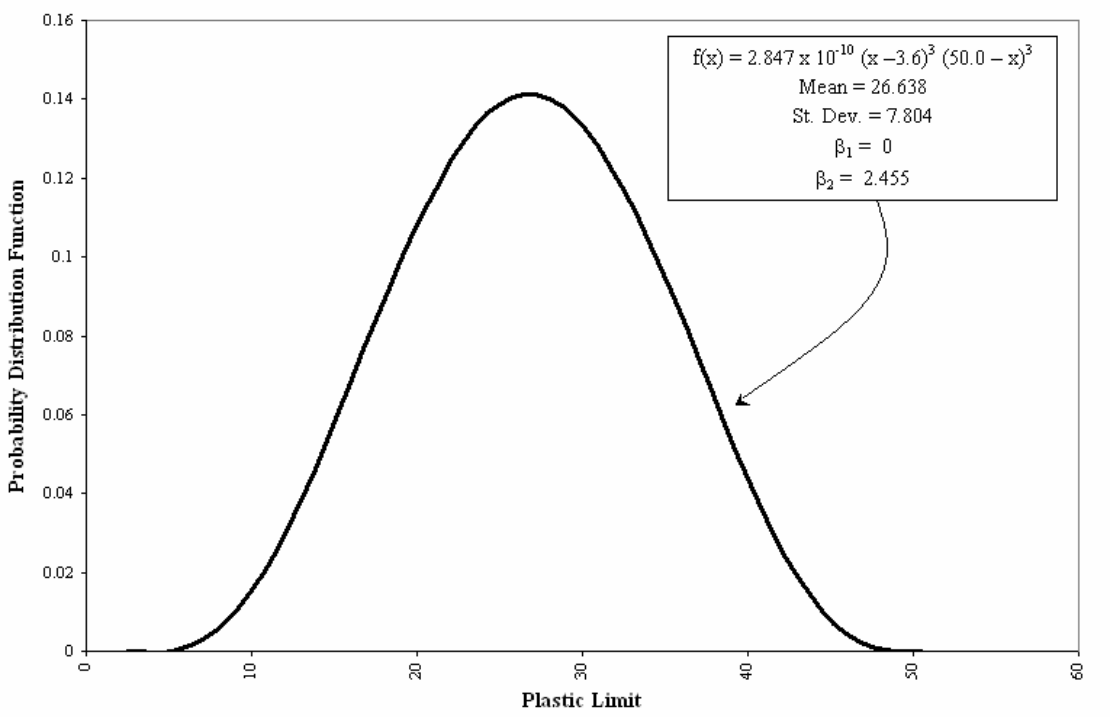

Figure 4.8 Probability Distribution Function of Site C Plastic Limits

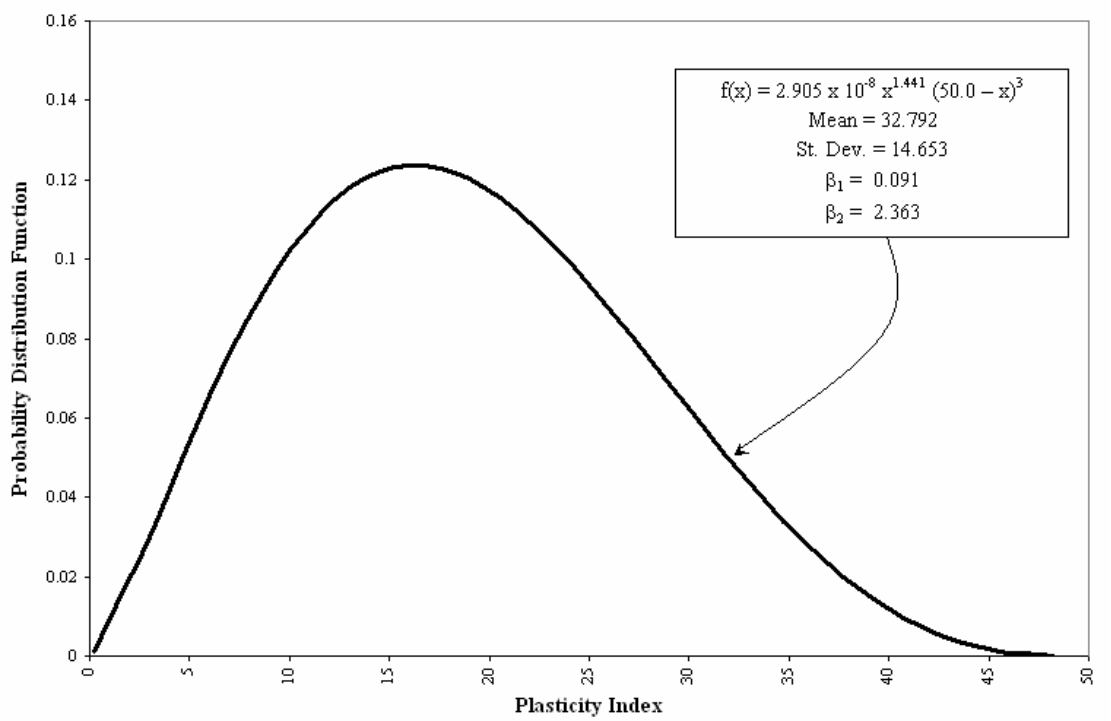

Figure 4.9 Probability Distribution Function of Plasticity Indices at Site C

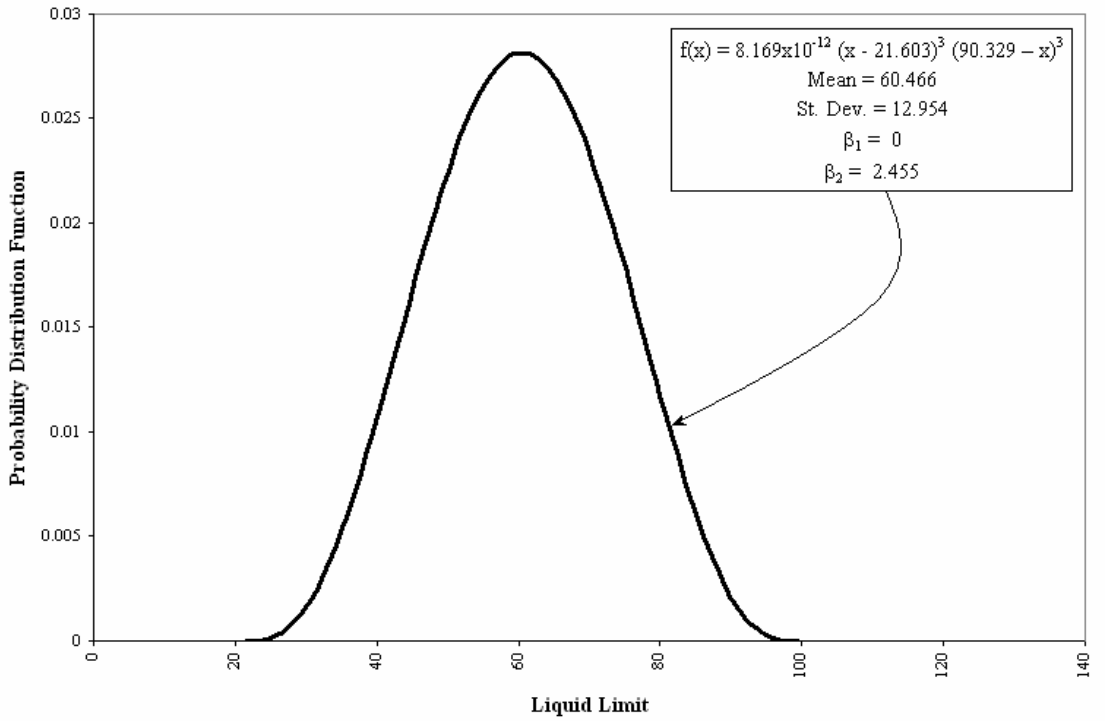

Figure 4.10 Probability Distribution Function of Liquid Limits for Davis (1999) Data

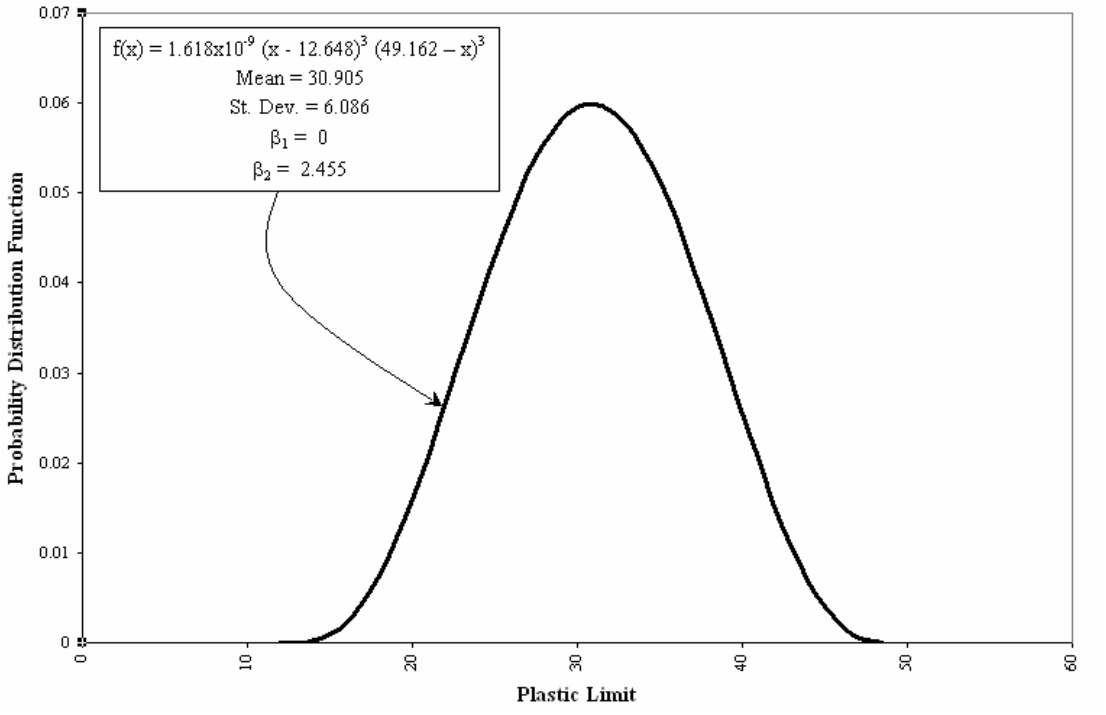

Figure 4.11 Probability Distribution Function of Plastic Limits for Davis (1999) Data

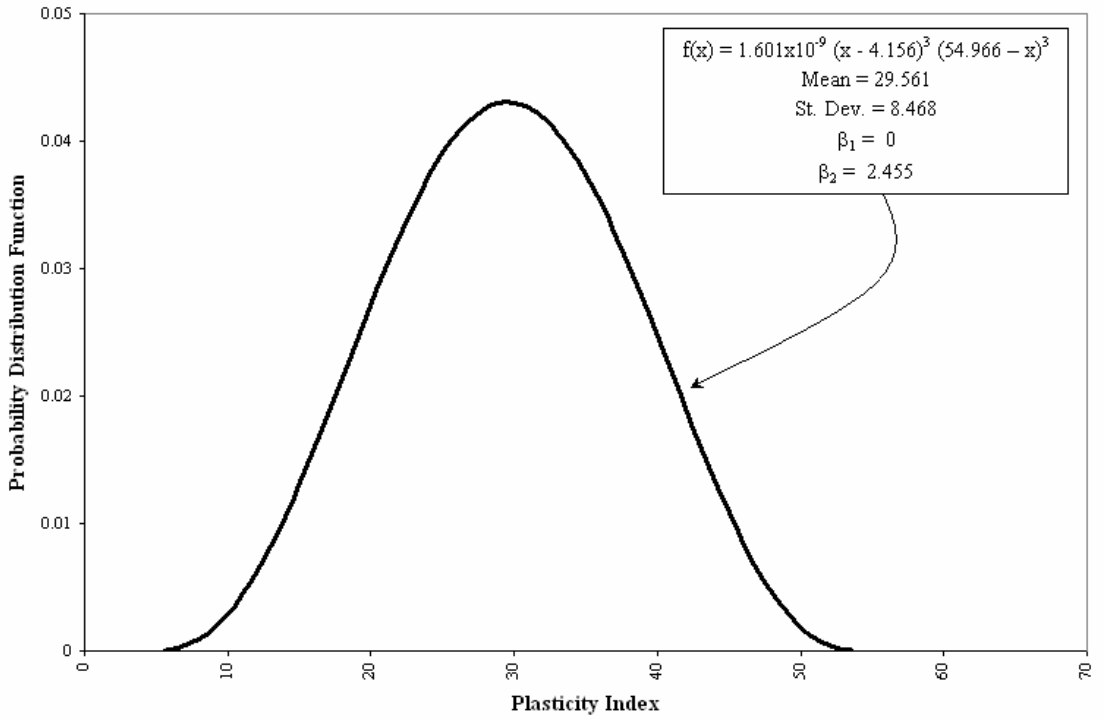

Figure 4.12 Probability Distribution Function of Plasticity Indices for Davis (1999) Data

Overall mean and standard deviation values of Atterberg Limits and plasticity index are given in Table 4.3.

Table 4.3 Statistical Properties for Atterberg Limits of Queensland Clays

Parameter	Liquid Limit, LL	Plastic Limit, PL	Plasticity Index, PI
Mean	**59.6**	**27.8**	**31.8**
Standard Deviation	**17.3**	**7.8**	**13.6**
Coefficient of Variation (%)	**29.0**	**28.0**	**42.8**

Casagrande's (1943) chart of liquid limit-plasticity index representation is currently used by engineers for soil classification. Figure 4.13 details the positioning for all of the natural clay samples on this chart. As shown, a strong overall trend was apparent. Using linear regression, the relationship between liquid limit and plasticity index can

be established for each individual site, as well as overall for Queensland clays as a whole.

As suggested by Gutierrez (2006) and summarised in Chapter 2, any relationship between liquid limit and plasticity should be presented in terms of liquid limit and plastic limit, not plasticity index. Thus, the relationships between plastic limit and liquid limit for each separate source of data are described in Equations 4.12 to 4.15. An overall equation for all Queensland clays is further presented in Equation 4.16.

Site A:	PL = 0.108LL + 14.705	(Eqn. 4.12)
Site B:	PL = 0.055LL + 22.513	(Eqn. 4.13)
Site C:	PL = 0.293LL + 9.235	(Eqn. 4.14)
Davis (1999):	PL = 0.415LL + 5.412	(Eqn. 4.15)
All Queensland Clays:	PL = 0.289LL + 10.326	(Eqn. 4.16)

Similar general relationships were found by linear regression analysis undertaken by Gutierrez (2006) on Uraguay clays, and also by Costet and Sanglerat (1975) for French and Spanish soils. These correlations are given below by Equations 4.17 and 4.18 respectively.

French and Spanish Soils:	PL = 0.30LL + 9	(Eqn. 4.17)
Uruguayan Clays:	PL = 0.28LL + 9.76	(Eqn. 4.18)

4.7 Natural Water Content, w_n

Water contents for each of the clay samples were determined using the method described in AS1289.2.1.1 (SAI Global, 2005) for Sites A and B, and Queensland Materials Testing Manual Q171 (Queensland Department of Main Roads, 1988) for Site C.

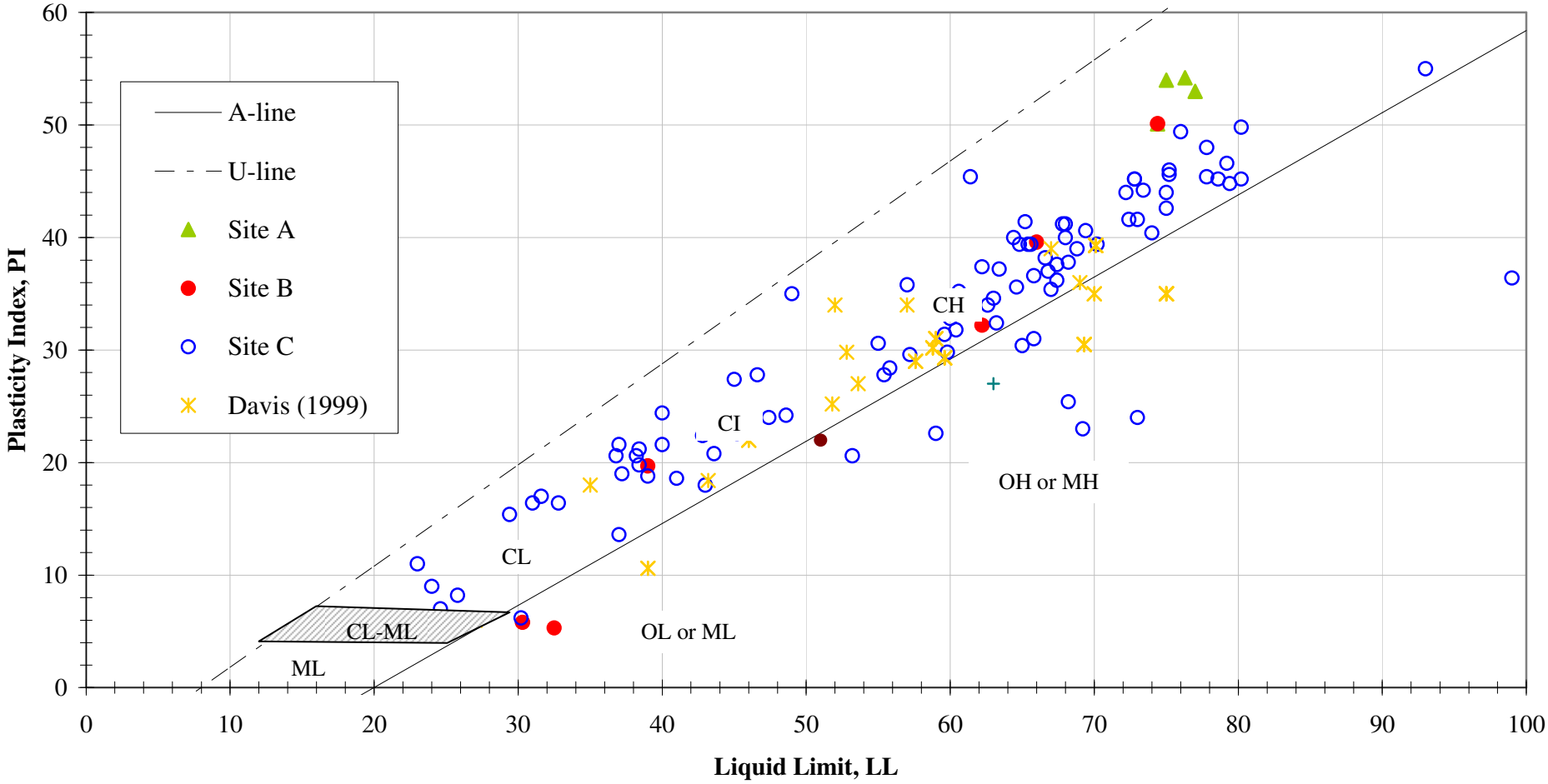

Figure 4.13 Plot showing Natural Sample Positioning upon Casagrandes Plasticity Chart

As undertaken with Atterberg limits for the sites, a beta distribution curve was fitted to data, and a distribution function also established for Sites B and C, and also Davis (1999) data. These functions are displayed together in Figure 4.14, and discussed in Section 4.7.6. Due to the limited data available (only 4 samples tested) for Site A, no function was derived. Furthermore, the values of mean and standard deviation for water content on this site should be viewed with caution. They have been included for informational purposes only.

4.7.1 Site A

Again, the relative variation measured between the samples taken at Site A was minimal, with all water contents tested falling between 59.0% and 62.3%. Mean and standard deviation values for the samples were 60.6 and 1.43 respectively.

4.7.2 Site B

The range of water contents measured for Site B extended from 24.9 to 69.6, and had a mean value of 48.3. Furthermore, the standard deviation and coefficient of variation for the sample population was calculated to be 12.5 and 0.26 respectively. The beta distribution curve that characterises natural water content for this site is given by:

$$f(x) = 1.521 \times 10^{-11} (x - 10.739)^3 (81.862 - x)^3 \qquad \text{(Eqn. 4.19)}$$

4.7.3 Site C

Significantly larger scatter was measured between the water contents determined for Site C, when compared to Site B data. This is evidenced by the coefficient of variation for Site C being in the order of 0.41, while Site B's coefficient of variation is only 0.26. The mean and standard deviation evaluated for this site were 80.6 and 33.2 respectively. Equation 4.20 typifies the beta distribution curve for Site C.

$$f(x) = 4.112 \times 10^{-11} x^{1.817} (180.545 - x)^{2.476} \qquad \text{(Eqn. 4.20)}$$

4.7.4 Davis (1999) Data

Water content values for these records ranged between 18.2 and 138.4. The mean and standard deviation values of this site were 68.1 and 24.2 respectively. Using the three sigma rule discussed in Section 4.5, the minimum and maximum values for the distribution were established to be 0 and 140.6 respectively. The beta distribution developed to describe this data is:

$$f(x) = 1.261 \times 10^{-12} x^{2.61} (140.600 - x)^{2.846} \qquad \text{(Eqn. 4.21)}$$

4.7.5 Overall Trends

From this analysis, it is clear that regardless of the source from which the clays were taken, the general overall distribution curve for natural water content for Queensland clays will follow a bell shape, exhibit little or no skew from the mean, and have a coefficient of kurtosis in the order of 2.4.

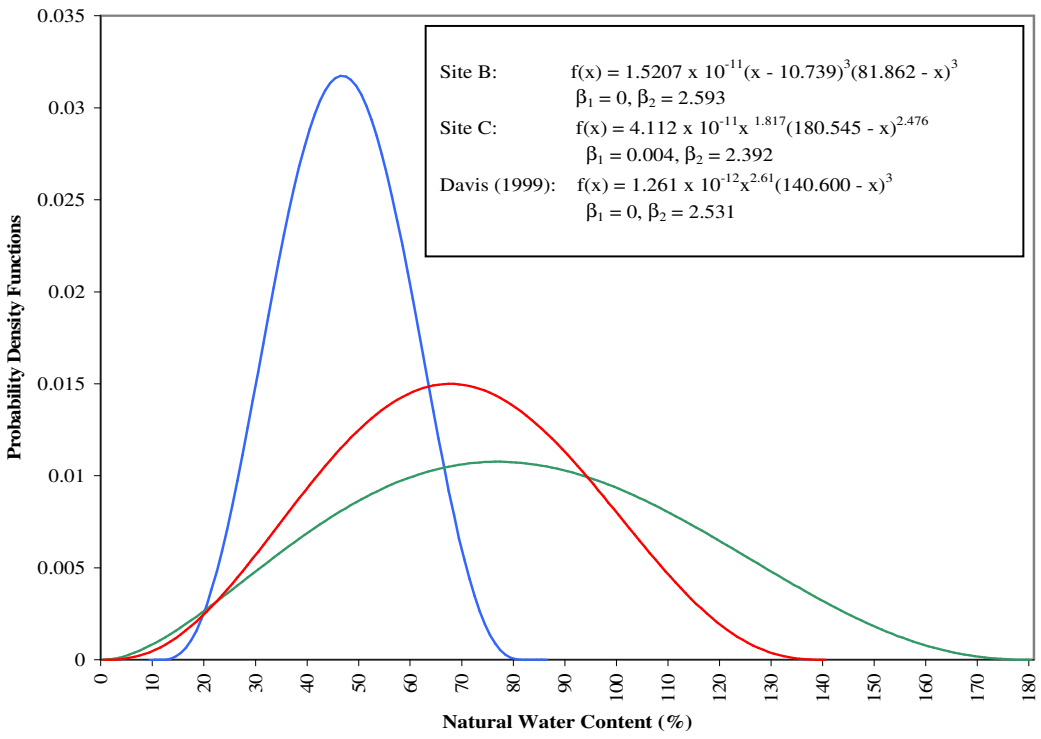

Figure 4.14 Probability Distribution Functions for Natural Water Contents

The curves for Site C and Davis (1999) data, indicate that the data from these two sources was very spread, while the flatness of the curve for the Site C data indicates a larger coefficient of variation, and means that the confidence with which the mean natural water content can be predicted is quite low.

The Site B curve is more peaked than both the Site C or Davis (1999) curves, and its average value is also slightly lower than established for either of these data sets. However, the number of samples from which this curve was established is also less than both of the other sites, and it is believed that if more samples were tested, the geometry of the curve would resemble the other two curves more closely.

4.8 Specific Gravity, G_s

Specific gravity is the ratio of density of a material to the density of water. Table 4.4 details the specific gravity of some common rocks and minerals.

Specific gravity tests for the soil samples were carried out with two 250 mL density bottles, as outlined in AS1289.3.5.2 guidelines. The density bottles were filled one third full with soil from the site under consideration. Distilled water was then added until each bottle was approximately two thirds full. Following this, each individual bottle was placed in a warm water bath for 30 to 45 minutes to remove any entrapped air from the specimen. Following a cooling period, the bottles were then placed in a desiccator, and a vacuum of 13 kPa applied for approximately an hour, to ensure that any remaining air entrapped in the soil-water mixture is expelled. Specific gravity of the specimens is then calculated according to Australian Standards specified formulae. If results from the two tests differed by more than 0.03, the results were discarded and the test undertaken again. The quoted specific gravity is the average of these two results.

A copy of the results for specific gravity testing at each site is shown in Appendix B. These are further summarized in Table 4.5 which details the mean and standard deviation values established for each data set. Due to the limited amount of sample available for Site A, only one value for specific gravity determined for the site. Thus,

no standard deviation could be quantified for the site. The number of tests results analysed with respect to Site B and Site C were 14 and 84 respectively. As shown, negligible difference was apparent between the mean values of specific gravity measured at any of the sites. Indeed, the range over which soils specific gravity measurements spanned for Sites B and C were very similar, with identical minimums and a measure equivalent to only one standard deviation between their maximum values. No data was available for Davis (1999) data with respect to this parameter.

Overall, the mean value for all 99 samples from Sites A, B and C, is 2.56 with a standard deviation of 0.09, and a coefficient of variation of about 0.04. This value lies outside of the realm of the commonly accepted range of 2.6 – 2.8 for soils. However, specific gravity values as low as 2.0 (for organic soils) and 4.4 (for mine tailings) (Sivakugan et al., 2006) have been reported in literature. It is hypothesised that the reason for this low quantity is the presence of organic matter. Tropical soils, such as those found in Queensland, frequently contain organic matter of significant amounts.

4.9 Overconsolidation Ratio (OCR), Preconsolidation Pressure (σ_p), Compression and Recompression Indices (C_c and C_r)

Parameters examined within this section are derived from the void ratio versus effective stress plot of individual oedometer tests. The methods adopted for these tests are outlined previously. Establishing such a plot is straightforward and may be formulated by first establishing initial void ratios for the samples using simple phase relations (Equation 4.22) and then the subsequent changes in void ratio over each load increment (Equation 4.23):

$$e_0 = \frac{w.G}{S_s} \qquad \text{(Eqn. 4.22)}$$

$$\Delta e = \frac{\Delta H}{H_0}(1 + e_0) \qquad \text{(Eqn. 4.23)}$$

Table 4.4. Specific Gravities for Selected Common Minerals and Rocks

Mineral/Rock Type	Specific Gravity, G_s
Basalt	2.7 – 3.1
Chalcopyrite	4.1 – 4.3
Chalk	1.9 – 2.1
Chromite	4.5 – 4.8
Coal	1.2 – 1.5
Gabbro	2.7 – 3.3
Gneiss	2.65 – 2.75
Granite	2.5 – 2.7
Hematite	5.0 – 5.2
Limestone	2.6 – 2.7
Peridotite	3.1 – 3.4
Pyrite	4.9 – 5.2
Pyrrhotite	4.4 – 4.7
Quartzite	2.6 – 2.7
Salt	2.1 – 2.4
Serpentinite	2.5 – 2.6
Sphalerite	3.8 – 4.2

Table 4.5 Statistical Properties for Specific Gravity of Queensland Clays

Parameter	Site A	Site B	Site C	Davis (1999)
Mean	2.68	2.67	2.55	No data
Standard Deviation	N/A	0.10	0.08	available

4.9.1 Preconsolidation Pressure, σ_p

The behaviour of soil is dependent, among other things, on the maximum effective vertical stress to which it has been exposed in the past. This stress 'memory' is referred to as preconsolidation pressure, and may be a product of a variety of mechanisms such as changes in pore water pressure due to the change in water table elevation, removal of overburden or past structures, chemical changes (for example, pH and temperature) or secondary compression (ageing) of the soil.

This pressure is usually determined from the void ratio versus effective stress plots using Casagrandes (1936) method, in which the point of maximum curvature is chosen on the consolidation curve, and two lines are drawn from this point – one horizontal and one tangent to the curve. The angle made by these two lines is bisected with an additional line, and then another line extended up from the virgin compression line (VCL) to meet it. The pressure at which these two last lines intersect is treated as the most probable preconsolidation pressure of the soil (see Figure 4.15).

A further method used by engineers to determine the 'most probable' preconsolidation pressure is to simply extend the two straight line portions of the consolidation curve, and define the preconsolidation pressure as the stress at which they intersect (Holtz, 1981). Both methods were utilised within this analysis – the first for clearly defined void ratio curves, and the second for the more disturbed samples.

4.9.2 Overconsolidation Ratio, OCR

The ratio of preconsolidation pressure to the current effective overburden pressure for a soil is defined as its overconsolidation ratio. Soils with an overconsolidation ratio of greater than one are described as overconsolidated, while soils with an overconsolidation ratio equal to one are defined as normally consolidated. The mechanical behaviour of clay is highly dependent on this measure of stress state. The relationship of overconsolidation ratio with the coefficient of volume compressibility is examined later within this chapter.

4.9.3 Compression Index, C_c

The compression index of a soil is defined as the gradient of the virgin consolidation line on a void ratio versus effective stress plot. It is denoted by C_c, and is directly related to settlements in normally consolidated soils.

Due to its importance in the settlement prediction of clays, several researchers have developed correlations which relate it to other index properties of soil. In the majority of cases, these relate compression index to three main parameters – the liquid limit, water content or initial void ratio of the soil.

Liquid limit is the most statistically significant Atterberg property for all four data sets in this study. This is evident by simply comparing the coefficients of variation for each of the parameters. Also, as outlined in Section 4.6.6, property values which are calculated by a linear trend between two other variables, present misguiding values with regards to their regression coefficients.

Table 4.6 outlines correlations which exist to describe compression index in terms of liquid limit only, along with their regions of applicability. It should be noted that the latter three equations presented by Look and Williams (1994) were actually produced for data collected on Queensland clays, but showed only weak correlations for their analysed dataset.

To assess the validity of using these published correlations in quantifying the compression indices of Queensland clays, it was necessary to produce equations which best characterised the collated data. By applying regression methods, power trends were found to provide the best fit in all three cases. These equations are shown below.

$$C_c = 0.0034*LL^{1.282} \qquad \text{(Eqn. 4.24)}$$

$$C_c = 0.005*\ w_n^{1.156} \qquad \text{(Eqn. 4.25)}$$

$$C_c = 0.303*e_0^{1.383} \quad \text{(Eqn. 4.26)}$$

To demonstrate the applicability of the correlations cited in Tables 4.6, 4.7 and 4.8, to the prediction of compressibility for Queensland clays, the compression indices predicted by each of these equations were plotted alongside either Equations 4.24, 4.25 or 4.26. The results from this exercise are shown in Figures 4.16 to 4.18 respectively.

From Figure 4.16 it can be seen quite definitively that, on a whole, correlations using liquid limit underestimate the compression indices of Queensland clays. The only exception to this statement is related those calculated using Look and Williams (1994) equation for overconsolidated clays. For liquid limits less than 35, this equation tends to overestimate the compression indices slightly. The degree to which indices are overestimated increases significantly with decreasing liquid limit.

A list of C_c values for each of the sources are shown in Appendix I. From this table, it can be seen that the minimum and maximum compression indices measured for Site A were 0.0003 and 0.012 respectively, while for Site B values ranged between 0.127 and 1.052. Lastly, Site C and Davis (1999) data recorded minimums of 0.121 and 0.071, and maximums of 1.959 and 1.562 respectively.

4.9.4 Recompression Index, C_r

The recompression index, C_r, is another important parameter in soft soil settlement analysis. It is defined in the same way as the compression index, C_c, however it correlates to the slope of unloading/reloading phase of the consolidation test.

In most cases, C_r is assumed to range between 0.015 and 0.035 (Leonards, 1976) and to be in the order of $1/5^{th}$ to $1/10^{th}$ the magnitude of the compression index (Das, 1994). Generally, the higher the plasticity index of a soil, the larger the ratio between compression and recompression indices (C_c/C_r).

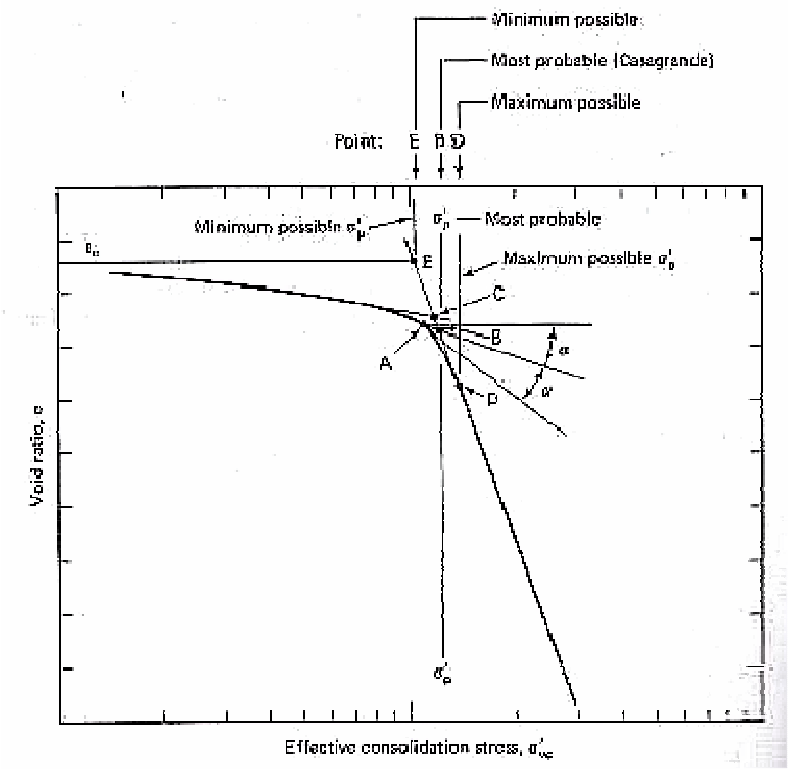

Figure 4.15 Graph showing Casagrandes (1936) Determination of Preconsolidation Pressure

Table 4.6 Existing Correlations relating Liquid Limit to Compression Index

Equation	Region of Applicability	Reference
$C_c = 0.006$ (LL – 9)	All natural soils	Azzous et al. (1976)
$C_c = 0.0046$ (LL – 9)	Overconsolidated Brazilian Clays	Bowles (1979)
$C_c – 0.008$ (LL – 7)	Normally Consolidated Queensland Clays	Look and Williams (1994)
$C_c = 0.004$ (LL + 48)	Overconsolidated Queensland Clays	Look and Williams (1994)
$C_c = = 0.008$ (LL – 10)	All Queensland Clays	Look and Williams (1994)
$C_c = 0.007$ (LL – 10)	Remoulded Normally Consolidated Clay Samples	Skempton (1944)
$C_c = 0.009$ (LL – 10)	Undisturbed Clay Samples of Low to Medium Sensitivity	Terzaghi and Peck (1967)

Table 4.7 Existing Correlations relating Natural Water Content to Compression Index

Equation	Region of Applicability	Reference
$Cc = 0.01\ (w_n - 5)$	All Clays	Assouz et al. (1976)
$C_c = 0.009\ (w_n - 1)$	Normally Consolidated Queensland soils	Look and Williams (1994)
$C_c = 0.009\ (w_n + 3)$	Overconsolidated Queensland soils	Look and Williams (1994)
$C_c - 0.009\ (w_n - 4)$	All Queensland clays	Look and Williams (1994)
$C_c = (1.15 \times 10^{-2})\ w_n$	Organic Soils	Moran et al. (1958)
$C_c = 0.0115 w_n$	All Clays	Herrero (1989)

Table 4.8 Existing Correlations relating Initial Void Ratio to Compression Index (after Aysen and Atilla, 2001)

Equation	Region of Applicability	Reference
$C_c = 1.15(e_0 - 0.35)$	All Clays	Nishida (1956)
$C_c = 0.30(e_0 - 0.27)$	Inorganic Soils	Hough (1957)
$C_c = 0.256 + 0.43(e_0 - 1.87)$	Motley Clays from Sao Paulo, Brazil	Cozzolino (1961)
$C_c = 0.2(e_0)^{1.6}$	Naturally Sedimented Young Soils	Shorten (1995)
$C_c = 0.4(e_0 - 0.25)$	All Natural Soils	Assouz (1976)

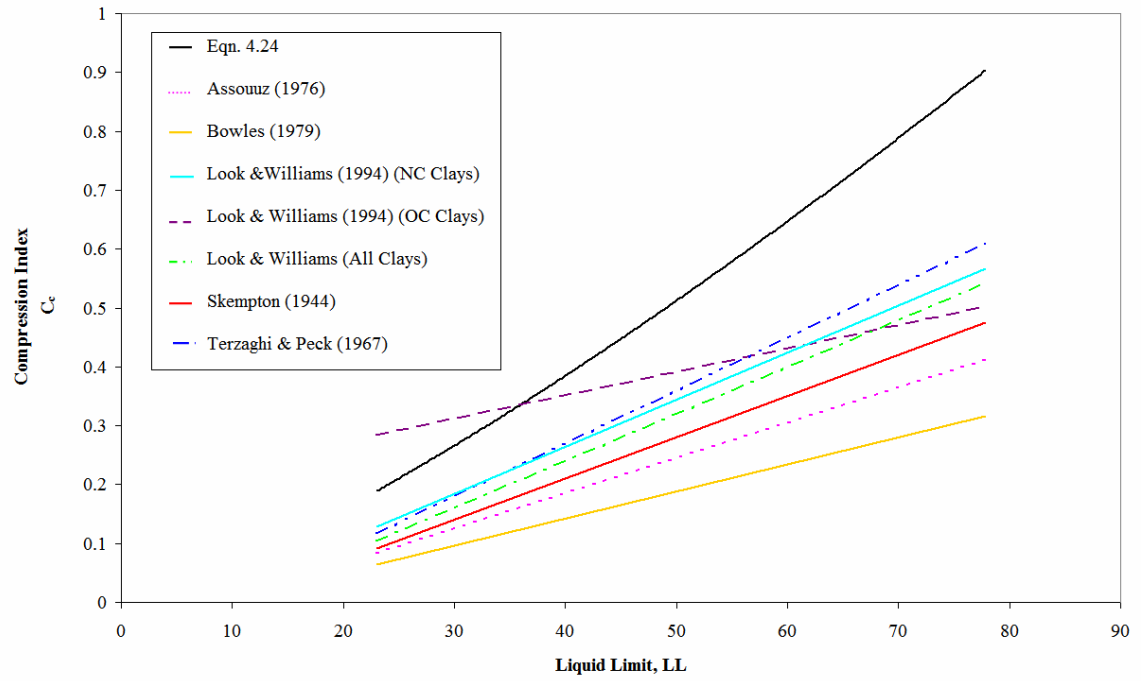

Figure 4.16 Comparison of Correlations relating Liquid Limit to Compression Index

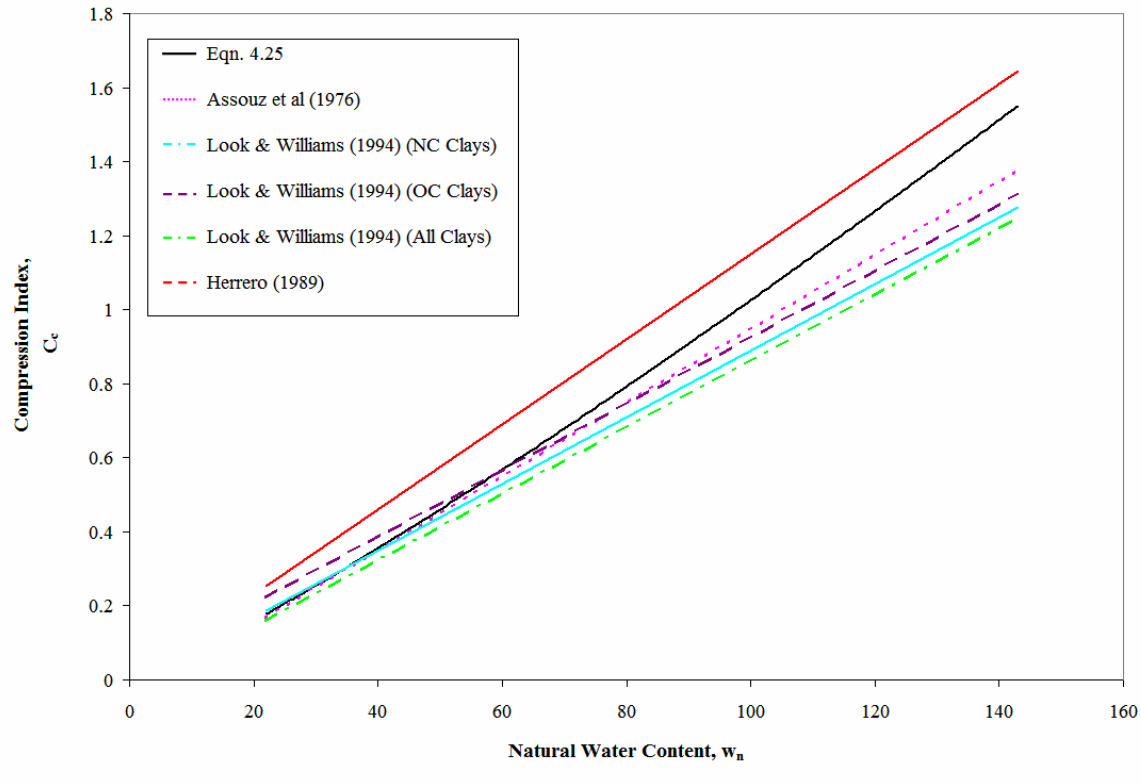

Figure 4.17 Comparison of Correlations relating Natural Water Content to Compression Index

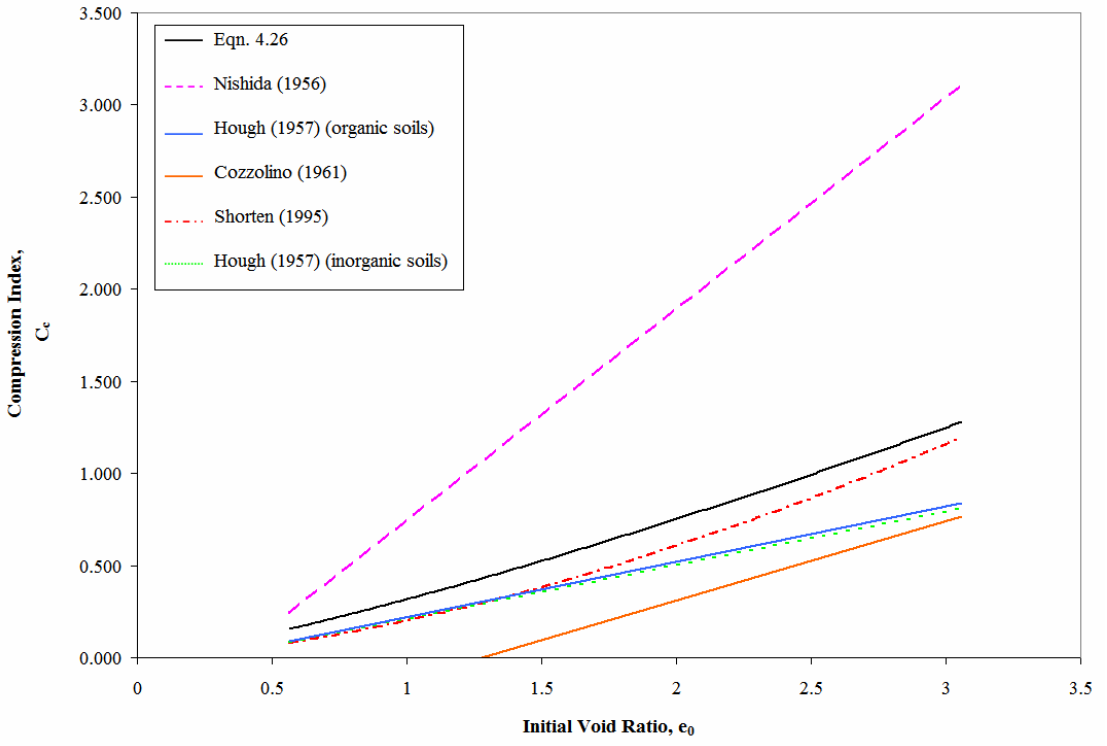

Figure 4.18 Comparison of Correlations relating Initial Void Ratio to Compression Index

Source data with regards to recompression indices are also shown in Appendix I. Ranges for C_r values were 0.0003 to 0.001 (Site A), 0.013 to 0.186 (Site B), 0.053 to 0.209 (Site C) and 0.033 to 0.454 (Davis, 1999) respectively. Thus, it is clearly seen that not all of the C_r results fell within the range outlined by Leonards (1976). The Das (1994) estimates of between $1/5^{th}$ and $1/10^{th}$ the compression index value was also found to be inconsistent with this data, with 55% of the samples recording C_r/C_c ratios outside this range.

4.10 Coefficient of Volume Compressibility (m_v)

4.10.1 General

The coefficient of volume compressibility describes the volumetric strain that a soil will experience per unit stress, and is determined by means of a simple oedometer test using the following equation.

$$m_v = \left(\frac{\Delta e}{1 + e_0} \right) \frac{1}{\Delta \sigma_v} \qquad \text{(Eqn. 4.26)}$$

Although it is the most popular of the compressibility coefficients for the direct calculation of settlements, its variability with stress level makes it less useful when quoting typical compressibilities or correlating compressibility with other properties of the soil.

The m_v method of calculating the primary settlement of clays due to application of a load is described using the following equation (Holtz and Kovacs, 1981):

$$s_c = m_v . H . q \qquad \text{(Eqn. 4.27)}$$

where s_c = soil settlement for a clay layer, H = the height of the clay layer before load application, m_v = coefficient of volume compressibility for the soil, and q = the normal stress applied to the sample.

Typically, a standard oedometer test adopts a load increment ratio (LIR) of 1. That is, with each additional loading increment, the pressure being applied to the clay sample is doubled. The load increment ratio was generally kept constant at 1 for all samples to ensure the points on the e-vs-log σ_v' plot are evenly spaced. However, in some cases LIR is reduced around the preconsolidation pressure to define it better, and even spacing is not maintained.

The coefficient of volume compressibility, m_v for each load increment can be calculated using the e-vs-log σ_v' plot, and a graph of m_v with vertical stress created. Typically, an m_v value at the appropriate stress level is selected from this plot, and used in settlement calculations. However, establishing the stress dependence of m_v using this method is not only misleading, but in many cases incorrect.

4.10.2 Determination of 'True' m_v Plot

The 'true' plot for describing soil's compressibility may be determined using an EXCEL spreadsheet developed in this research. In addition to knowing the specific gravity (G_s) and water content (w) of the soil sample, it is essential also to have a record of the sample dimensions for the oedometer sample, along with the vertical load increments, and the corresponding consolidation settlements (s_c) caused by them.

The first two entries, w and G_s, are used to calculate initial void ratio of the sample, whilst the last three are used in computing subsequent void ratios for the actual oedometer load increments. The preconsolidation pressure of the plot is determined using Casagrande's method, and the appropriate compression index (C_r or C_c) calculated for each loading stage. For loading stages less than the preconsolidation pressure, this compression index will be C_r. Conversely, for loading stages greater than the preconsolidation pressure, the compression index which needs to be used will be C_c. The load increment which includes the preconsolidation pressure is not considered within any of the calculations.

These incremental indices are then used in computing a 'weighted' average which is implemented into the EXCEL spreadsheet. Separate averages are derived for both the overconsolidated and normally consolidated sections of the plot. These weighted values are denoted by C_{rw} and C_{cw} respectively and described by Equations 4.28 and 4.29:

$$C_{rw} = \frac{\sum (C_r * \Delta\sigma_v)}{\sum (\Delta\sigma_v)} \qquad \text{(Eqn. 4.28)}$$

$$C_{cw} = \frac{\sum (C_c * \Delta\sigma_v)}{\sum (\Delta\sigma_v)} \qquad \text{(Eqn. 4.29)}$$

Following this, a 'theoretical' void ratio versus effective stress plot can be plotted by drawing two straight lines – the first from the initial void ratio to the preconsolidation pressure using C_{rw} as the gradient of the line, and the second from the preconsolidation pressure, using C_{cw} as its gradient. From this plot, the 'true' compressibility plot can be developed by calculating m_v (using Equation 4.26) at smaller, equally sized increments.

A sensitivity analysis undertaken on the sizing of these calculation increments indicated that increments in the order of 10 kPa should be used. Smaller discretization of the stress increments yielded negligible difference to the plot produced.

4.10.3 Example Problem of 'True' m_v Determination

The following example uses actual data obtained from an oedometer test on a soft clay sample (see Table 4.9), and calculates the m_v versus effective stress plot for the soil sample using the current conventional method, as well as the method proposed in Section 4.9.2. 1t shows the correct derivation of the m_v plot, and illustrates why significant errors are introduced using the current method of plotting.

Problem Statement

Given the following sample data, what is the overall settlement of an 8 metre layer of clay subjected to a 30 kPa loading applied in four equivalent stages?

Sample Data

Sample No.: 506049
Sample Depth (m): 4.0
Height (mm): 19.5
Specific Gravity, G_s: 2.70
Water Content (%): 46.8
Wet Density, ρ (kg/m^3): 1757
Initial Saturation (%): 94.0

Table 4.9: Oedometer Results Summary

Increment No.	Pressure (kPa)	Height (mm)
Seating Load	6.25	19.440
1	12.5	19.420
2	25.0	19.294
3	50.0	19.118
4	100.0	18.728
5	200.0	18.110
6	400.0	17.492
7	800.0	16.852

Example Calculations

Conventional m_v Method

Firstly, initial void ratio of the sample:

$$e_0 = \frac{wG_s}{S}$$

$$= \frac{(0.468)(2.70)}{0.94}$$

$$= 1.345$$

Now, calculated values using the conventional method of adopting the oedometer loading increments are shown in Table 4.10, Figure 4.19 and Figure 4.20.

Table 4.10 Void ratio and m_v values using Oedometer Loading Increments

Increment No.	Pressure Range (kPa)	Void Ratio prior to loading, e	Incremental Change in Void Ratio, Δe	Incremental Coefficient of Volume Compressibility, m_v (MPa^{-1})
1	6.25 – 12.5	1.295	0.002	0.164
2	12.5 – 25.0	1.293	0.015	0.517
3	25.0 – 50.0	1.278	0.021	0.361
4	50.0 – 100.0	1.257	0.046	0.400
5	100.0 – 200.0	1.211	0.073	0.317
6	200.0 – 400.0	1.137	0.072	0.156
7	400.0 – 800.0	1.065	0.076	0.082

For the midpoint of the clay layer, the initial effective vertical stress is:

$$\sigma_v' = 4(\gamma_{sat} - \gamma_w)$$

$$= 4\left[(1757)(9.81) - (1000)(9.81)\right]$$

$$= 29.7 \text{ kPa}$$

Thus, following 30 kPa loading, the effective vertical stress at the mid-layer will be 59.7 kPa. Using Figure 4.20, $m_v \cong 0.380$ MPa^{-1} at a pressure of 59.7 kPa

Thus, the total settlement using this method is:

$$S_c = m_v.q.H$$

$$= (0.380)(30)(8)$$

$$= 91.2 \text{ mm}$$

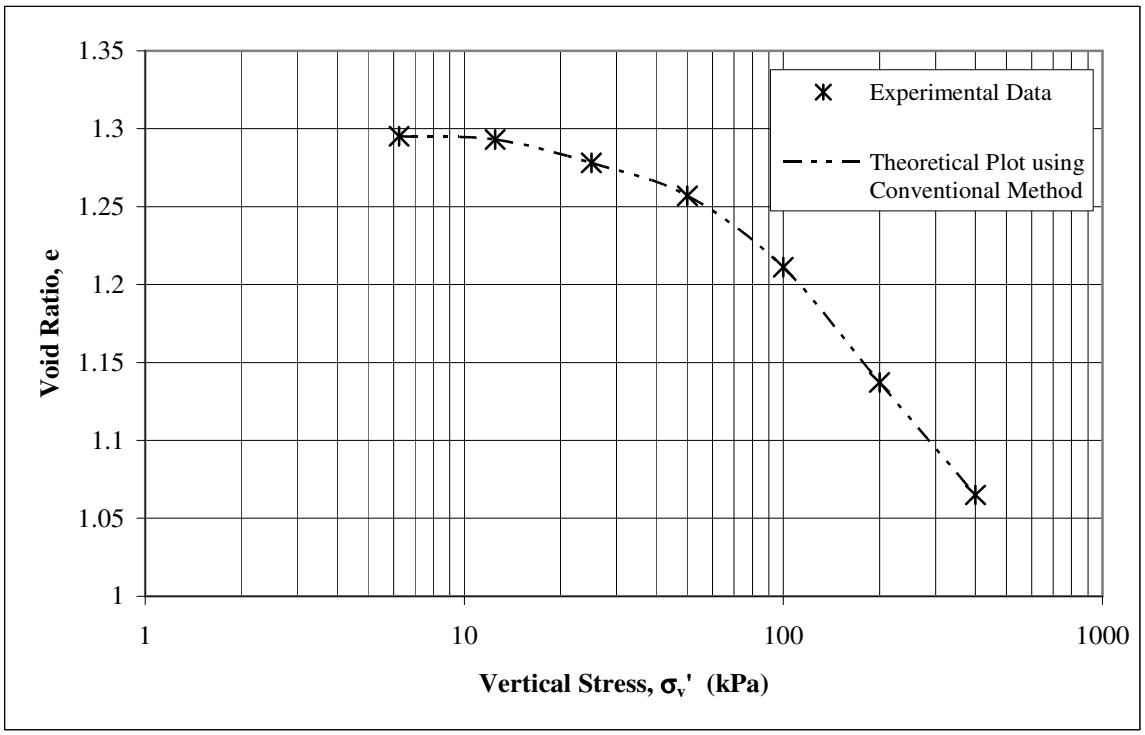

Figure 4.19 Void Ratio vs. Effective Stress Plot using Conventional Method

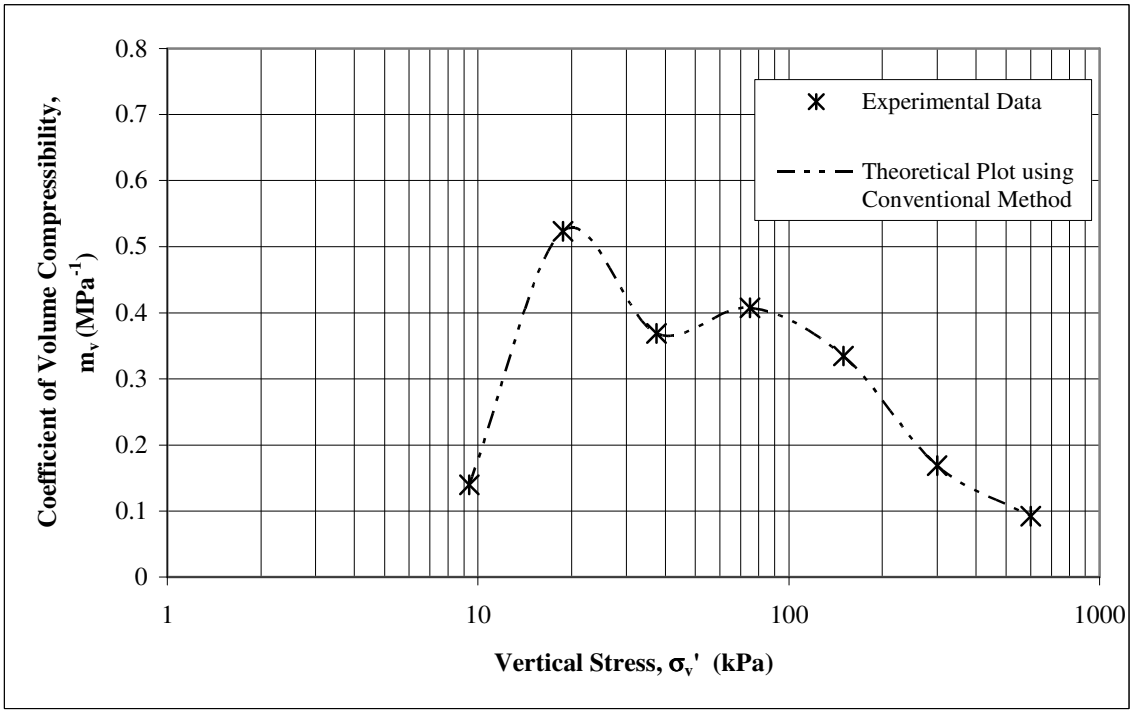

Figure 4.20 Coefficient of Volume Compressibility vs. Effective Stress Plot using Conventional Method

C_r-C_c-σ_p' Method

Using Casagrande's method and Figure 4.19, the preconsolidation pressure can be determined as 75 kPa. The in situ overburden pressure on the sample is 29.7 kPa. Thus, preconsolidation pressure has not yet been reached and only C_r need be used to calculate the settlement following 20 kPa loading. The average C_r value across the loading increments is 0.055.

$$\Delta e = C_r .\log\left(\frac{\sigma_{v0}' + \Delta\sigma_v}{\sigma_{v0}'}\right)$$

$$= 0.055 * \left(\log\left(\frac{59.7}{39.7}\right)\right)$$

$$= 0.010$$

Thus, total settlement using this method, is:

$$S_c = \frac{\Delta e}{1+e_0} H$$

$$= \left(\frac{0.010}{1+1.345}\right).8000$$

$$= 33.4 \text{ mm}$$

Proposed Method

Using the previously determined values of C_r, e_0 and σ_p' (= 0.055, 1.345 and 75 kPa respectively), the plots shown in Figures 4.21 and 4.22 were developed. These figures display the measured lab values, alongside the theoretical plot determined from calculating each parameter at smaller equivalent intervals of 10 kPa.

The 30 kPa increment in the above problem was discretised into four 7.5 kPa increments, taking the effective stress from 29.7 kPa to 59.7 kPa. Using Figure 4.22, the m_v values for these four stages are given below:

$[m_v]_{inc\ 1}$ = 0.252 MPa^{-1}.

$[m_v]_{inc\ 2}$ = 0.214 MPa^{-1}.

$[m_v]_{inc\ 3}$ = 0.186 MPa^{-1}.

$[m_v]_{inc\ 4}$ = 0.165 MPa^{-1}.

In this proposed method, the total settlement is calculated as the sum of individual settlements induced by each pressure stage (using appropriate m_v for each stage):

$$S_c = \sum_{1}^{i} (m_v q)_i H$$

$$= [(0.252)(7.5) + (0.214)(7.5) + (0.186)(7.5) + (0.165)(7.5)](8)$$

$$= 49.02 \text{ mm}$$

This example details the importance of using smaller stress increments when deriving the relationship between coefficient of volume compressibility and effective stress for clays.

It is widely accepted that the compressibility of a clay sample increases considerably at its preconsolidation stress. However, due to the unit LIR conventionally adopted during oedometer testing, the full magnitude of this parameter is quite frequently estimated incorrectly. As a result, settlements are miscalculated.

Using the C_r-C_c-σ_p' settlement calculation as a basis for comparison, we can clearly observe that, in this case, predicting settlement from m_v values obtained using the conventional method produced values approximately 2.7 times larger than those calculated using the C_r-C_c-σ_p' method. Predicting m_v using the proposed method yielded significantly smaller differences in settlement.

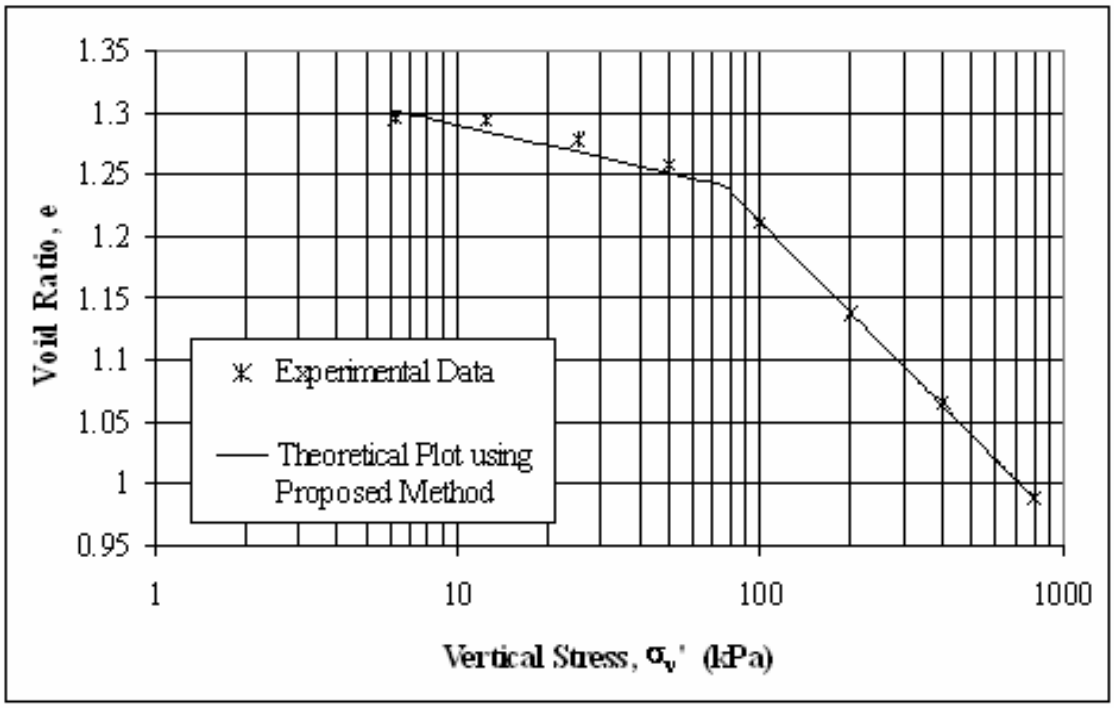

Figure 4.21 Void Ratio vs. Effective Stress Plot using Smaller Stress Increments

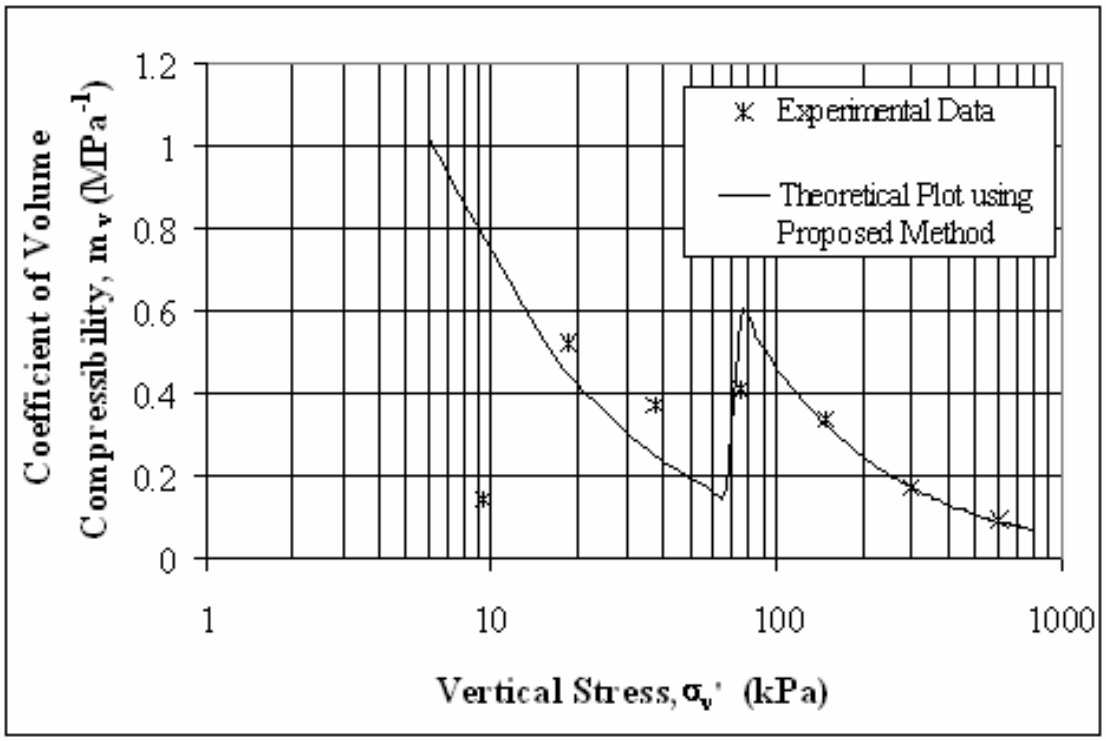

Figure 4.22 Coefficient of Volume Compressibility vs. Stress Plot using Smaller Stress Increments

4.10.4 Influence of OCR on m_v Value

Raw data from oedometer tests undertaken on Site B samples were used to study the influence of overconsolidation ratio on m_v. Results from these tests were then used to establish the true m_v plot for the sample. Overconsolidation ratios of 1.5, 2, 2.67, 3, 5, 7.5 and 10 were tested for each of the samples. These were achieved by initially loading the sample to 800 kPa so that it achieves normally consolidated state. Following this, the sample was unloaded to an OCR of 10 kPa, and allowed to stand for 24 hrs. Subsequent loading increments were calculated to coincide with the desired OCR levels. A standing period of 24 hrs was maintained between each load stage to ensure that the appropriate OCR level was attained.

For clarity, only results for the OCR values of 2, 3 and 5 are shown in Figures 4.23 to 4.28. The general expression for these figures can be written as:

$$m_v = L\left(\frac{\sigma_{v,current}}{\sigma_{p(initial)}}\right)^{0.9} \qquad \text{(Eqn. 4.30)}$$

where $\sigma_{p(initial)}$ is the in situ preconsolidation pressure (in kPa) and $\sigma_{v,current}$ is the vertical stress at which m_v is being calculated (in kPa). That is, $\sigma_{v,current}$ will increase from the left to right of the plot.

The coefficient L for these equations is specific to each sample and is shown in Figure 4.29. L has been further related to overconsolidation ratio, and can be expressed as Equation 4.31. The parameters of L and Q have units of MPa^{-1}, while the N parameter has no units.

$$L = Q * (OCR)^N \qquad \text{(Eqn. 4.31)}$$

By examining Figure 4.29, two trends are apparent. The first, is that as the overconsolidation ratio of the soil increases, L decreases. The second is that a relationship appears to be present between L and the parameters of liquid limit,

plasticity index and linear shrinkage. An increase in any one of the index properties limits listed corresponds to an increase in L. No trend is apparent with regards to plastic limit.

Only four lines are evident within Figure 4.29. This is due to the coefficients of samples JCU2_L5, JCU2_L6 and JCU_L7 being close to identical, and plotting basically on top of one another. The overall trendline corresponding to these samples is situated second from the top. The uppermost line corresponds to JCU2_L4, and the bottom two are JCU2_L2 and JCU2_L3 respectively (where JCU2_L2 is the lower of them).

To investigate the apparent relationship between these index properties and each of the components of the power trend for L (see Equation 4.31), the coefficients of Q and N were plotted individually against liquid limit, plasticity index and linear shrinkage. The relationships determined, and their corresponding r^2 values are detailed below, and shown diagrammatically in Figures 4.30 and 4.31 respectively. As shown, liquid limit had the strongest correlation with the Q coefficient, while linear shrinkage influenced N most significantly.

$$Q = 0.0024(LL) - 0.0541 \qquad (r^2 = 0.87) \qquad \text{(Eqn. 4.32a)}$$

$$Q = 0.0022(PI) + 0.0099 \qquad (r^2 = 0.73) \qquad \text{(Eqn. 4.32b)}$$

$$Q = 0.0057(LS) + 0.0120 \qquad (r^2 = 0.72) \qquad \text{(Eqn. 4.32c)}$$

$$N = 2.7647 - 0.5486*\ln(LL) \qquad (r^2 = 0.68) \qquad \text{(Eqn. 4.33a)}$$

$$N = 1.3507 - 0.2452*\ln(PI) \qquad (r^2 = 0.88) \qquad \text{(Eqn. 4.33b)}$$

$$N = 1.1930 - 0.2585*\ln(LS) \qquad (r^2 = 0.93) \qquad \text{(Eqn. 4.33c)}$$

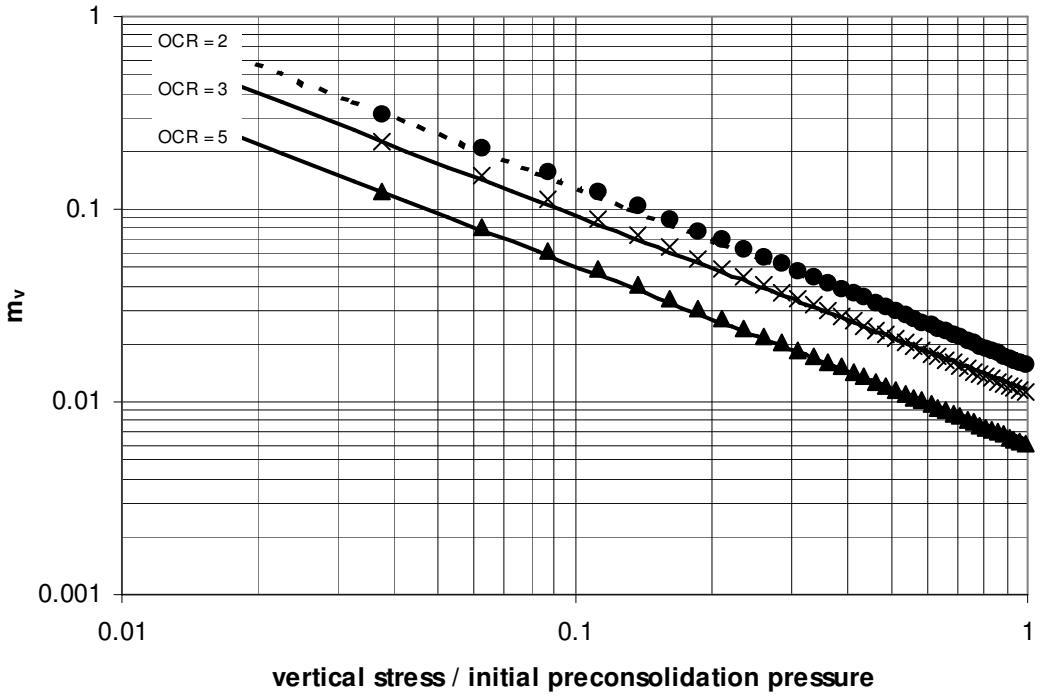

Figure 4.23 Coefficient of Volume Compressibility vs. Normalised Stress Plot for JCU2_L2

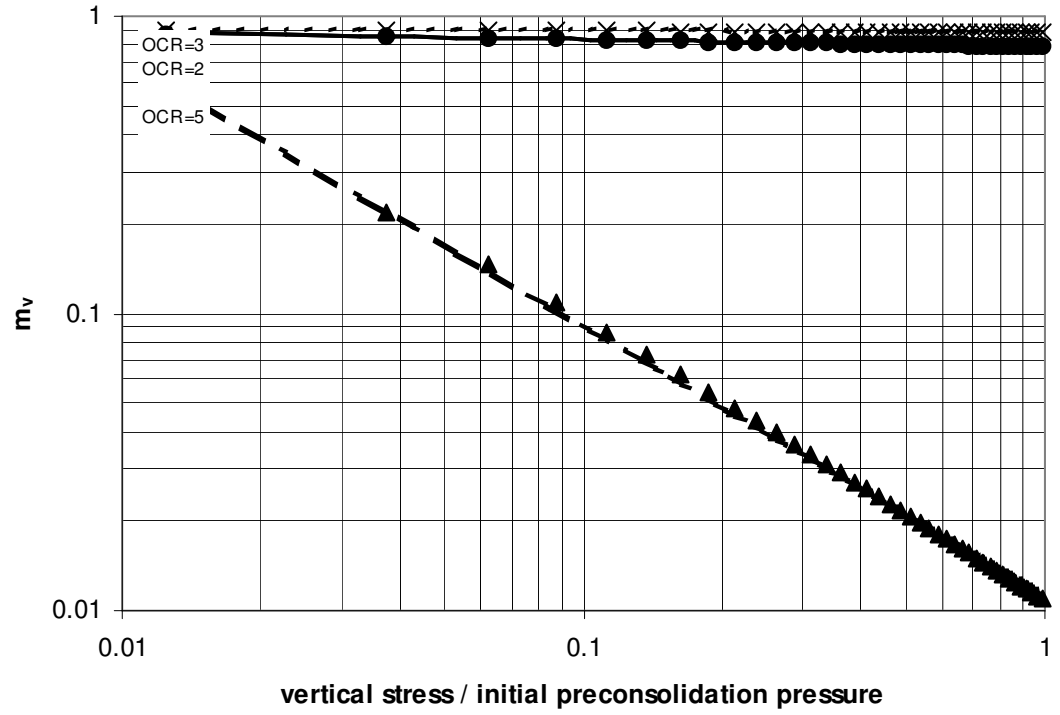

Figure 4.24 Coefficient of Volume Compressibility vs. Normalised Stress Plot for JCU2_L3

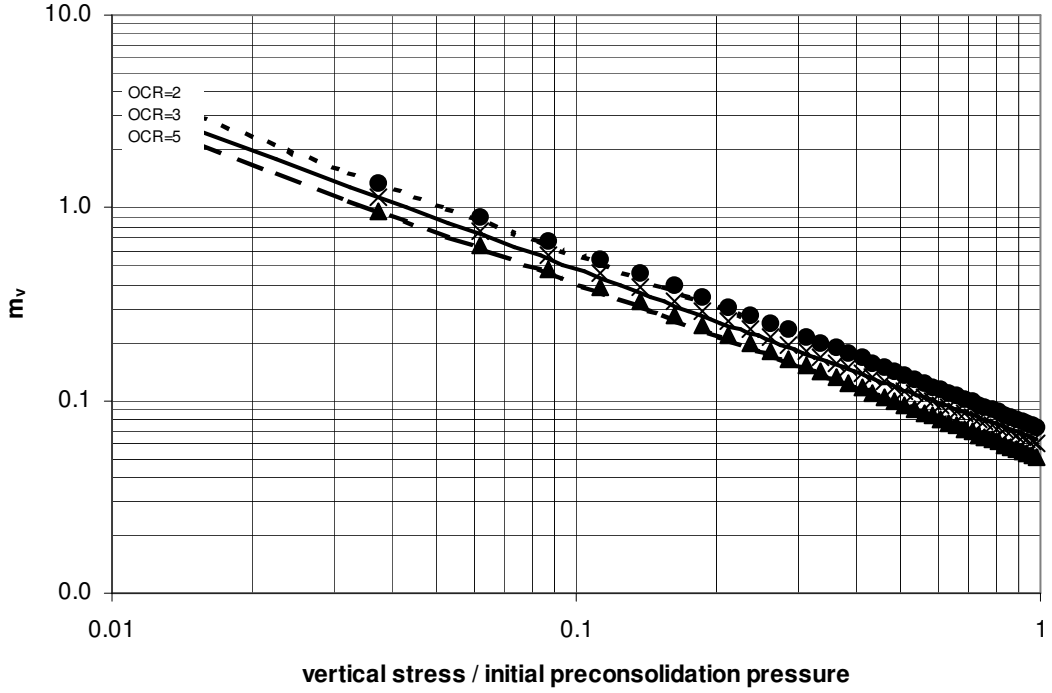

Figure 4.25 Coefficient of Volume Compressibility vs. Normalised Stress Plot for JCU2_L4

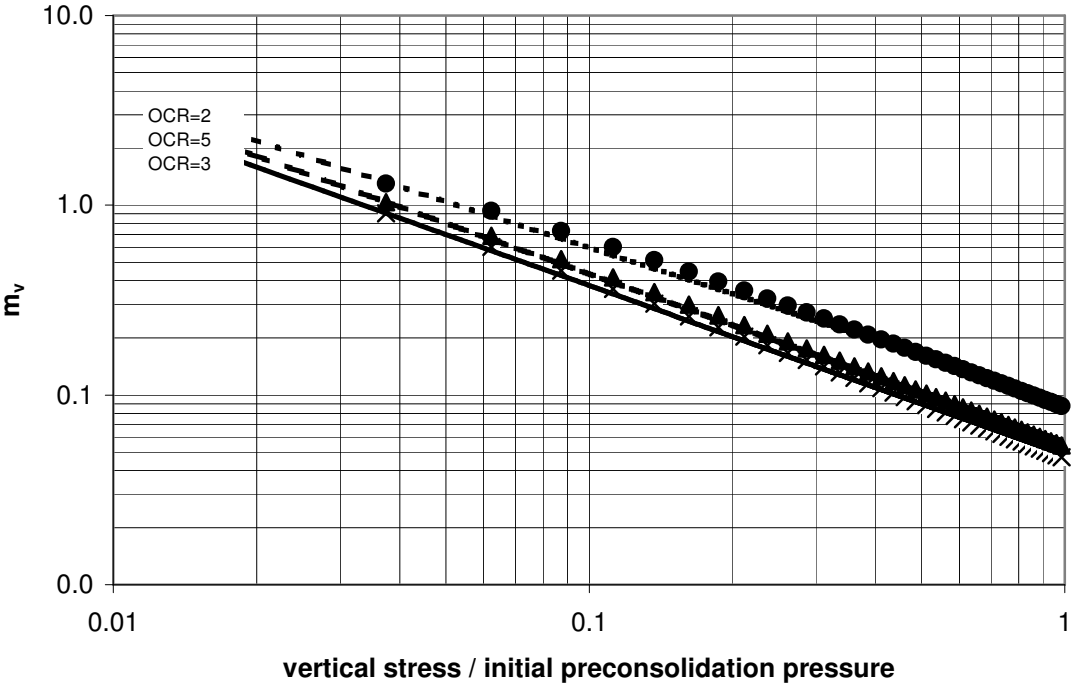

Figure 4.26 Coefficient of Volume Compressibility vs. Normalised Stress Plot for JCU2_L5

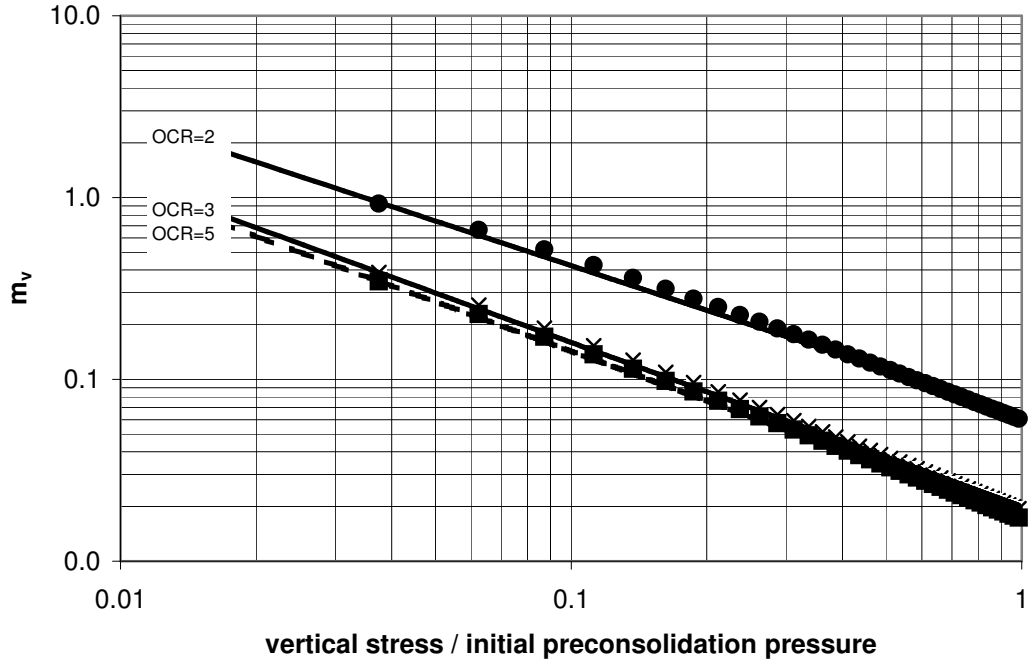

Figure 4.27 Coefficient of Volume Compressibility vs. Normalised Stress Plot for JCU2_L6

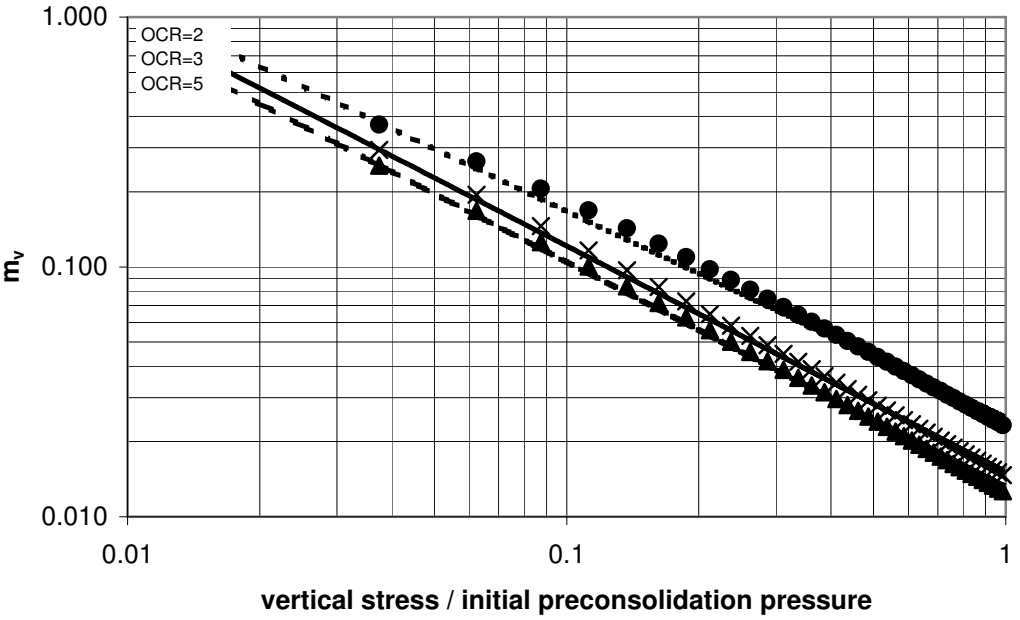

Figure 4.28 Coefficient of Volume Compressibility vs. Normalised Stress Plot for JCU2_L7

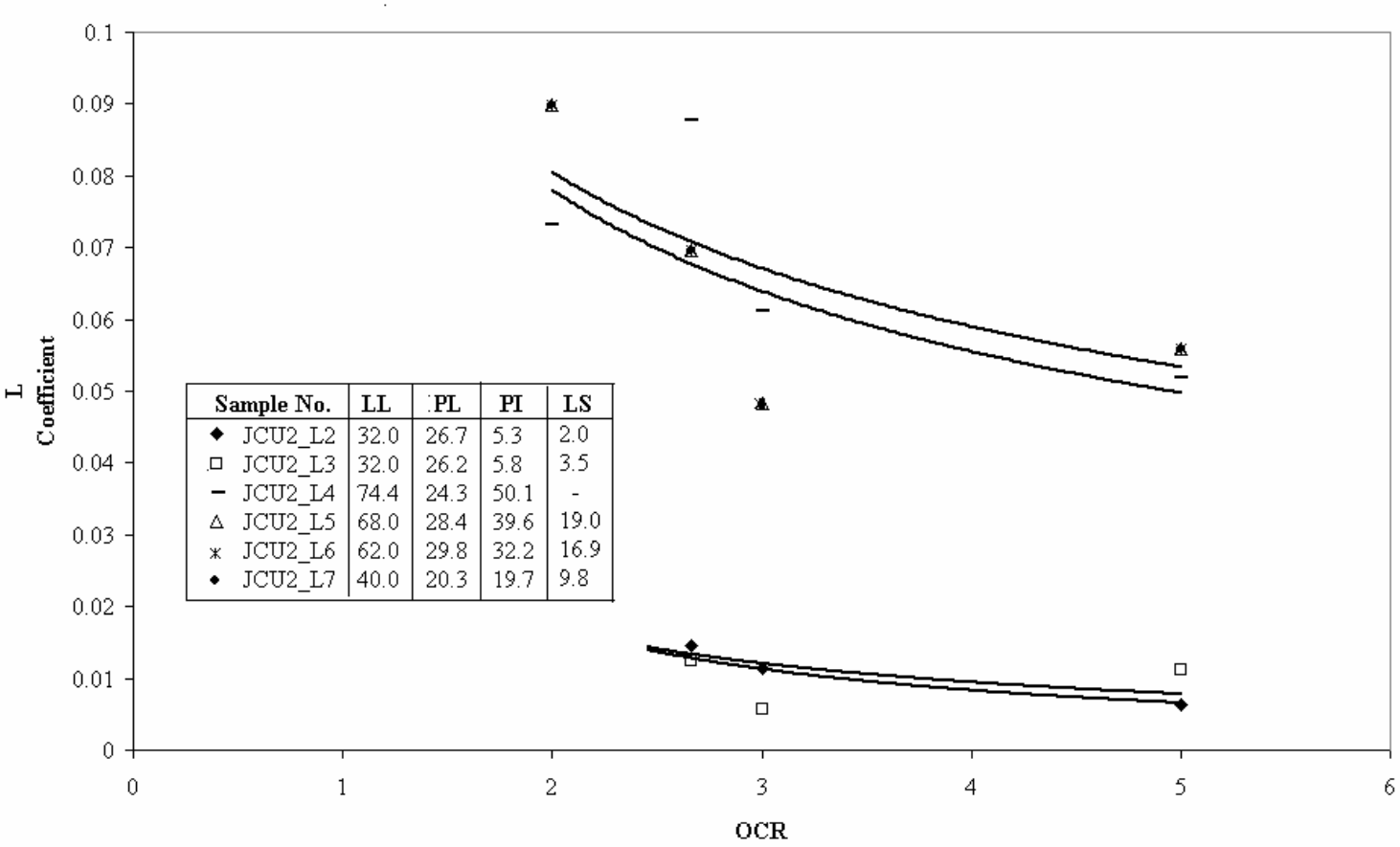

Figure 4.29 L Coefficient for Empirical m_v Equation

By substituting Equations 4.31, 4.32a and 4.33c back into Equation 4.30, an overall equation relating m_v (in MPa^{-1}) to OCR and index properties is obtained. It should be noted that the preconsolidation pressure referred to by this equation is the in-situ preconsolidation pressure of the specimen, and $\sigma_{v,current}$ is the pressure equivalent to the current vertical pressure that the sample is under. This ratio $\frac{\sigma_{v,current}}{\sigma_{p(initial)}}$ is not, therefore, equivalent to 1/OCR, and can achieve values less than or greater than 1.

$$m_v = (0.002LL - 0.054)(OCR)^{1.193-0.259\ln(LS)}\left(\frac{\sigma_{v,current}}{\sigma_{p(initial)}}\right)^{0.9} \qquad \text{(Eqn. 4.33)}$$

4.11 Coefficient of Consolidation (c_v)

4.11.1 General

The primary consolidation behaviour of a soil is commonly characterised using linear elastic Terzaghi's consolidation theory. Although not strictly correct, due to its assumption of constant coefficients of volume compressibility and permeability, this theory is widely taught and is commonly used for predicting the primary settlement of structures on soft soil. One of the fundamental parameters for this theory is the coefficient of consolidation.

Coefficient of consolidation, c_v, describes the rate at which the compression of the soil layer takes place for the primary consolidation phase, and is obtained using the time-compression data from a routine one-dimensional consolidation test.

Typically, either of the two popular curve-fitting methods developed by Casagrande and Fadum (1940) or by Taylor (1942) is used. Often, the coefficient of consolidation determined using Taylor's method is slightly greater than calculated using the Casagrande method.

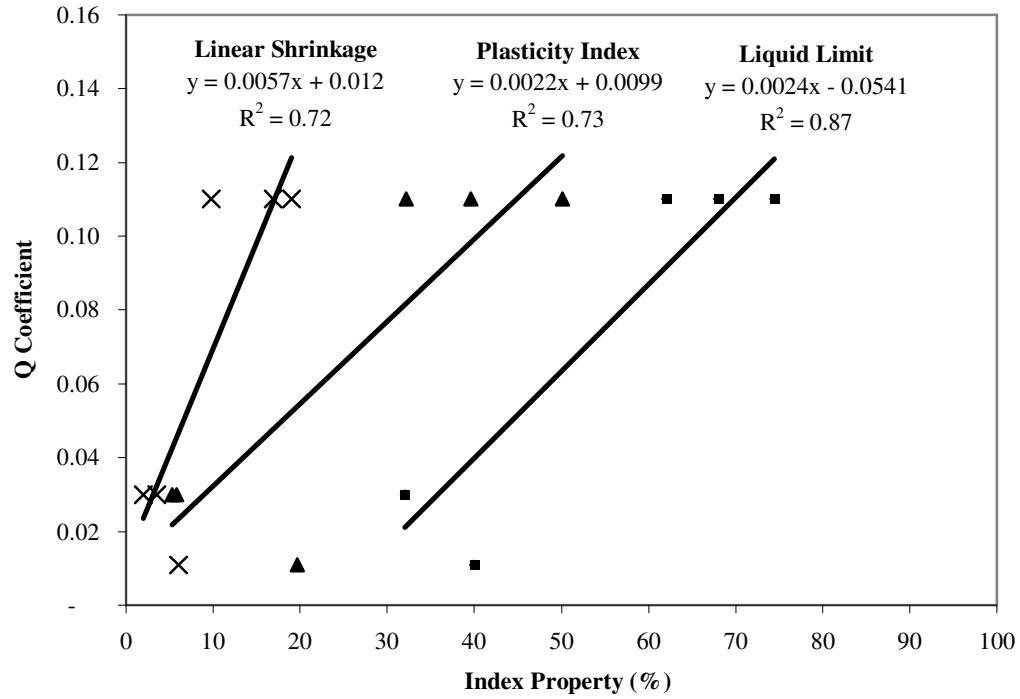

Figure 4.30 Correlation of Q Coefficient with Liquid Limit, Plasticity Index and Linear Shrinkage

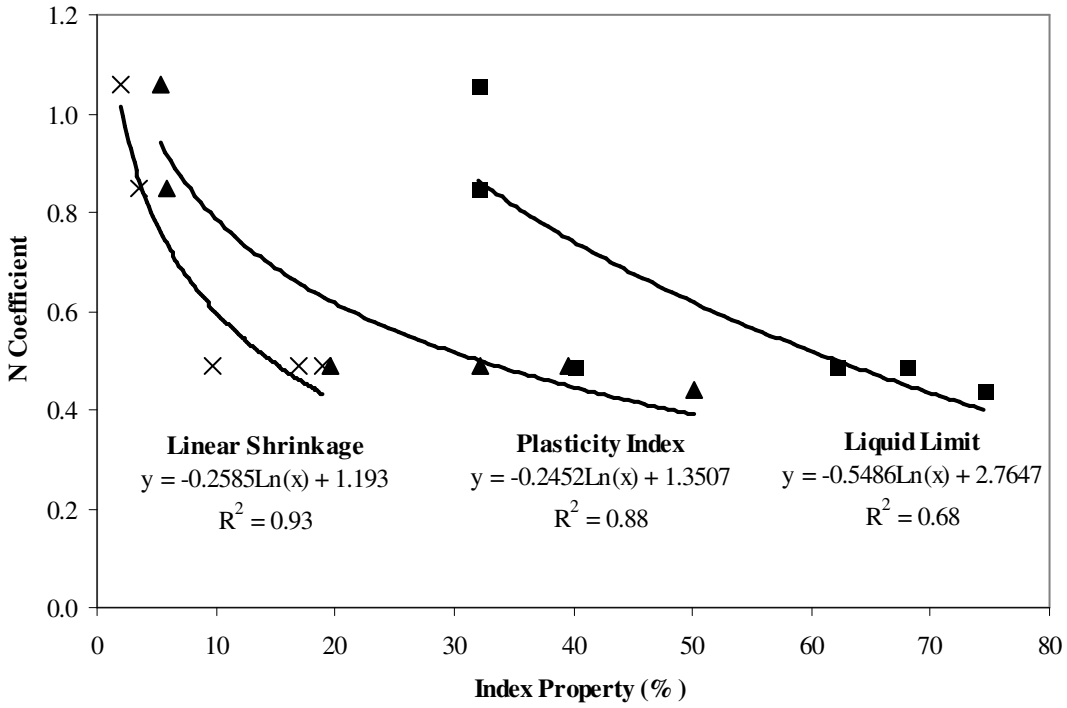

Figure 4.31 Correlation of N Coefficient with Liquid Limit, Plasticity Index and Linear Shrinkage

However, a large number of other curve fitting procedures have also been published, including the velocity method (Pankin et al, 1978), hyperbola method (Sridharan and Prakash, 1985), early stage log-t method (Robinson and Allam, 1996), inflection point method (Pankin et al., 2000), and least squares method (Chan, 2003). Sridharan and Prakash (1995) discussed five of the different approaches and their individual shortcomings.

4.11.2 Correlation of c_v with Index Properties

The presence of so many methods suggests that none are completely satisfactory in the evaluation of c_v, and that prediction by means of a correlation between c_v and index properties would be both desirable and highly useful for design purposes.

Limited research has been published with regards to this field. The first relationship documented was within an internal design manual (NAVFAC DM-71) formulated by the US Navy in 1971. It presented a figure that plotted coefficient of consolidation against liquid limit, and marks a generalised curve for undisturbed soils in the range of the virgin compression line. Lower and upper limit curves are also marked on the plot. These curves correspond to soils in the recompression phase (lower curve) and completely remoulded soils (upper curve) respectively.

Subsequent to this, Carrier (1985) suggested an expression for c_v in terms of activity (A), liquidity index (LI) and plasticity index (PI). Carrier (1985) concluded within his paper that this prediction equation is strongly influenced by the water content of the given clay and that c_v decreases with decreases in water content.

$$c_v = \frac{9.09x10^{-7}}{PI}\left(\frac{\left(1.192+A^{-1}\right)^{6.993}\left(4.135LI+1\right)}{\left(2.03LI+1.192+A^{-1}\right)^{7.993}}\right) \qquad \text{(Eqn. 4.34)}$$

Most recently, Sridharan and Nagaraj (2004) found the following relationship relating shrinkage index (SI) to coefficient of consolidation. Shrinkage index is equal to plastic limit minus shrinkage limit. The units for c_v in this equation are m^2/s.

$$c_v = 0.03*(SI)^{-3.54} \quad \text{(Eqn. 4.35)}$$

However, shrinkage limit is considered subject to significant uncertainty and is thus no longer commonly conducted. This test is prone to errors resulting from entrapped air bubbles in the dry soil specimen, as well as cracking during drying and weighing (Holtz, 1981).

Due to the absence of Atterberg Limits for Site C, no analysis could be undertaken on that data. Analyses of the results suggest that the index property showing the strongest correlation is plasticity index. However, this association is not considered significant, as correlation coefficients for all loading stages registered values of 0.55 or less.

4.11.3 Measured c_v Values

Minimum and maximum values of c_v for both the overconsolidated and normally consolidated regions of the void ratio plot are shown in Appendix I. Generally, coefficient of consolidation is an order of magnitude larger for the overconsolidated region as compared to the normally consolidated region. The results from this investigation (shown in Appendix I), showed that the average $\frac{(c_v)_{OC}}{(c_v)_{NC}}$ ratios for both the minimum and maximum values were less than 10 in most cases (see Table 4.11).

Table 4.11 Minimum and Maximum Measured $\frac{(c_v)_{OC}}{(c_v)_{NC}}$ Ratios

Location / Source	Average $[(c_v)_{OC} / (c_v)_{NC}]_{min}$	Average $[(c_v)_{OC} / (c_v)_{NC}]_{max}$
Site A	1.87	3.30
Site B	1.11	7.74
Site C	3.15	10.88
Davis (1999) Data	11.80	4.94

4.12 Coefficient of Secondary Compression, C_α

As previously stated, determination of the total amount of settlement, as well as the rate of settlement, are integral to any embankment analysis. Furthermore, often it is the settlement criterion that governs many of the design considerations.

Secondary compression is the compression that fine grained soils experience following the dissipation of all excess pore pressure resulting from loading. It occurs under constant vertical effective stress, and is also sometimes referred to as 'creep'. It is characterised using the coefficient of secondary compression, C_α. This coefficient is defined as the slope of the final portion of time compression curve on the semi-log plot, and is given by:

$$C_\alpha = \frac{\Delta e}{\Delta \log t} \qquad \text{(Eqn. 4.36)}$$

Significant research has been undertaken within this field, an extensive number of factors have been cited in literature as the causes of secondary compression. A number of these were described by Sridharan and Prakash (1998) and include, but are not restricted to, the plastic deformation of the adsorbed water, gradual readjustment of the frictional forces, creep jumping of bonds and viscous structural reorientation. Clearly, despite the extensive research, the mechanisms controlling the secondary compression of soils are very complex phenomena which are not yet understood.

Four main assumptions were summarised by Raymond and Wahls (1976) for consideration when calculating the secondary compression of fine grained soils. These assumptions were:

- C_α is independent of time (at least during the time span of interest)
- C_α is independent of the thickness of the soil layer
- C_α is independent of the LIR, as long as some primary consolidation occurs; and

- The ratio of C_α/C_c is approximately constant for many normally consolidated clays over the normal range of engineering stresses

The results and analysis presented within this section deal with the last two assumptions.

4.12.1 C_α/C_c Ratios

Mesri and Godlewski (1977) examined the fourth of these assumptions, and found that the C_α/C_c ratio ranged between 0.025 and 0.085 for a wide variety of soils (see Table 4.12). Mesri and Castro (1987) extended this range slightly to suggest typical values between 0.02 and 0.1. Furthermore, they suggested that a nominal value of $C_\alpha/C_c = 0.05$ be used for natural soils in the absence of any data. Ameratunga (2006) suggests that C_α for South East Queensland clays varies between the values of 0.005 to 0.02, with higher values obtained in the case of peats or organic clays.

Oedometer testing on Site A samples did not allow for the calculation of C_α, and thus, ratios were not determined. C_α/C_c ratios calculated for Sites B and C, as well as the Davis (1999) data, registered ranges lesser than that suggested by Mesri (1977). Site B ratios were between 0.007 and 0.038, Site C between 0.005 and 0.081 and Davis (1999) data between 0.006 and 0.021. Lower values such as these were also measured for soft clays underneath the Ballina bypass near the New South Wales border (Ewers, 2000) and also for Hong Kong marine clays (Zhu, 2001). The C_α measurements used to compute this ratio for each sample are detailed in Appendix J.

4.12.2 Dependence of Creep on Soil Index Properties

A review of available literature indicated that the majority of research on secondary compression was on the methods of determining C_α, mechanisms causing it and factors governing it. Very few, however, appeared to have attempted to relate this parameter to the index properties of a soil.

To examine the relationship between Atterberg Limits and the coefficient of secondary compression, samples from each of the source sets were plotted with the Atterberg limit on the x-axis, and its C_α on the y-axis.

As seen in Figure 4.32, a distinctly increasing trend of C_α with increasing index propety was observable for Site B. Equations for these trends are given below. The correlation coefficient values for each of these equations were 0.96, 0.97 and 0.93 respectively. No further trend was detected with respect to plasticity limit.

Liquid Limit: $C_\alpha = 0.0002e^{0.0607(LL)}$ (Eqn. 4.39)

Plasticity Index: $C_\alpha = 0.0007e^{0.0642(PI)}$ (Eqn. 4.40)

Linear Shrinkage: $C_\alpha = 0.0008e^{0.1093(LS)}$ (Eqn. 4.41)

These graphs suggest that C_α correlates most strongly with plasticity index, however, that it is also strongly influenced by both liquid limit and linear shrinkage. However, further attempts to correlate the coefficient of secondary compression yielded vastly different and varying results for Site C and Davis (1999) data. No discernable trend was apparent for Site C, while Davis (1999) data actually showed a decrease in C_α with increasing Atterberg Limit (see Figure 4.33). Correlation of C_α with the Atterberg limits examined for Site B produced the strongest trend for linear shrinkage, followed by liquid limit, and then linear shrinkage. Again, no further trends were discernable for plastic limit or liquidity index.

4.12.3 Stress Level Dependency of Creep

The effect of creep on preconsolidation pressure was first presented conceptually by Bjerrum (1972). Figure 4.34 illustrates his concept of 'artificial aging'. It shows that if an oedometer soil sample is loaded from its in-situ effective stress at Point "a" to end of primary consolidation at Point "c", and then the surcharge removed after a certain time period (Point "d"), then the stress level is reduced to that of Point "e". The creep rate at this point will now be significantly lower than its in-situ stress state. The

parallel lines (or isotaches) on this figure, represent the creep independent of stress level. The reducing creep strain rate is equivalent to one order of magnitude reduction with each log time cycle (Wong, 2006a).

Table 4.12. Values of C_α/C_c for Natural Soils (after Mesri & Godlewski, 1977)

Soil	C_α / C_c
Organic Clays and Silts	0.035 – 0.060 0.040 – 0.060
Amorphous and Fibrous Peats	0.035 – 0.085
Canadian Muskeg	0.090 – 0.100
Leda Clay (Canada)	0.030 – 0.060
Post-glacial Swedish Clay	0.050 – 0.070
Soft Blue Clay (Victoria, B.C.)	0.026
Sensitive Clay, Portland, ME	0.025 – 0.055
San Francisco Bay Mud	0.040 – 0.060
New Liskeard (Canada) Varved Clay	0.030 – 0.060
Mexico City Clay	0.030 – 0.035
Hudson River Silt	0.030 – 0.060
New Haven Organic Clay Silt	0.040 – 0.075

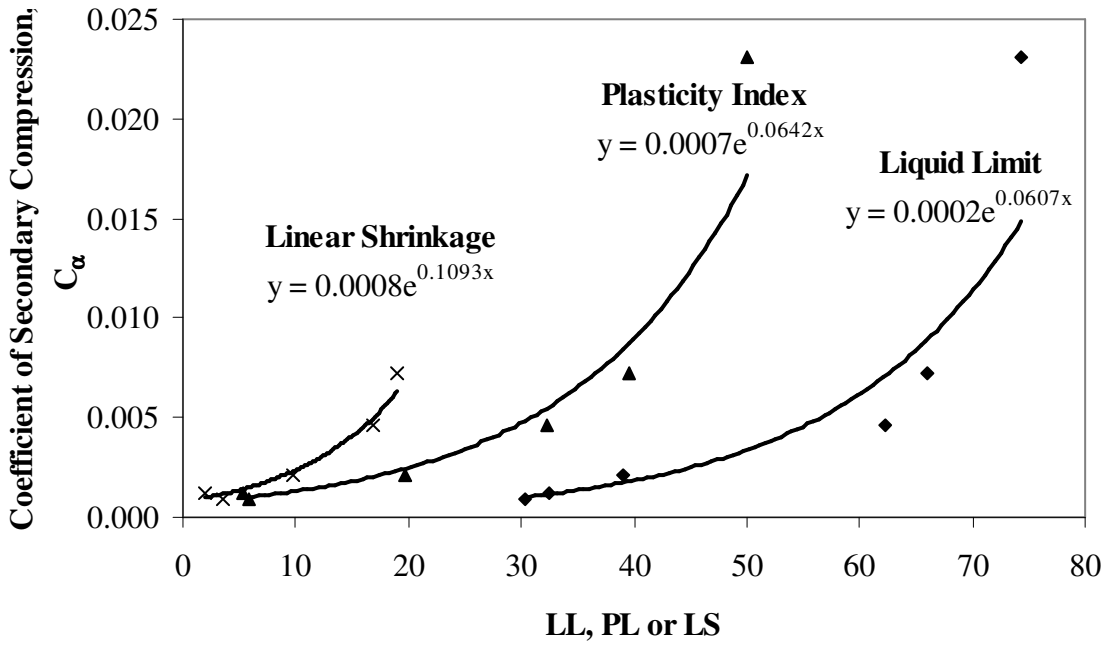

Figure 4.32 Correlation of C_α with Atterberg Limits for Site B

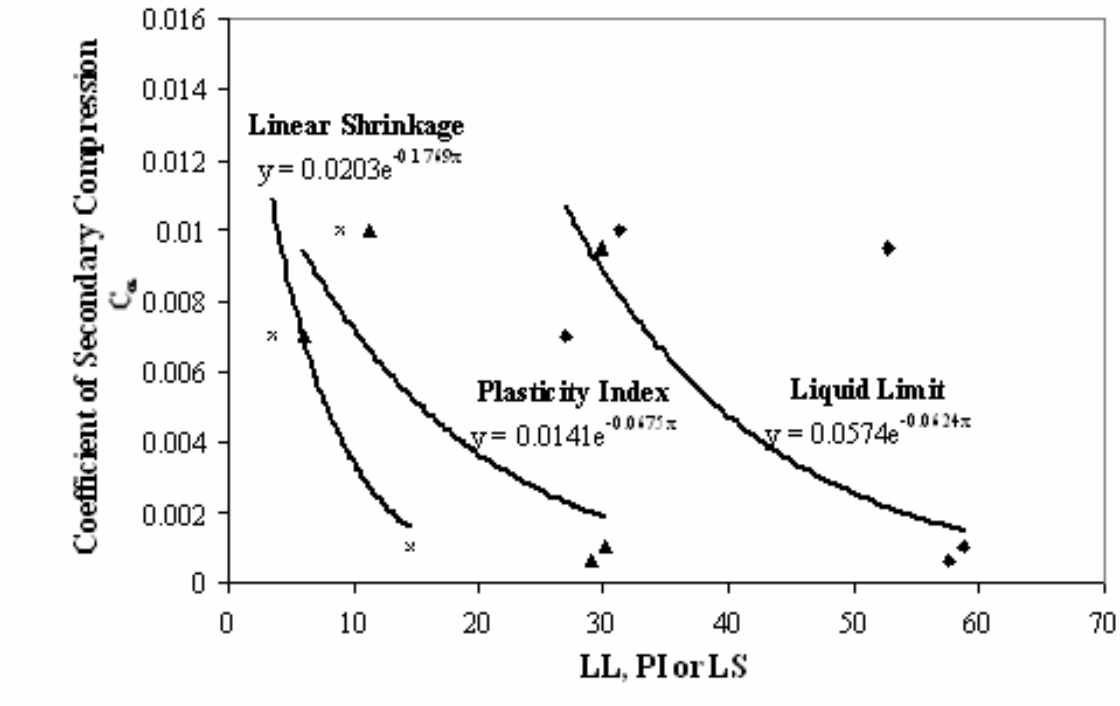

Figure 4.33 Correlation of C_α with Atterberg Limits for Davis (1999) Data

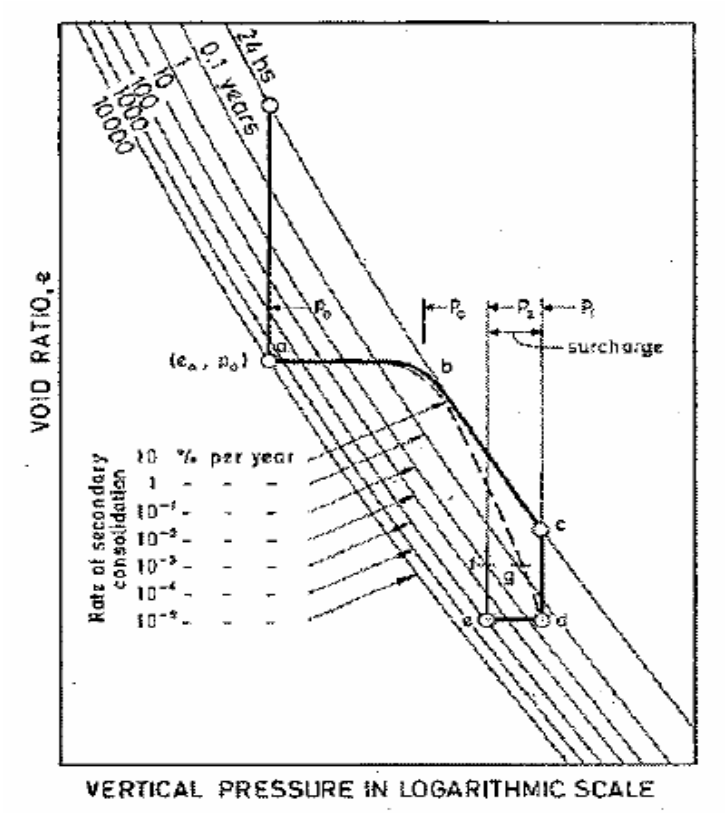

Figure 4.34 Effects of Geological History on Rate of Creep (Bjerrum, 1972)

The coefficient of secondary compression is both history and stress level dependent. Studies of the stress level dependence of this parameter have been carried out by Nash et al. (1992) and Ewers and Allman (2000). The results of these tests are shown in Figure 4.35 (a) and (b).

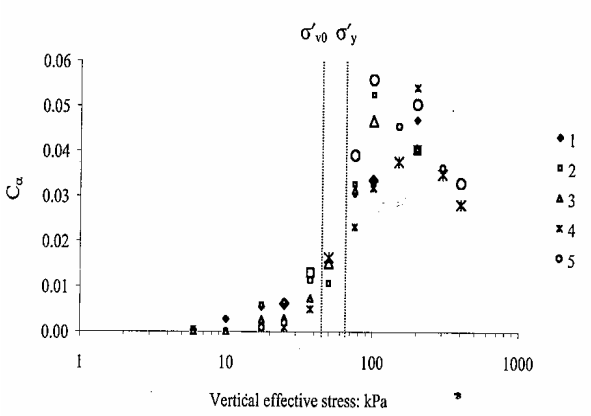

(a)

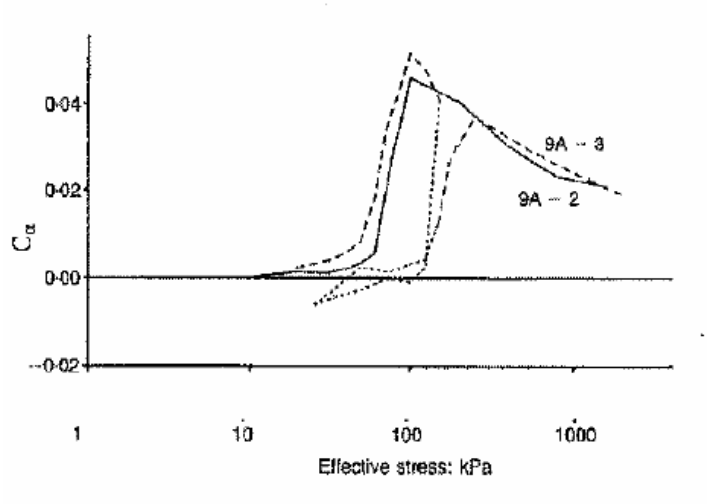

(b)

Figure 4.35 Results of Studies involving the Stress Dependence of Creep (a) Nash et al. (1992) and (b) Ewers and Allman (2000)

Alonso et al. (2000) alternatively presented this stress dependence by graphing the reduction in rate of creep with overconsolidation ratio. Further studies by Magnan (2001) produce a smooth 'S' shaped plot of 1/OCR against creep strain. Wong (2006b) described this plot using Equation 4.37.

$$\frac{C_{\alpha e(OC)}}{C_{\alpha e(NC)}} = \frac{(1-m)}{e^{(OCR-1)n}} + m \qquad \text{(Eqn. 4.37)}$$

where OCR = overconsolidation ratio

$C_{\alpha e\,(OC)}$ = creep strain rate per log time cycle for an overconsolidated soil at a particular OCR

$C_{\alpha e\,(NC)}$ = creep strain rate per log time cycle for an normally consolidated soil (OCR = 1)

m and n = constants depending on soil type (in the absence of site specific data, m = 0.1 and n = 6 may be used for organic soils)

$C_{\alpha e}$ within this equation relates to the creep strain rate, and is defined using Equation 4.38 (where e_0 = initial void ratio).

$$C_{\alpha e} = \frac{C_{\alpha}}{1+e_0} \qquad \text{(Eqn. 4.38)}$$

Implementation of this equation, however, is difficult due to the site specific *m* and *n* constants, and also determination of $C_{\alpha e\,(NC)}$, as this parameter is not constant within the normally consolidated range.

Using Site B samples, the dependence of C_{α} with OCR was examined. Results from the laboratory testing yielded a very distinct trend of decreasing C_{α} with increasing overconsolidation ratio.

An example of this decreasing trend is shown in Figure 4.36. For clarity, only nine of samples have been plotted, and power trendlines fitted. From this plot, the overall general relationship between C_{α} and OCR is given by Equation 4.39.

$$C_{\alpha} = 0.01(OCR)^{-1.25} \qquad \text{(Eqn. 4.39)}$$

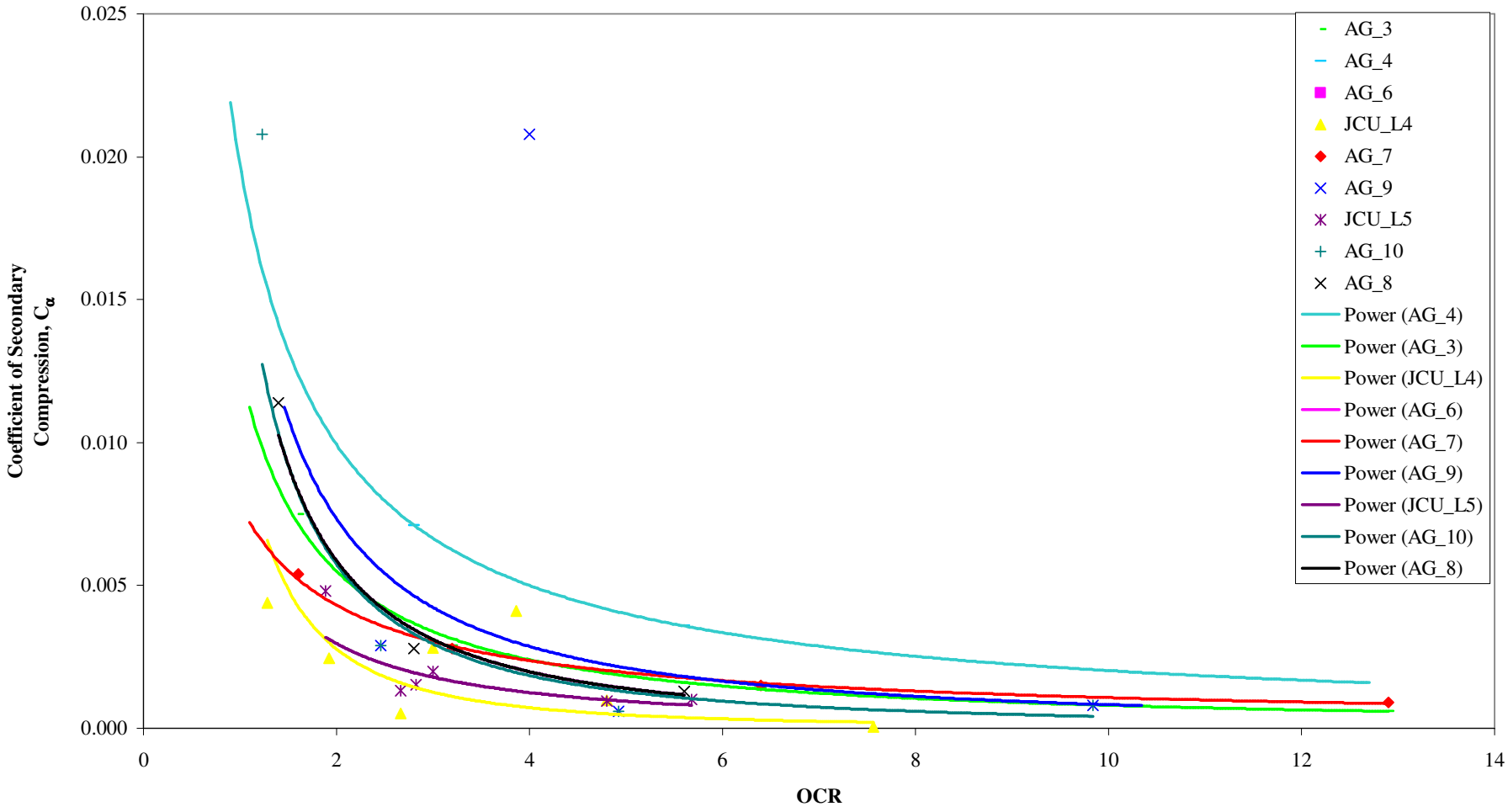

Figure 4.36 Results of Studies involving the Stress Dependence of Creep in Overconsolidated Soils at Site B

Furthermore, it can be seen from this plot that for samples with an OCR of less than approximately 3.5, the difference in C_α magnitude between unit OCRs is significant. While still showing a decrease in C_α with increased OCR, the rate of change in C_α magnitude is much more gradual for samples with OCR's greater than 3.5.

However, caution is urged when using this general relationship. This relationship has been developed for soils similar to Site B (LL_{mean} = 50.7, PL_{mean} = 25.2). As described previously within Section 4.12.2, C_α is also affected by the index properties of a soil. This influence has not been taken into account when deriving this equation.

Figure 4.35 shows examples of the stress dependence of C_α in normally consolidated clays. C_α remains low for stress increments below the in situ vertical stress and increases to a peak stress value slightly larger than the preconsolidation pressure of the sample before decreasing again in value. The results by both Ewers and Allman (2000) and Nash et al. (1992) show this behaviour to a degree (see Figure 4.35). This decreasing trend continued to a further low point, before C_α once again started increasing.

The author believes that the behaviour displayed with regards to the magnitude of creep coefficient with increasing effective stress is similar to that displayed by the volume compressibility coefficient (m_v) used in primary consolidation. To evaluate this hypothesis, the data presented by Ewers and Allman (2000) was reanalysed. This data was selected for examination in lieu of the data from Sites B and C because of its reduced pressure increments. The reduced pressure increments of this data allowed examination of the behaviour around the preconsolidation stress of the soil.

By using the method outlined in Sections 4.10.2 and 4.10.3, the true m_v vs effective stress plot was determined for the Ewers and Allman (2000) results. The e_0, C_r, C_c and σ_p' of the sample analysed were 2.74, 0.28, 1.23 and 70 kPa respectively. Figure 4.38 presents this analytical plot alongside corresponding C_α values for the sample.

As with the m_v trend, the peak in C_α values is easily noticeable. However, this peak occurs at a pressure which exceeds the preconsolidation pressure of the soil. This shift

is hypothesised to be a result of the onset of creep during primary consolidation. This concept of simultaneous primary consolidation and creep has been examined and presented by Mesri et al. (1994).

Additionally, the initial decrease in values (at lower effective stress) does not appear to follow the same rate of change. The gradient of this decrease is calculated using C_r.

Thus, it is further suggested that the value of C_r also decreases in value as a result of the creep during consolidation.

4.13 Conclusions

A statistical study of data from laboratory testing taken from four different sources around Queensland was performed, and suitable correlations for estimating the consolidation response have been determined.

With respect to Atterberg limits, probability distribution functions were developed for each of the sites to establish the overall distribution of each limit over the sites. Such distributions can be used to examine the mean value of each of the Atterberg Limits, and also to give an indication of the probability of a given measurement falling close to this value for soils in the vicinity of these sites.

From these beta distribution curves it can be seen that, with the exception of plasticity index for Site B, index properties followed a bell shape which is perfectly symmetrical, or only slightly skewed to the right. Furthermore, it shows that triangular distributions should be expected for sites with clays of low plasticity (as was the case with Site B).

Studies also yielded the following relationship to describe the dependence of liquid limit on plastic limit. Similar general relationships ere found by linear regression analysis undertaken by Gutierrez (2006) on Uruguay clays, and also by Costet and Sanglerat (1975) for French and Spanish soils.

$$PL = 0.289LL + 10.326$$

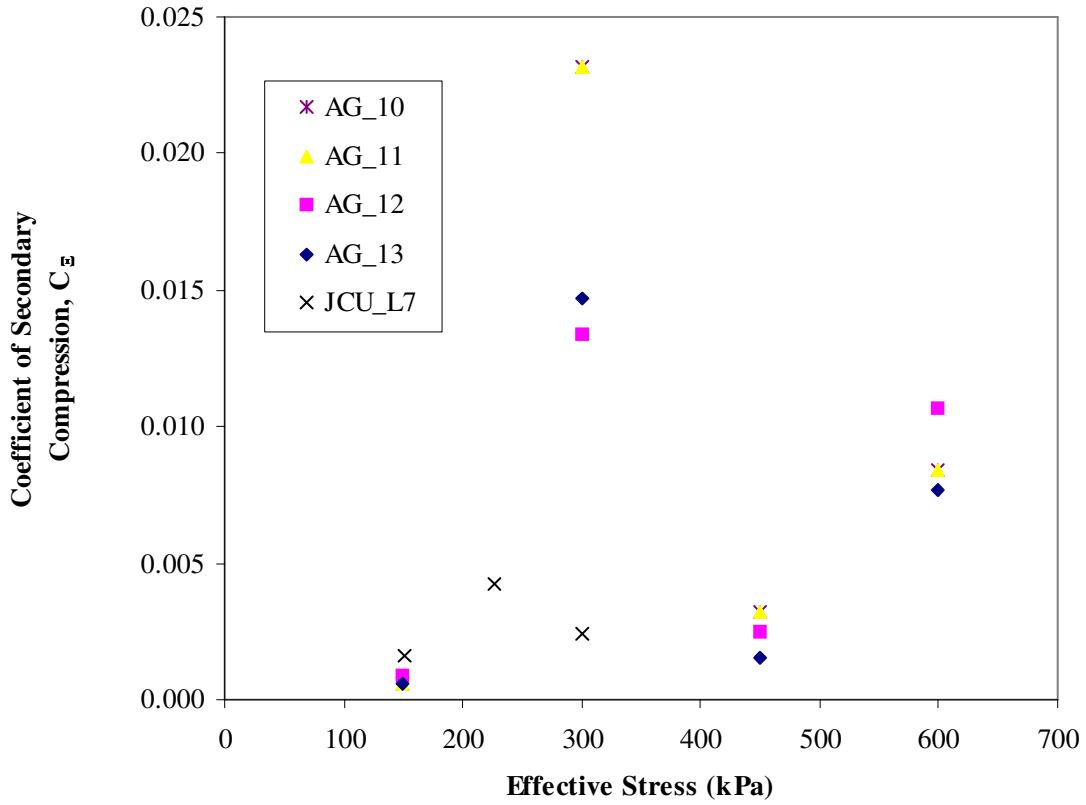

Figure 4.37 C_α vs Effective Pressure for Normally Consolidated Samples

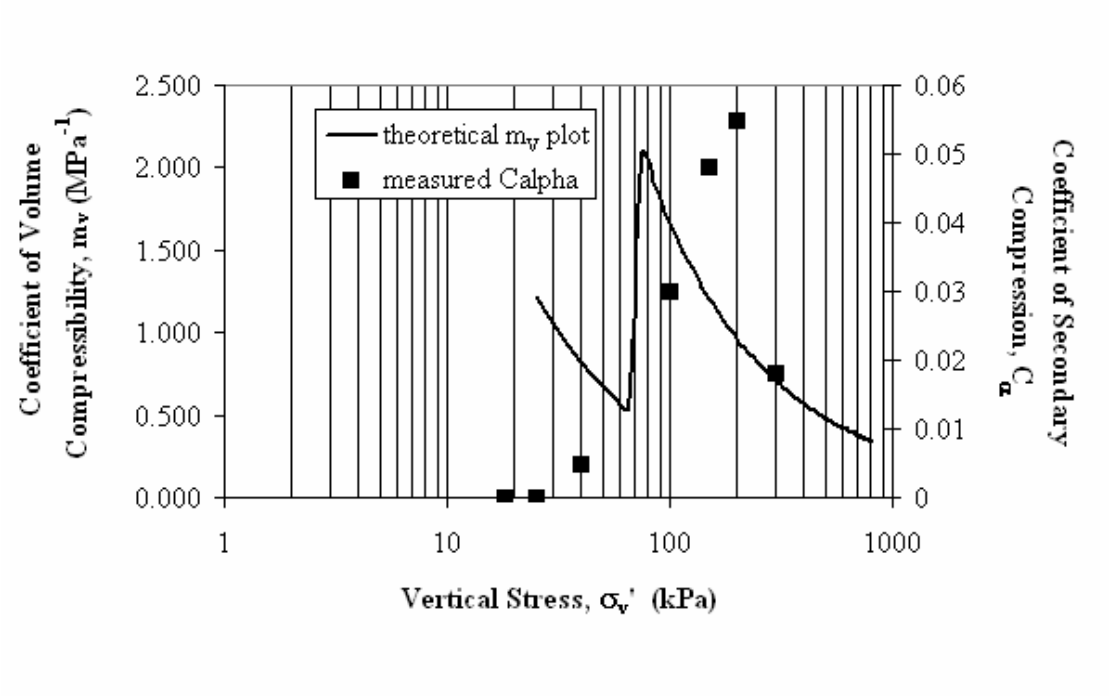

Figure 4.38 C_α and m_v vs. Effective Pressure for Ewers and Allman (2000) Data

From this analysis, it is also quite clear that regardless of the source from which the clays were taken, the general overall distribution curve for natural water content of Queensland clays will follow a bell shape, exhibit little or no skew from the mean, and have a coefficient of kurtosis in the order of 2.5.

Results of 99 samples from Sites A, B and C yielded a mean value of 2.56 with a standard deviation of 0.09, and a coefficient of variation of about 0.04. This slightly lower value of specific gravity is hypothesised to be a result of the high organic matter frequently present within Queensland clays along the Eastern coastal belt.

The applicability of a number published correlations in quantifying the compression indices of Queensland clays was investigated. It can be seen from Figure 4.16 that correlations involving liquid limit tend underestimate the compression index on a whole. Equations that best characterised the compression indices in terms of liquid limit, natural water content and initial void ratio.

$$C_c = 0.0034*LL^{1.282}$$

$$C_c = 0.005* w_n^{1.156}$$

$$C_c = 0.303*e_0^{1.383}$$

An analytical study on the derivation and selection of representative m_v values identified flaws in present practice, and also detailed the importance of stress increment reduction from the conventional unit LIR to approximately 10 kPa during m_v calculation. An example outlined within Section 4.9.3 further demonstrated this point.

Further testing was undertaken to determine the influence of index properties and OCR on the parameter m_v. As a result of these tests, the general equation below was able to be established. As defined previously in Section 4.10.4, the preconsolidation pressure referred to by this equation is the in-situ preconsolidation pressure of the specimen, and $\sigma_{v,current}$ is the pressure equivalent to the current vertical pressure that

the sample is under. This ratio $\frac{\sigma_{v,current}}{\sigma_{p(initial)}}$ is not, therefore, equivalent to 1/OCR, and can achieve values less than or greater than 1.

$$m_v = (0.002LL - 0.054)(OCR)^{1.193-0.259\ln(LS)}\left(\frac{\sigma_{v,current}}{\sigma_{p(initial)}}\right)^{0.9}$$

The above relationship was established by analysing the laboratory testing results of 6 different Site B samples and considering the r^2 values produced. Its applicability is therefore limited. To ensure the relevance of this generalised equation, further testing on a variety of different soils is required.

Examination of the correlation of coefficient of secondary compression with index properties yielded mixed results. Site B data suggested that liquid limit, plasticity index and linear shrinkage all influence the magnitude of C_α, however no discernable trend was apparent for Site C, and Davis (1999) data actually showed a decrease in C_α with increasing Atterberg Limit (see Figure 4.32). No further trends were discernable for plastic limit or liquidity index.

Data was also further investigated in terms of the dependence C_α on effective stress in both overconsolidated and normally consolidated samples. Results suggest that the magnitude of C_α decreases with increased overconsolidation ratio. An overall general relationship between C_α and OCR was suggested (see Equation 4.38). However, it is hypothesised that both the coefficient and power displayed by this relationship will change with increasing index properties.

As a result of this analysis, it is suggested that the relationship between effective stress and coefficient of secondary compression is similar to that of the coefficient of volume compressibility with effective stress. One can see intuitively that these two parameters are linked – m_v is slope of the consolidation curve during primary consolidation, and C_α is the slope of the consolidation line during secondary compression. The relationship of m_v with overburden is discussed in Section 4.10.

The stress at which maximum m_v was encountered was the in situ preconsolidation pressure of the soil. C_α peaks at a stress value in exceedance of this pressure. This shift in positioning is hypothesised to be a result of the onset of creep during primary consolidation. The recompression index of the soil is also hypothesised to decrease in value as a result of the creep during consolidation, as is the ratio of m_v to C_α.

However, it should also be stressed that consolidation settlement predictions are strongly dependent on the quality of sampling. As shown in Figure 4.39, the virgin compression curve obtained by high quality sampling is curvilinear for soft clays. Poor sampling will result in underestimation of the compression index C_c and overestimation of the recompression index, C_r, making determination of the overconsolidation pressure difficult. This topic is further discussed by Holtz and Kovacs (1981), and while every effort was taken to ensure high quality sampling on those tested within this research, some of the data obtained for analysis did show signs of poor sampling, and may have introduced slight errors into the equations obtained.

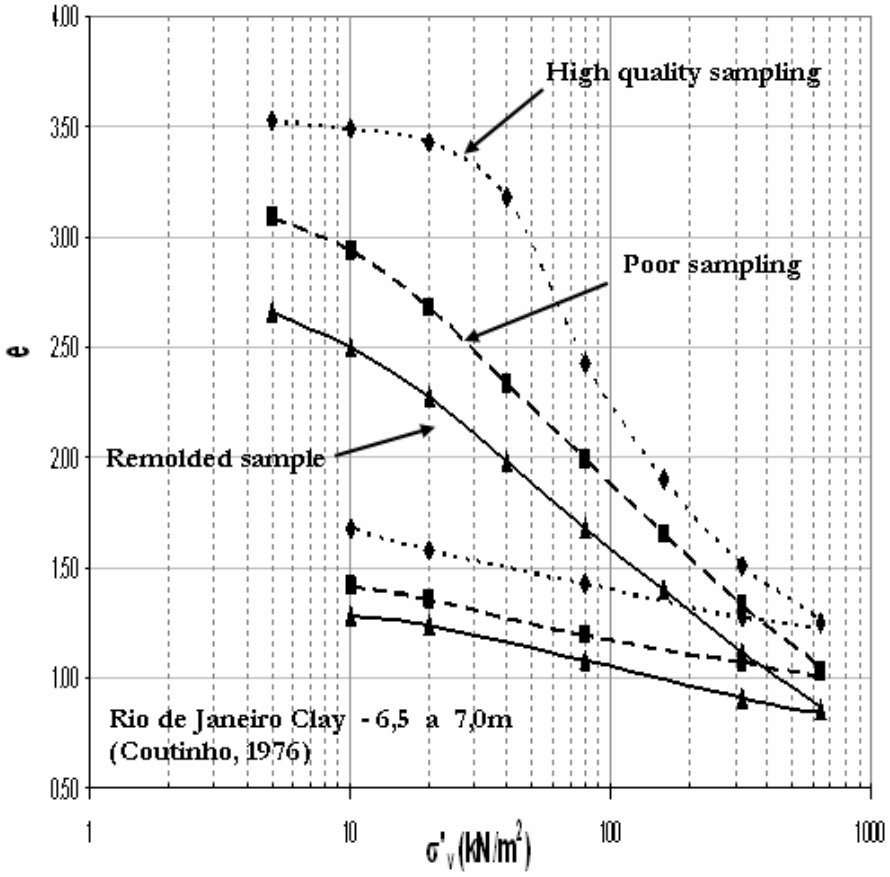

Figure 4.39 Effect of sample quality on Consolidation Curves (Coutinho, 1976)

CHAPTER 5

ANALYSIS OF A CASE HISTORY: SUNSHINE COAST MOTORWAY TRIAL EMBANKMENT

5.1 General

Located approximately 100 km north of Brisbane, the Sunshine Coast is one of Queensland's main tourist attractions, and one of Australia's fastest growing regions recording a high .rate of annual population growth of 3.6%, i.e. approximately 0.5 million by the end of 2021. As one of the major carriageways for the region, the Sunshine Coast Motorway provides an integral part of the South East Queensland road network, and not surprisingly is one of the key development projects for the Queensland Department of Main Roads.

A proposed route alignment through Area 2 of the 2nd stage of the Motorway (Figure 5.1) was fixed in October 1990. This particular area of the Motorway extends from the lowlands adjacent to the Maroochy River, and terminates 1.5 km south of Yandina-Coolum Road. Overall, the total length of this section measures approximately 4.7 km. The topography to be traversed within this stage of the Motorway was predominantly low lying (RL < 1.0 m) requiring significant earthworks along the majority of the route. Embankment construction was mainly in the order of 2-3 m in height, however, increased up to 7 m or more on the approaches to various structures along the route.

Initial site investigations were used primarily for the purpose of profiling the soil conditions along the proposed route. These tests showed that the original alignment would inevitably cross over large sections of highly compressible soft clays (undrained shear strength less than 10 kPa).

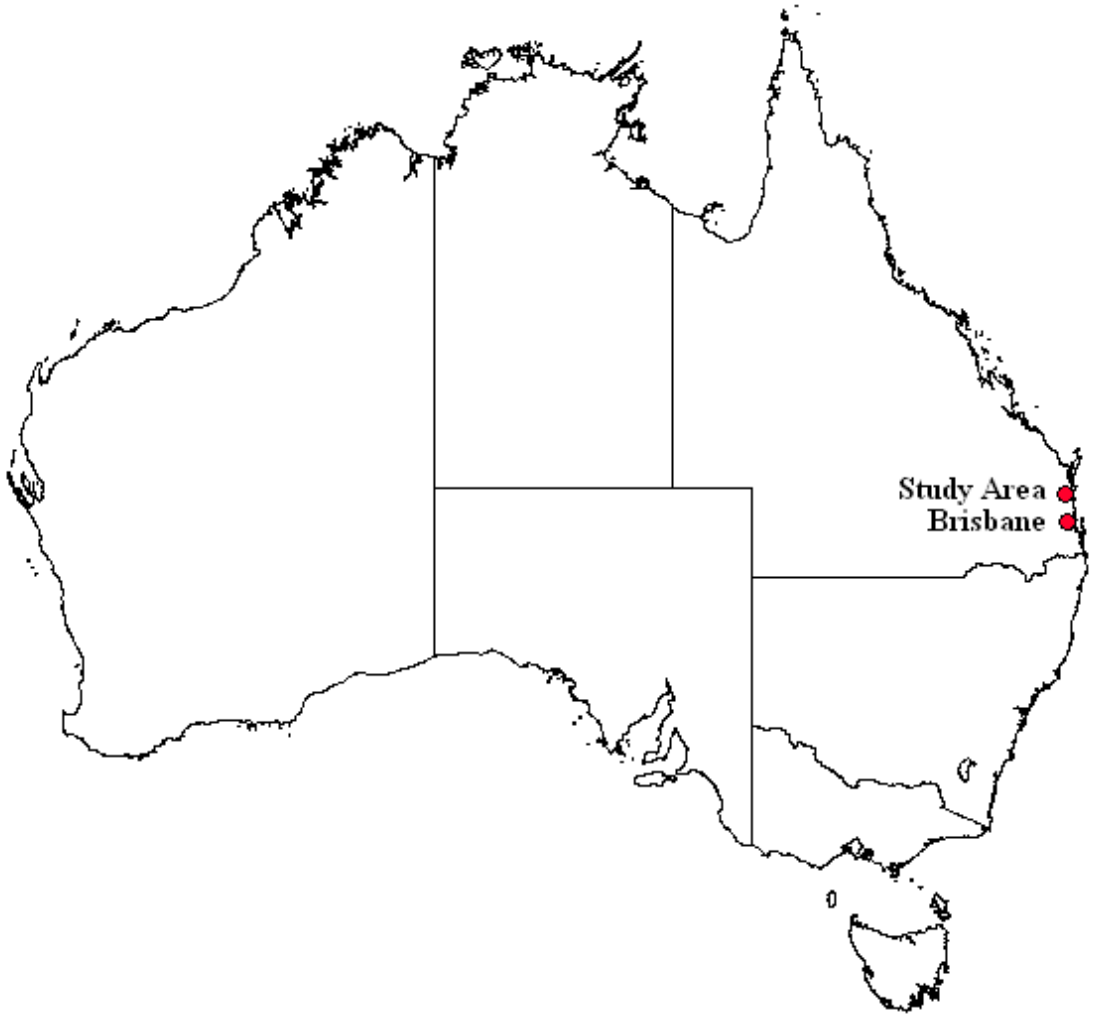

Figure 5.1 Map showing approximate location of Area 2, Stage 2 of the Sunshine Motorway

Road embankments constructed on soft soils are often subjected to large deformations, and can be rendered unserviceable due to excessive settlements. Following careful consideration, the proposed development path was moved further east, and a new alignment was fixed in December 1990. Additional geotechnical investigations undertaken along this new alignment showed that although soft clays were still traversed along the changed route, the area being crossed had been significantly reduced.

In order to meet several contractual requirements stipulated for the Motorway construction, and given the geotechnical problems expected with traversing such a large proportion of soft clay, a trial embankment was built to ensure the overall success of the project. This fully instrumented embankment (maximum height of

2.85m) allowed the soft clay foundation behaviour to be observed, and the parameters established for preliminary design to be verified. More significantly, this embankment provided a means of evaluating the effectiveness of prefabricated vertical drains (PVD). Construction was undertaken in multiple lifts over a period of approximately 2 months. PVDs were installed in a triangular pattern under two separate sections of the embankment.

This chapter describes the predicted and measured behaviour of the embankment and the underlying soft clay foundation. Field behaviour was simulated using a fully coupled Biot consolidation model, and the Modified Cam Clay theory was adopted for all clay layers, except for the compacted surface crust and the sand layer, which were modelled according to the Mohr-Coulomb theory. The effectiveness of PVDs was evaluated on the basis of excess pore pressure dissipation and both the vertical and lateral displacements below the embankment.

5.2 Geotechnical Investigations

Due to the large amounts of earthworks required, an extensive in-situ and laboratory testing schedule was undertaken by Queensland Dept. of Main Roads (1991a, 1991b, 1992) to profile the soils. The total scope of the investigation included:

- forty-eight (48) drill boreholes[1];
- ten (10) electric static friction cone penetrometer tests;
- sixty-four (64) standard bridge probes[2] and
- six (6) backhoe pits.

Standard Penetration Testing (SPT) and undisturbed soils sampling were also undertaken at boreholes drilled close to the pier or abutment locations. Boreholes were extended until the bedrock had been cored to a depth of 3m. Additionally, in-situ shear vanes were conducted along the entire length of the proposed route. The

[1] In some cases, holes were redrilled to obtain additional samples. The additional samples were identified using prefixes (e.g. DH5A)
[2] Several probes were redone. These probes were identified using suffixes (e.g. P15B)

recovered samples had a diameter of either 50 mm or 75 mm, and were individually tested for obtaining their index properties, organic content, natural moisture content and particle size distribution curves. Additionally, unconsolidated-undrained, isotropically consolidated undrained and consolidated-drained triaxial tests were performed on selected soft clay samples.

As mentioned previously, during initial profiling of the original route alignment, significant areas of soft and very soft, sensitive clay were encountered. Therefore, the alignment of the proposed development route was moved further east, and a new alignment fixed. Additional geotechnical investigations undertaken along this new alignment showed that although soft clays were still traversed along the route, the quantity being crossed was significantly reduced. The additional testing along this new alignment was limited and mainly used to verify that the soft clays present along the new route were similar in geotechnical properties to those along the old alignment.

5.3 Subsoil Conditions

Due to the limited amount of testing undertaken along the final alignment, soil properties were estimated using results from laboratory and field testing carried out along both the new and old alignments. A typical soil profile within Area 2, Stage 2 of the Sunshine Motorway is shown in Figure 5.2. As shown, testing revealed the existence of a 0.5 m thick weathered crust above 10 m of silty clay. Laboratory testing conducted on this clay layer indicated that it could be divided into three additional layers. The uppermost of these layers exhibited an average water content of 82% and an approximate liquid limit of 60%. The middle layer of clay, was a more plastic, and exhibited average water content and liquid limit values of 90% and 65%, respectively. The bottom layer of clay was much less plastic, with averaged water content and liquid limit of approximately 75% and 66%, respectively. Wijekulasuriya et al (1999) noted that the liquidity index exceeded 1.0 for all soil layers below the weathered crust, indicating a highly sensitive nature. Further underlying this soft clay was a clayey sand layer which extended to a depth of approximately 16 m below the ground level.

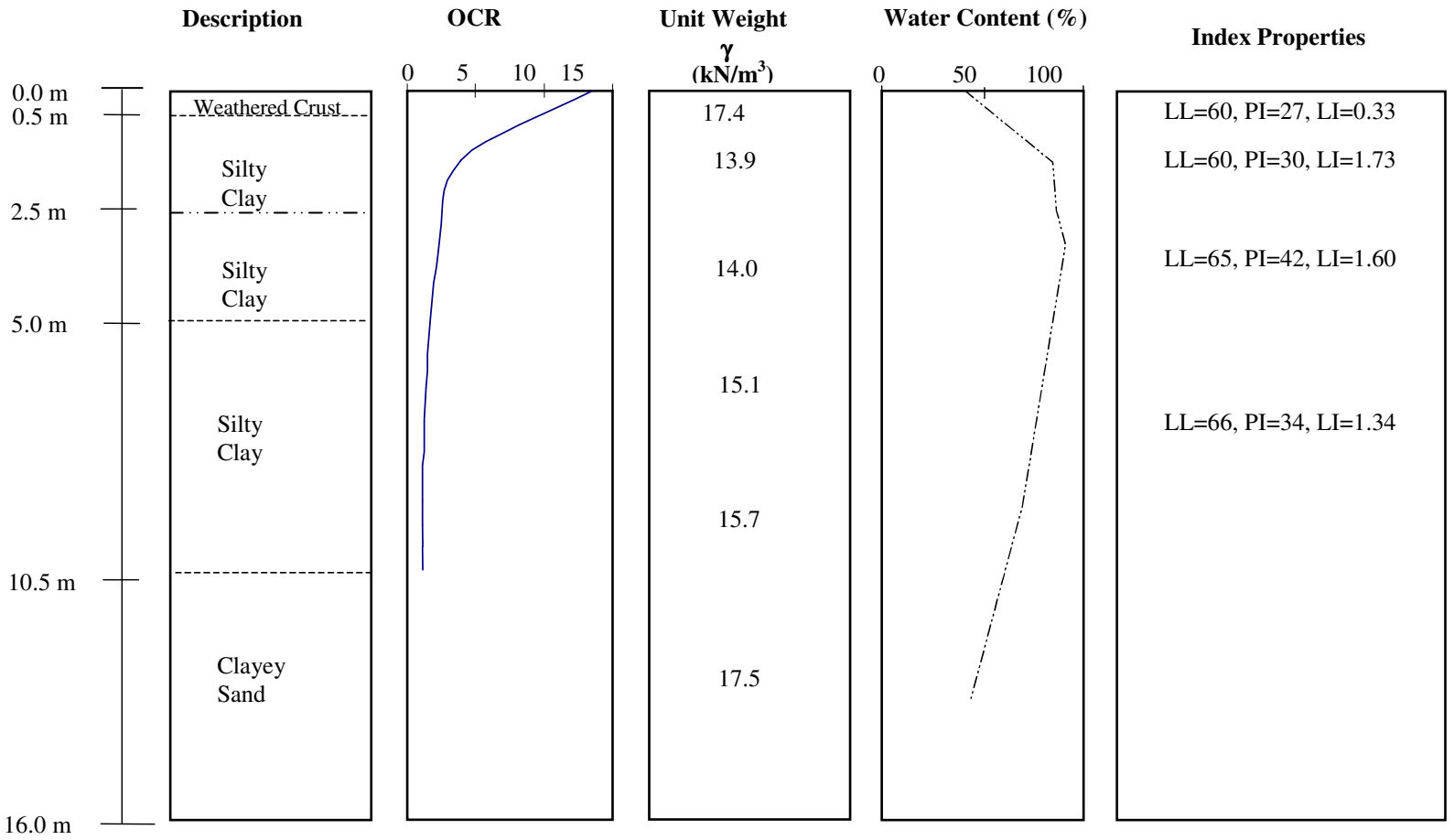

Figure 5.2 Typical Soil Profile beneath Area 2, Stage 2A of the Sunshine Motorway Alignment

Although many soft clays are normally consolidated, overconsolidation can sometimes occur close to the soil surface due to weathering, erosion and desiccation (Figure 5.2). It was also observed that the unit weight of the clay was fairly consistent with depth, ranging between 13.9 kN/m^3 and 15.7 kN/m^3, with the exception of the topmost compacted crust which measured 17.4 kN/m^3. Interestingly, the average specific gravity for all five layers varied between 2.48 and 2.63. These values are lower than the range normally expected for clayey soils (usually around 2.65) and can be attributed to the presence of organics within the soil. Average values of organic content reported by Litwinowicz (1994) range between 4.8% and 10.7% for layers within 10 m below the ground level.

Samples used in evaluating the subsoil conditions were taken in both vertical and horizontal directions. Consolidation tests were also undertaken on both vertically and horizontally orientated specimens. To obtain an indication of the permeability anisotropy, the average horizontal permeability was divided by the average vertical permeability giving a k_h/k_v ratio of 2.85. Field measurements also suggested a k_h/k_v ratio exceeding 2. Such anisotropy in permeability is comparable to observations made by other researchers for marine clays of similar properties (Bo et al, 2003). Table 5.1 details the permeability coefficients in the horizontal and vertical directions for selected samples.

Soil properties established through laboratory and in situ testing were unique to this project and differed substantially from any other soils encountered previously by Main Roads. This, in addition to the possibility of sample disturbance due to the high sensitivity of the soil, warranted the construction of a trial embankment to observe the real foundation behaviour, and also verify the design parameters previously established. In order to ensure effective sub-surface drainage of the Motorway, PVDs were chosen as the method of ground improvement below the surcharge loading, and .two different drain spacings (1 m and 2 m) were implemented.

5.4 Embankment Conditions

An observational approach, based on performance monitoring, is generally undertaken by Main Roads to address issues associated with uncertainties in ground conditions, design parameters and calculation methods (Wijeyakulasuriya et. al., 1999). The trial embankment considered herein, more specifically, was constructed to:

- assess the feasibility and stability of staged construction of the embankment,
- assess the effectiveness of the mandrel driven PVDs, and
- verify the compressibility and consolidation characteristics assumed for design calculations

The overall trial embankment design (see Figure 5.3) comprised of three sections (referred forthwith in this paper as Sections A, B and C respectively). The two primary sections (Sections A & B) were 35 m in length. Section A represented the design case (vertical drains installed at 1 m spacing) and Section B was the control (i.e. undisturbed virgin ground with only preloading applied). Section C measuring 20 m was used as an intermediate case with PVDs installed at 2 m spacings. Installation of vertical drains was in a triangular grid arrangement, and to a depth of 10 metres for both sections. In conjunction with Section A, Section C was used to assess the influence of drain spacing and the suitability of PVD in the stabilisation of Sunshine Coast soft clays.

The nominal crest width and height of all sections of the embankment were 17 m and 2.85 m respectively. Berms were constructed to widths of 5 m on the instrumented side of the embankment and 8 m on the opposite side. The height of all berms was approximately 1 m.

Table 5.1 Permeability Coefficients for Untreated Foundation Soils

Section ID	Parameter	Soil Layer					
		Layer	1	2	3	4	5
		Description	Weathered Crust	Silty Clay	Silty Clay	Silty Clay	Clayey Sand
		Depth (m)	0 – 0.5	0.5 – 2.5	2.5 – 5.0	5.0 – 10.5	10.5 – 16.0
All Sections	Vertical Permeability (m/s)	k_v	3.845×10^{-8}	4.136×10^{-8}	3.288×10^{-8}	9.400×10^{-9}	7.782×10^{-8}
	Horizontal Permeability (m/s)	k_h	6.298×10^{-8}	6.776×10^{-8}	5.438×10^{-8}	1.540×10^{-8}	1.324×10^{-7}

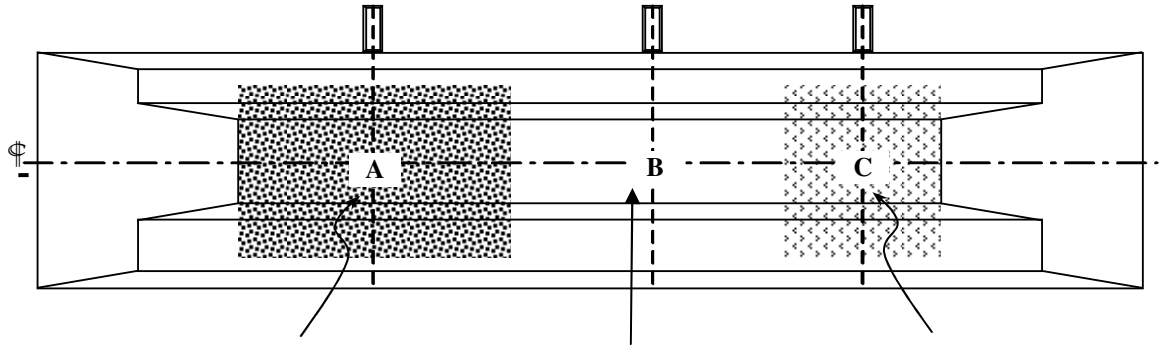

Figure 5.3 Sketch of Trial Embankment Design (Plan View)

Layout of instrumentation below the embankment was designed to optimize the range of equipment installed without sacrificing the quality and extent of information being gathered. The bulk of instruments were placed on one half of the embankment cross section.

A mixture of measurement devices were installed beneath the trial embankment for cross referencing purposes. The type of instrumentation included inclinometers, settlement gauges, horizontal profile gauges, piezometers (pneumatic, standpipe and vibrating wire) and earth pressure cells. The total number of instruments located below Section C was greatly reduced compared with both the design and untreated sections. The locations of each of the piezometers (PP & PV)[3], settlement gauges (SC) and inclinometers (I) used for verification purposes are shown in Figures 5.4, 5.5 and 5.6. These figures relate to Sections A, B and C respectively.

5.5 Numerical Modelling of Case Study

5.5.1 General

A numerical analysis of the trial embankment from this case study was undertaken using *FLAC*. A fully coupled Biot consolidation model was adopted to mimic the soft clay foundation behaviour below the embankment. This type of model has been found by other researchers, including Indraratna et al. (1997) to realistically represent the actual field behaviour of soft clays.

An overview of basics concerning *FLAC,* the programming of consolidation modelling, and also the conversion of 3-dimensional vertical drain systems to plane strain, is given in Chapter 2.

[3] PP = pneumatic piezometer; PV = vibrating wire piezometer

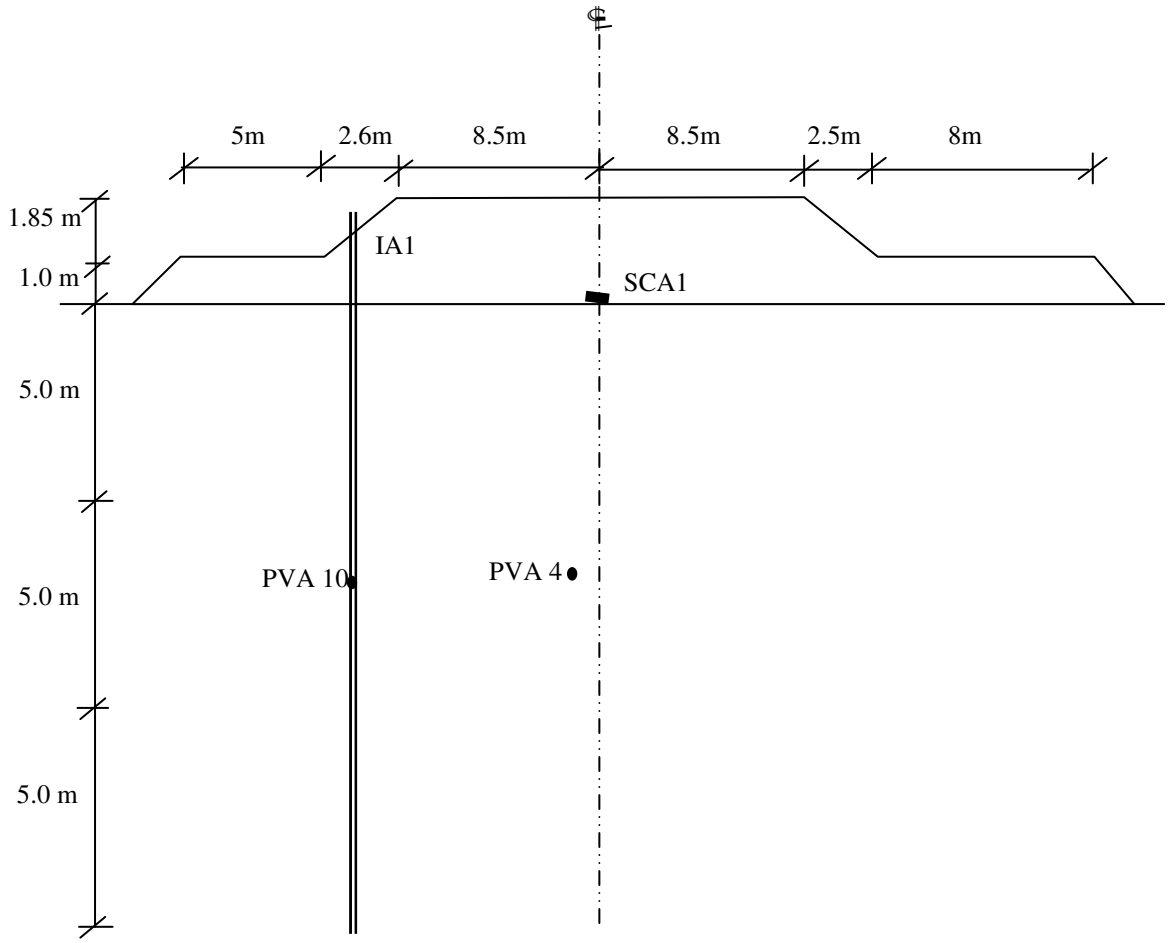

Figure 5.4 Instrumentation Layout for Section A (Elevation View)

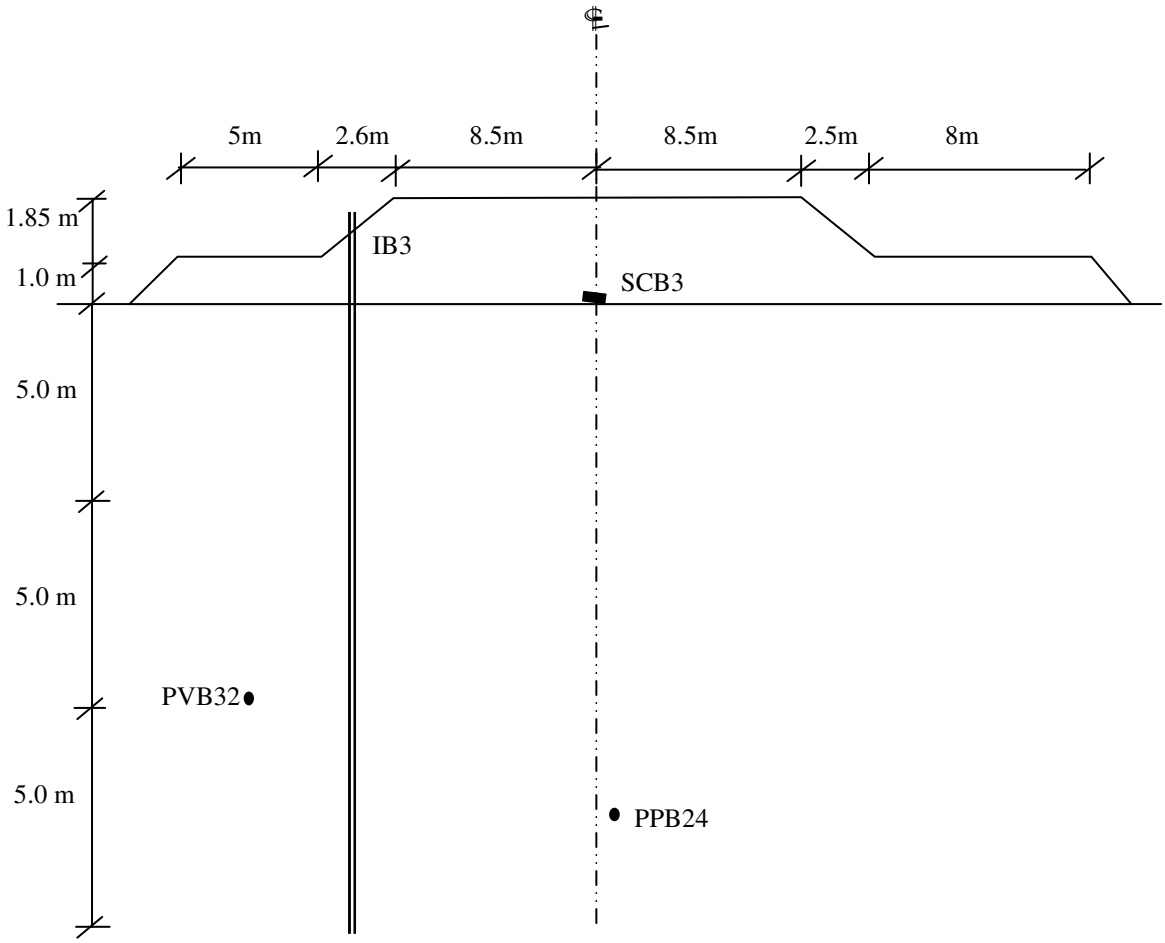

Figure 5.5 Instrumentation Layout for Section B (Elevation View)

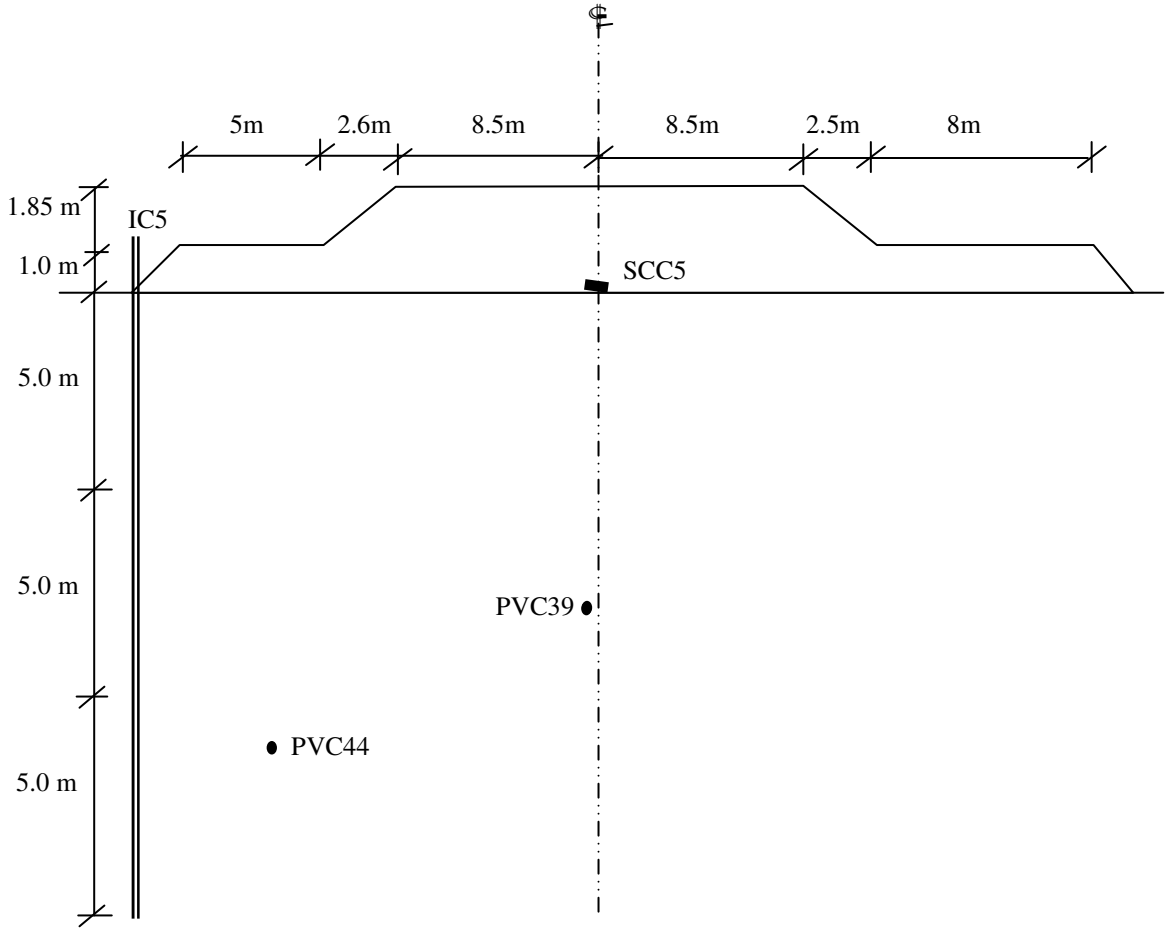

Figure 5.6 Instrumentation Layout for Section C (Elevation View)

5.5.2 Applied Constitutive Models and Material Properties

The Modified Cam-Clay constitutive model, derived by Roscoe and Burland (1968) was used to describe each of the clay sub layers (excluding the crust). Parameters required in describing this model, include the gradients of volume against log pressure relations for consolidation and swelling (λ and κ respectively), the frictional constant (M) and the void ratio at unit normal pressure on the CSL (e_{cs}). The crust and remaining sand layer were modelled assuming Mohr-Coulomb constitutive behaviour. Definition and derivation of all of these factors are outlined in Chapter 2. Values for the parameters used in both types of foundation models are shown in Table 5.2.

For the treated foundations, base horizontal permeabilities were calculated using the method derived by Indraratna and Redana (2000), and outlined in Chapter 2. The extent of the smear was assumed as 5 times the equivalent radius of the drain. Calculated values for both the undisturbed and smeared sections of the affected foundation layers are shown in Table 5.3.

The surcharge loading associated with the embankment construction was described using a Mohr-Coulomb model. The soil parameters of the embankment fill are shown in Table 5.4. Due to the lack of symmetry along the centreline of the embankment sections, it was necessary to model the whole width of the embankment for each simulation.

5.5.3 Grid Generation

The basic finite difference grid used to compute lateral and vertical displacements, as well as excess pore water pressure for this study is shown in Figure 5.7. Foundations were modelled to a depth of 16 m. The lateral boundaries of the finite difference mesh were fixed at 150 metres from the centreline. By exceeding the vertical boundary dimension by at least five times, boundary effects were able to be minimised. The mesh density was increased below the embankment to improve the computational accuracy.

Table 5.2 Parameters used in FLAC Analysis

Parameter	Soil Layer					
	Layer	1	2	3	4	5
	Description	Weathered Crust	Silty Clay	Silty Clay	Silty Clay	Clayey Sand
	Depth (m)	0 – 0.5	0.5 – 2.5	2.5 – 5.0	5.0 – 10.5	10.5 – 16.0
	Model	MC[4]	MCC[5]	MCC	MCC	MC
Lambda	λ		0.27	0.48	0.27	
Kappa	κ		0.013	0.016	0.013	
Slope	M		1.2	1.2	1.06	
Critical Void Ratio	e_{cs}		5.514	7.409	5.566	
Drained Poisson's Ratio	ν	0.3	0.45	0.45	0.45	0.3
Dry Density (kg/m^3)	ρ	1249	850	725	1000	1280
Shear Modulus (MPa)	G	9				3
Cohesion (kPa)	c'	13.5				13.5
Friction Angle (degrees)	ϕ'	35.0				35.0

[4] MC = Mohr Coulomb model
[5] MCC = Modified Cam Clay Model

Table 5.3 Plane Strain Permeability Values for Treated Sections of the Foundation Layers

Section ID	Parameter	Soil Layer				
		Layer	1	2	3	4
		Description	Weathered Crust	Silty Clay	Silty Clay	Silty Clay
		Depth (m)	0 – 0.5	0.5 – 2.5	2.5 – 5.0	5.0 – 10.5
Section A	Plane Strain Horizontal Permeability (no smear) (m/s)	$k_{hp(SA)}$	5.324×10^{-8}	7.023×10^{-8}	5.586×10^{-8}	1.596×10^{-9}
	Plane Strain Horizontal Permeability (with smear) (m/s)	$k_{hp}'_{(SA)}$	1.635×10^{-9}	2.116×10^{-8}	1.683×10^{-9}	4.808×10^{-9}
Section C	Plane Strain Horizontal Permeability (no smear) (m/s)	$k_{hp,(SC)}$	4.218×10^{-8}	5.459×10^{-8}	4.342×10^{-8}	1.240×10^{-8}
	Plane Strain Horizontal Permeability (with smear) (m/s)	$k_{hp}'_{(SC)}$	1.144×10^{-8}	1.480×10^{-8}	1.177×10^{-8}	3.363×10^{-9}

Table 5.4 Mohr Coulomb Parameters of Embankment Fill

Parameter	Symbol	Value
Dry Density (kg/m^3)	ρ	2039
Shear Modulus (MPa)	G	10
Cohesion (kPa)	c'	10
Friction Angle (degrees)	ϕ'	32

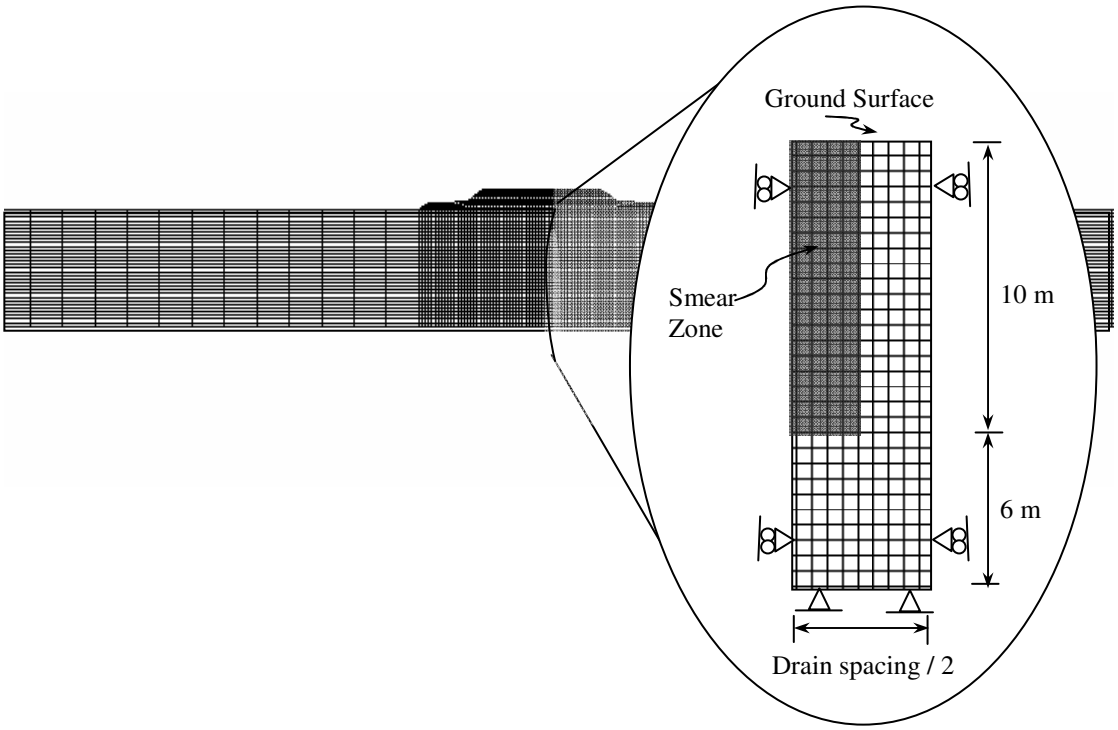

Figure 5.7 Finite Difference Mesh for Full Embankment Analysis (main) and Unit Cell Analysis (subset)

In order to include the smear zones, the mesh was adjusted slightly for each of the sections which included the vertical drains. Prior to full multi-drain simulation of each section, a single drain model was run and calibrated for establishing the relevant soil layer properties. The total width of a single drain model equated to the drain spacing under consideration. The total width of the embankment modelled for multi-drain simulation was 35 metres.

5.5.4 Boundary and Initial Conditions

The boundary conditions along both sides of the foundation model used were fixed in the x-direction to prevent lateral deformations, while still allowing movement in the y-direction. Full fixation in both the x and y-directions was assigned for the bottom boundary of the model, as the soil below it was dense enough to neglect any deformations associated with it.

The groundwater table was assumed at ground surface level for this analysis. Although the results from standpipe piezometers installed in the trial embankment indicated a slight variability in the height of the water table, this assumption was considered reasonable as the mean height of these variations corresponded to ground level. This bottom boundary was further assumed as non-draining, while the uppermost was assumed as freely draining. Full saturation was assumed for all zones below water table height.

To account for the multiple layering within each of these models and to ensure equilibrium, gravity was switched on following the specification of all initial in-situ stress and pore water pressures, and all models solved to an equilibrium ratio of 0.1%. Displacements resulting from this ‘solve command’, were initialized back to zero prior to the first embankment loading.

5.5.5 Stages of Construction

The actual construction sequence of the embankment loading is shown in Figure 5.8. Simulation of loading was achieved using a multi-staged approach.

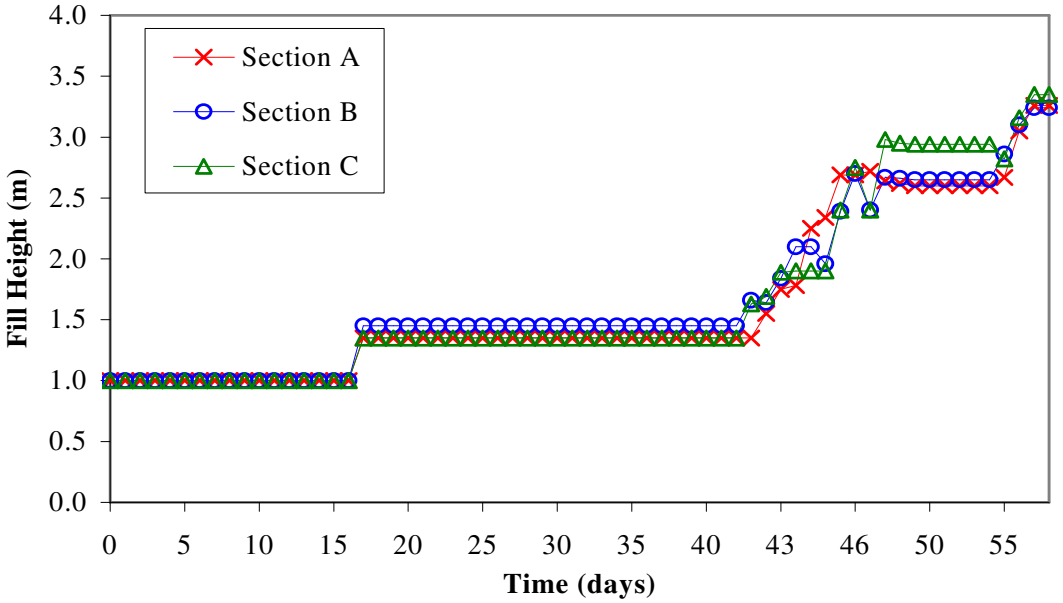

Figure 5.8 Actual Construction Sequence for Trial Embankment Sections

For numerical modelling purposes, the total height of the embankment was divided into 10 individual embankment layers of varying heights. To model the raising of the embankment, all 10 layers were initially assigned as null, and then 'applied' to the model at the appropriate times by changing the constitutive model to a Mohr-Coulomb material.

5.6 Analysis of Results

Actual field measurements of the foundation response were monitored by Queensland Department of Main Roads (1991a, 1991b, 1992). The follow sections compare and discuss the values predicted from this modelling exercise with field measurements of surface settlements, pore water pressures, and lateral displacement.

5.6.1 Excess Pore Pressures

Pore pressure generation was analysed at two separate locations within each section. Piezometers PPA4, PPA10, PPB 28, PPB32, PVC39 and PPC44 were selected for comparison. The locations of these piezometers were shown previously in Figures 5.4, 5.5 and 5.6. Plots of pore pressure variation versus time for each of the piezometers are given in Figure 5.9.

Excess pore pressures were estimated extremely well for the initial stages of Sections B and C, however, a slight overestimation of pressures was observable for Section A. The maximum deviation between the observed and predicted pore pressures within these stages occurred at PVA4, and measured approximately 10 kPa. This overestimation is hypothesised to be an effect of excessive groundwater pumping from machinery installing adjacent instrumentation or vertical drains. The overall maximum excess pore pressures achieved following these initial loading stages were also predicted well, with a discrepancy of only 5 kPa observable at the point of maximum pore pressure.

Significant disparity can be seen with regards to the rate of dissipation present for the treated sections of the embankment. This difference is primarily due to a phenomenon known as the Mandel-Cryer effect.

The Mandel-Cryer effect is characterised by stress redistribution associated with large lateral strains, where the increase in localised stresses in some regions of the soils due to stress redistribution can in fact generate additional pore pressures, hence mimicking the effect of retarded pore water pressure dissipation (Mandel, 1950; Mandel, 1953; Cryer, 1963). Such a phenomenon has been observed in the development of excess pore water pressures in thick deposits of normally consolidated clays, and similarly below various surcharge loadings, including trial embankments built upon soft clays from the Muar Plains, Malaysia (Indraratna, 1994).

5.6.2 Surface Settlements

Comparisons of predicted and observed surface settlement were made for each of the three sections. The points selected for comparison were located at settlement gauges SCA1 (Section A), SCB3 (Section B), and SCC5 (Section C). Gauges SCA1 and SCB3 were located under the centreline of the embankment, and at SCC5, 1 m left of the centreline. (see Figures 5.4, 5.5 and 5.6). Figure 5.10 shows the predicted and observed settlements for each embankment section.

As clearly demonstrated, the magnitudes of vertical settlement under the embankment are generally well computed. Slight underestimations and overestimations were predicted for Sections A and C respectively. As expected, for the treated sections displayed a faster consolidation rate compared to the untreated Section B. Furthermore, the settlement consolidation rate for Section A, in which the drains were spaced at 1 m, was quicker than Section C, which was treated with drains at 2 m spacing. The difference, however, between values (both predicted and observed) for Sections A and C was minimal, and thus, any benefits derived from installing the vertical drains at spacings closer than 2 m is negligible, as the smear effect produced by drain installation in such sensitive soils negates it.

The divergence observed between the predicted settlement-time relationships for the treated sections is greater than that which is shown by the field readings. This may be due to physical problems with the vertical drains installed (i.e. kinking and/or clogging of the drain), but is more likely to be due to the differences with the smear effects assumed from drain installation.

5.6.3 Lateral Displacements

The predicted and measured lateral soil deformations were measured for inclinometers IA1, IB3 and IC5 (locations shown in Figures 5.4, 5.5 and 5.6). Displacements have been

compared at 69 days (end-of-construction) for all three sections. Inclinometer displacement profiles for measured and predicted results in each of the sections are shown in Figure 5.11.

It is observed that the maximum lateral movement below the embankment was predicted well with only slight overestimation for Sections A and C, and only slight underestimation for Section B. The predicted displacement profiles for Section A and Section B also compared favourably when evaluated with respect to that which was measured in the field. These inclinometers were installed 10 m left of the centreline.

A less favourable comparison was found for Section C, where although the maximum lateral displacement was predicted reasonably, the displacement profile generated by the model was quite different to that which occurred in the field. Errors in the prediction of lateral movement for Section C may be partly due to the corner effects of the embankment. These are not properly modelled in 2D plane strain. Such effects would be less of a concern for inclinometers IA1 and IB3, as they are located away from the toe of the embankment. The inclinometer in Section C, IC5, was however located at the toe of the embankment and would be subjected to such effects in the field.

Also, anisotropy of the mechanical properties of the soil may also have contributed to differences between the predicted and measured lateral deformations). Inability to input such directional variation is one of the major drawbacks of the Cam-clay model (Parry and Wroth, 1977).

5.7 Conclusions

This chapter presented a classic case history of a trial embankment built on soft, organic marine clay in Area 2A of the Sunshine Coast Motorway in South East Queensland, Australia. It detailed both the pore pressure response, as well as the vertical and lateral deformations produced during the construction of a fully instrumented trial embankment.

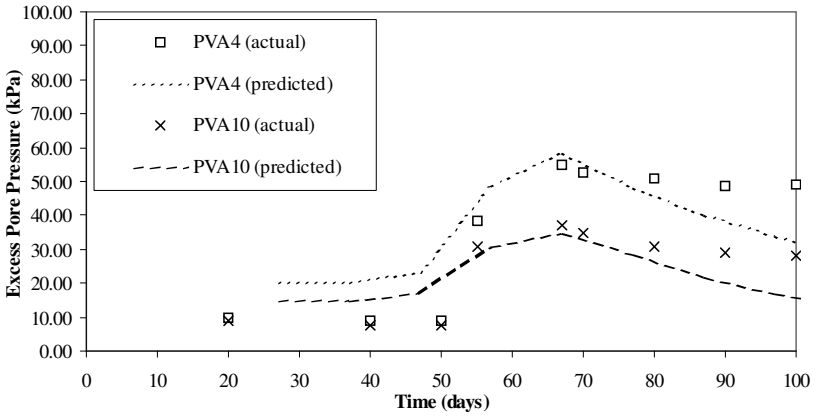

(a)

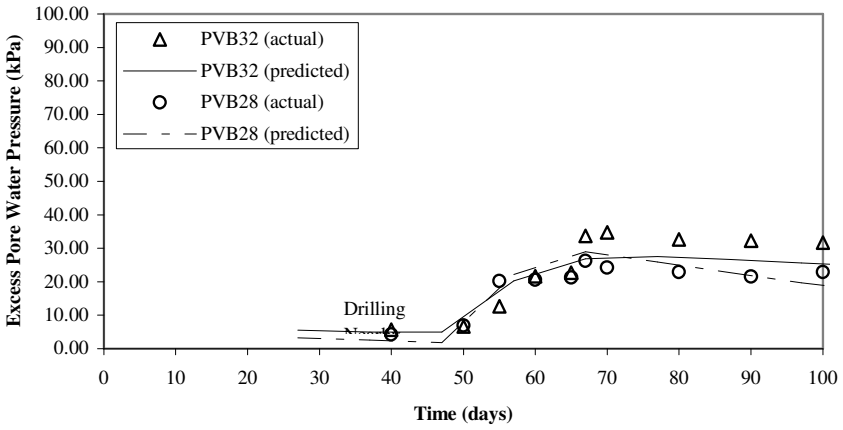

(b)

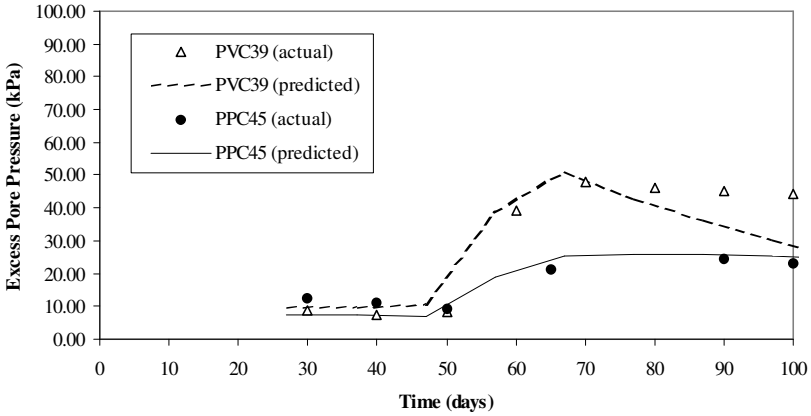

(c)

Figure 5.9 Excess Pore Water Pressure Variation in (a) Section A, (b) Section B and (c) Section C

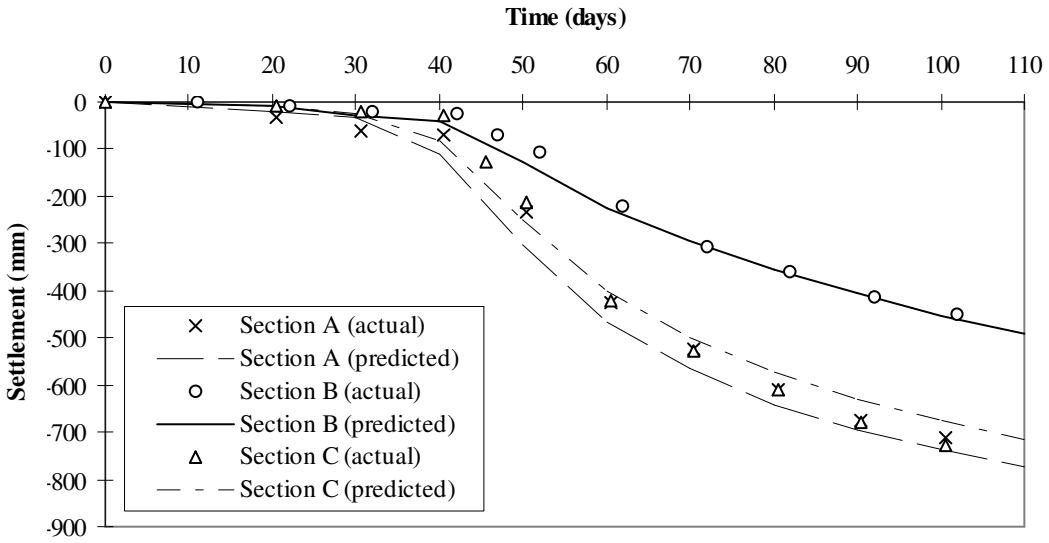

Figure 5.10 Settlement Plot for Gauges SCA1, SCB3 and SCC5 during the Embankment Construction Phase

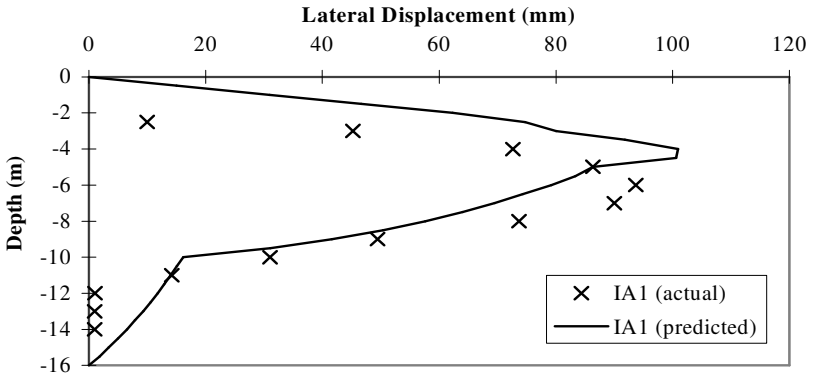

(a)

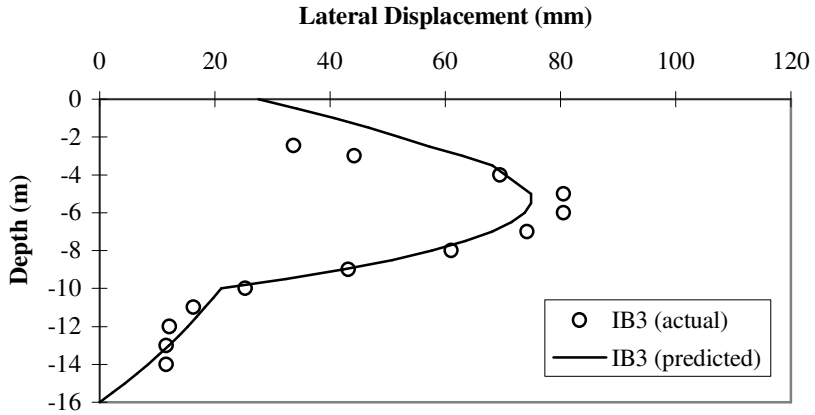

(b)

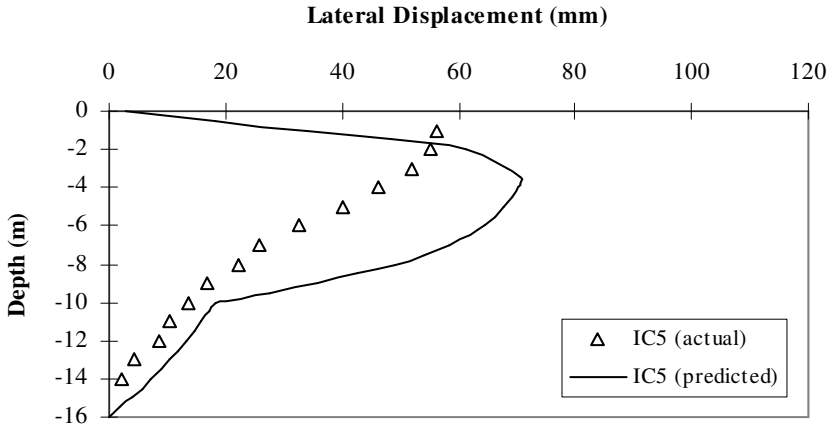

(c)

Figure 5.11 Lateral Displacement profiles for Inclinometers (a) IA1 (Section A), (b) IB3 (Section B) and (c) IC5 (Section C) at 69 days (end-of-construction)

The trial embankment was used to assess the feasibility and stability of staged construction of the embankment, the effectiveness of installing prefabricated vertical drains, and to verify the compressibility and consolidation characteristics.

The embankment was constructed using a multi-staged approach, and three separate sections were considered. These sections represented the design case (vertical drains installed at 2 m spacings), a control case (virgin undisturbed soil) and an intermediate case (vertical drains installed at 1 m spacings). A fully coupled plane strain analysis of each of these sections was carried out and compared with in situ measurements.

The deviations between the measured field values and the values of excess pore water pressure predicted by each Section's numerical model were considered acceptable. The maximum deviation between observed and predicted excess pore pressure occurred at PVC44 at 60 days. Maximum deviation in Sections A and C were predicted at 60 days and 75 days, respectively. With the exception of PVC44, excess pore water pressure was slightly overestimated for each of the prediction points. Discrepancies between measured and predicted pore pressures may have been due to disparities between the actual and assumed loading conditions, or disparities related to the clay permeabilities employed in the numerical analysis.

The numerical model predictions of surface settlement were in excellent agreement with the field measurements. Both numerical and field measurements showed that reducing the drain spacing from 2 metres (Section C) to 1 metre (Section A) has no significant difference on the settlement at any point in time. It should be noted that the presence of drains irrespective of the spacing, has no effect on the final magnitude of the consolidation settlement; it only has effect on hastening the rate of settlement.

The magnitude of maximum lateral displacement was predicted well by all three sections, however, while the displacement profile for Sections A and B compared favourably with the movements measured in the field, the profile for Section C differed significantly from

the field profile. This difference may be due to the positioning of each of the inclinometers. IC5, which was located at the embankment toe. This inclinometer would be subjected to corner effects from the embankment. Such effects are not properly modelled in a 2D plane strain analysis. Inclinometers IA1 and IB3 would not have been significantly affected in this regard due to their positioning (10 m left of the centreline).

CHAPTER 6

SHORT TERM LATERAL DEFORMATIONS INDUCED IN AN ELASTIC MEDIUM THROUGH THE APPLICATION OF RIGID EMBANKMENT LOADING

6.1 General

The development of lateral deformations during and after embankment construction has been the subject of numerous studies over the years, the necessity having arisen from observations of the damage to adjacent structures including bridge abutments, piles and utilities. When soft clays are present, these lateral soil movements are particularly large, and frequently quite significant stresses can be generated (Broms, 1972; Huder and Bucher, 1981). This stress-strain behaviour conforms to the idea that when a load is applied to the soil surface, the vertical stress within the soil mass is increased and extends indefinitely in all directions. The lateral soil movements induced through the intensity of these applied loads will generate passive loadings and subsequently passive stresses on nearby structures.

Such significant loading and displacement on the structures adjacent to the movement of the soil mass may result in unserviceable behaviour of these structures (Ellis, 1997). Furthermore, in the particular case of piles installed close to or within embankments, lateral displacements have been found to produce important bending moments which result in undesirable movement of these pile bridge abutments (Stewart, 1999; Hsi and So, 1999), and even structural failure of the piles (Tavenas et al., 1979).

Of the existing research that has been conducted in the field of deformation analysis below embankment loading, the majority focuses upon deformations in relation to the stability of the embankment and soil behaviour within the system. In this respect,

lateral soil deformations have been analysed and their magnitude and rate of generation found to be related to an embankment's stability (Hunter and Fell, 2003).

This chapter describes the development of a series of equations and design charts useful in determining the location and magnitude of short-term lateral soil displacements. They describe the displacement profile not only at the embankment toe, but also at various distances away from it. All equations and charts have been non-dimensionalised so that they can be used for a variety of soil types and dimensions (in any units).

6.2 Review of Lateral Displacement Theory

The deformation behaviour of clay foundations under embankments, both during undrained loading and consolidation, is often analysed using finite element and/or difference methods (Ohta, 1991; Indraratna et. al., 1994; Hsi and MacGregor, 1999) However, as noted previously by many researchers (Poulos, 1972; De Beer, 1977; Tavenas, 1979), the prediction of lateral displacement under embankment loading is a very difficult task in comparison with vertical settlements, and still appears to be inaccurate for both short-term and long term conditions (Tavenas, 1979; Hsi and MacGregor, 1999).

Burland (1971) developed a theoretical model to estimate the vertical and horizontal displacement due to consolidation beneath embankment loadings. Based on simple stress-strain theory, this model seemed to produce acceptable results compared with field data, and the subsequent analysis yielded the conclusions that during the consolidation, the lateral displacement develops rapidly at the surface and remains approximately constant as the deformation spreads downwards

Further observations by Holtz and Lindskog of the generation of lateral displacement were published in 1971. They state that significant horizontal movements occurred at the toe of the embankment and the rate of movement decreased significantly after achieving the maximum point. They also found that the rate of movement of lateral displacement was rapid during the early stages and decreased gradually with time.

However, the corresponding depths to maximum displacement point were quite consistent.

Poulos and Davis (1974) presented elastic solutions derived by Clough and Woodward (1967) to account for the distribution of horizontal and vertical displacement within a foundation of finite depth. These displacements were predicted at the base of the embankment and are described using Equation 6.1. Use of this equation for lateral deformation prediction is, however, severely limited due to its development and consideration of only one geometry (see Figure 6.1). Within Equation 6.1, the influence factor $I_{\rho v,h}$ is interpreted from either Figure 6.2a (horizontal displacement) or 6.2b (vertical displacement), and E_1, γ and H are the Young's Modulus, unit weight and height of the embankment soil respectively.

$$\delta_{v,h} = 5.55 \frac{\gamma H}{E_1} I_{\rho_{v,h}} \qquad \text{(Eqn. 6.1)}$$

An extensive study of lateral deformations induced in the clay foundations beneath 21 embankments during construction and consolidation phases was carried out by Tavenas et. al (1979). These observations revealed that the magnitude and distribution profile of lateral displacements is governed by the drained and undrained conditions of clay foundations. It was suggested that lateral deformations developed could probably be predicted using the elastic theory, provided drained characteristics and a Poisson's ratio of 0.3 were assigned to the foundation clay. The displacement profile at end of construction was further proposed to be governed by the thickness of the normally consolidated clay layer, which behaved similarly to an elastic solution. However, if the clay layer was not entirely normally consolidated, then an abnormal shape was obtained within the foundation. The lateral deformation profile was found to remain stationary during the long term consolidation phase. A linear relationship was developed to describe the lateral displacement with vertical settlement.

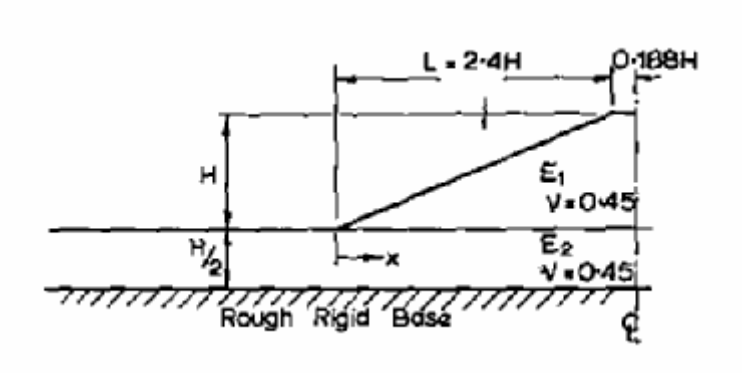

Figure 6.1 Geometry of Embankment considered by Clough and Woodward (1967) (after Poulos and Davis, 1974)

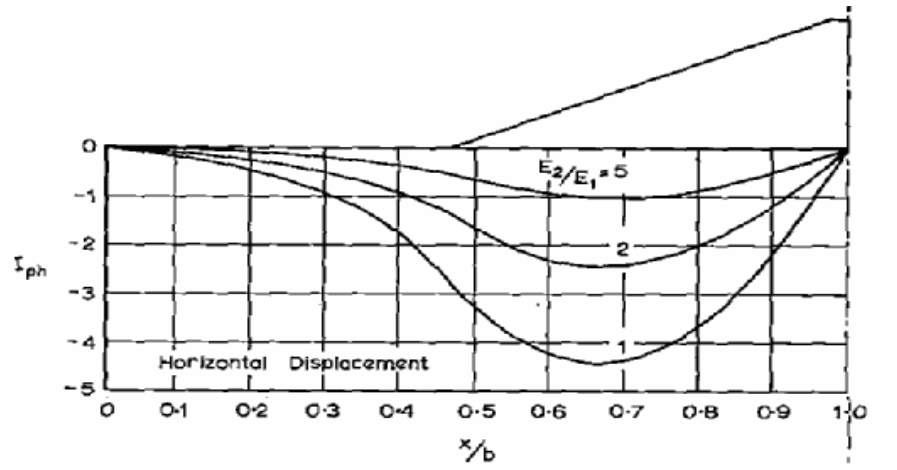

(a)

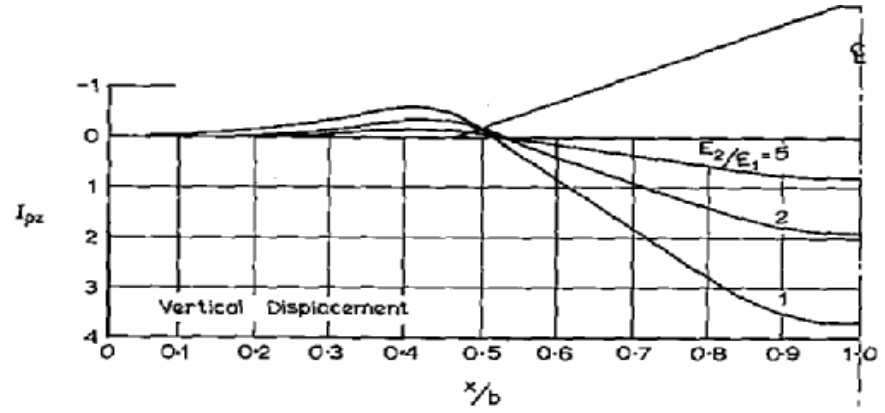

(b)

Figure 6.2 Influence Factors for the Embankment considered by Clough and Woodward (1967) (after Poulos and Davis, 1974)

Loganathan et al. (1993) presented a new methodology termed "Field Deformation Analysis (FDA)", to identify and quantify the different components of settlement from the total settlement measured during field observations. Finite element models were developed to reflect the foundation behaviour below two untreated full scale test embankments at the Muar Flats, and the results from these analyses compared with results from the FDA method. This comparison concluded that the FDA method was useful in predicting the settlement components of low embankments, however, that it should be used only for high embankments provided it had a short period of construction. Additionally, using the results of the finite element analyses, it was found that the maximum lateral deformation beneath the toe of the embankment was approximately 0.28 times the maximum settlement below the centre of an embankment at the end of construction.

It is apparent from the literature review that, with the exception of Clough and Woodward (1967), the majority of prediction methods are only applicable to deformations which occur below the toe of the embankment, and not to those which occur in the soil adjacent to it.

6.3 Modelling Assumptions and Considerations

A number of assumptions were made during formulation of the equations and design charts shown subsequently within this chapter. Foremost to these, was the assumption of an elastic constitutive model.

Deflections of soil which occur under undrained loading, and as a result of the rate of loading being fast with respect to the soils permeability characteristics are sometimes termed 'immediate settlement'. This expression is misleading, however, as it is not actually settlement, because no volume changes occur. Elastic deformation is used for calculation purposes of both the undrained deformation of loaded area on clay foundations, and the total (drained) settlement of sandy foundations. Application of the elastic constitutive model to soil mechanics is further discussed in Chapter 2 of this dissertation.

The second principal assumption was that of a plane strain condition. Some common engineering problems such as a tunnel under external pressure, strip footings, embankment loading and a dam subjected to water loading have significant strains in only two directions. If the strains in the remaining direction are small enough, they can be neglected and a plane strain condition can be assumed.

The third main assumption was that of a homogeneous, isotropic material in a semi-infinite half space in which the soil medium initially assumed to be bounded with a horizontal ground surface extending infinitely in both width and depth. This assumption, has been applied previously by many researchers (Fadum, 1948; Foster and Ahlvin, 1954; Osterberg, 1957) and is detailed more thoroughly in Poulos and Davis (1974). Finite depth layers were accounted for through correction factors.

Under linear, homogeneous and isotropic soil conditions, the related equations for the special case of plane-strain in the x-z plane where $\varepsilon_y = 0$ are shown below where ε, σ, γ and τ are the normal stress, normal strain, shear strain and shear stress in the particular plane as noted in the subscript (Poulos and Davis, 1974).:

$$\sigma_y = v(\sigma_x + \sigma_z) \qquad \text{(Eqn. 6.2)}$$

$$\varepsilon_x = \frac{1+v}{E}[\sigma_x(1-v) - v\sigma_z] \qquad \text{(Eqn. 6.3)}$$

$$\varepsilon_z = \frac{1+v}{E}[\sigma_z(1-v) - v\sigma_x] \qquad \text{(Eqn. 6.4)}$$

$$\gamma_{xz} = \frac{1}{G}\tau_{xz} \qquad \text{(Eqn. 6.5)}$$

With respect to the horizontal deformations of the soil mass, factors involved in the horizontal strain (ε_x) equation must be considered. These include Young's modulus, Poisson's ratio, vertical and horizontal stress.

A simplified and more general form of the deformation equation is utilised for many elastic solutions (see Equation 6.6).

$$\delta = \frac{qB}{E} I \qquad \text{(Eqn. 6.6)}$$

As shown, the displacement, δ, depends on parameters including applied stress, q, foundation width, B, equivalent elastic soil modulus, E, and displacement influence factor, I (Mayne and Poulos 1999). Factors that may influence I value are Poisson's ratio, soil layering, finite layer thickness, foundation roughness, and interface adhesion. From Equation 6.6, it is clearly evident that the relationship between deformation, δ, and both the applied pressure, q, and width of loaded area, B, is a directly proportional one.

Burland et. al (1977) observed that in soft soils where the applied stress exceeded the preconsolidation pressure, immediate settlement accounted for approximately 10% of consolidation settlement. This fraction was found to increase to approximately 50 to 60% of the total settlement in stiff materials where applied stress was below the preconsolidation pressure (Fang, 1991). With respect to lateral displacements induced through embankment loading, Tavenas et al. (1979) found that lateral displacements conformed to elastic theory by increasing at the same rate as vertical settlement during the construction phase.

Observations by Perloff and Baron (1976) showed that different sized footings subjected to identical unit pressures should not be expected to have equivalent immediate settlements. Observations found that the immediate settlements were directly proportional to the size of the footings, with larger footings registering larger immediate settlements (Fang 1991).

In view of the large loaded area and applied load of embankment, the effect of immediate settlements is considered to be relatively significant to its total foundation settlements.

6.4 Idealised Soil Model Geometry and Loading Conditions

The model used for design chart development assumes the standard embankment geometry of a trapezoid of crest width, a, base width, B, and height, h. Its shape is assumed to be symmetrical around the centreline, and no lateral movement or force is assumed to cross the centreline. As a result of such assumptions, and in the interest of ensuring time efficiency, only half the embankment was generated for modelling purposes. The embankment is assumed to be rigid enough such that no stability failure occurs within the embankment during simulation.

The depth of foundation modelled was ensured to be ten times the height of the embankment. This bottom boundary was considered to be rigid and was fixed in the y-direction. The far lateral boundary of the finite difference mesh was placed a distance of four times the half base width from the embankment centreline, and also fixed in the y-direction. By assigning the lateral and vertical dimensions in this manner, boundary effects were minimised. The ground surface boundary was assumed free moving.

A sensitivity study conducted upon the model using different meshes showed that 1 m x 1 m grid struck the right balance between solution time and accuracy for the foundation soil. For simplicity, the embankment grid also adopted this mesh sizing. Figure 6.3 further shows the geometry and boundary conditions previously discussed.

For any geotechnical model, an in-situ state of stress must be applied to the *FLAC* grid prior to any construction or application of loading occurring. Thus, gravity was applied to the model, and an in situ state of stress solved prior to loading in any of the models.

Embankment loading was assumed to be instantaneous for all models, and applied following the development of in-situ conditions phase of the model. Loadings were described using an elastic model.

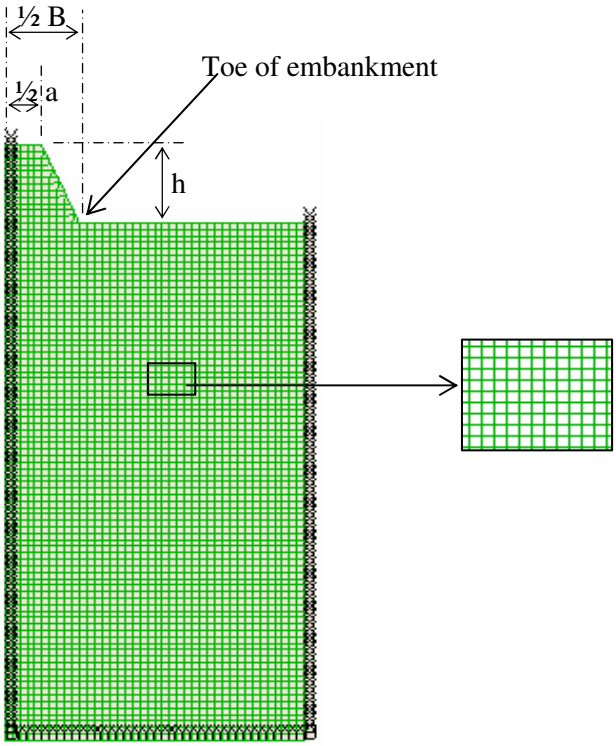

Figure 6.3 Model Geometry and Boundary Conditions

Staged construction was not accounted for within the development of these equations. Also, to ensure that equilibrium was achieved for each case, histories of both the unbalanced force and equilibrium factor in *FLAC* were monitored.

As elastic deformation is not related to volumetric change and consolidation, it was not necessary to consider the expulsion of water and the effect of pore pressure in these soil models.

6.5 Input Parameters

In modelling the lateral deformations, the input parameters of the soil properties included the bulk (K) and shear (G) moduli of the foundation soils, as well as the soil density (ρ), of both the embankment and foundation soils. Bulk and shear moduli

were calculated internally through programming a *FISH*[*] code into the *FLAC* model, by specifying the Young's Modulus (E) and Poisson's Ratio (ν) for the model.

Input parameters for the geometry of the embankment and foundation soils were the height of the embankment (h), height of the soil layer (H), and widths of the base (B) and crest (a) of the embankment.

In order to interpret the deformation analysis, the input parameters of a and h have been normalized with B. A select range of ratios for ν, h/B, a/B and B were simulated in *FLAC*. The results obtained are believed to be sufficient to represent the whole range of results due to the linearity of the elastic solution. The Young's modulus and density of soil were chosen arbitrarily over a wide range of values. Input values for the lateral deformation simulations are shown in Table 6.1.

A correction factor has been determined to account for situations in which the compressible layer was of finite thickness H. To develop this coefficient, models were simulated at depths equivalent to 2, 3, 5, 8 and 10 times the height of the embankment.

It was also found, and is observable in Figure 6.4 that the maximum lateral displacement does not necessarily occur underneath the toe of the embankment. Therefore, a correction factor was also formulated to account for how far the point under consideration was away from the toe of the embankment. This distance from the embankment toe is described within this chapter using the symbol L_x.

6.6 Approximate Solutions of Lateral Displacements in an Elastic Medium due to Rigid Embankment Loading

The general profile of simulated lateral soil deformations beneath the toe of the embankment is shown in Figure 6.5. As clearly shown in the plot, lateral deformation increases relatively rapidly with depth, reaching the maximum displacement at

[*] *FISH* is the internal programming language of *FLAC* which allows user definition of variables, and in some cases, constitutive models.

relatively shallow depths below the ground surface. After reaching this maximum, it then decreases gradually with depth to a point where the lateral deformation is negligible.

In view of the similar profiles obtained between lateral displacement and vertical settlement of the soil foundation, the triangular strain influence factor distribution of Schmertmann et al. (1978) was employed as an analytical tool for approximation of the lateral displacement profile.

This triangular distribution was specified by four parameters (see Figure 6.6):

- Maximum lateral displacement, δ_{lat},
- Depth of maximum lateral displacement, z_{max}
- Influence depth, z_{inf}
- Distance from the embankment toe, L_x

Two idealized straight lines were used to represent the curve. The first of these lines connects the point for which lateral displacement is to be calculated to the maximum lateral displacement, δ_{lat}, at a depth of z_{max}. This origin point is expressed using the symbol, L_x. The second line is then drawn to connect this point of maximum displacement, to the point at which negligible deformation along the profile occurs (i.e. deformation magnitude remains equivalent with depth). At this point, zero displacement can be assumed (z_{inf}). This point, z_{max}, was visually determined for each profile. The area bounded by the triangle is related to total lateral displacement for the particular loading condition.

As shown by Figure 6.5, the commencement points of the lateral displacement plots vary from negative to positive on the vertical-axis depending on the Poisson's ratio selected. Thus, an inward movement of soil could be expected in some cases. This phenomenon has also been observed in the field. However, within this research, analysis of this point was not undertaken.

Table 6.1 Input values of FLAC for Lateral Deformation Simulation.

Input Parameter	Input value
Young's Modulus, E (MPa)	1 and 10
Density of soil, ρ (kg/m^3)	1800 and 2000
Poisson's ratio, ν	0.1, 0.2, 0.3, 0.4
Width of embankment, B (m)	10, 20, 30, 40 and 50
a/B	0.1, 0.2, 0.5, and 0.8
h/B	0.1, 0.4, 0.6, 0.8 and 1.0

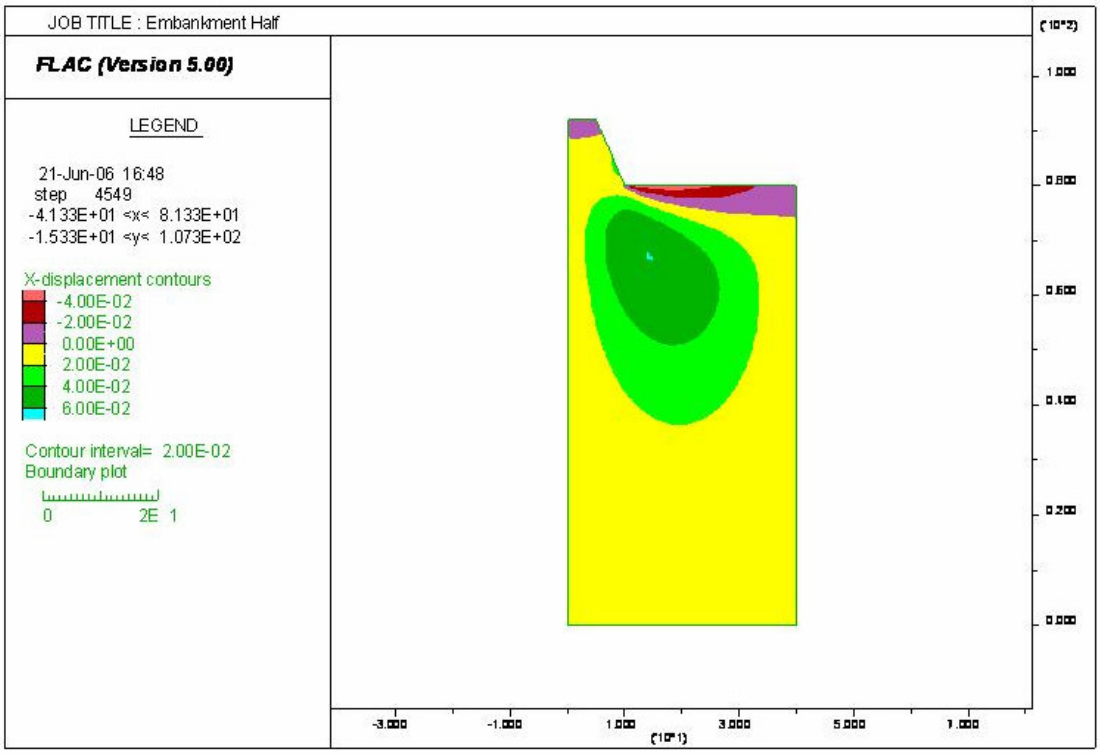

Figure 6.4 Horizontal Displacement Contours for Model Simulation

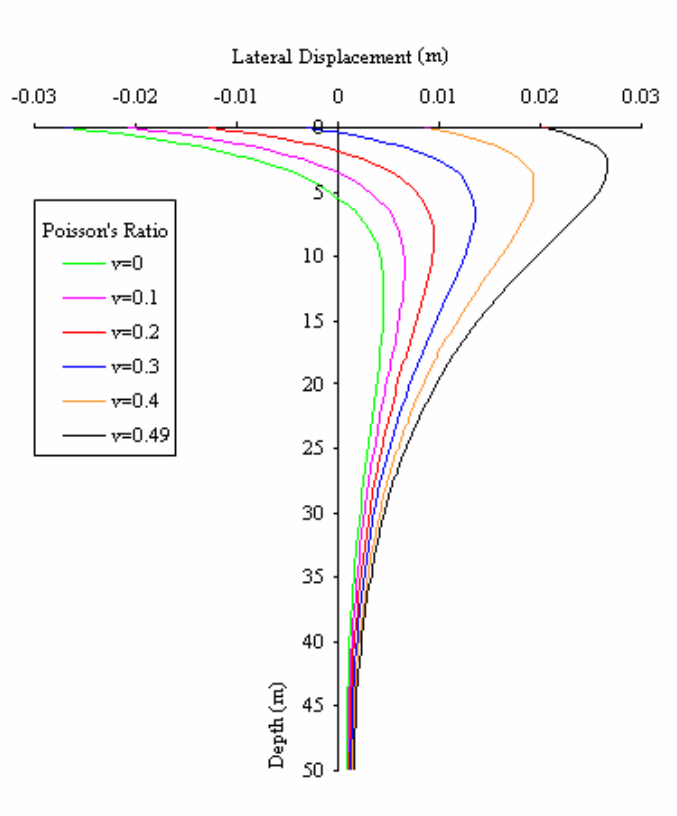

Figure 6.5 Variation of lateral deformation profile under the embankment toe with various Poisson's ratios (Embankment dimension: B=10 m, a/B=0.5 and h/B=0.6)

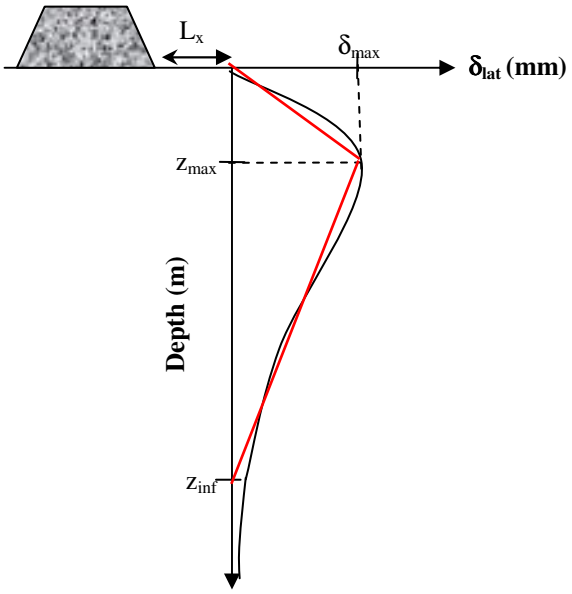

Figure 6.6 Schematic Diagram showing Triangular Distribution assumed for Lateral Displacement Approximation.

For all cases, the vertical axis of the lateral deformation profile and the commencement point for the lateral displacement approximation was assumed at the desired L_x away from the embankment toe.

In order to non-dimensionalise these 4 parameters described above, each of the geometrical parameters – z_{max}, z_{inf}, L_x – were divided by B, and the deformation equation (Equation 6.6) rearranged to describe the influence factor, I_{peak} (see Equation 6.7), instead of δ_{max}. By generalising the solutions in this manner, they can be used to suit different types of soil properties and embankment geometries.

$$I_{peak} = \frac{\delta_{max} E}{qB} \qquad \text{(Eqn. 6.7)}$$

This analysis has been concluded from the examination of tabulated results from 516 different cases. Equations for I_{peak}, z_{max}/B, z_{inf}/B were initially derived for layers of infinite depth. Infinite depth in these situations was defined to encompass any situations in which the compressible layer exceeded the influence depth, z_{inf}.

The factors Φ_1 and Φ_2 were derived for use in conjunction with I_{peak}, and are used to account for the distance (L_x) away from the embankment toe, and also the depth of foundation layer respectively. The third correction factor, Φ_3, is used in calculating the depth of maximum displacement, z_{max}, and accounts for the depth of foundation layer.

Details of the derivation of equations and design charts are discussed subsequently in Sections 6.6.3, 6.6.4 and 6.6.5. In order to clearly define when the infinite depth solution should be used, and when finite layer correction factors should be applied, z_{inf} has been discussed first. Following z_{inf}, analysis of both I_{peak} and z_{max} are given.

6.6.1 Effect of Young's Modulus, Foundation Density, Embankment Fill Density and Embankment Height

The results of these *FLAC* simulations suggest that the effects of Young's Modulus and the foundation density on values of I_{peak}, z_{max}/B, z_{inf}/B are negligible. Changes in both Young's Modulus, from 1 to 10 MPa, and foundation density, from 1800 to 2000 kg/m^3 yielded almost identical results. Therefore, they were not considered as governing parametersor used in developing approximate solutions.

The effects of both embankment fill density and fill height were accounted for in the pressure, q, constituent of the deformation equation (Equation 6.6).

6.6.2 Governing Parameters of z_{inf}/B

A number of steps were taken in determining the influence depth ratio, z_{inf}/B, due to embankment loading. Foremost to these, was to plot the lateral deformation profile induced in each embankment loading. Lateral displacement profiles were plotted not only at the toe of the embankment, but also at distances of 0.5B, 0.75B, B, 1.5B, 2B and 2.5B away.

Observations suggested that Poisson's ratio is the only governing parameter for determining influence depth. Investigations showed that z_{inf}/B remained constant for the entire range of a/B and h/B tested. The relationship between z_{inf}/B and ν can be expressed as

$$\frac{z_{\inf}}{B} = 3.2 - 1.4\nu \qquad \text{(Eqn. 6.8)}$$

It is evident from this equation, that with increased Poisson's ratio, the influence depth for a soil will decrease. Furthermore, given that Poisson's ratio can vary

between 0 to 0.5 for soils[¥], it is obvious that the minimum and maximum values of z_{inf}/B are 2.5 and 3.2, regardless of the width of the loading. Variation of z_{inf}/B with ν is shown in Figure 6.7.

Investigations by Tavenas et al (1979) found that lateral displacement increases linearly with vertical settlement during the construction phase, and up to the initial period of consolidation. They also suggested that the lateral displacements could be predicted by means of elastic theory. Thus, based on the elastic stress-strain relationships of a material under vertical loading, we can hypothesise that the lateral soil movement is primarily generated by the vertical settlement of the soil mass, and additionally, that the reliability of the developed results can be judged by means of this vertical settlement.

6.6.3 Governing Parameters of I_{peak}

A study of the simulation results revealed that there was a definite connection between the magnitude of I_{peak} and the factors of Poisson's ratio, ν and the crest to base width ratio, a/B, of the embankment. Increases of either of these parameters show a definite increase in the value of I_{peak} (see Figure 6.8). The governing of these two parameters is Poisson's ratio.

In the context of a compressible layer of infinite depth (i.e. $H > z_{inf}$), Equation 6.9 may be used to determine the peak influence factor attributable to embankment loading. The factor Φ_1, described using Equation 6.10, accounts for circumstances in which the lateral deformation profile is required for points located away from the embankment toe.

$$I_{peak} = \left[0.030\left(\frac{a}{B}\right) + 0.032 \right]^{\Phi_1 \nu} \qquad \text{(Eqn. 6.9)}$$

[¥] such soils should have high permeability. See Section 6.7 for notes regarding the method recommended specifically for loading upon clays.

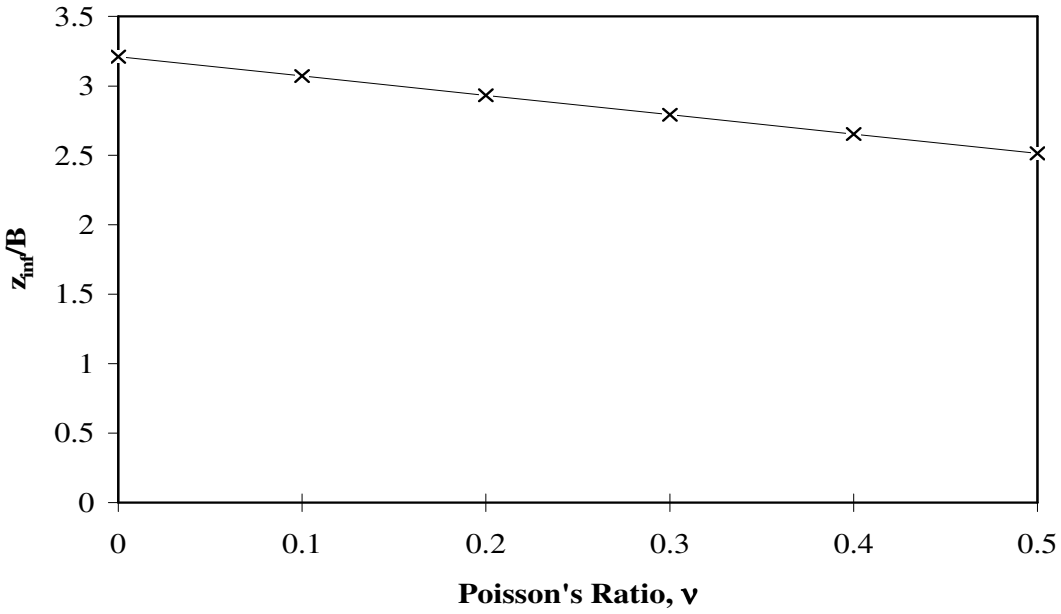

Figure 6.7 Normalised depth of influence, z_{inf}/B, with varying Poisson's Ratio

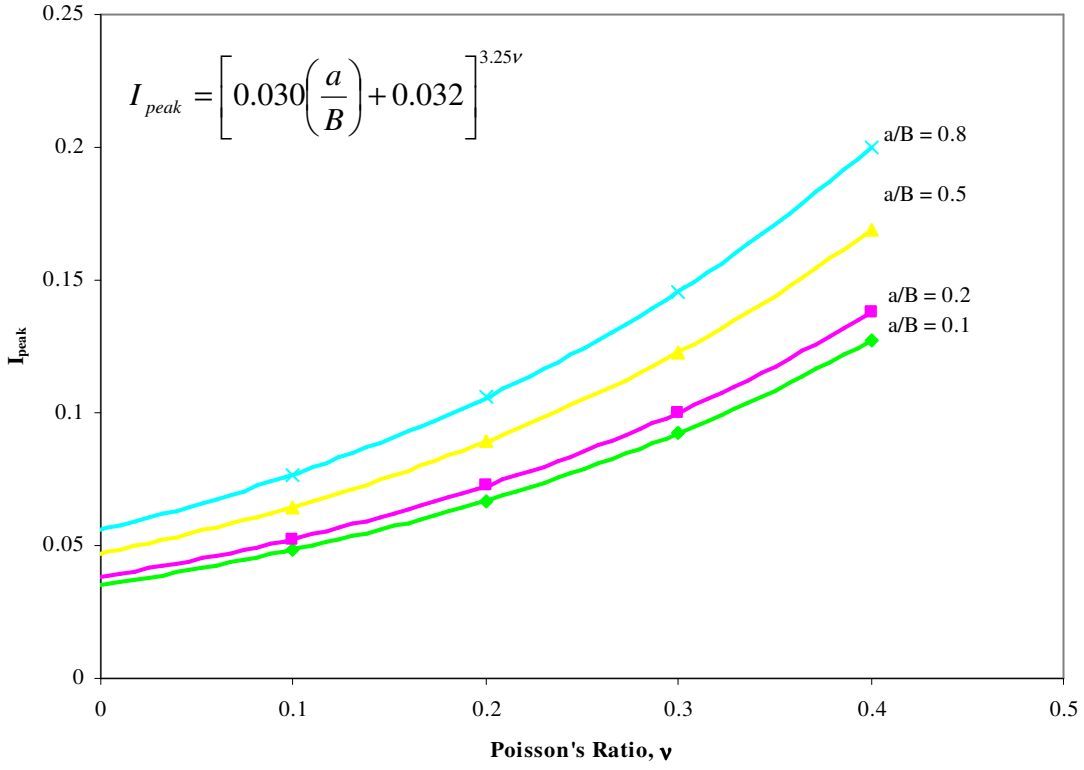

Figure 6.8 Plots of I_{peak} against Poisson's Ratio, ν, for Various a/B Ratios at the Toe of an Embankment

$$\Phi_1 = 0.067\left(\frac{L_x}{B}\right)^2 - 0.475\left(\frac{L_x}{B}\right) + 3.25 \qquad \text{(Eqn. 6.10)}$$

For finite depths (i.e. depths which do not exceed the influence depth, (z_{inf}), a further factor, Φ_2, has been produced to account for the amplification of lateral deformations (see Equation 6.11).

$$\Phi_2 = 0.88\left(\frac{H}{5B}\right)^{-0.44} \qquad \text{(Eqn. 6.11)}$$

This factor is applied following the calculation of maximum lateral displacement using I_{peak} for foundations of infinite depth. Thus, the overall maximum lateral displacement is calculated using Equation 6.12. Φ_2 is assumed as 1 in situations of "infinite" depth.

$$\delta_{lat,\max} = \Phi_2 \frac{qBI_{peak}}{E_{foundation}} \qquad \text{(Eqn. 6.12)}$$

6.6.4 Governing Parameters of z_{max}/B

As with z_{inf}, analysis suggests Poisson's ratio, ν, to be the only governing parameter for determination of the value of z_{max}/B, and that the position of maximum lateral displacement is independent of embankment geometry.

The relationship between z_{max}/B and ν was determined through a simple spreadsheet analysis, and may be expressed through the following numerical equation. The result of this equation will be negative, indicating the depth below ground level.

$$\frac{z_{\max}}{B} = 0.68\nu - 0.545 \qquad \text{(Eqn. 6.13)}$$

Analysis further showed that although the layer depth, H, had negligible difference on the position of maximum lateral displacement, however, the distance of the profile away from the toe (L_x) influenced the result. This effect can be quantified by applying the factor outlined in Equation 6.14.

$$\Phi_3 = 0.056\left(\frac{L_x}{B}\right) + 1.0 \qquad \text{(Eqn. 6.14)}$$

By combining these two equations, the overall equation for z_{max}/B is:

$$\frac{z_{max}}{B} = \Phi_3\left(0.68\nu - 0.545\right) \qquad \text{(Eqn. 6.15)}$$

Figure 6.9 presents a design chart of the above equations (where L_x=0). It should be noted that in the case of an embankment with berms, z_{max} should be determined with respect to the main embankment loading.

6.7 Approximate Solutions of Lateral Displacements in Clays due to a Rigid Embankment Load

Due to the low permeability of clays, the recommended method for the analysis of and prediction of clay foundation behaviour during the construction phase is to presume that the rate of construction for the embankment is sufficiently high to correspond to an undrained response. This undrained loading is characterised in analysis by assuming a Poisson's ration of 0.5, and an undrained modulus of elasticity, E_u.

6.8 Validation of Approximate Solutions

6.8.1 General

The approximate solutions developed and derived within this chapter are only applicable to short-term settlements, and thus correspond to the lateral displacement

induced as a result of the immediate vertical settlement of the foundation. Differentiation between the three different phases of settlement (immediate; consolidation; secondary compression) is notoriously difficult with regards to in-field data.

Thus, in order to validate these equations, results were obtained from running the numerical model previously established for the Sunshine Motorway Trial Embankment (described in Chapter 5), and not allowing pore pressure dissipation. By excluding fluid flow from the model, an accurate gauge of the immediate settlement, and thus, the short-term deformations was able to be obtained.

6.8.2 Geometric and Parametric Assumptions

The approximate layout assumed for the Sunshine Motorway Trial Embankment and used for validation purposes is shown in Figure 6.10. As shown, this geometric arrangement consists of two trapezoids in half symmetry. The primary trapezoid corresponds to the main embankment with a crest width of 17 metres, base width of 22 metres and total height of 2.85 metres. The second, shorter trapezoid corresponds to a crest width of 33 metres, base width of 55 metres, and height of 1 metre.

Two points of comparison were selected for validation. Point A is situated at the toe of the main embankment. Point B, on the other hand, is located 6.5 metres away from the toe of the embankment, at the edge of the berm. Foundation depth is assumed as one single, homogeneous layer with a thickness of 16 metres.

In accordance with the numerical model, embankment density was assumed to be 2039 kg/m^3. For Young's Modulus of the foundation, a weighted value was calculated using actual values from the layered situation. Overall, the weighted value was evaluated to 10.48 MPa. Poisson's ratio for the homogeneous foundation was also calculated using this method.

6.8.3 Discussions and Conclusions

Table 6.2 displays a comparison of the values calculated using the equations derived above[℘] with the numerical model results (assuming undrained loading).

While slightly underestimating the actual magnitude, the equations produced acceptable results for points both at the toe of the embankment (Point A) and also at a short distance away from the toe (Point B). The depth at which this maximum lateral displacement occurs was also slightly underestimated. However, with the level of underestimation being in the order of 5% or less for both profiles, this deviation is also considered acceptable.

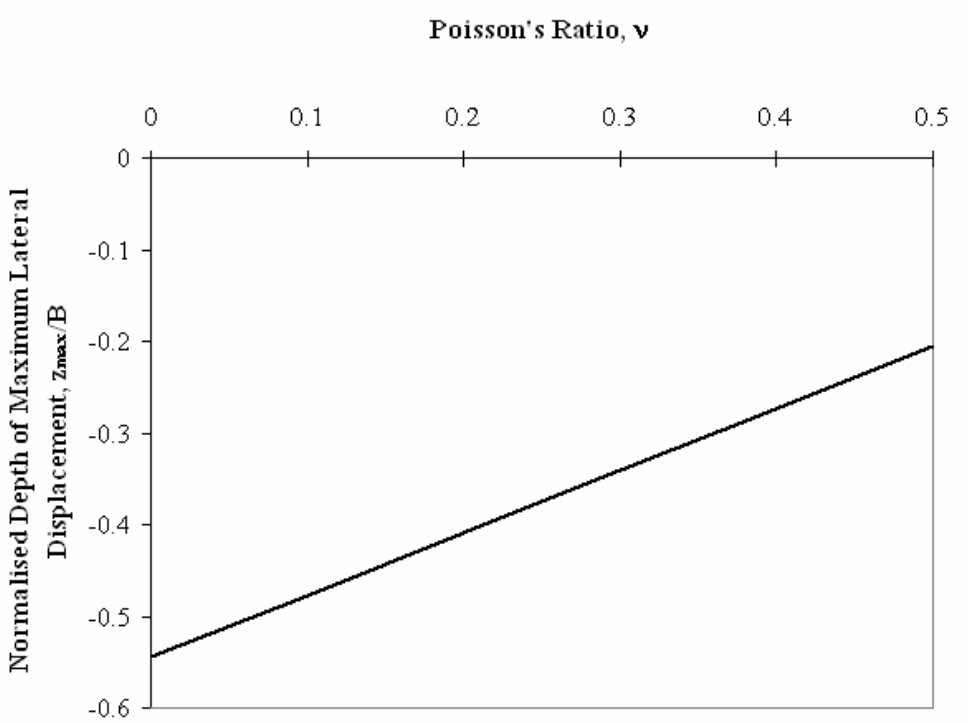

Figure 6.9 Normalized Depth of z_{max}/B for the Lateral Displacement beneath the Toe of Embankment

[℘] Full calculations are shown in Appendix K

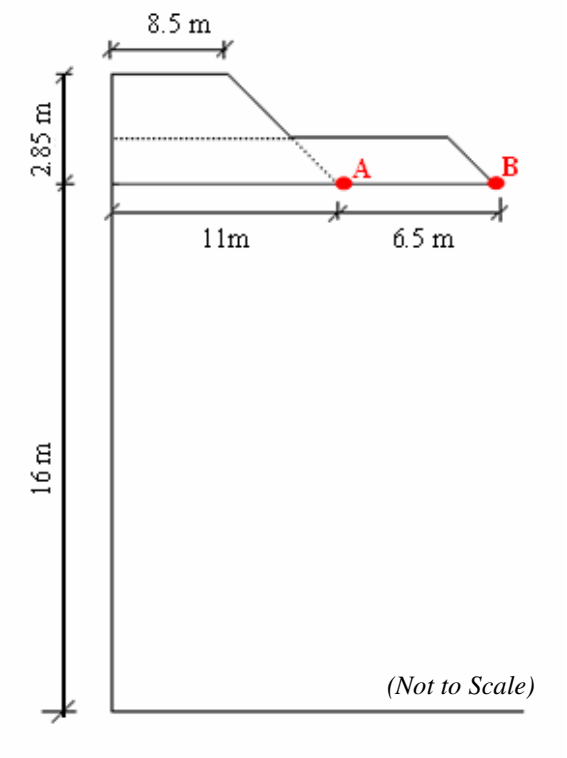

Figure 6.10 Approximated Layout for Validation of Lateral Displacement Solutions

Table 6.2 Comparison of Analytical and Numerical Predictions for $\delta_{lat,\max}$ and z_{max}

Parameter	Units	Point A		Point B	
		Analytical Solution	*Numerical Model*	*Analytical Solution*	*Numerical Model*
$\delta_{lat,\ max}$	mm	65.2	73.8	90.2	87.9
z_{max}	m	4.31	5	4.59	5
z_{inf}	m	27.5	n/a	27.5	n/a

Discrepancies between the analytical and numerical modelling solutions can be primarily attributed to the approximation of a single, homogeneous layer which is used for the analytical solutions. It is acknowledged that such an approximation will be erroneous, however, is also necessary in the production of generalised equations.

6.9 Conclusions and Recommendations for Further Research

This chapter overviewed the development of approximate solutions for the lateral displacement not only beneath the toe of the embankment, but also within the adjacent soils. These analytical solutions were developed by analysing the results of FLAC simulations, with the main assumption of an elastic model to describe soil behaviour. A triangular influence factor distribution similar to that hypothesised by Schmertmann (1978) was assumed for the approximated profiles.

Within this chapter, the primary solutions developed in relation to lateral displacement include:

- A dimensionless influence factor, I_{peak}, developed from the general form of the deformation equation, and used to describe the maximum lateral deformation induced from the loading
- The normalized depth at which the maximum deformation occurs, z_{max}/B where z_{max} is the depth at which maximum deformation occurs and B is the width of embankment.
- The normalized influence depth of the deformation zone, z_{inf}/B where z_{inf} is the maximum depth below the toe of embankment at which negligible displacement is encountered and B is the width of embankment.

In each case, these solutions have been expressed in the form of numerical equations. However, design charts are also included for points underneath the toe of the embankment.

A comparison of values obtained using these approximate solutions and results of the numerical model developed and verified in Chapter 5 were carried out to validate the accuracy of the solutions. The validity of z_{inf} is judged by means of maximum depth of influence strain zone for vertical settlement. The range obtained for z_{inf}/B was 2.5 to 3.2.

It should be stressed that these solutions only approximate the short term lateral displacement induced, and does not take into account any lateral spreading due to consolidation or creep.

Suggested future research within this area includes:

- Refinement of the developed models to incorporate layering
- Investigation of effect of Gibson-type (linearly increasing modulus) profiles on the lateral displacement profiles produced
- Establishment of approximate solutions to estimate the commencement point of lateral displacement profile. This variation in the displacement profiles is clearly apparent when Poisson's ratio increases from 0 to 0.5 (see Figure 6.5).
- Investigate the lateral displacement of embankment in a non-homogeneous and anisotropic soil mass

CHAPTER 7

SUMMARY, CONCLUSIONS AND RECOMMENDATIONS

7.1 Summary

During its formation, soil is exposed to innumerable geomorphic processes which affect its composition and ultimately its behaviour. Such varied environmental and physical interaction leads to a natural variation between the soil properties of different sites. In this respect, soil – as an engineering material – is unique, and a holistic approach toward geotechnical calculations should be adopted.

While a wealth of experience has been accumulated with respect to the theoretical behaviour of soils, our knowledge of soil properties still remains fragmentary.

A thorough geotechnical characterisation of four different sites across Queensland was conducted as part of this dissertation, and typical consistency and deformation properties of the clays discussed. Furthermore, empirical correlations have been developed from the laboratory works which describe, among other things, the dependence of both coefficient of volume compressibility and coefficient of secondary compression on the overconsolidation ratio of a clay.

An analytical study of the derivation of the m_v vs. effective stress plot identified flaws in current practice. A new discretised method of analytically determining the settlement of a foundation taking into account the stress dependence of m_v, and also the loading sequence of an embankment has been formulated, and is described within this thesis.

A fully coupled 2-dimensional numerical model was developed in the commercially available finite difference package *FLAC* to describe the foundation response below a trial embankment constructed in South East Queensland. The soil below this embankment was fully instrumented, and considered as three different sections. The first of these sections, the control case, examined surcharge loading only on undisturbed virgin soil. The other two sections were installed with vertical drains at spacings of 1 metre and 2 metres respectively. This plane strain model was validated against field results recorded by the Queensland Department of Main Roads, and used to assess the effectiveness of prefabricated vertical drains in these types of soils.

The results of this two dimensional model were also used to validate approximate solutions produced by the author to describe the short term lateral deformations generated as a result of embankment loading.

7.2 Conclusions

The following conclusions can be drawn from this research, and are divided into the sections corresponding to the chapters of the thesis.

7.2.1 Laboratory Induced Variation in Atterberg Limit Testing

This statistical analysis was undertaken on published NATA data and used to quantify levels of variation introduced into the results of liquid limit, plastic limit, plasticity index and linear shrinkage solely as a result of laboratory test methods. Beta distributions were developed specific to each of the soils tested. With a few minor exceptions, index properties were determined to behave like normal variates

Using the assumption of normal variate behaviour, the following general expression was established to describe the probability distribution functions of laboratory induced

variation for each of these index properties. The minimum and maximum range limits, *a* and *b*, have been assumed as $\mu - 3\sigma$ and $\mu + 3\sigma$ respectively.

$$f(x) = \frac{(6\sigma)^{-7}}{0.0071}\left(X - (\mu - 3\sigma)\right)^3\left((\mu + 3\sigma) - X\right)^3$$

From this study, it is also suggested that standard deviations for index properties may be assumed in the order of 10% of the mean value of both liquid and plastic limits, and 15% of the mean value of plasticity index.

In addition to this variance quantification, the well known empirical correlation which relates linear shrinkage to the plasticity index of a soil has been evaluated using the proficiency test results. Calculated plasticity index / linear shrinkage ratios ranged between 1.78 (loam) and 3.70 (clay).

While no overall trend could be determined to estimate the plasticity index / linear shrinkage ratio for all of samples, for soils with medium to high liquid limits (greater than 40%), this ratio was found to approximately equal 0.05 times the liquid limit.

7.2.2 Characterisation of Queensland Natural Clay Properties

A study of the consolidation, compressibility and consistency characteristics of soils from four different locations was completed as part of this thesis. These sites included Cairns, Townsville, Brisbane and the Sunshine Coast[#].

The results from this laboratory work were then analysed statistically, and probability distribution functions were developed to establish the overall distribution of each property over the sites. A number of important conclusions identified from this statistical analysis are listed below.

[#] Davis (1999) data included results from both Townsville and Cairns

- Beta distributions developed to describe the liquid limit and plastic limits of clays can be expected to follow a bell shape which is either perfectly symmetrical, or slightly skewed to the right (β_1 ranges from 0 to 0.03) however, with regards to plasticity index, these distributions vary significantly depending on the plasticity of the clay under consideration. For clays of low plasticity (as was the case for those tested at Site B), a triangular distribution should be expected, whereas for clays of medium to high plasticity, distributions tend to be the symmetrical shape expected for plastic and liquid limits.
- Regardless of the source from which the clays are taken, the general overall distribution curve for natural water content of Queensland clays will follow a bell shape, exhibit little or no skew from the mean, and have a coefficient of kurtosis in the order of 2.5.
- The mean value of specific gravity for the Queensland clays tested was 2.56. Deviations from this value fall within a very narrow band. The standard deviation and coefficient of variation resulting from an analysis of the 99 samples taken from Sites A, B and C were 0.09 and 0.04 respectively. This G_s value is slightly lower than the commonly assumed range of 2.6 to 2.8, and is hypothesised to be a result of the high levels of organic matter frequently present within clays along the Eastern coastal belt.
- An examination of the correlation between coefficient of secondary compression and various index properties produced mixed results. A distinctly increasing trend of C_α with increasing values of liquid limit, plasticity index and linear shrinkage was observable for Site B. There was, however, no discernable trend for Site C data, and Davis (1999) data showed the decreased values of C_α with increases in these index properties. No trends were detectable for plastic limit or liquidity index for.

- Overconsolidation ratio is suggested to have a significant influence on C_α. The laboratory test results analysed in Chapter 4 indicate that the magnitude of C_α decreases with increased overconsolidation ratio.

Investigations were also undertaken to ascertain the applicability of a number of published correlations which quantify the compression and consistency values of clays, and develop a number of correlations which were specific to Queensland clays. These further conclusions were made:

- The dependence of liquid limit on plastic limit for Queensland clays may be described as:

$$PL = 0.289LL + 10.3$$

- Previously published correlations involving liquid limit tend underestimate the compression index. Equations which best characterise the compression indices in terms of liquid limit, natural water content and initial void ratio are described below.

$$C_c = 0.0034*LL^{1.282}$$

$$C_c = 0.005*\ w_n^{1.156}$$

$$C_c = 0.303*e_0^{1.383}$$

- The influence of index properties and OCR on the coefficient of volume compressibility (m_v) may be expressed using the following equation:

$$m_v = (0.002LL - 0.054)(OCR)^{1.193-0.259\ln(LS)}\left(\frac{\sigma_{v,current}}{\sigma_{p(initial)}}\right)^{0.9}$$

This equation was established using the results of laboratory testing on Site B samples.

The $\left(\frac{\sigma_{v,current}}{\sigma_{p(initial)}}\right)$ term within this equation uses the initial in-situ preconsolidation stress of the sample and not the current preconsolidation

stress. Furthermore, this term is not synonymous with $\frac{1}{OCR}$, and its values can be both less than or greater than 1.

Prior to developing the above equation, an analytical study on the derivation and selection of representative m_v values identified flaws in present practice. Currently, the stress increments over which m_v values are established follow the loading stages of the corresponding oedometer test. However, as shown through an example in Chapter 4 of this thesis, this method produces m_v vs. effective stress plots that are not true representations of the compressibility behaviour. A new method of plot determination is proposed within Chapter 4 of this thesis. This approach involves the discretization of stress increments into smaller, equivalent increments, and is easily coded into EXCEL to reduce the calculation time.

A sensitivity analysis undertaken on the sizing of these calculation increments indicated that increments in the order of 10 kPa should be used. Smaller discretization of the stress increments yielded negligible difference to the plot produced.

- C_α was found to decrease with increased overconsolidation ratio. An overall general relationship between C_α and OCR was suggested (see Equation 4.38). However, it is hypothesised that both the coefficient and power displayed by this relationship will change with increasing index properties
- It is suggested that the relationship between effective stress and coefficient of secondary compression is similar to that of the coefficient of volume compressibility with effective stress

Results of the analyses undertaken in Chapter 4, particularly with respect to the influence of overconsolidation ratio on secondary compression, provide significant advances in estimation of residual settlements in highway embankments on soft clays. Furthermore, it provides greater understanding on the reduction of secondary settlement by removal of part of the surcharge used in preloading.

7.2.3 Analysis of a Case History: Sunshine Coast Motorway Trial Embankment

A fully coupled plane strain analysis has been developed and verified within Chapter 5 of this thesis. It presents the case study of a trial embankment constructed on soft, organic marine clay along the Sunshine Coast Motorway in South East Queensland, Australia. Developed in *FLAC*, this numerical model has been used to:

- predict the pore pressure response, as well as the vertical and lateral deformations produced not only in virgin undisturbed foundation soil, but also in foundations installed with different ground improvement schemes
- assess the feasibility and stability of staged construction of the embankment
- assess the effectiveness of installing prefabricated vertical drains, and
- verify the compressibility and consolidation characteristics computed from laboratory test results

Results from this numerical model were used in Chapter 6 to verify the approximate solutions developed to predict the lateral displacements below embankment loading.

7.2.4 Short Term Lateral Deformations Induced in an Elastic Medium through the Application of Rigid Embankment Loading

Within Chapter 6, a 2-dimensional embankment loading program was designed and coded in *FLAC*. This program is capable of predicting the short term lateral deformations produced in elastic foundations below rigid embankment loading, and investigated the

influence of various material properties and geometric arrangements. Approximate solutions have been developed from the results of these numerical simulations. These solutions predict the lateral displacement not only beneath the toe of the embankment, but also within soils immediately adjacent to the toe.

These approximate solutions were specified by four parameters – peak influence factor (I_{peak}), depth of maximum lateral displacement (z_{max}), influence depth (z_{inf}) and distance from the embankment toe (L_x).

Analysis suggests Poisson's ratio, ν, to be the only governing parameter for determination of the value of z_{max}/B, and that the position of maximum lateral displacement is independent of embankment geometry. The relationship between z_{inf}/B and ν can be expressed as:

$$\frac{z_{\inf}}{B} = 3.2 - 1.4\nu$$

Additionally, the magnitude of the peak influence factor (I_{peak}) used to describe the maximum lateral deformation induced from the loading was found to be directly related to the factors of Poisson's ratio, ν, crest to base width ratio, a/B, of the embankment, and ratio of distance from the embankment toe to embankment base width (L_x/B). The following equation has been developed to describe this non-dimensional parameter:

$$I_{peak} = \left[0.030\left(\frac{a}{B}\right) + 0.032 \right]^{\Phi_1 \nu}$$

where the factor $\Phi_1 = 0.067\left(\frac{L_x}{B}\right)^2 - 0.475\left(\frac{L_x}{B}\right) + 3.25$

The maximum lateral displacement, $\delta_{lat,max}$, is described using:

$$\delta_{lat,\max} = \Phi_2 \frac{qBI_{peak}}{E_{foundation}}$$

This second factor, Φ_2, accounts for the depth of foundation layer. If the foundation layer depth (H) is greater than the influence depth, z_{inf}, then this factor equals 1. However, if the foundation layer depth is less than z_{inf}, then it expressed as:

$$\Phi_2 = 0.88\left(\frac{H}{5B}\right)^{-0.44}$$

Studies of the normalized depth of maximum lateral displacement, z_{max}/B suggest it is independent of both embankment geometry and foundation layer height. It was found to essentially only be governed by Poisson's ratio and distance from the embankment toe. The relationship between z_{max}/B and ν was determined through a simple spreadsheet analysis, and may be expressed through the following numerical equation. The result of this equation will be negative, indicating the depth below ground level.

$$\frac{z_{\max}}{B} = \Phi_3(0.68\nu - 0.545)$$

The factor, Φ_3, allows for the distance of profile from the embankment toe, and is described using:

$$\Phi_3 = 0.056\left(\frac{L_x}{B}\right) + 1.0$$

These solutions were validated using results from the numerical model developed and verified in Chapter 5. It should be stressed that these solutions only approximate the short term lateral displacement induced, and does not take into account any lateral spreading due to consolidation or creep.

7.3 Recommendations for Future Research

Whilst considerable literature exists defining the assessment and analysis of clays, there are many areas that deserve further study. The recommendations outlined have been presented under the same titles as the chapters presented in this dissertation.

7.3.1 Laboratory Induced Variation in Atterberg Limit Testing

- Statistical analyses similar to that described in Chapter 3 should be undertaken to quantify the levels of variation induced solely as a result of other remaining geotechnical testing methods. Producing probability distribution functions to describe the variation and the probability of certain levels occurring would provide an invaluable tool for risk-benefit analysis.

7.3.2 Characterisation of Queensland Natural Clay Properties

- The database of soil properties developed within this chapter should be expanded to encompass more clay sites around Queensland. These properties should include consolidation and consistency parameters, as well as basic soil descriptors such as specific gravity and water content. Such extension to the database would be invaluable when computing design study calculations. Purely through examining the database, and finding entered data from the sites in the vicinity of that being examined, engineers would be able to gauge a rough estimate of the soil properties.

Verification of these estimates would only require minimal testing, and thus, there would be significant time and economical benefits.

- Further and continual development of empirical relationships specific to the prediction of Queensland clay properties should also be identified as an important research area. Extension to the database, as suggested above, would only improve the accuracy of empirical correlations produced for the region
- The relationships between index properties and m_v were developed using only a small number of points. Thus, further oedometer and index property testing is warranted and should be completed on a wider range of values to confirm these relationships, or, if needs be, amend them.
- Further investigation of the relationship between overconsolidation ratio, consistency limits and coefficient of secondary compression. This correlation is hypothesised to be similar to that of the coefficient of volume compressibility with overburden pressure.

7.3.3 Analysis of a Case History: Sunshine Coast Motorway Trial Embankment

- Currently, there are very few published case studies which present the behaviour of Australian soft soils when installed with vertical drains and subjected to surcharge loading. Thus, publication of such case studies should be encouraged within the engineering community.

7.3.4 Short Term Lateral Deformations Induced in an Elastic Medium through the Application of Rigid Embankment Loading

- The models developed should be refined to incorporate the effect of layering, and the approximate solutions adjusted accordingly
- Investigation should be undertaken into the effect of Gibson-type (linearly increasing modulus) profiles on the lateral displacement profiles produced

- Approximate solutions to estimate the commencement point of lateral displacement profile should be developed. This variation in the displacement profiles is clearly apparent when Poisson's ratio increases from 0 to 0.5
- The effect of anisotropy on the magnitude of lateral displacements produced in the foundation is also a field of study warranting attention.
- Incorporate fully coupled consolidation into the models developed and produce approximate solutions to predict long term lateral deformations. Observations from the field suggest that the development of approximate solutions of this nature should be considered possible as the depth of influence (z_{inf}) and depth of maximum lateral displacement (z_{max}) do not appear to change significantly during consolidation.

REFERENCES

Aboshi, H. and Monden, H. 1963. "Determination of the Horizontal Coefficient of Consolidation of an Alluvial Clay", *Proceedings of the 4th Australian New Zealand Conference on Soil Mechanics and Foundations Engineering*, pp 159 - 164

Akagi, T. 1977. "Effect of Mandrel-Driven Sand Drains on Strength", *Proceedings of the 9th International Conference on Soil Mechanics and Foundation Engineering,* Tokyo, Vol. 1, pp 3 - 6

Akagi, T. 1981. "Effect of Mandrel-Driven Sand Drains on Soft Clay", *Proceedings of the 10th International Conference on Soil Mechanics and Foundation Engineering*, Stockholm, pp 581 - 584

Alonso, E. E., Gens, A. and Lloret, A. 2000. "Precompression Design for Secondary Settlement Reduction", *Geotechnique*, Vol. 50 (6) pp 645 - 656

Ameratunga, J. 2006. *Personal Communication*

Atterberg, A. 1911. "Lerornas Forhallande till Vatten, deras Plasticitetsgranser och Plasticitetsgrader (The Behaviour of Clays with Water, their Limits of Plasticity and their Degrees of Plasticity)", *Kungliga Lantbruksakademiens Handlingar och Tidskrift,* Vol. 50. No. 2. pp 132 - 158

Aysen, M. and Atilla, M. 2001. "Regression Analysis of Soil Compressibility", Turkish Journal of Engineering and Environmental Sciences, Vol. 25 No. 2 pp 101 - 109

Azzous, A.S., Krizek, R.J. and Corotis, R.B., 1976. "Regression Analysis of Soil Compressibilty", *Soils and Foundations*, Vol. 16 No. 2 pp 19 - 29

Balasubramaniam, A.S. 2002. *Compiled Notes from Short Course on Advanced Soil Behaviour and Critical State Soil Mechanics*, Griffith University, Brisbane, Australia

Barron, R.A. 1948. "Consolidation of Fine-Grained Soils by Drain Wells", Transactions of the American Society of Civil Engineers, Vol. 113 pp 718 - 724

Bergardo, D., Asakami, H., Alfaro, M.C. and Balasubramaniam, A.S. 1991."Smear Effects of Vertical Drains on Soft Bangkok Clay", *Journal of Geotechnical Engineering*, American Society of Civil Engineers, Vol. 117 (10), pp 1509 - 1530
Bergado, D.T., Alfaro, M.C. and Balasubramaniam, A.S. 1993. "Improvement of Soft Bangkok Clay using Vertical Drains", *Geotextiles and Geomembranes*, Vol. 12 No. 7 pp 727 - 745
Bergado, D.T., Chai, J.C., Alfaro, M.C. and Balasubramaniam, A.S., 1994. *Improvement Techniques of Soft Ground in Subsiding and Lowland Environment*. A.A. Balkema Publishers, Rotterdam, Netherlands
Bergado, D.T. and Long, P.V., 1994. Numerical Analysis of Embankment on Subsiding Ground Improved by Vertical Drains and Granular Piles. *Proceedings 13th International Conference on Soil Mechanics and Foundation Engineering*, New Delhi, India, pp 1361 – 1366
Bergado, D.T., Mannivannan, R., Balasubramaniam, A.S. 1996. "Proposed Criteria for Discharge Capacity of Prefabricated Vertical Drains", *Geotextiles and Geomembranes*, Vol. 14, pp 481 - 505
Bergado, D.T., Balasubramaniam, A.S., Fannin, R.J., Anderson, L.R., and Holtz, R.D. 1997. "Full Scale Field Test of Prefabricated Vertical Drains (PVD) on Soft Bangkok Clay and Subsiding Environment", *Ground Improvement, Ground Reinforcement and Ground Treatment Developments 1987 – 1997 (Geologan '97),* Edited by V.R. Schaefer, American Society of Civil Engineers, Geotechnical Special Publication 69, pp 372 - 393
Bergardo, D.T., Chai, J.C., Miura, N., and Balasubramaniam, A.S. 1998. "PVD Improvement of Soft Bangkok Clay with Combined Vacuum and Reduced Sand Embankment Preloading", *Journal of Geotechnical Engineering*, Southeast Asian Geotechnical Society, Vol. 29(1), pp 95 - 122
Bjerrum, L. 1972. "Embankments on Soft Ground", *Proceedings of Specialty Conference: Performance of Earth and Earth-Supported Structures*, American Society of Civil Engineers, New York, NY, Vol. II pp 1 - 54
Bo, M.W., Chu, J., Low, B.K., and Choa, V. 2004. *Soil Improvement: Prefabricated*

Vertical Drain Techniques, Thomas Learning, 5 Shenton Way, Singapore, Singapore
Britto, A.M. & Gunn, M.J., 1987. *Critical State Soil Mechanics via Finite Elements*, Elis Horwood Limited, England
Broms, B.B. 1971. "Stability of flexible structures (piles and pile groups)", *Proceedings of the 5th European Conference on Soil Mechanics and Foundations Engineering*, Vol. 2. pp 239 - 269
Budhu, M., 2000. "Soil Mechanics and Foundations", *John Wiley and Sons Inc*., New York, USA
Burland, J. B. (1971). A method of estimating the pore pressures and displacements beneath embankments on soft, natural clay deposits. *Stress-strain behaviour of soils: Proceedings of the Roscoe Memorial Symposium*, Cambridge University, pp.29-31.
Carrier, W.D., 1985. "Consolidation Parameters derived from Index Tests". *Geotechnique*, Vol. 35, No. 2, pp 211 - 213
Casagrande, A., 1932. "Research on the Atterberg Limits of Soils", *Public Roads*, Vol. 13 No. 8 pp 121 - 136
Casagrande, A., 1936. "The Determination of the Preconsolidation Load and Its Practical Significance", *Proceedings of the First International Conference on Soil Mechanics and Foundation Engineering*, Cambridge, Vol 3 pp 60 - 64
Casagrande, A. and Fadum, R. E. 1940. "Notes on Soil Testing for Engineering Purposes", *Harvard University Graduate School of Engineering Publication* No. 8
Casagrande, A., 1942. "Classification and Identification of Soils", *Proceedings of the American Society of Civil Engineers*, pp 901 - 991
Casagrande, A., 1958. "Notes on the Design of the Liquid Limit Device", *Geotechnique*, Vol. 13 No. 2 pp 84 - 91
Chai, J.C., Miura, N., Sakajo, S., and Bergado, D. 1995. "Behaviour of Vertical Drain Improved Subsoil under Embankment Loading", *Soils and Foundations*, Vol. 35 (4), pp 49 - 61
Chai, J.C.and Miura, N., 1997. "Method of Modelling Vertical Drain Improved Subsoil", *Proceedings of China-Japan Joint Symposium on Recent Developments of Theory and Practice in Geotechnology*, Shanghai, China. pp 1 – 8

Chan, A.H.C. 2003. "Determination of the Coefficient of Consolidation using a Least Squares Method", *Geotechnique*, 53 (7) pp 673 - 678
Choa, V., Bo, M.W. & Chu, J. 2001. "Soil Improvement Works for Changi East Reclamation Project", *Ground Improvements*, Vol. 5 No.4 pp 141 - 153
Chu, J., Bo, M.W., Choa, V. 2004. "Practical Considerations for Using Vertical Drains in Soil Improvement Projects", *Geotextiles and Geomembranes*, Vol. 22 pp 101 - 117
Clough, R.W. and Woodward, R.J., 1967. "Analysis of Embankment Stresses and Deformations", *Journal of Soil Mechanics and Foundations Division*, American Society of Civil Engineers, Vol. 93 (SM4) pp 529 - 549
Coutinho, R.Q., 1976. "Radial drainage consolidation characteristics of Fluminense Plains soft clay (in Portuguese)", *M. Sc. Thesis*, COPPE/UFRJ, Rio De Janeiro, Brazil
Cozzolino, V.M. 1961. "Statistical Forecasting of Compression Index", *Proceedings of the 5th International Conference of Soil Mechanics and Foundation Engineering*, Paris Vol 1 pp 51 - 53
Craig, R.F. 1995. *Soil Mechanics: 5th Edition*. London, Chapman and Hall
Cryer, C.W., 1963. "A Comparison of the 3-Dimensional Theories of Biot & Terzaghi", *Quarterly Journal of Mechanics and Applied Mathematics*, Vol. 16, pp 401 - 412
Das, B.M. 2002. *"Principles of Geotechnical Engineering – 5th Edition"*, Thomson Learning Inc., California, USA
Davis, R.O. and Selvadurai, A.P.S. 1996. *Elasticity and Geomechanics*, Cambridge University Press, 40 West 20th St., New York, NY, USA
Davis, R.E. 1998. "Geotechnical Characterisation of Soft Clays in Tropical North Queensland", *Masters Thesis*, James Cook University
De Beer, E.E. 1977. "Piles subjected to Static Lateral Loads", *State of the Art Report*, Specialty Session, No.10., 9th International Conference on Soil Mechanics and Foundations Engineering, Tokyo, Japan
Duncan, J.M. 1994. "The Role of Advanced Constitutive Relations in Practical Application", *Proceedings of the 12th International Conference on Soil Mechanics and Foundation Engineering*, New Delhi, India, Vol. 5 pp 31 - 48
Duncan, M. 2000. "Factors of Safety and Reliability in Geotechnical Engineering",

Journal of Geotechnical and Geo-Environmental Engineering, ASCE, Vol. 126 No. 4 pp 307 - 316
Ellis, E. A. 1997. "Soil-structure Interaction for Full Height Piled Bridge Abutments constructed on Soft Clay" *PhD Dissertation*, University of Cambridge, Cambridge, United Kingdom
Ewers, B and Allman, M.A. 2000. "Secondary Compression of Soft Clay from Ballina Bypass", *Proceedings of GeoEng2000*
Fadum, R.E. 1948. "Influence Values for Estimating Stresses in Elastic Foundations", *Proceedings of the 2nd International Conference on Soil Mechanics and Foundation Engineering*, Vol. 3, pp 77 - 84
Fang, H.Y. 1991. *Foundation Engineering Handbook*, 2nd Edition, Van Nostrand, Reinhold
Foster, C.R. and Ahlvin, R.G., 1954. "Stresses and Deflections Induced by a Uniform Circular Load", *Proc. High. Res. Board*, Vol. 36. pp 467 - 470
Goodman, R.E. 1998. *Karl Terzaghi: The Engineer as Artist*, American Society of Civil Engineers Press, 1801 Alexandar Bell Drive, Reston, Virginia, USA
Gutierrez, A. 2006. "Determination of Atterberg Limits: Uncertainty and Implications", *Journal of Geotechnical and Geo-Environmental Engineering,* ASCE, Vol. 132 No. 3 pp 420 - 424
Hansbo, S. 1957. "A New Approach to the Determination of the Shear Strength of Clay by the Fall-Cone Test", *Proceedings No. 14*, Swedish Geotechnical Institute pp 47
Hansbo, S. 1979. "Consolidation of Clay by Band-Shaped Prefabricated Drains", *Ground Engineering*, Vol. 12(5) pp 16 - 25
Hansbo, S. 1981."Consolidation of Fine-Grained Soils by Prefabricated Drains", *Proceedings of the 10th International Conference on Soil Mechanics and Foundation Engineering*, Stockholm, pp 677 - 682
Harr, M.E. 1977. *"Mechanics of Particulate Media – A Probabilistic Approach",* McGraw-Hill International Book Company, USA.
Hines, W.H., Montgomery, D.C., Goldsman, D.M. and Borror, C.M. 2003. *Probability and Statistics in Engineering – 4th Edition*, John Wiley and Sons Inc., New Jersey, USA

Hird, C. C, Pyrah, I.C. and Russell, D. 1992. "Finite Element Modelling of Vertical Drains beneath Embankments on Soft Ground", *Geotechnique*, Vol. 42 (3), pp 499 - 511
Holtz, R. D. and Lindskog, G. 1972. "Soil movements below a test embankment" *Proceedings of the ASCE Specialty Conference on Performance of Earth and Earth-Supported Structures*, West Lafayette, Indiana, Vol. 1, pp.273-284.
Holtz, R.D. and Kovacs, W.D., 1981. *An Introduction to Geotechnical Engineering*, Prentice Hall Inc., New Jersey, USA
Holtz, R.D., Jamiolkowski, M., Lancellotta, R. and Pedroni, S. 1988. Behaviour of Bent Prefabricated Vertical Drains", *Proceedings of the 12th International Conference on Soil Mechanics and Foundations Engineering*, Rio De Janeiro, Vol. 3, pp 1657 - 1660
Holtz, R.D. 1991. Prefabricated Vertical Drains: Design and Performance*, CIRIA Ground Engineering Report: Ground Improvement* , Oxford: Butterworth – Heinemann Ltd.
Hough, B.K. 1957. *"Basic Soil Engineering"*, The Ronald Press Company, New York
Hsi, J.P. and MacGregor J.P. 1999. "Prediction and Monitoring of Embankment Performance" *Proceedings of the 8th Australian and New Zealand Conference on Geomechanics*, Hobart, Australia, pp. 259-265.
Hsi, J.P. and So, B.S. 1999. "Design Considerations of Bridge Abutment Piles Subjected to Embankment Settlement. *Proceedings of the 8th Australian and New Zealand Conference on Geomechanics*, Hobart, Australia, pp. 397 - 403.
Huder, J. and Bucher, F. 1981. "Underpinning of a Pile Foundation in Soft Clay", *Proceedings of 10th International Conference on Soil Mechanics and Foundations Engineering*, Vol. 2. pp 741 - 745
Hunter, G. and Fell R. 2003. "Prediction of Impending Failure of Embankments on Soft Ground". *Canadian Geotechnical Journal,* Vol. 40: pp.209-220
Indraratna, B., Balasubramaniam, A.S. and Ratnayake, P.1994, "Performance of Embankment Stabilized with Vertical Drains on Soft Clay", *Journal of Geotechnical Engineering*, ASCE, Vol. 120, No 2, pp: 257-273.
Indraratna, B., Balasubramaniam, A. and Sivaneswaran, N., 1997. Analysis of Settlement and Lateral Deformation of Soft Clay Foundation Beneath Two Full-Scale

Embankments, *International Journal of Numerical and Analytical Methods in Geomechanics*, Vol. 21 No. 9, pp 599 – 618
Indraratna, B. & Redana, I.W. 1998. "Laboratory Determination of Smear Zone due to Vertical Drain Installation", *Journal of Geotechnical Engineering*, American Society of Civil Engineers, Vol. 125 (1) pp. 96 - 99
Indraratna, B. & Redana, I.W. 2000. "Numerical Modelling of Vertical Drains with Smear and Well Resistance installed in Soft Clay", *Canadian Geotechnical Journal*, Vol. 37, pp 132 - 145
ITASCA Consulting Group, 2002. *FLAC 5.0 Users Guide*, Itasca Consulting Group, 708 South Third Street, Suite 310, Minneapolis, MN 55415 USA
Jamiolkowski, M. & Lancellotta, R. "Consolidation by Vertical Drains – Uncertainties Involved in Prediction of Settlement Rates", *Proceedings of 10th International Conference on Soil Mechanics and Foundations Engineering*, Stockholm
Jamiolkowski, M., Lancelotta, R. and Wolski, W. 1983. "Precompression and Speeding Up Consolidation", *Proceedings of the 8th European Conference on Soil Mechanics and Foundations Engineering*, Vol. 3. Helsinki
Kjellman, W. 1948. "Accelerating Consolidation of Fine Grain Soils by means of Cardboard Wicks", *Proceedings of the 2nd International Conference on Soil Mechanics and Foundation Engineering*, Vol. 2, pp 302 - 305
Krizek, R.J. and Sheeran, D.E.,1971. "Preparation of Homogeneous Samples by Slurry Consolidation", *Journal of Materials*, Vol 6, pp 356 - 373
Krizek, R.J., Edil, T.B. and Kutay Ozaydin, I.,1975. "Preparation and identification of Clay Samples with a Controlled Fabric", *Journal of Engineering Geology*, 9, pp 13 - 38
Lee, I.K., White, W. & Inglas, O.G. 1983. *"Geotechnical Engineering",* Pitman
Litwinowicz, A., Wijeyakulasuriya, C. V. and Brandon, A. N., 1994. "Performance of a Reinforced Embankment on a Sensitive Soft Clay Foundation", *Proceedings of the 5th IGS Conference*., Singapore, pp. 11 - 16
Loganathan, N., Balasubramaniam, A.S. and Bergado, D.T. 1993. "Deformation Analysis of Embankments", *Journal of Geotechnical Engineering*, Vol. 119 (8), pp 1185 - 1206

Lumb, P. 1966. "Variability of Natural Soils", *Canadian Geotechnical Journal*, Vol. 3 No. 2

Magnan, J.P., Bertaina, G., Khemissa, M., and Reiffsteck, Ph. (2001). "A Propos des Indices de Fluage Determines a L'Oedometre", *Proceedings of the 15th International Conference on Soil Mechanics and Geotechnical Engineering*, Istanbul, Vol. 1 pp 203 - 206

Mandel J., 1950. "Etude Mathematique de la Consolidation des Sols, Actes Due Colloque International De Mechanique", *Ppoitier*, Vol. 4, pp 9 – 19

Mandel, J., 1953, "Consolidation des Sols (Etude Mathematique)", *Geotechnique*, 3, pp 287 - 299

Mayne, P.W. and Poulos, H.G. 1999. "Approximate Displacement Influence Factors for Elastic Shallow Foundations", *Journal of Geotechnical and Geoenvironmental Engineering*, Vol. 125 (6) pp 453 - 460

Mesri, G. and Godlewski, P.M. 1977. "Time and Stress-Compressibility Interrealationship", *Journal of Geotechnical Engineering Division*, ASCE, 103, pp 417 - 430

Mesri, G. and Castro, A. 1987. "C_α/C_c Concept and K_0 during Secondary Compression", *Journal of Geotechnical Engineering Division*, ASCE, 113, 230 - 247

Mesri, G., Lo, D.O.K. and Feng, T. 1994. *ASCE Specialty Conference on Geotechnical Engineering*, Special Publication No. 40 (1) pp 8 - 76

Miura, N. & Chai, J.C. 2000. "Discharge Capacity of Prefabricated Vertical Drains Confined in Clay", *Geosynthetics International*, Vol. 7 (2) pp 119 - 135

Nagaraj, T.S. & Miura, N. 2001. *Soft Clay Behaviour – Analysis and Assessment*, A.A. Balkema Publishers, Rotterdam, Netherlands

Nash, D.F.T., Sills, G.C. & Davision, L.R. 1992. "One Dimensional Consolidation Testing of Soft Clay from Bothkennar", Geotechnique, Vol. 42 (2) pp 241 - 256

National Association of Testing Authorities, 1984. *Soils Interlaboratory Test – September 1984 – PTAC Report No. 19*, National Association of Testing Authorities, Chatswood, NSW

National Association of Testing Authorities, 1989. *Soils Proficiency Test Program –*

November 1989 – PTAC Report No. 60, National Association of Testing Authorities, Chatswood, NSW

Nishida, Y. 1956. "A Brief Note on Compression Index of Soils", *Journal of Soil Mechanics and Foundations*, American Society of Civil Engineers, Vol 32 SM3 pp 1027.1 – 1027.14

Ohta, H., Iizuka, A., Mitsuhashi, Y. and Nabetani, M. 1991. "Deformation analysis of Anisotropically Consolidated Clay Foundation Loaded by 5 Embankments" *Proceedings of the 7th International Conference on Computer Methods and Advances in Geomechanics*, Cairns, A.A. Balkema. Vol.2.

Onoue, A., Ting, N.H., Germaine, J.T., and Whitman, R.V. 1991. "Permeability of Disturbed Zone around Vertical Drains", *Proceedings of the American Society of Civil Engineers*, Geotechnical Engineering Congress, Colorado, pp 879 - 890

Osterberg, J.O. 1957. "Influence values for Vertical Stresses in Semi-Infinite Mass due to Embankment Loading", *Proceedings of the 4th International Conference on Soil Mechanics and Foundation Engineering*, Vol. 1. pp 393

Pankin, A.K., Mesri, G., Feng, T.W. and Shahien, M. 2000. "Coefficient of Consolidation by Inflection Point Method", *Journal of Geotechnical and Geoenvironmental Engineering,* 126 (12) pp 1211 - 1212

Parkin, A. K. (1978). "Coefficient of consolidation by the velocity method." *Géotechnique*, London, 28(4), 472–474.

Parry, R.H.G and Wroth, C.P., 1977. "Shear Properties of Soft Clays", *Report presented at Symposium on Soft Clay*, Bangkok, Thailand

Perloff, W.H. and Baron, W. 1976. "Soil Mechanics – Principles and Applications", The Ronald Press Company, New York

Potts, D.M. and Zdravkovic, L., 1999. *Finite Element Analysis in Geotechnical Engineering: Theory*, Thomas Telford, London

Potts, D.M. 2003. "Numerical Analysis: A Virtual Dream or Practical Reality?", *Geotechnique*, Vol. 3 No. 6, pp 235 - 273

Poulos, H.G. 1972. "Difficulties in the Prediction of Horizontal Deformations of Foundations", *Journal of Soil Mechanics and Foundations Division*, American Society

of Engineers, Vol. 98 (SM8) pp 843 - 848
Poulos, H.G. and Davis, E.H. 1974. "Elastic Solutions for Soils and Rock Mechanics", John Wiley and Sons, New York, United States of America
Prakash, K. and Sridharan, A. 2002. "Determination of Liquid Limit from Equilibrium Sediment Volume", Technical Note, *Geotechnique*. Vol. 53 No. 9 pp 693 - 696
Proficiency Testing Australia. 2006. *Guide to Proficiency Testing Australia*, Proficiency Testing Australia, Silverwater, New South Wales
Queensland Department of Main Roads. 1978. *Queensland Materials Testing Manual Q103C - Particle Size Distribution (Hydrometer),* Materials and Geotechnical Services Branch (Internal Document)
Queensland Department of Main Roads. 1978. *Queensland Materials Testing Manual Q183 -Oedometer Consolidation Test*, Materials and Geotechnical Services Branch (Internal Document)
Queensland Department of Main Roads. 1987. *Queensland Materials Testing Manual Q105 – Plastic Limit and Plasticity Index,* Materials and Geotechnical Services Branch (Internal Document)
Queensland Department of Main Roads. 1988. *Queensland Materials Testing Manual Q104D - One point Liquid Limit (Cone Penetrometer),* Materials and Geotechnical Services Branch (Internal Document)
Queensland Department of Main Roads. 1989. *Queensland Materials Testing Manual Q171 - Moisture Content*, Materials and Geotechnical Services Branch (Internal Document)
Queensland Department of Transport, 1991. *Sunshine Motorway Stage 2 – Area 2 Geotechnical Investigation. Materials and Geotechnical Services Branch Report No. R1765,* Materials and Geotechnical Services Branch, Brisbane, Queensland
Queensland Department of Main Roads, 1991. *Sunshine Motorway Stage 2 – Area 2 Geotechnical Investigation (Report No. R1765),* Materials and Geotechnical Services Branch, Brisbane, Queensland
Queensland Department of Main Roads, 1991. "Sunshine Motorway Stage 2 – Area 2 Geotechnical Design (Report No. R1770)", Materials and Geotechnical Services

Branch, Brisbane, Queensland
Queensland Department of Main Roads, 1992. *Sunshine Motorway Stage 2 – Interim Report on the Performance of the Trial Embankment Area 2A (Ch 28490 – 28640) (Report No. R1802)* Materials and Geotechnical Services Branch, Brisbane, Queensland
Raymond, G.P., and Wahls, H.G. 1976. "Estimating 1-Dimensional Consolidation, Including Secondary Compression, of Clay loaded from Overconsolidated to Normally Consolidated State", Special Report, *Transportation Research Board*, Washington DC
Redana, I.W. 1999. "Effectiveness of Vertical Drains in Soft Clay with Special Reference to Smear Effect", *PhD Dissertation*, University of Wollongong, Wollongong, NSW, Australia
Robinson, R.G., and Allam, M.M. 1996. "Determination of Coefficient of Consolidation from Early Stage of log t Plot", *Geotechnical Testing Journal*, ASTM, 19(3) pp 316 - 320
Roscoe, K.H., and Burland, J. B., 1968. "On the Generalised Stress Strain Behaviour of Wet Clay", *Engineering Plasticity*, Cambridge University Press, Cambridge, U. K., pp 535 - 609
SAI Global. 1992. "AS 1289.2.1.1 – Methods of testing soils for engineering purposes – Determination of the moisture content of a soil – Oven drying method (Standard method)", *Standards Australia (Accessed via website: http://www.saiglobal.com/online/autologin.asp)*
SAI Global. 1995. "AS 1289.3.1.1 – Methods of testing soils for engineering purposes - Soil classification tests - Determination of the liquid limit of a soil - Four point Casagrande method", *Standards Australia (Accessed via website http://www.saiglobal.com/online/autologin.asp)*
SAI Global. 1995. "AS1289.3.2.1 – Methods of testing soils for Engineering Purposes – Soil Classification Tests – Determination of the Plastic Limit of a Soil – Standard Method ", *Standards Australia (Accessed via website http://www.saiglobal.com/online/autologin.asp)*
SAI Global. 1995. "AS 1289.3.3.1 – Methods of testing soils for engineering purposes - Soil classification tests - Calculation of the plasticity index of a soil", *Standards*

Australia (Accessed via website: http://www.saiglobal.com/online/autologin.asp)
SAI Global. 1995. "AS1289.3.4.1 – Methods of testing soils for Engineering Purposes – Soil Classification Tests – Determination of the Linear Shrinkage of a Soil – Standard Method ", *Standards Australia (Accessed via website http://www.saiglobal.com/online/autologin.asp)*
SAI Global. 1995. "AS 1289.3.5.1 – Methods of testing soils for engineering purposes – Soil classification tests – Determination of the Soil ", *Standards Australia (Accessed via website: http://www.saiglobal.com/online/autologin.asp)*
SAI Global. 1995. "AS 1289.3.5.2– Methods of testing soils for engineering purposes – Determination of the soil particle density of a soil – Standard method", *Standards Australia (Accessed via website: http://www.saiglobal.com/online/autologin.asp)*
SAI Global. 1998**.** "AS 1289.6.6.1 – Methods of testing soils for engineering purposes - Soil strength and consolidation tests - Determination of the one-dimensional consolidation properties of a soil - Standard method" *Standards Australia. (Accessed via website: http://www.saiglobal.com/online/autologin.asp)*
SAI Global. 1999. "AS 1289.1.3.1– Methods of testing soils for engineering purposes - Sampling and preparation of soils - Undisturbed samples - Standard method", *Standards Australia (Accessed via website http://www.saiglobal.com/online/autologin.asp*)
Schmertmann, J.H., Brown, P.R. and Hartman, J.P. 1978. "Improved Strain Influence Factor Diagrams", Journal of Geotechnical Engineering Division, Vol. 104 (8) pp 1131 - 1135
Schofield, A.N. and Wroth, C.P. 1968. *Critical State Soil Mechanics*, McGraw Hill, London, UK
Schultze, E. 1972. "Frequency Distributions and Correlations of Soil Properties", *Statistics and Probability in Civil Engineering*, Hong Kong University Press (Hong Kong International Conference) distributed by Oxford University Press, London
Sivakugan, N., Chameau, J., Holtz, R. and Altschaefft, A., 1988. "Servo-Controlled Cuboidal Shear Device" *Geotechnical Testing Journal*, Vol. 11 (2), pp 119 - 124
Sivakugan, N. 2006. *A FLAC Primer*, James Cook University, Townsville, Australia
Sivakugan, N., Rankine, R.M., Rankine, K.J., and Rankine, K.S. (2006). "Geotechnical

considerations in mine backfilling in Australia," *Journal of Cleaner Production*, Elsevier, 14, 1168-1175

Skempton, A.W. 1944. "Notes on the Compressibility of Clays", Quarterly Journal of Geological Society, London, Vol. 100 pp 119 – 135

Sridharan, A., and Prakash, K. 1985. "Inproved Rectangular Ref Hyperbola Method for Determination of Coefficient of Consolidation", *Geotechnical Testing Journal*, ASTM, 8(1) pp 37 - 40

Sridharan, A., and Prakash, K. 1995. "Critical Appraisal of Laboratory Determination of c_v", *Compression and Consolidation of Clayey Soils*, A.A. Balkema, Rotterdam, pp 567 - 572

Sridharan, A., and Prakash, K. 1998. "Secondary Compression Factor ", *Proceedings of Institution of Civil Engineers – Geotechnical Engineering*, 131(2) pp 96 - 103

Sridharan, A. and Nagaraj, H.B. 2004. "Coefficient of Consolidation and its Correlation with Index Properties of Remoulded Soils". *Geotechnical Testing Journal*, 27(5) pp 6

Stewart, D.P. and McInnes, D.B. 1993 "The Impact of Lateral Soil Displacements on the Goongoongup Rail Bridge, Perth" *Proceedings of the 8th Australian and New Zealand Conference on Geomechanics*, Hobart, Australia, pp. 345 - 351.

Tavenas, F., Mieussens, C. and Bourges, F. 1979. Lateral Displacements in Clay Foundations under Embankments, *Canadian Geotechnical Journal*, Issue 16, pg. 532 - 550

Taylor, D.W. 1942. "Research on Consolidation of Clays", *Serial No. 82*, Department of Civil and Sanitary Engineering, Massachusetts Institute of Technology, Cambridge, Mass

Ting, N.H., Onoue, A., Germaine, J.T., Whitman, R.V., and Ladd, C.C. 1990. "Effects of Disturbance on Soil Consolidation with Vertical Drains", *Research Report R90-11*, Department of Civil Engineering, MIT, MA, USA

U.S. Navy, 1971. "Soil Mechanics, Foundations and Earth Structures". *NAVFAC Design Manual DM-7*, Washington DC

Wijeyakulasuriya, V., Hobbs, G. and Brandon, A. 1999. "Some Experiences with Performance Monitoring of Embankments on Soft Clays", *Proceedings of the 8th ANZ*

Conference on Geomechanics, Hobart (preprint)
Wong, P. 2006. "*Preload Design, Part 1 – Review of Soil Compressibility Behaviour in Relation to the Design of Preloads*", Australian Geotechnical Society
Wong, P. 2006. "*Preload Design, Part 2 – An Analytical Method Based on Bjerrum's Time Line Principale and Comparison with Other Design Methods*", Australian Geotechnical Society
Wood, D.M. 1990. *Soil Behaviour and Critical State Soil Mechanics*. Cambridge University Press, 40 West 20th St., New York, NY, USA
Wood, D.M. 2004. Geotechnical Modelling, Spon Press, 29th West 35th Street, New York, NY, USA
Yoshikuni, H. & Nakanodo, H. 1974. "Consolidation of Fine-Grained Soils by Drain Wells with Finite Permeability", *Japanese Society of Soil Mechanics and Foundation Engineering*, Vol. 14 (2) pp 35 - 46
Youden WJ (1959) "Graphical Diagnosis of Inter-laboratory Test Results". *Industrial Quality Control*, 15, 24-28.
Zhu, G., Yin, J.H. and Graham, J., 2001. "Consolidation Modelling of Soils under the Test Embankment at Chek Lap Kok International Airport in Hong Kong using a Simplified Finite Element Method", *Canadian Geotechnical Journal*, 38(2) pp 349 - 364

Appendix A

Example of NATA Proficiency Test

Instructions and Results Sheets

NATA PROFICIENCY TESTING PROGRAM - SOILS

INSTRUCTIONS TO PARTICIPANTS

Laboratory Code: ____

To ensure that results from this program can be analysed properly, participants are asked to adhere carefully to the following instructions.

1. Each participant will be supplied with four soil samples, each of about 700 gms, labelled G, H, I and J. Samples G and H are clay soil types and Samples I and J are loam soil types.

2. Prior to testing, each sample is to be wet-sieved through a 425 μm sieve.

3. The following tests are to be performed ONCE ONLY per sample to the indicated part of AS 1289-1977, as amended (except as indicated in 4).

   (a) Liquid limit, to Part C1.1
   (b) Plastic limit, to Part C2.1
   (c) Plasticity index, to Part C3.1
   (d) Linear shrinkage, to Part C4.1

4. Laboratories registered with NATA for performing these tests solely to other methods are required to follow their registered methods and note this on the attached results sheet.

5. An additional objective of this program is to generate precision information. To achieve this a split level experimental design is being used.

   Therefore all tests must be performed on samples G and H concurrently, by the same operator. Similarly, though not necessarily with this same operator, all tests must be performed on samples I and J concurrently, by the same operator.

6. The results are to be reported on the attached form to the accuracy indicated. The additional information requested should also be supplied and any further comments are welcome.

7. NATA-registered laboratories are also to return an endorsed test report in the format that would be supplied to a customer.

8. Testing may commence as soon as samples are received. All laboratories must return results and reports **NO LATER THAN 13 JANUARY 1989 to:**

Mr J Neylan
Proficiency Testing Group
National Association of Testing Authorities, Australia
688 Pacific Highway
CHATSWOOD NSW 2067

Telephone: (02) 411 4000 Telex: 26378 Fax: (02) 411 8379

(NOTE: Similarly for Samples A, B, C, D, E, F)

Figure A.1. Example of Participant Instruction Sheet for Proficiency Testing (NATA, 1989)

NATA PROFICIENCY TESTING PROGRAM - SOILS

RESULTS SHEET

Laboratory Code: ____

TEST (Report to)	TEST METHOD	SAMPLE G	SAMPLE H	SAMPLE I	SAMPLE J
Liquid Limit (1%)					
Plastic Limit (1%)					
Plasticity Index (1%)					
Linear Shrinkage (0.5%)					

1. Dates of Tests: **Samples G and H** _____ **Samples I and J** _____

2. Which of the following grooving tool and height gauges as specified in AS 1289.C1.1 was used? Fig C1.1.2 or Fig C1.1.3 **(delete one)**

3. In determining plastic limit, was the soil formed into a thread by rolling between the operator's hand or two glass plates (delete one).

   If done differently across samples, please specify _____

4. In determining linear shrinkage please indicate:

   (a) mould size: _____

   (b) the manner in which excess soil was struck off the overfilled shrinkage mould (*)

   _____

5. Does your laboratory normally prepare samples by wet-sieving or dry-sieving? (delete one)

Signed: _____

(*) Two commonly practiced techniques are to either:

- **hold the palette blade perpendicular to the top of the mould, removing the excess material with a slow sawing action along the length of the mould; or^R**
- **hold the blade almost flat, removing excess material with long smooth strokes across the top of the mould.**

Figure A.2. Example of Participant Results Sheet for Proficiency Testing (NATA, 1989)

Appendix B

Z-Score Plots, Youden Diagrams and Relative Frequency Histograms for Liquid Limits

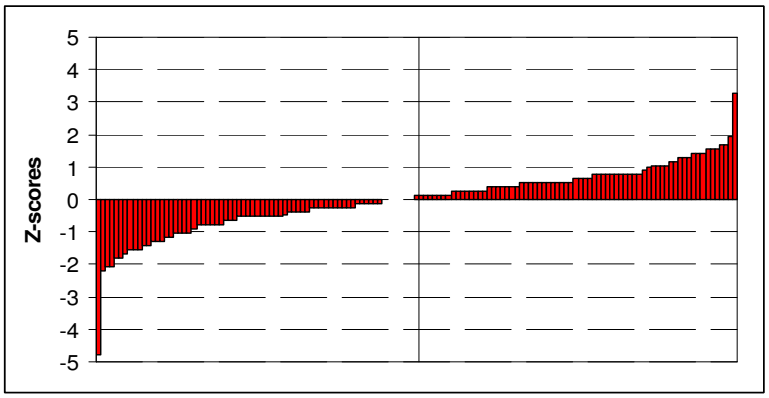

(a)

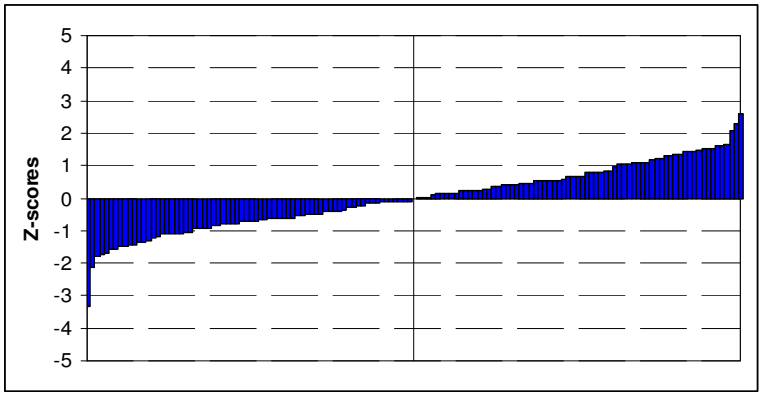

(b)

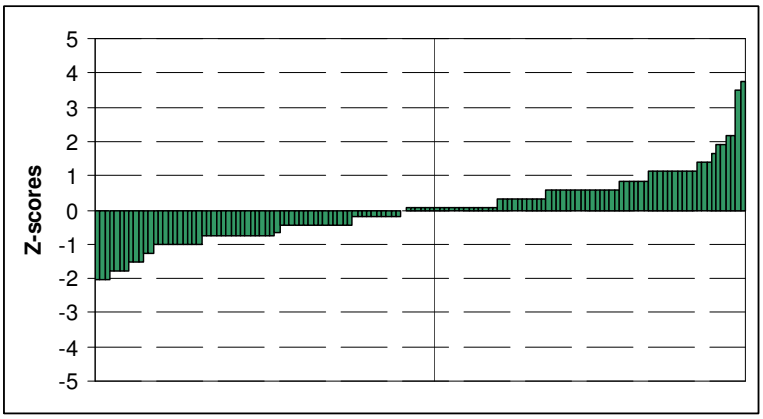

(c)

Figure B.1 Standardised Z-Scores for the Liquid Limit of (a) Sample A, (b) Sample B and (c) Sample C

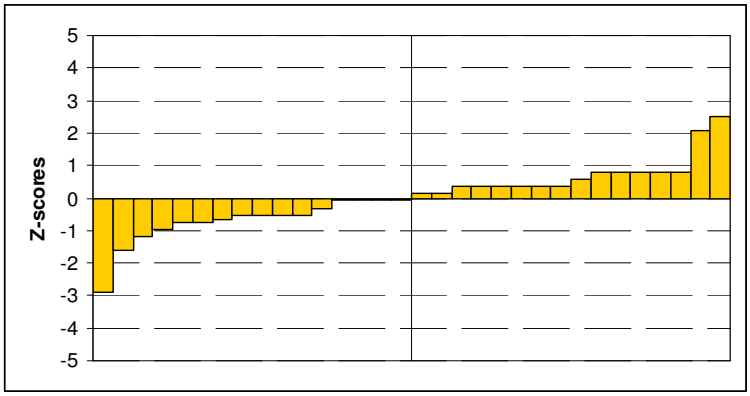

(a)

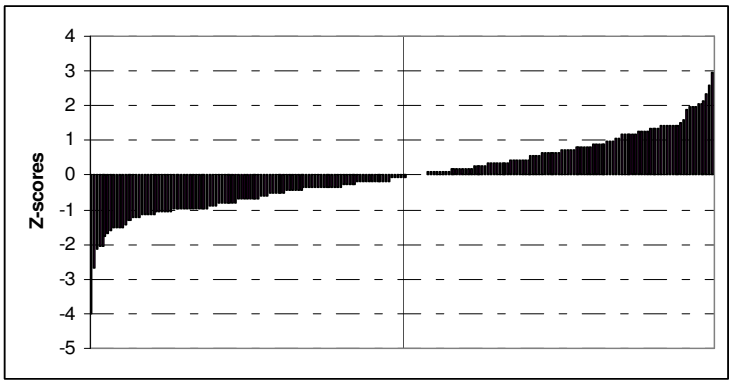

(b)

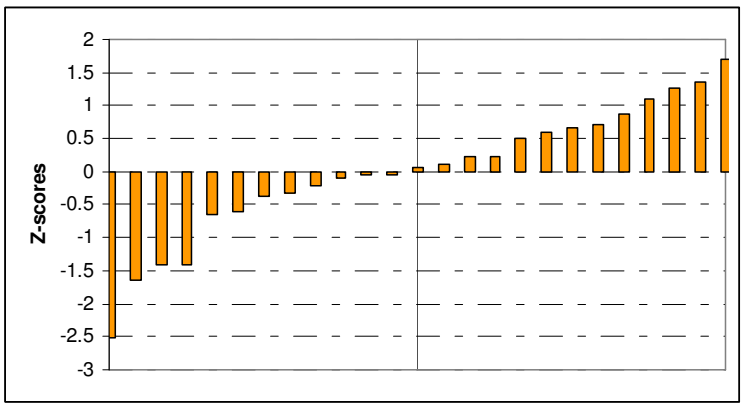

(c)

Figure B.2 Standardised Z-Scores for the Liquid Limit of (a) Sample D, (b) Sample E and (c) Sample F

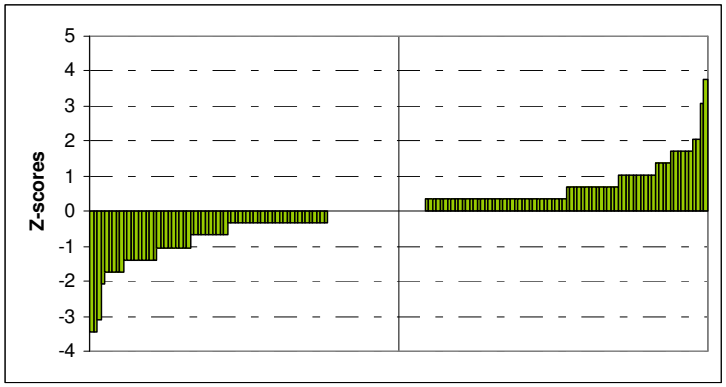

(a)

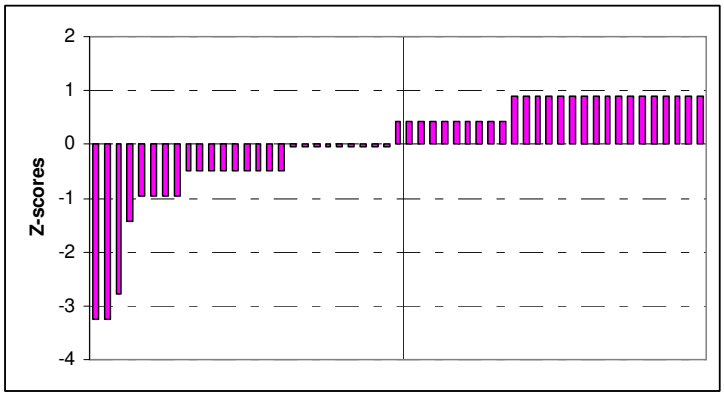

(b)

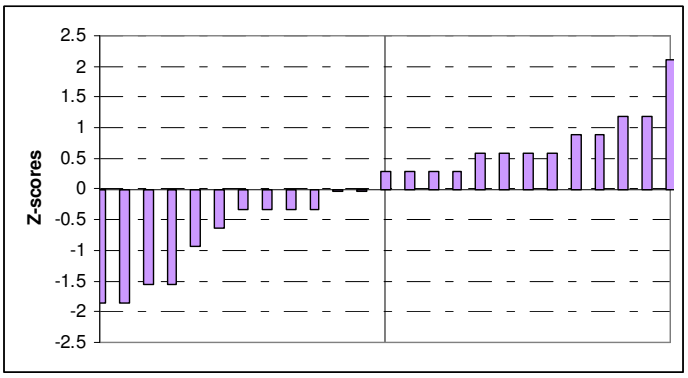

(c)

Figure B.3 Standardised Z-Scores for the Liquid Limit of (a) Sample G, (b) Sample H and (c) Sample I

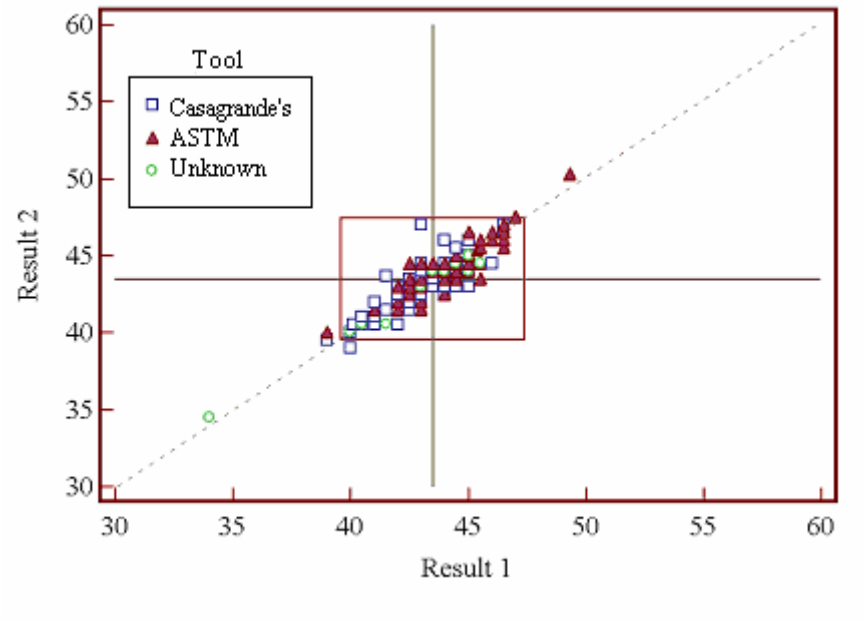

(a)

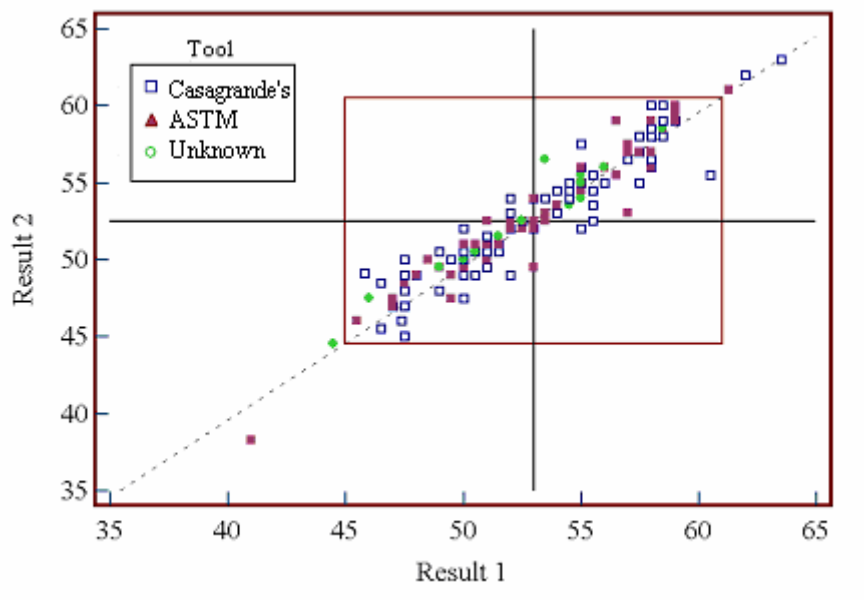

(b)

Figure B.4 Youden Plot for the Measured Liquid Limits of (a) Sample A and (b) Sample B

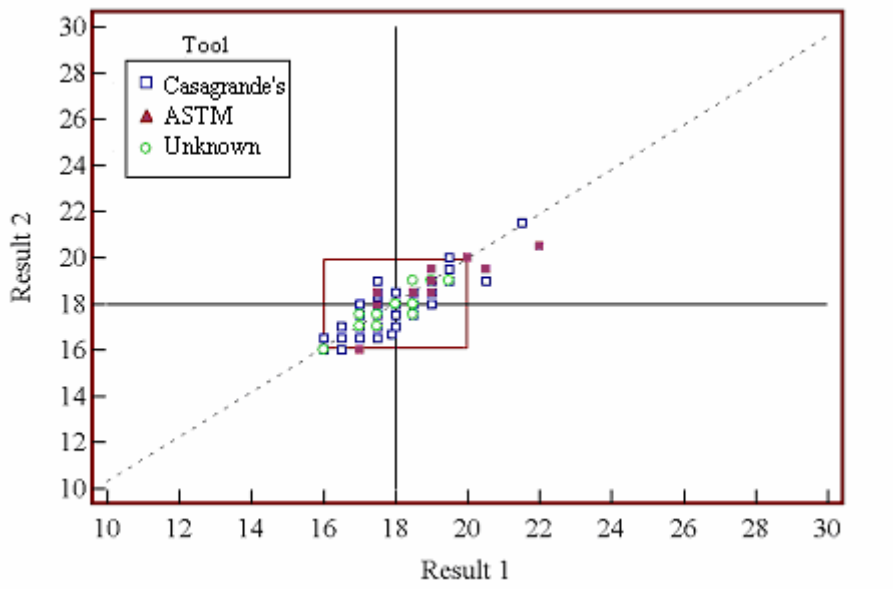

(a)

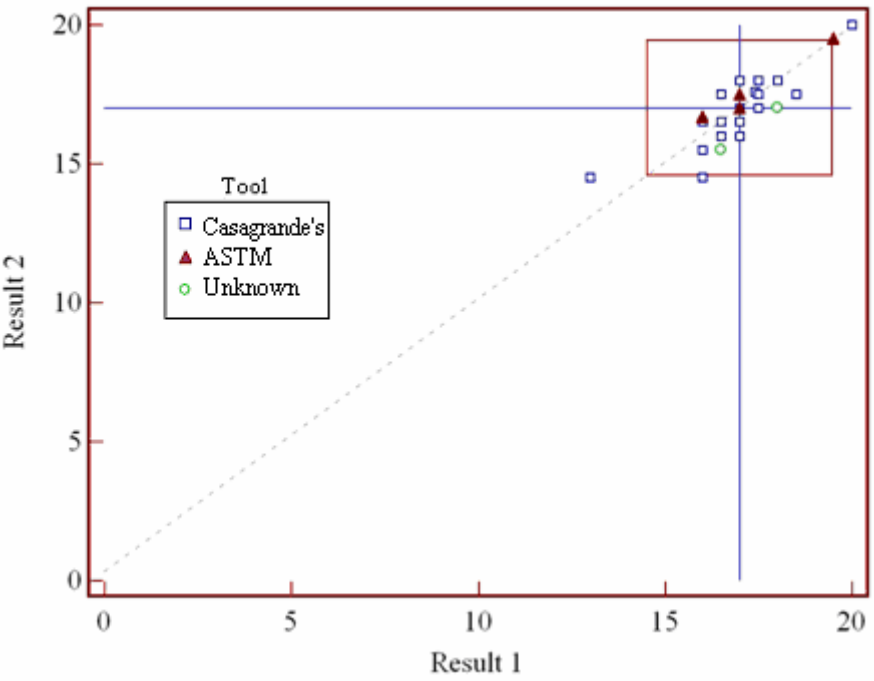

(b)

Figure B.5 Youden Plots for the Measured Liquid Limits of (a) Sample C and (b) Sample D

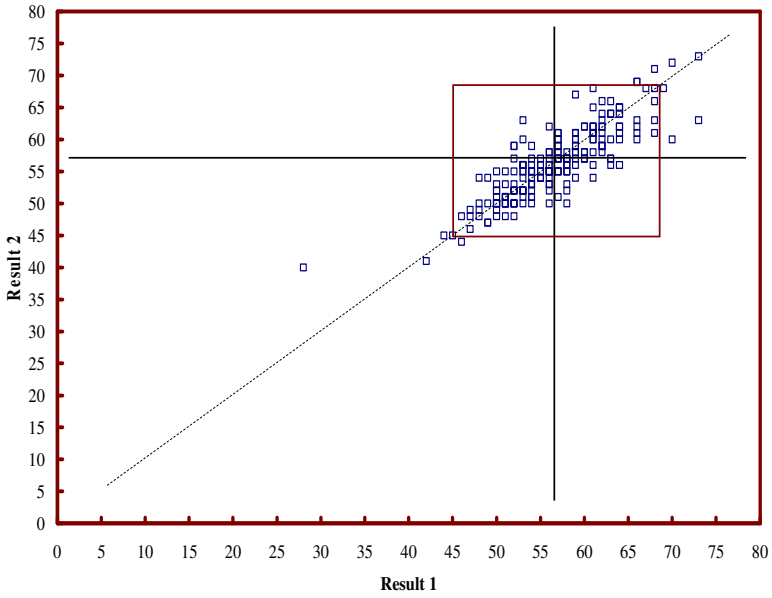

(a)

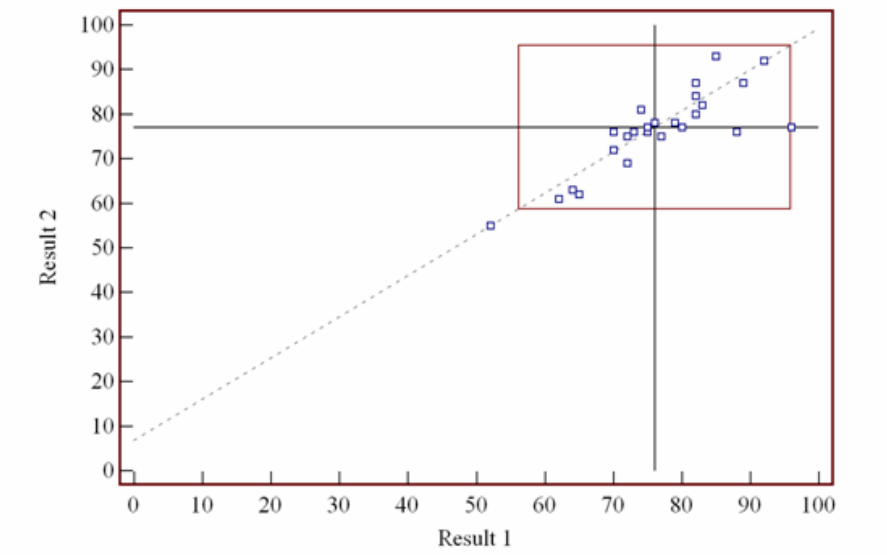

(b)

Figure B.6 Youden Plots for the Measured Liquid Limits of (e) Sample E and (f) Sample F

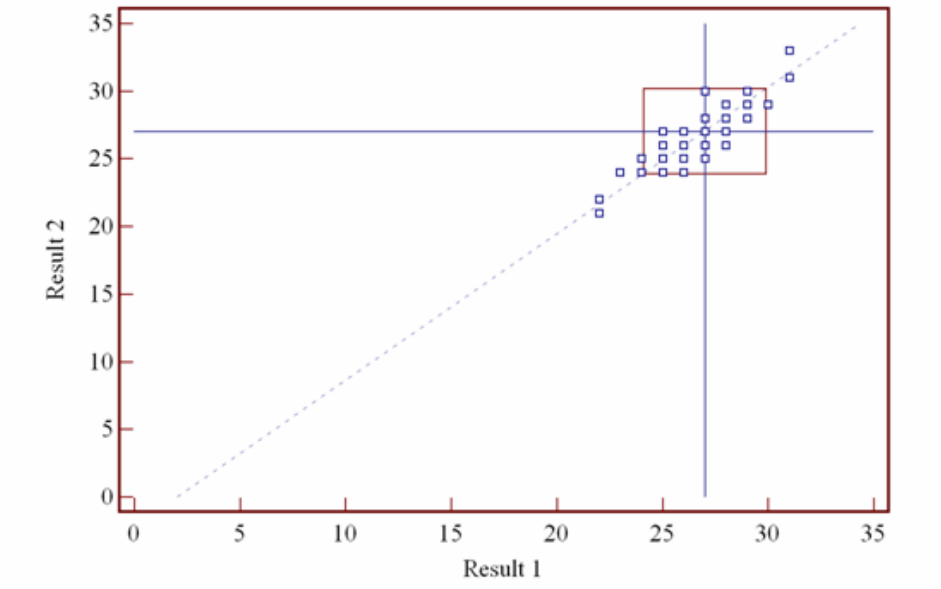

(a)

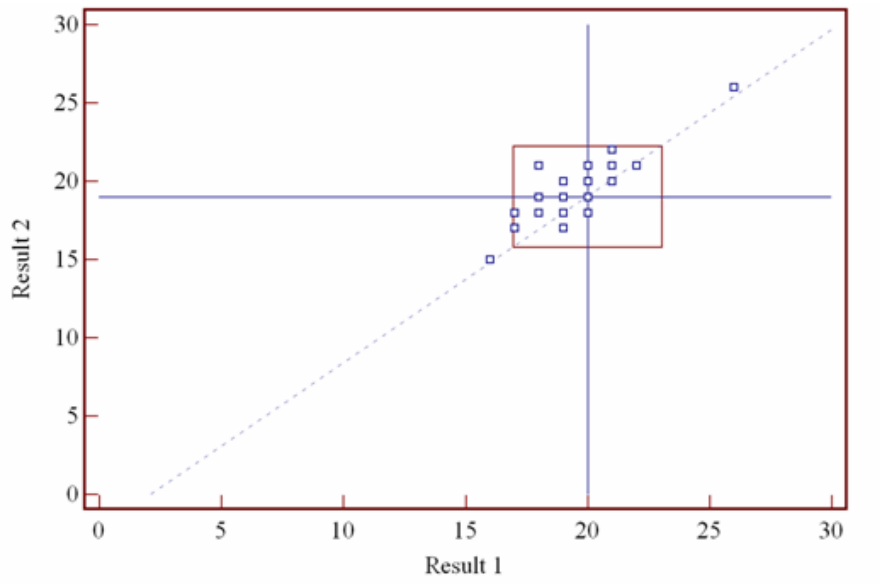

(b)

Figure B.7 Youden Plots for the Measured Liquid Limits of (a) Sample G and (b) Sample H

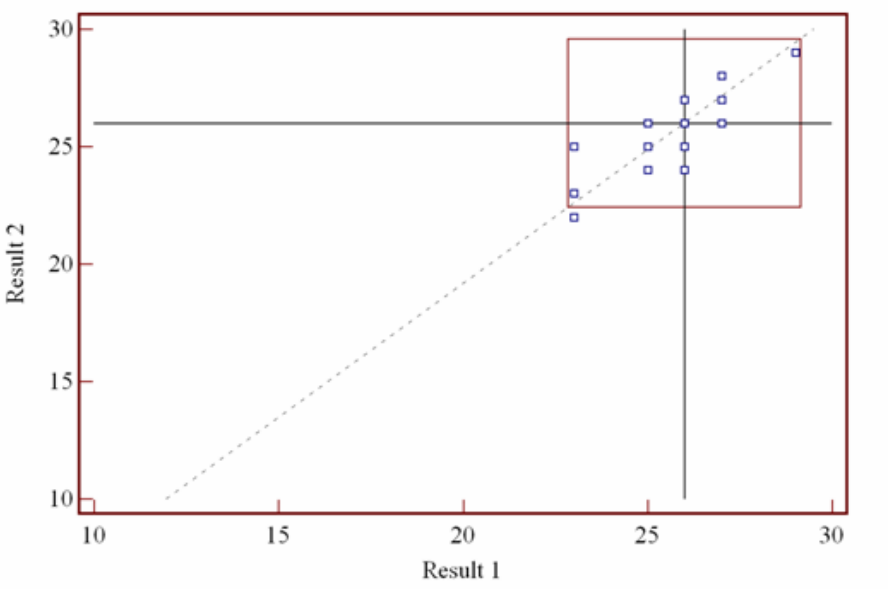

Figure B.8 Youden Diagram for the Measured Liquid Limits of Sample I

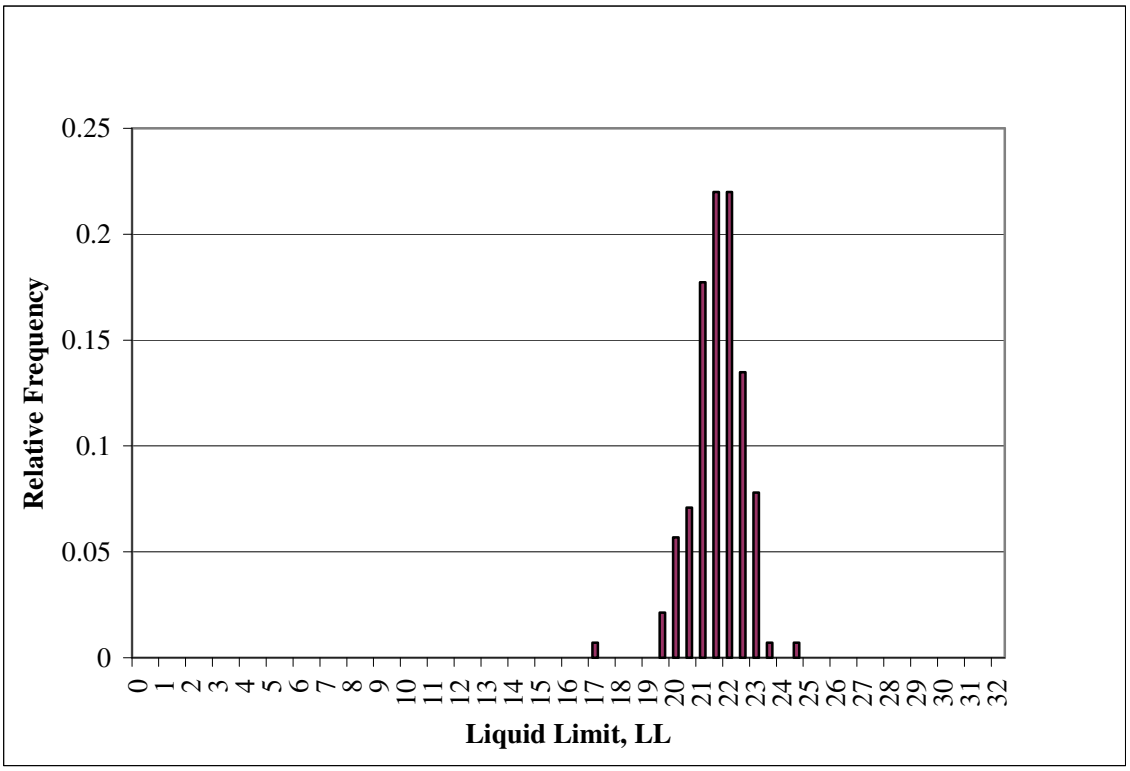

Figure B.9 Relative Frequency Histogram of Sample A Liquid Limits

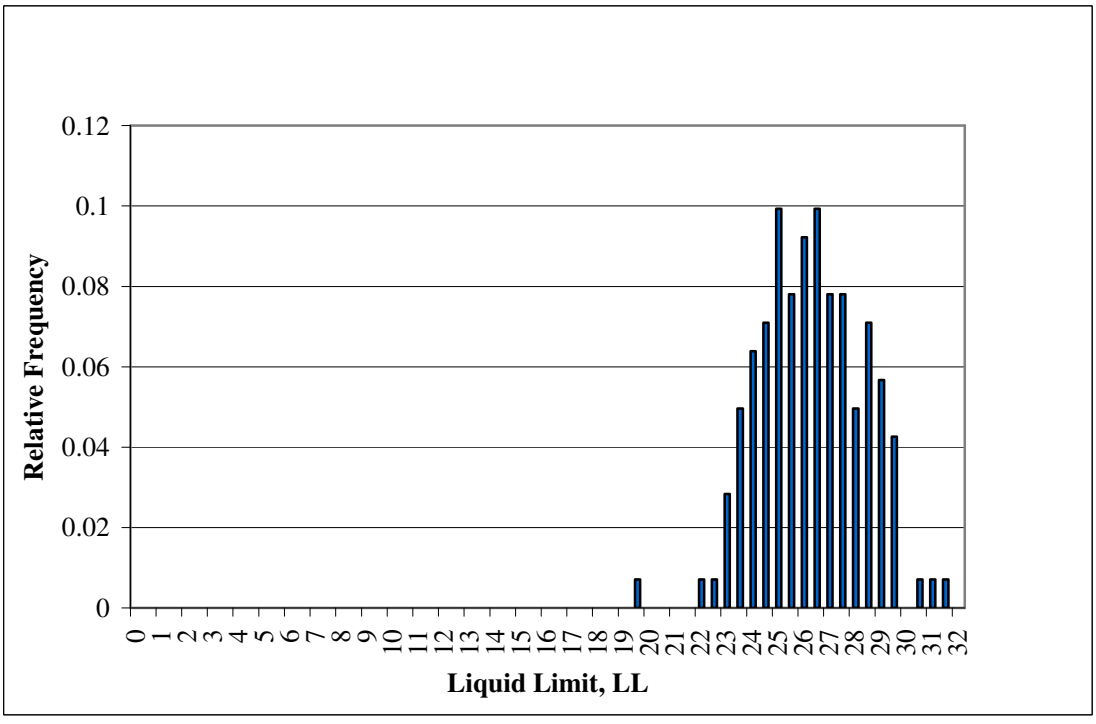

Figure B.10 Relative Frequency Histogram of Sample B Liquid Limits

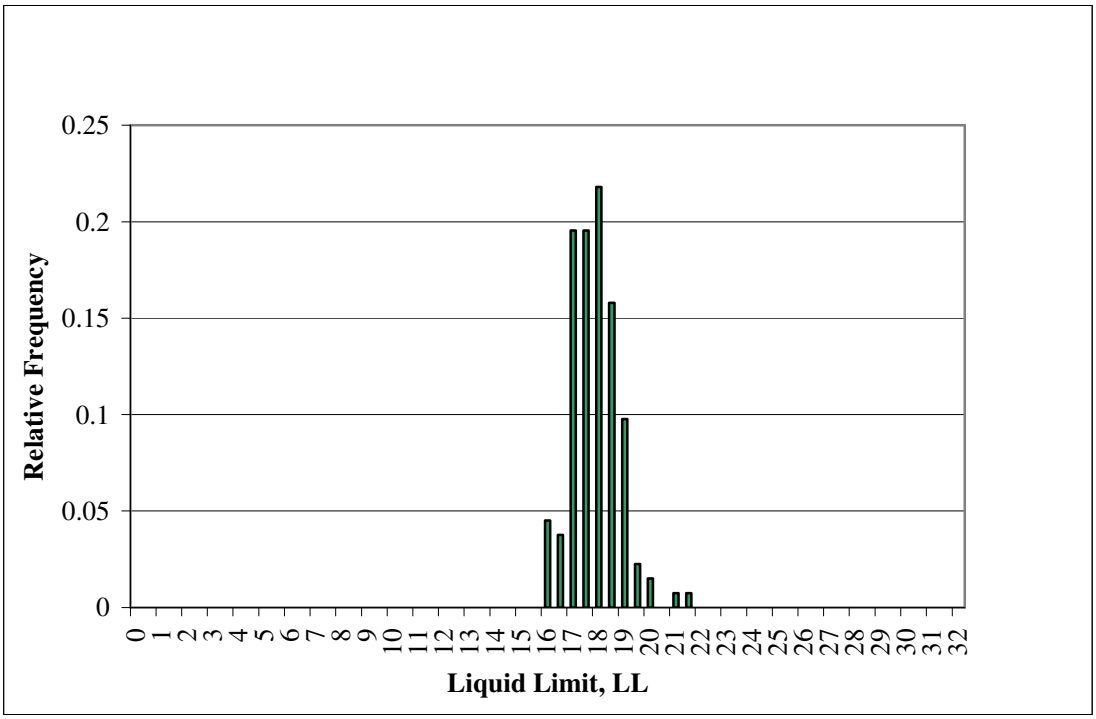

Figure B.11 Relative Frequency Histogram of Sample C Liquid Limits

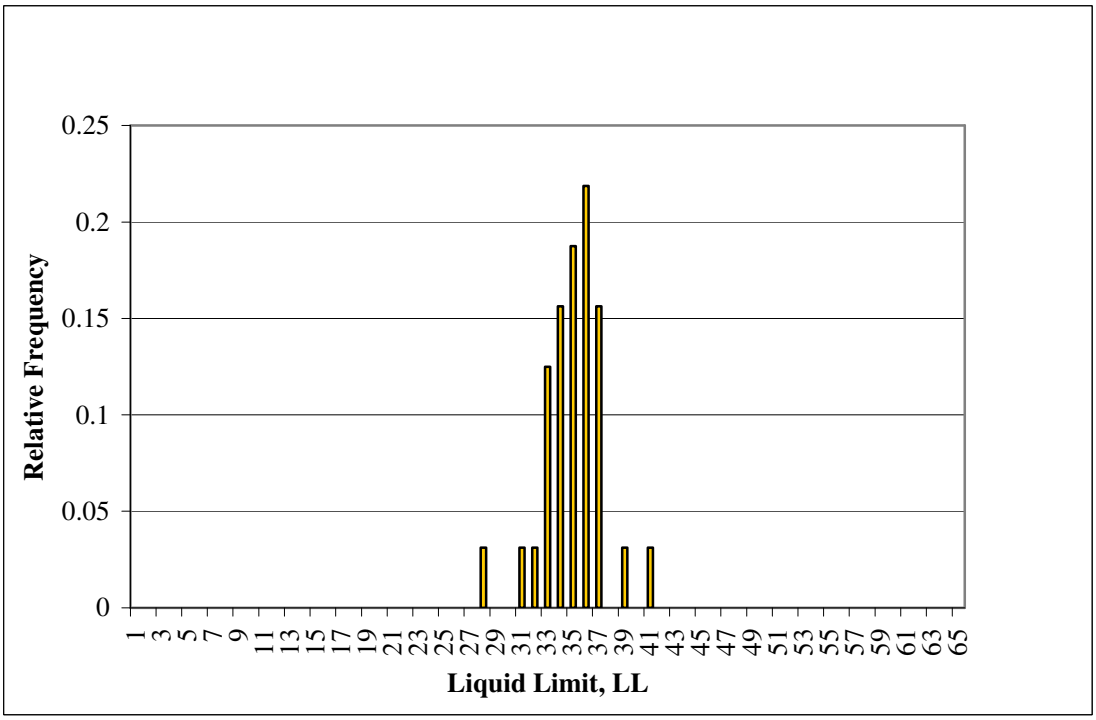

Figure B.12 Relative Frequency Histogram of Sample D Liquid Limits

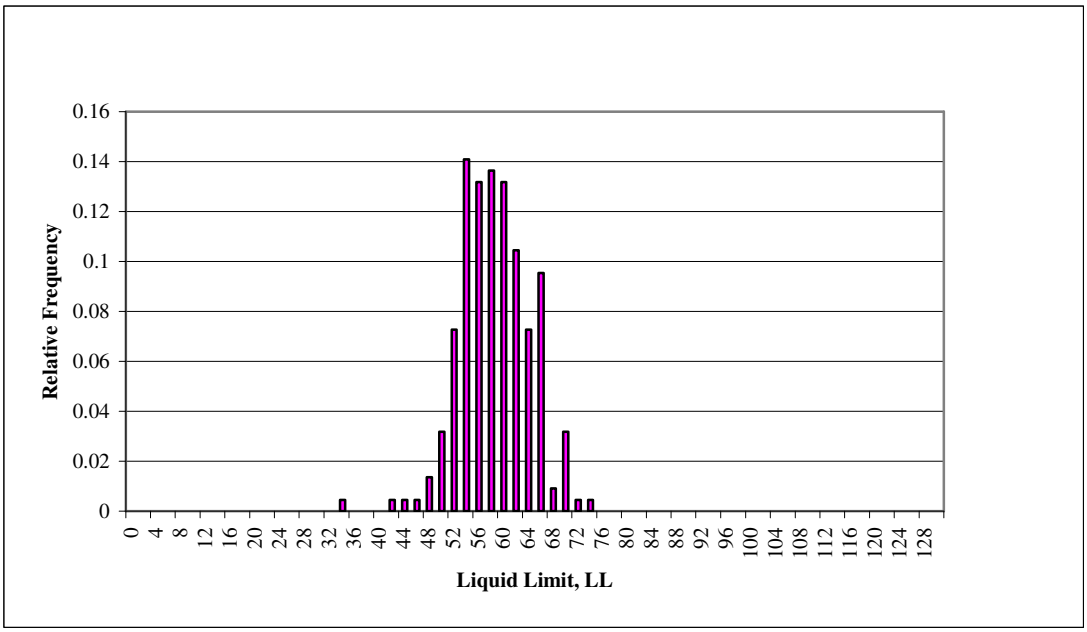

F**igure B.13** Relative Frequency Histogram of Sample E Liquid Limits

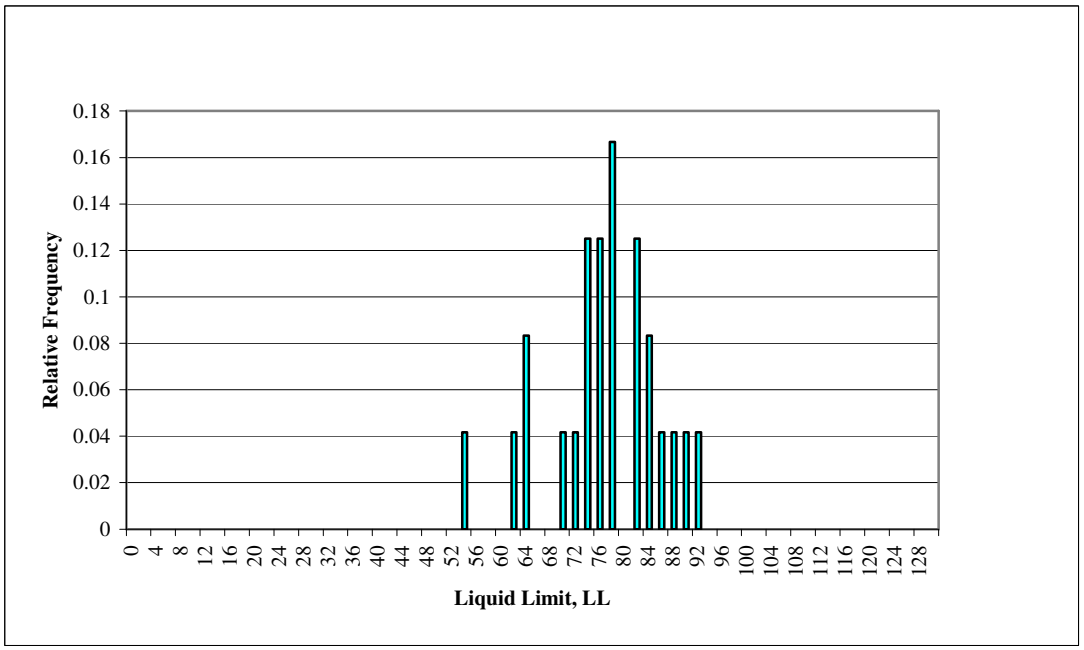

Figure B.14 Relative Frequency Histogram of Sample F Liquid Limits

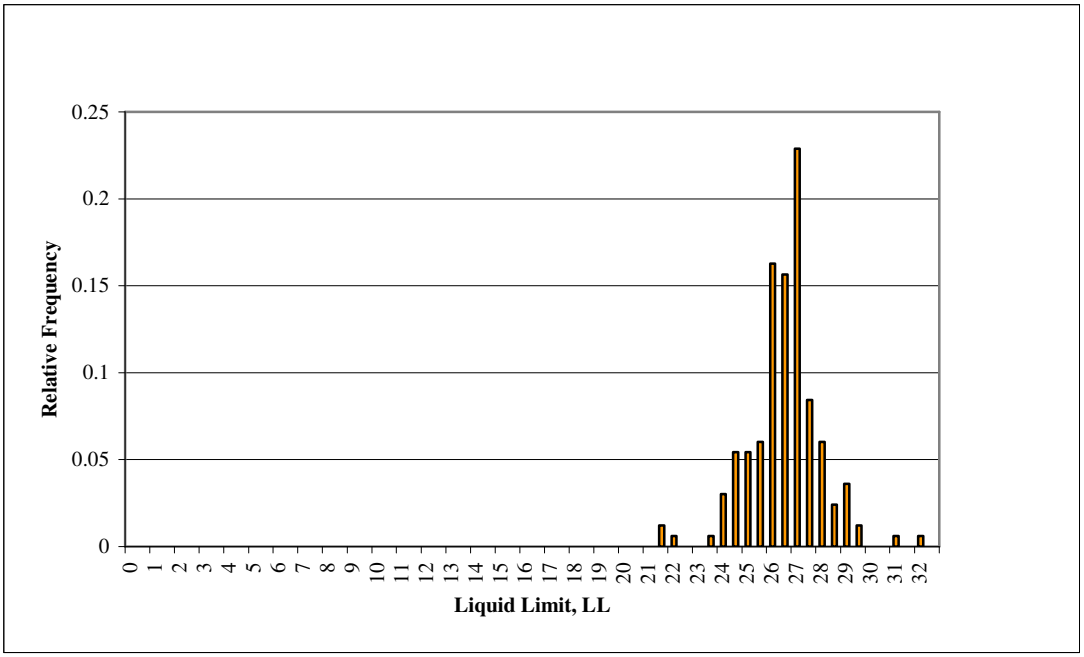

Figure B.15 Relative Frequency Histogram of Sample G Liquid Limits

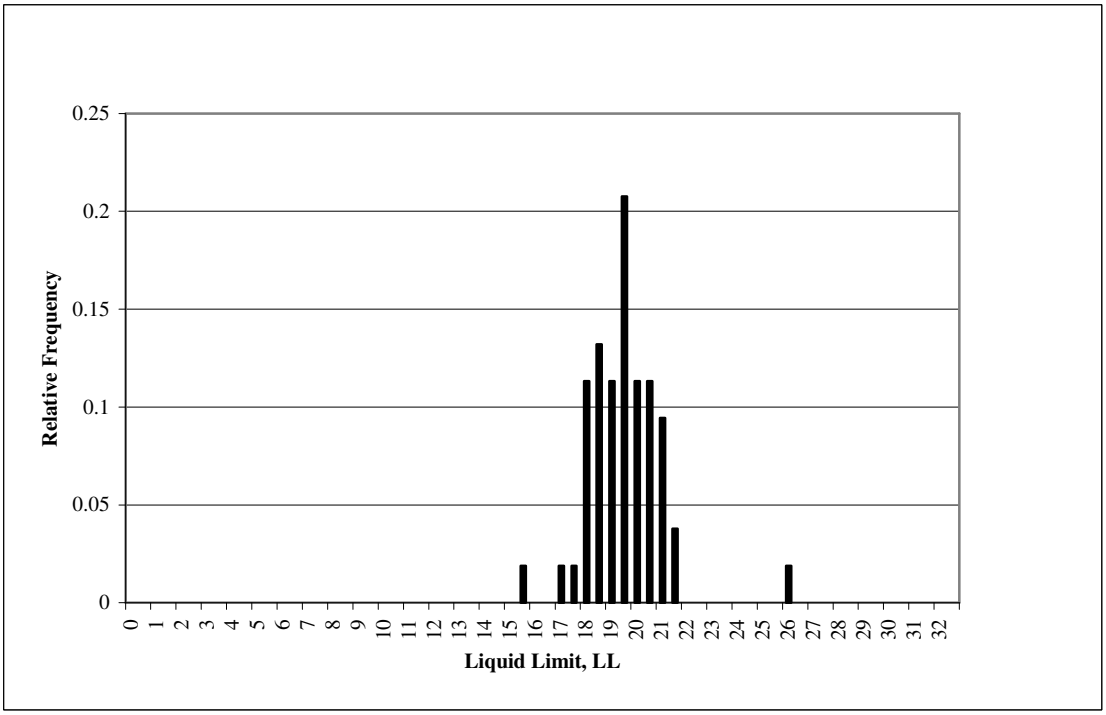

Figure B.16 Relative Frequency Histogram of Sample H Liquid Limits

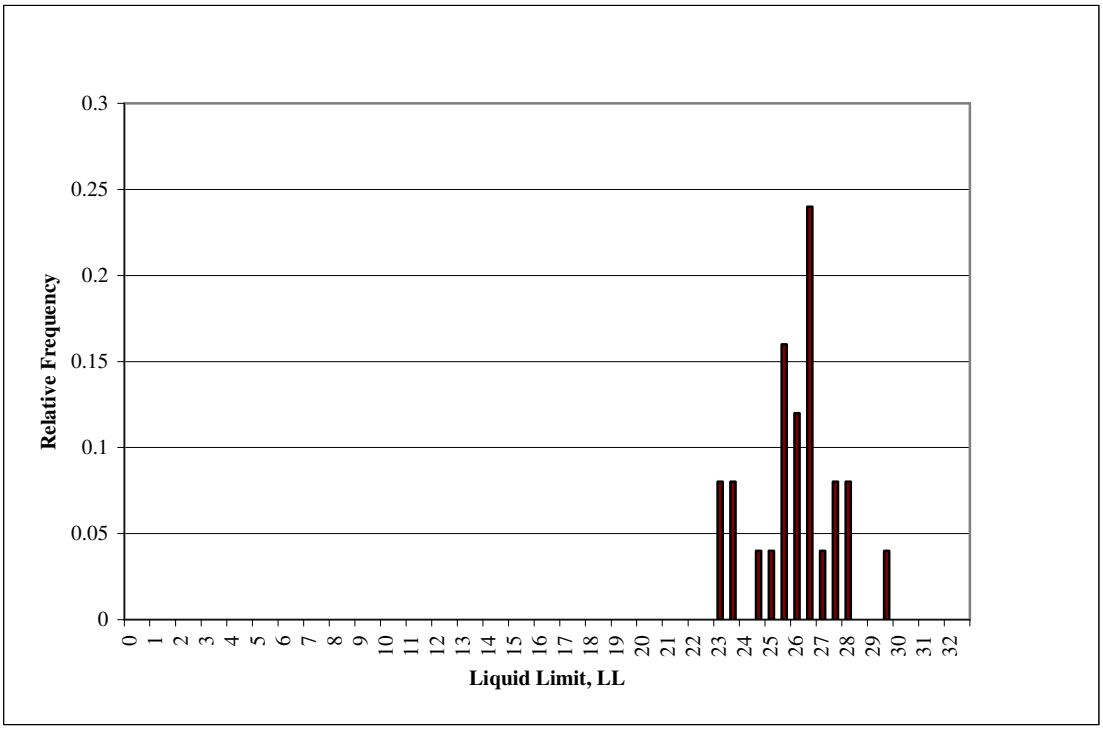

Figure B.17 Relative Frequency Histogram of Sample I Liquid Limits

Appendix C

Z-Score Plots, Youden Diagrams and Relative Frequency Histograms for Plastic Limits

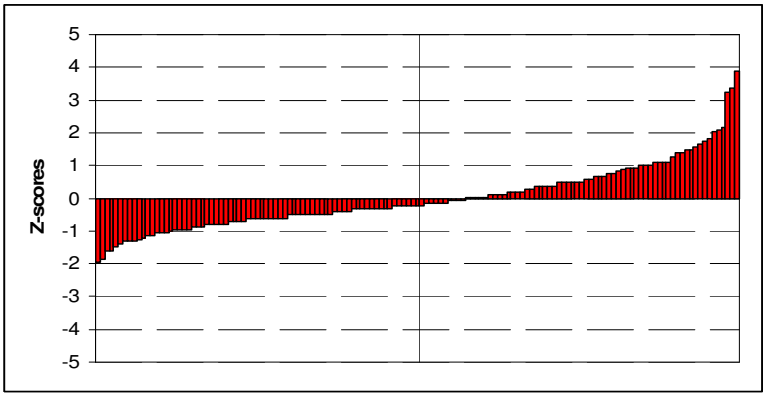

(a)

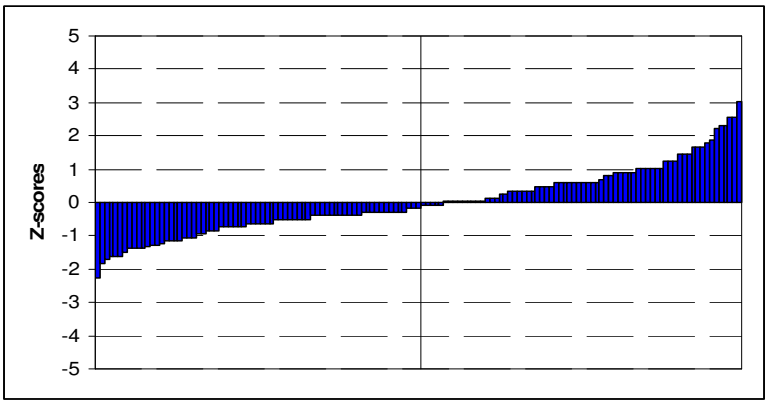

(b)

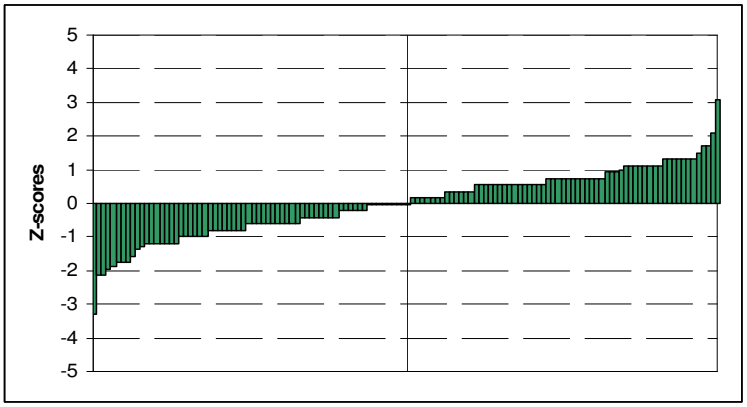

(c)

Figure C.1 Standardised Z-Scores for the Plastic Limit of (a) Sample A, (b) Sample B and (c) Sample C

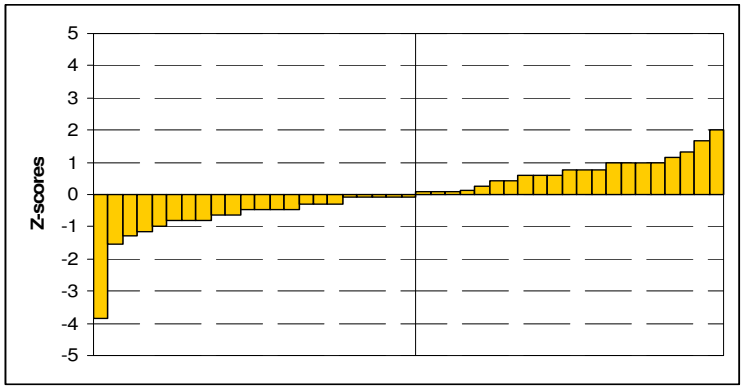

(a)

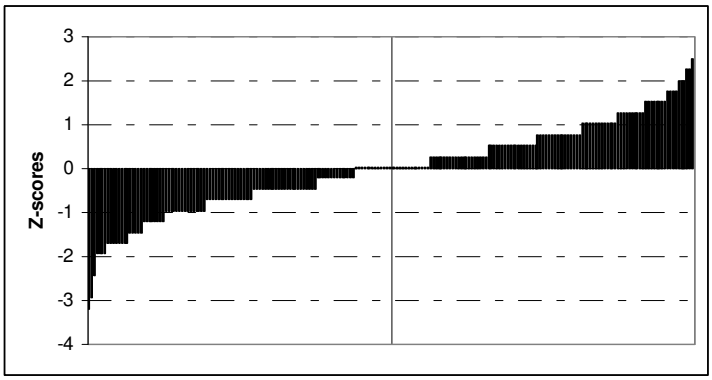

(b)

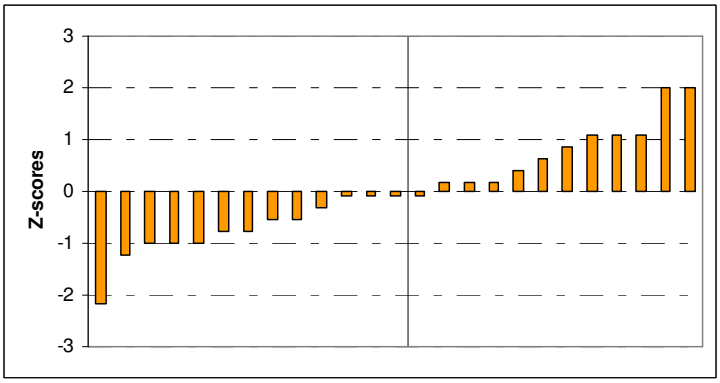

(c)

Figure C.2 Standardised Z-Scores for the Plastic Limit of (a) Sample D, (b) Sample E and (c) Sample F

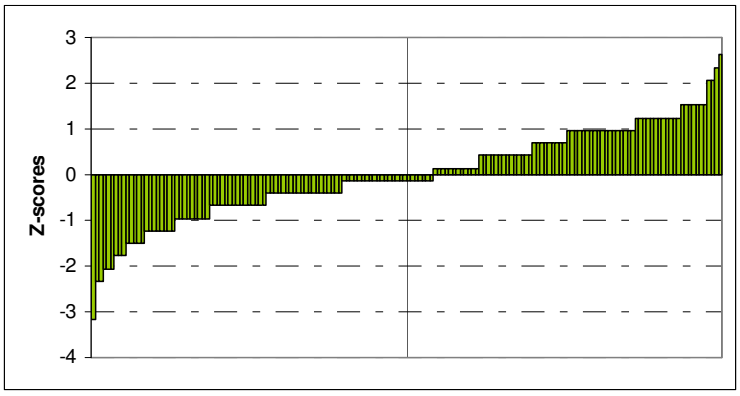

(a)

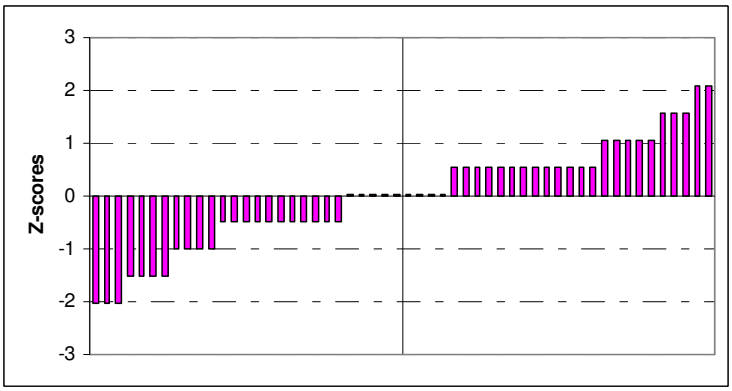

(b)

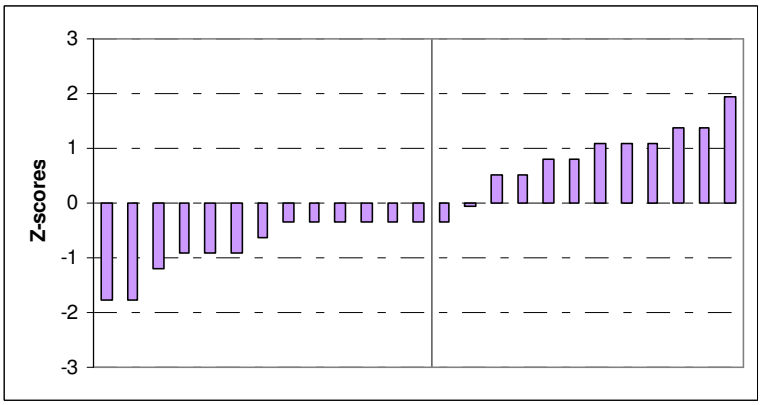

(c)

Figure C.3 Standardised Z-Scores for the Plastic Limit of (a) Sample G, (b) Sample H and (c) Sample I

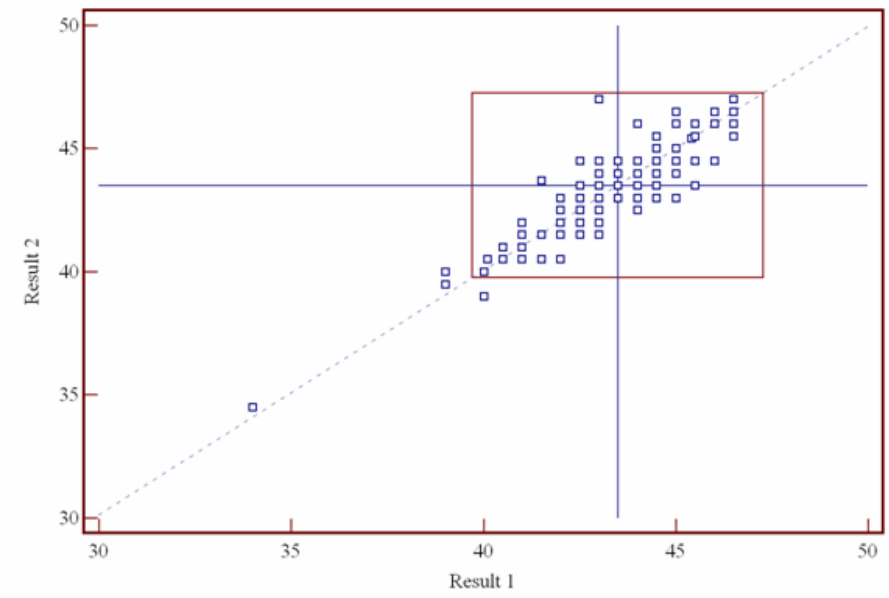

(a)

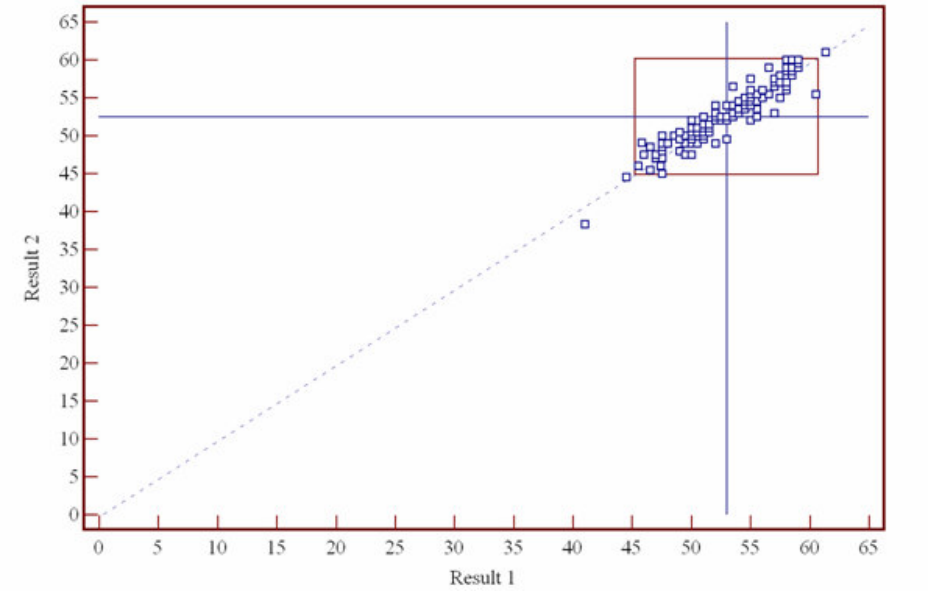

(b)

Figure C.4 Youden Plot for the Measured Plastic Limits of (a) Sample A and (b) Sample B

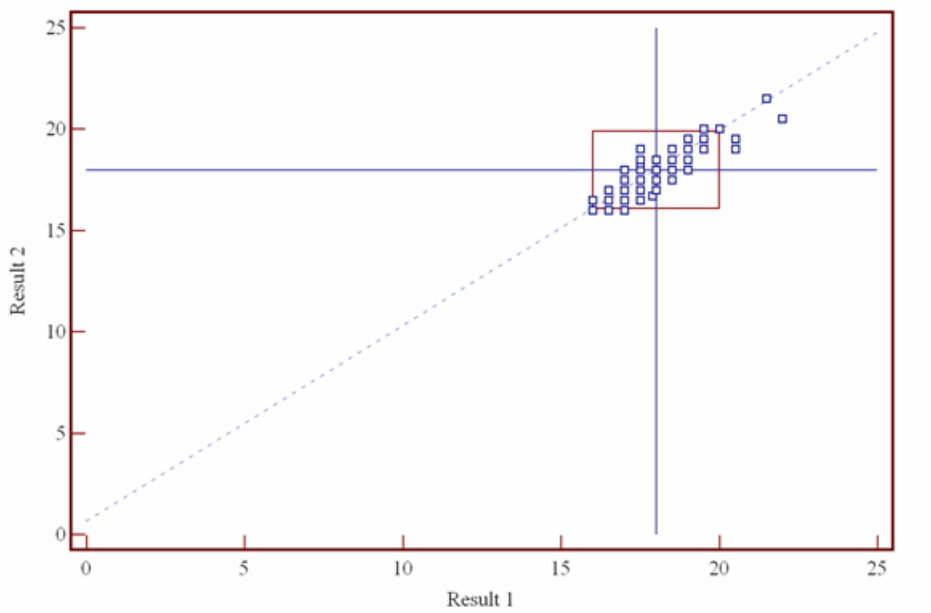

(a)

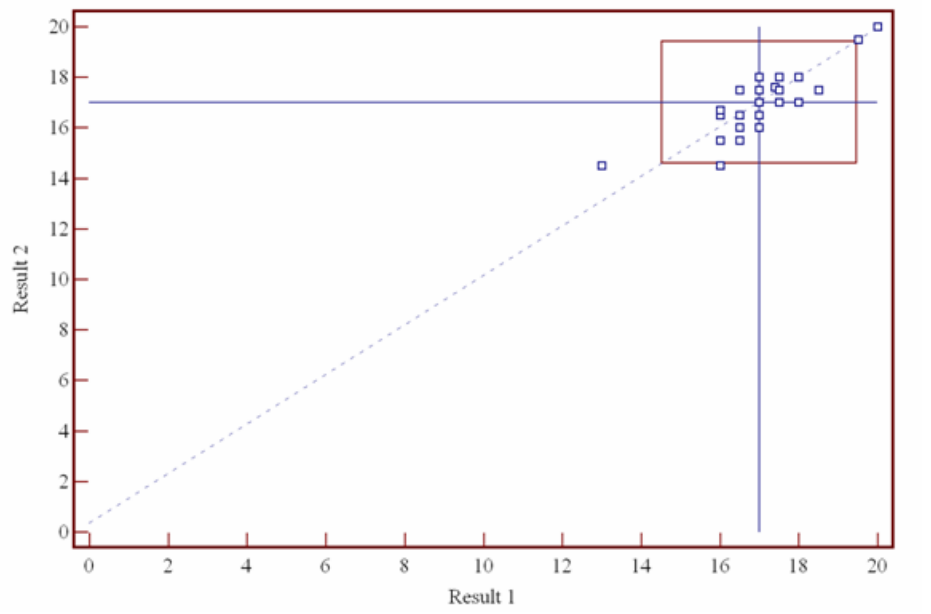

(b)

Figure C.5 Youden Plots for the Measured Plastic Limits of (a) Sample C and (b) Sample D

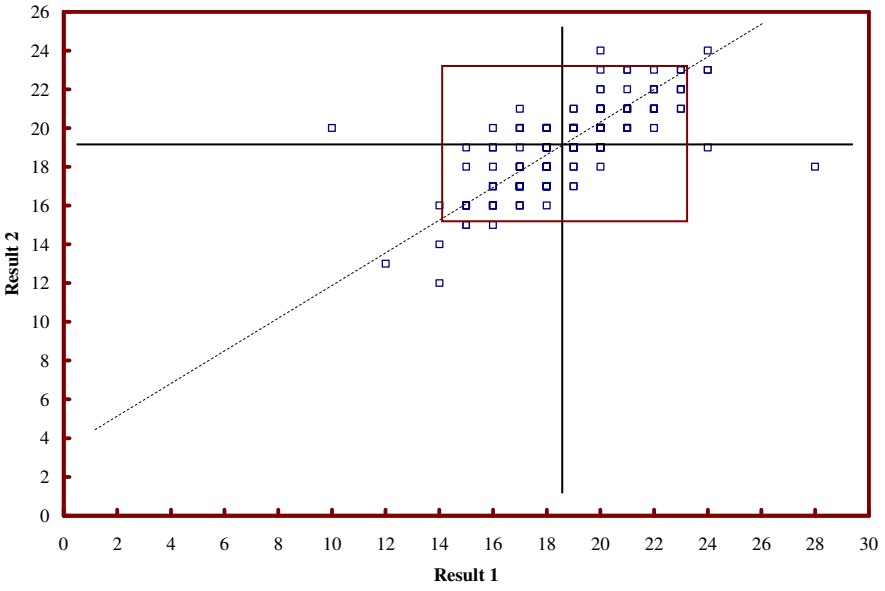

(a)

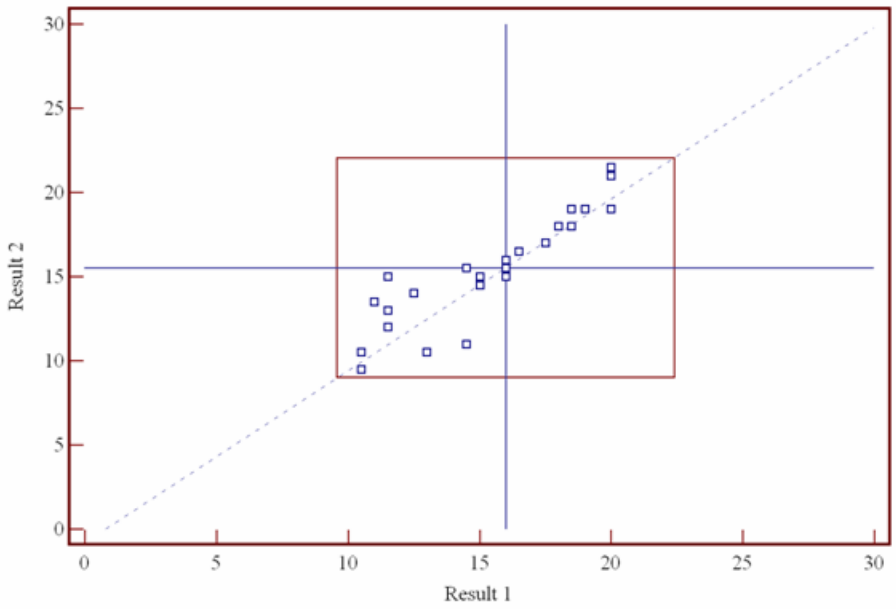

(b)

Figure C.6 Youden Plots for the Measured Plastic Limits of (e) Sample E and (f) Sample F

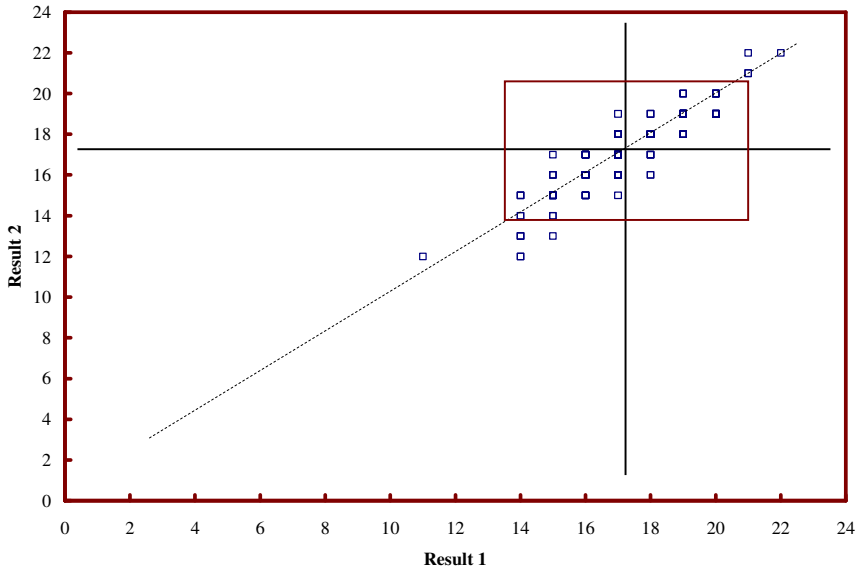

(a)

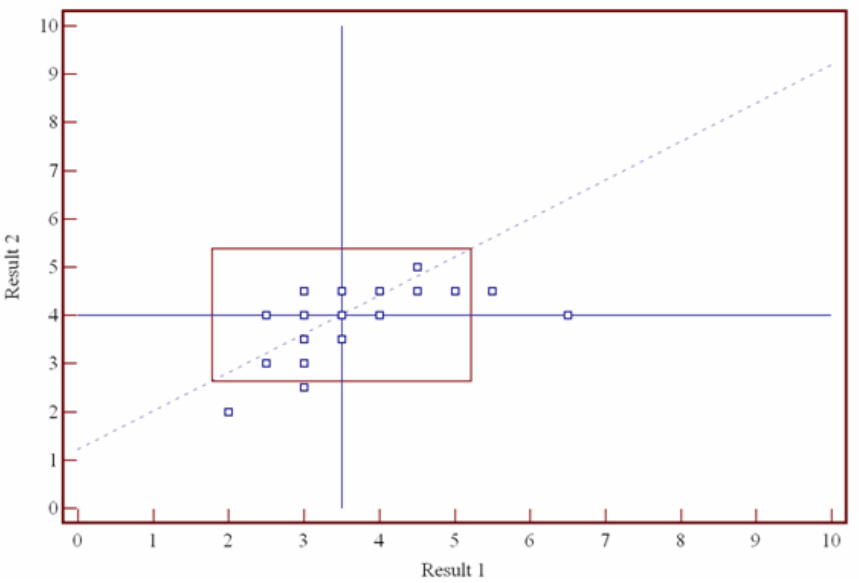

(b)

Figure C.7 Youden Plots for the Measured Plastic Limits of (a) Sample G and (b) Sample H

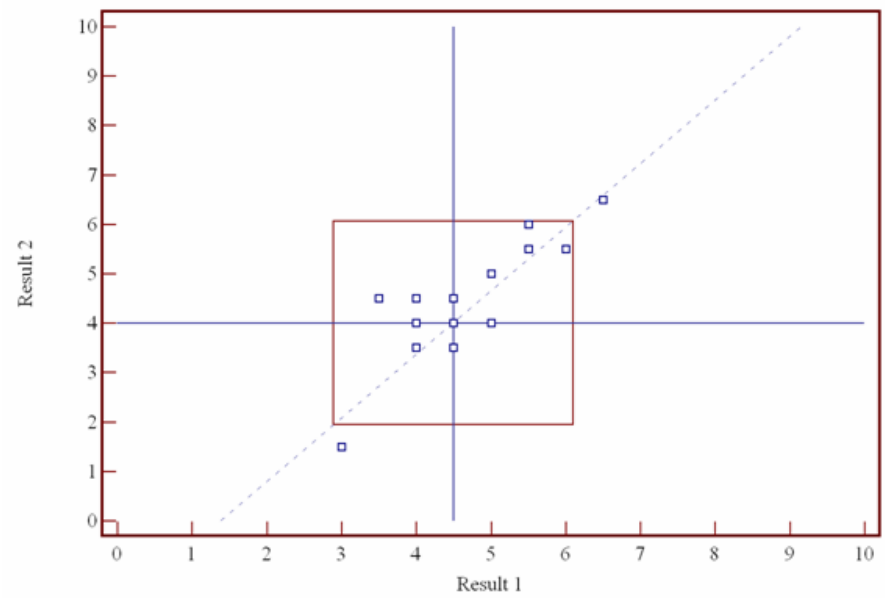

Figure C.8 Youden Plot for the Measured Plastic Limits of Sample I

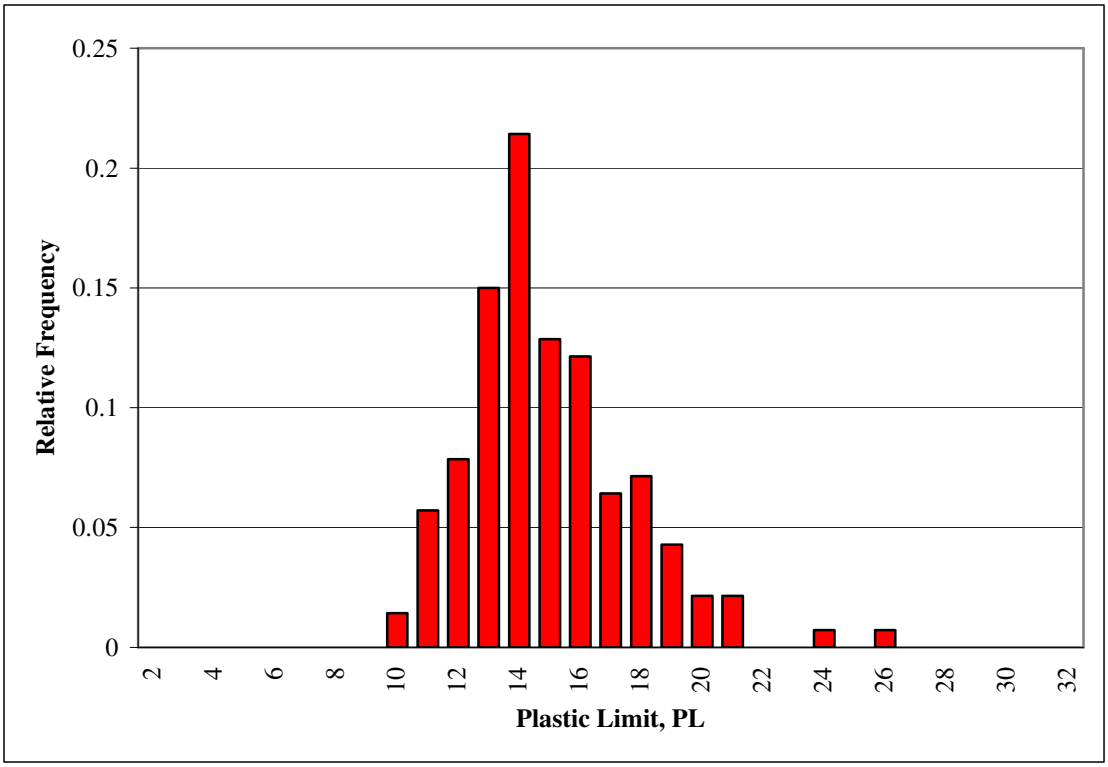

Figure C.9 Relative Frequency Histogram of Sample A Plastic Limits

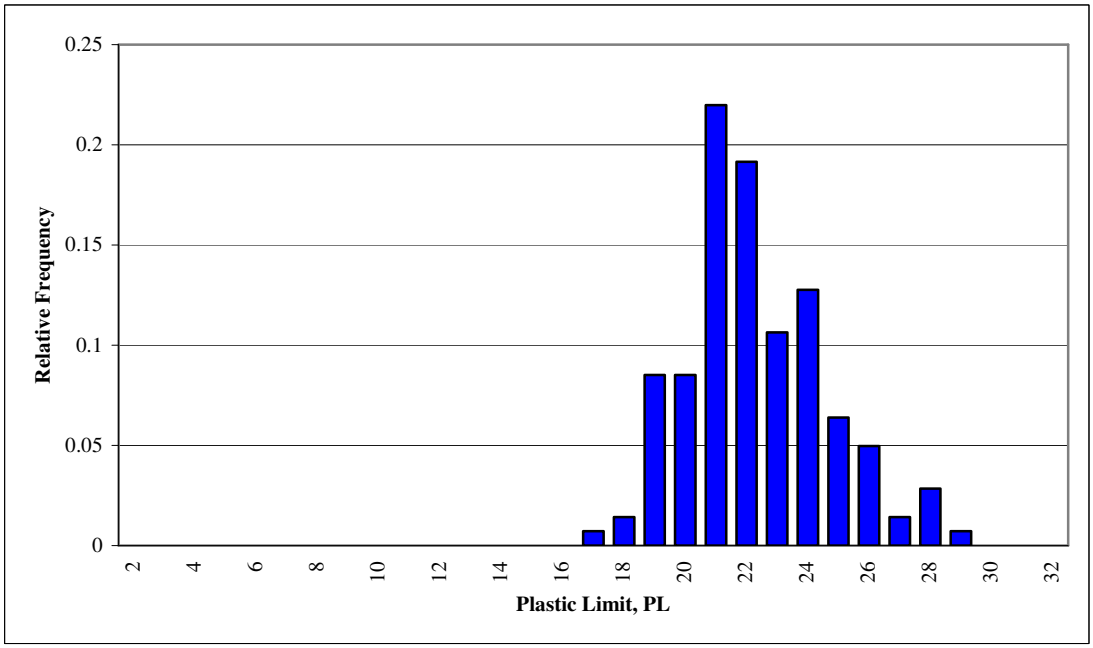

Figure C.10 Relative Frequency Histogram of Sample B Plastic Limits

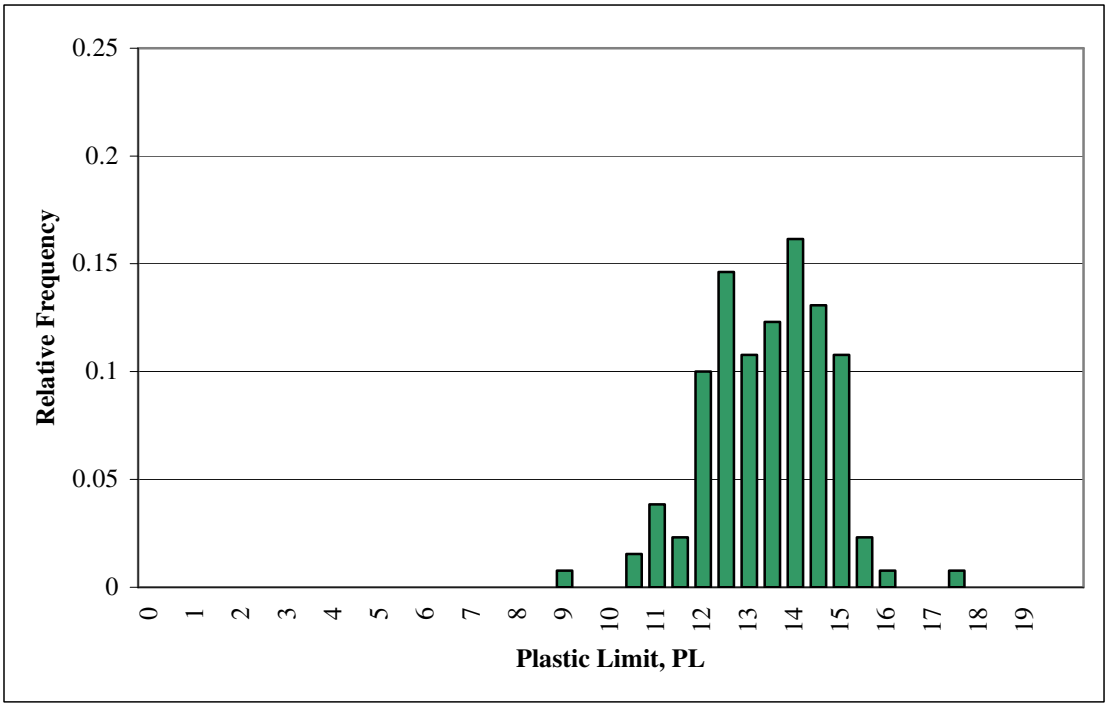

Figure C.11 Relative Frequency Histogram of Sample C Plastic Limits

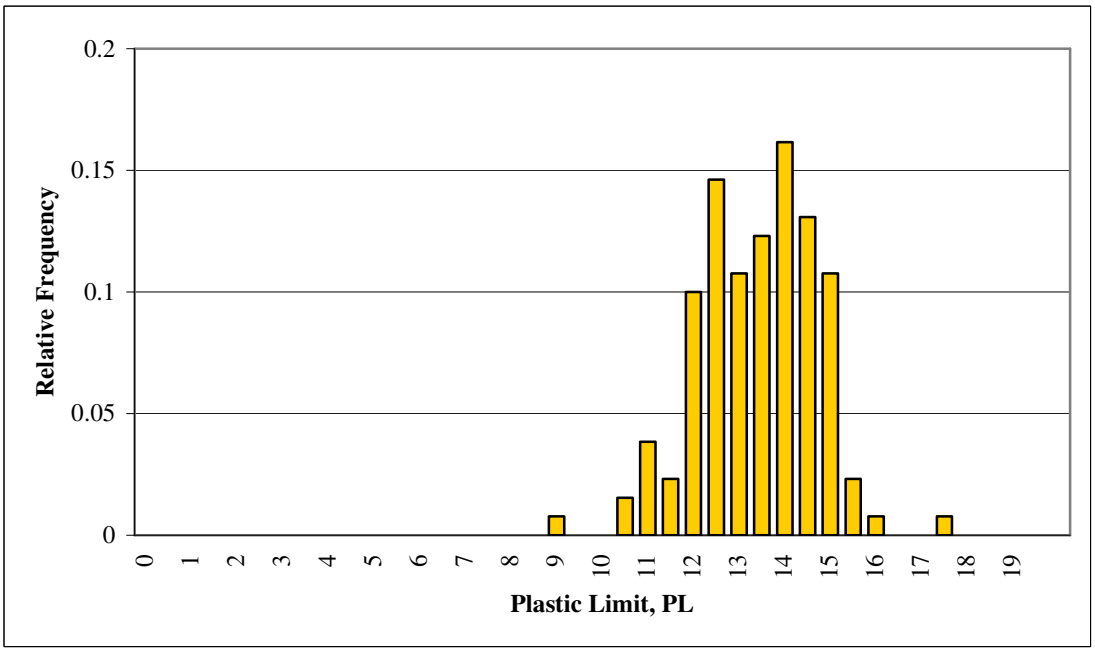

Figure C.12 Relative Frequency Histogram of Sample D Plastic Limits

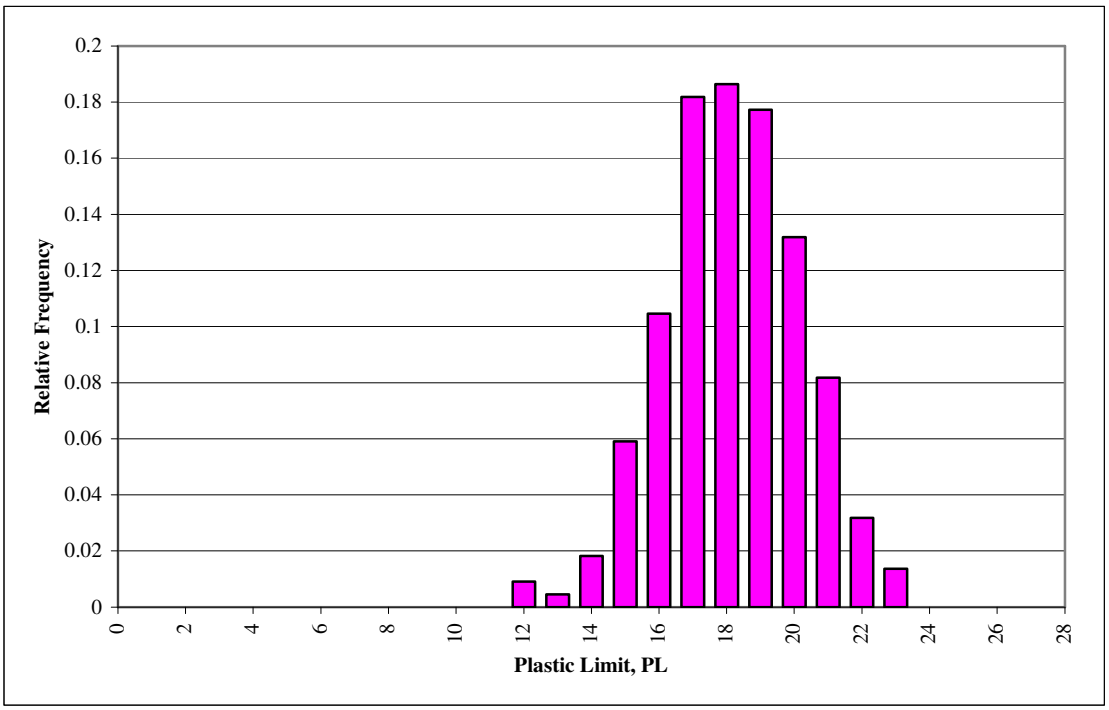

Figure C.13 Relative Frequency Histogram and of Sample E Plastic Limits

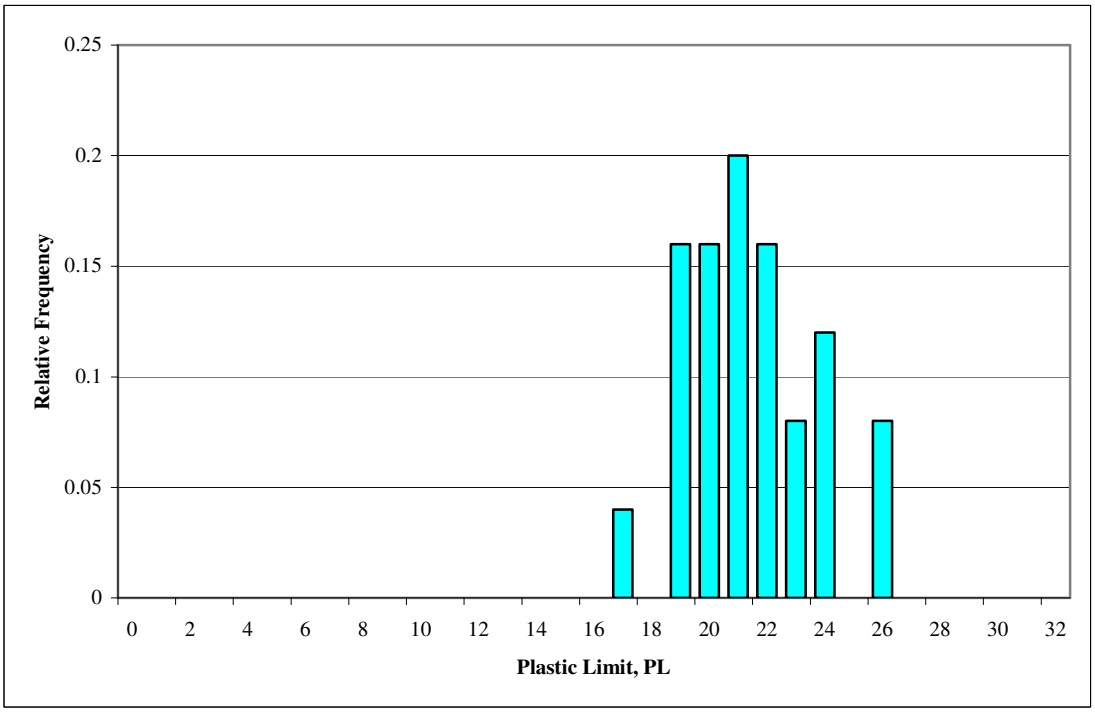

Figure C.14 Relative Frequency Histogram of Sample F Plastic Limits

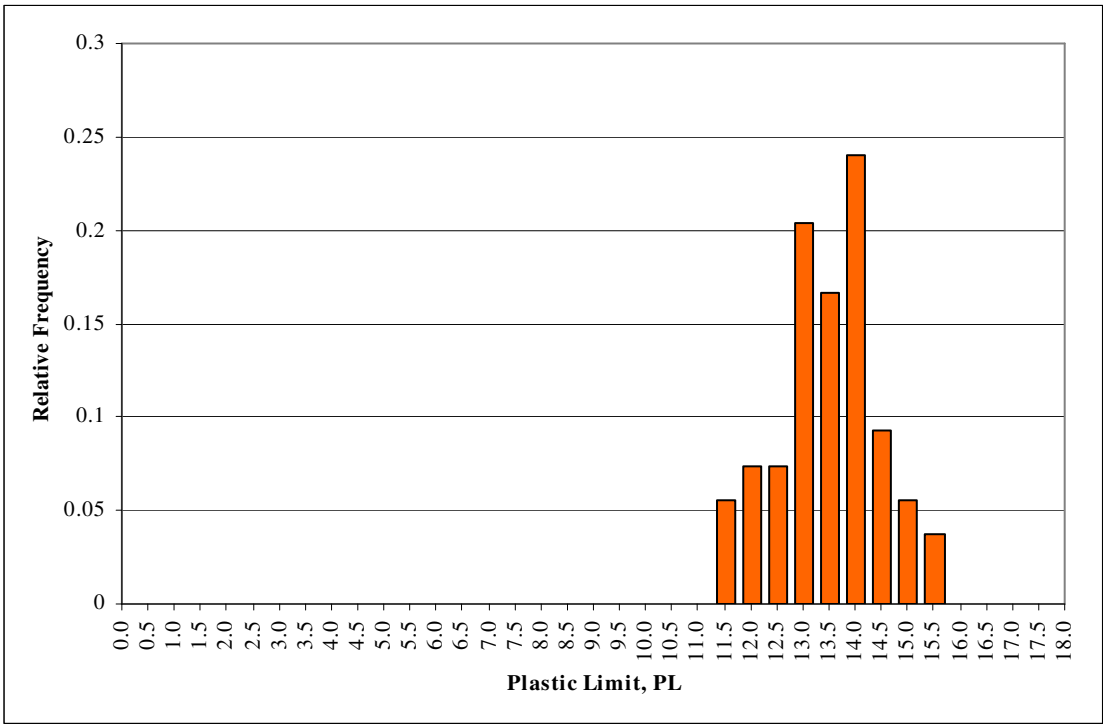

Figure C.15 Relative Frequency Histogram of Sample G Plastic Limits

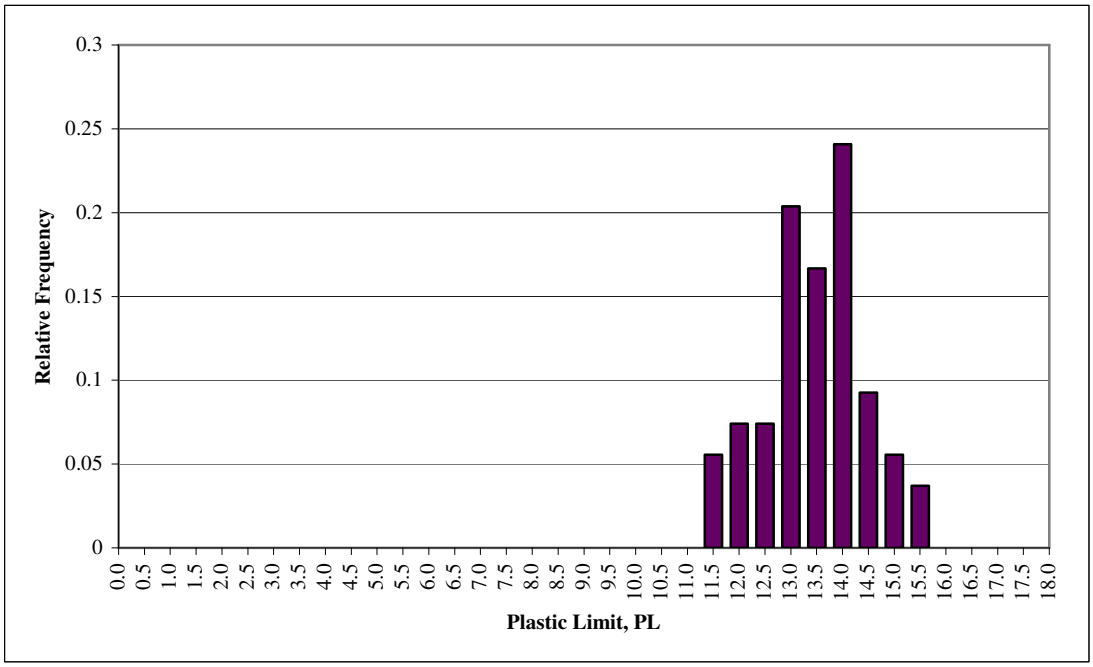

Figure C.16 Relative Frequency of Sample H Plastic Limits

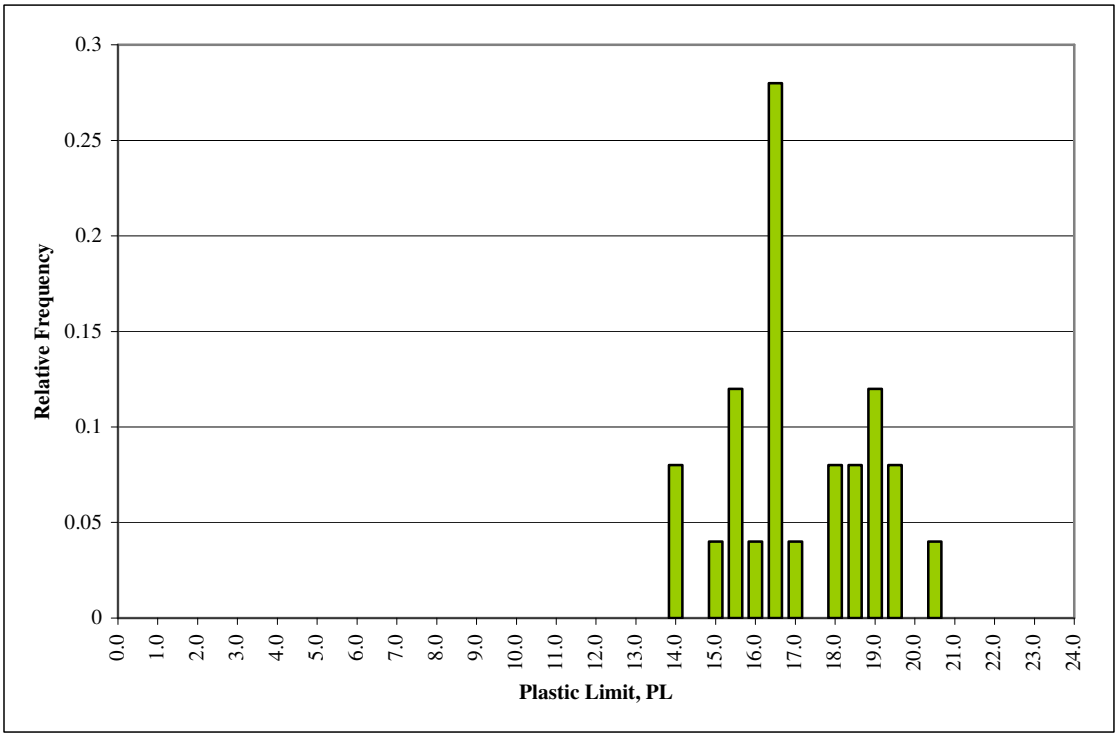

Figure C.17 Relative Frequency Histogram of Sample I Plastic Limits

Appendix D

Z-Score Plots and Relative Frequency Histograms for Plasticity Index

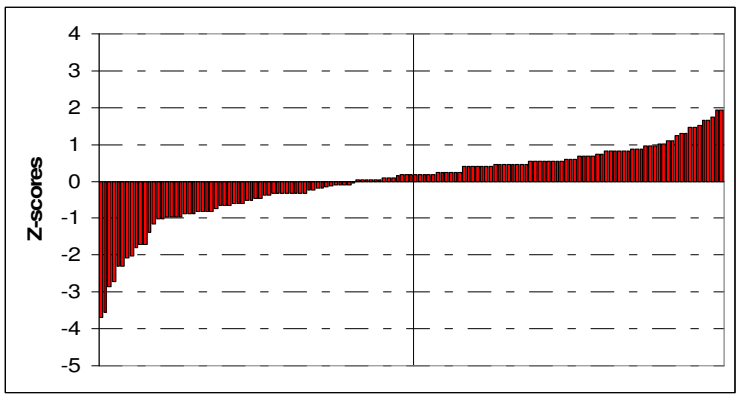

(a)

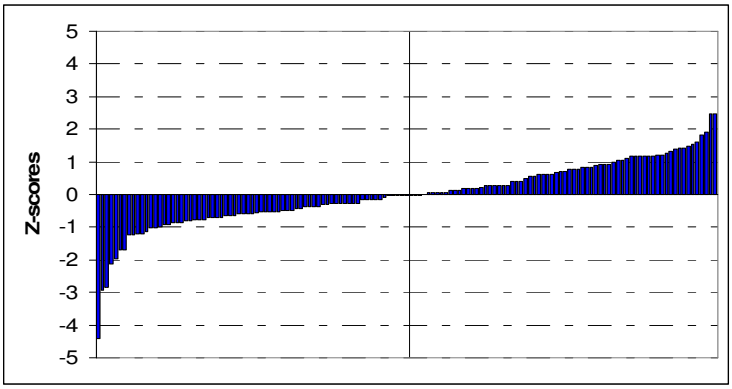

(b)

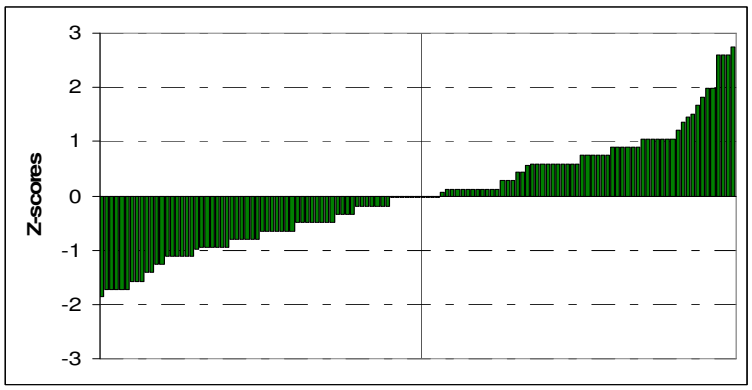

(c)

Figure D.1 Standardised Z-Scores for the Linear Shrinkage (a) Sample A, (b) Sample B and (c) Sample C

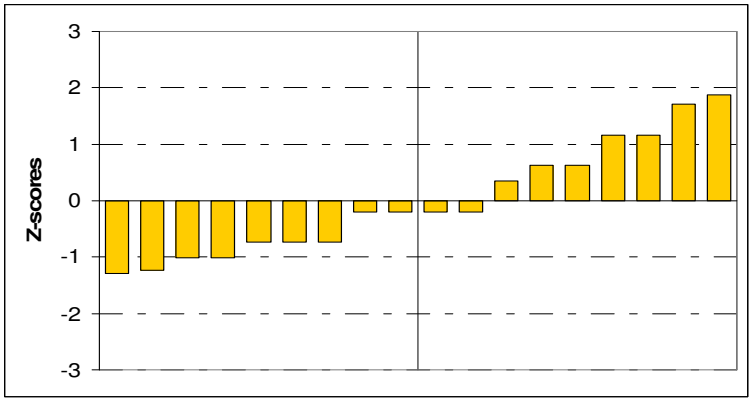

(a)

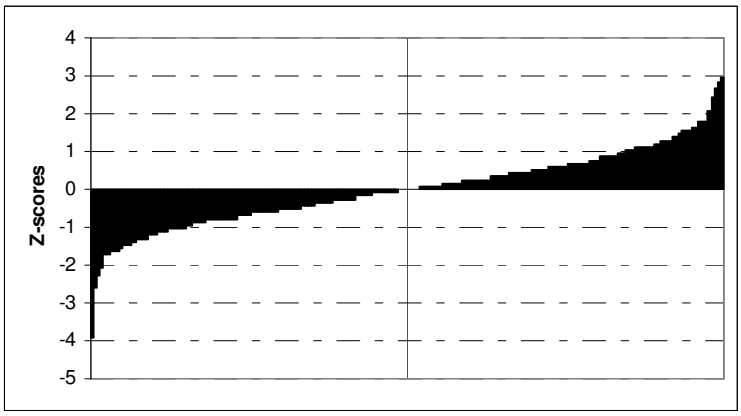

(b)

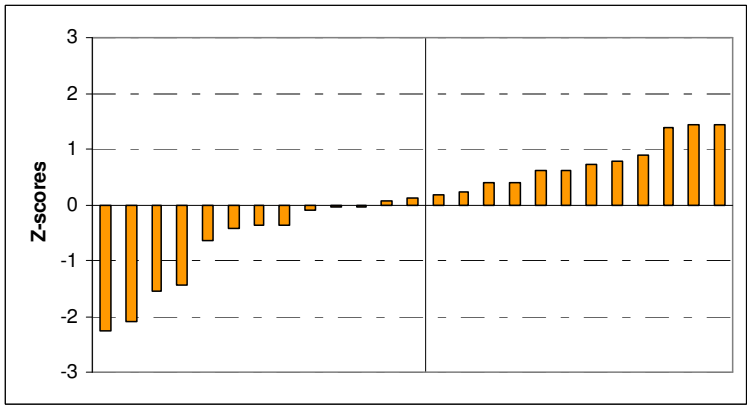

(c)

Figure D.2 Standardised Z-Scores for the Linear Shrinkage of (a) Sample D, (b) Sample E and (c) Sample F

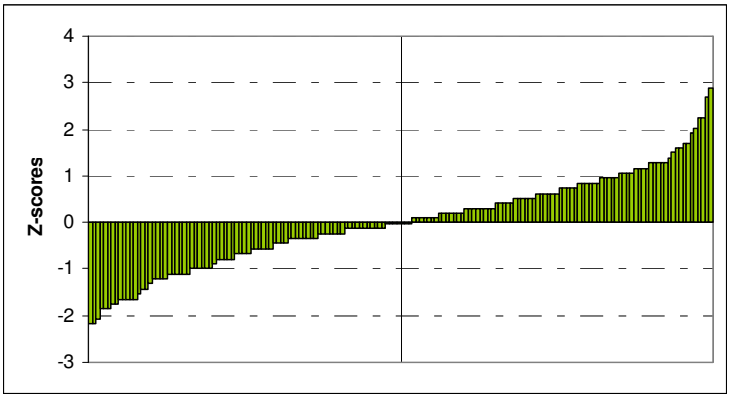

(a)

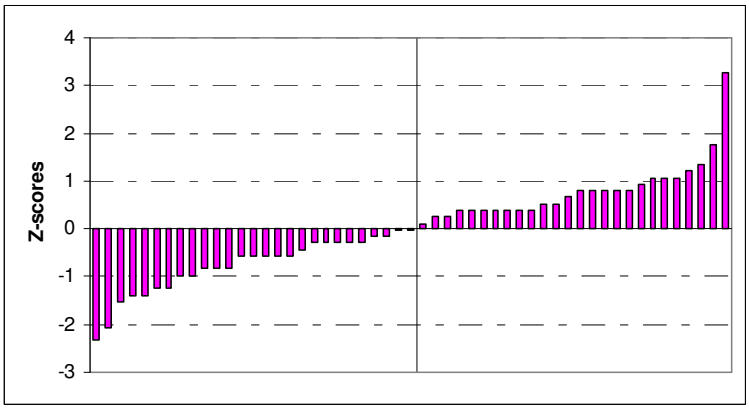

(b)

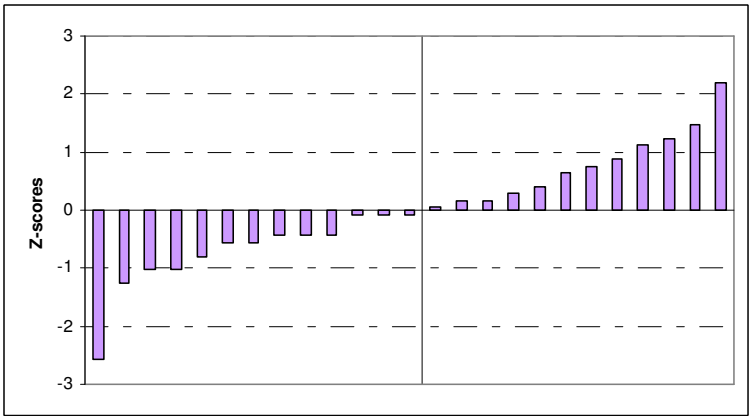

(c)

Figure D.3 Standardised Z-Scores for the Linear Shrinkage of (a) Sample G, (b) Sample H and (c) Sample I

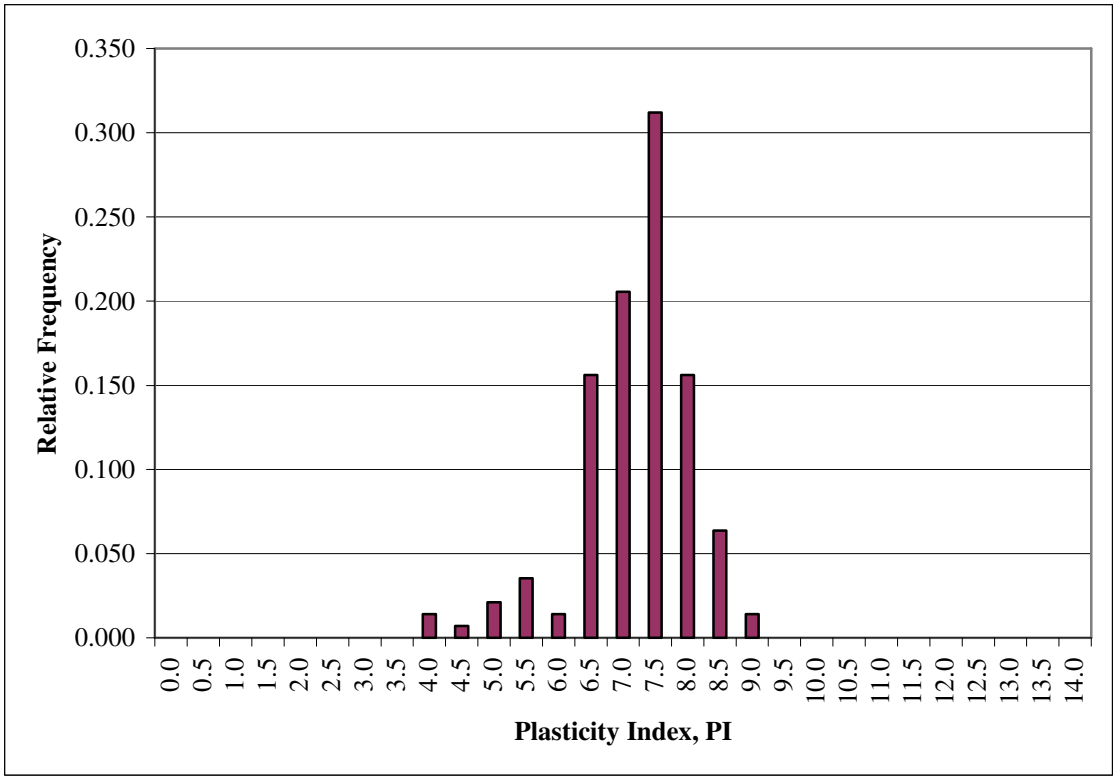

Figure D.4 Relative Frequency Histogram of Sample A Plasticity Index

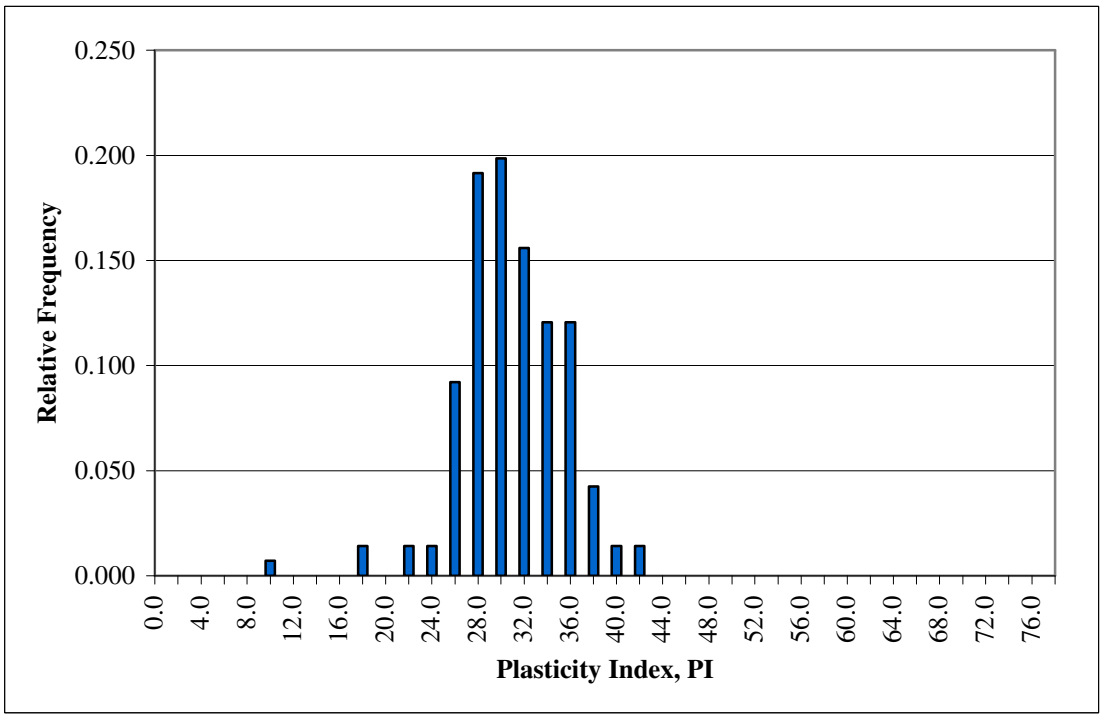

Figure D.5 Relative Frequency Histogram and of Sample B Plasticity Index

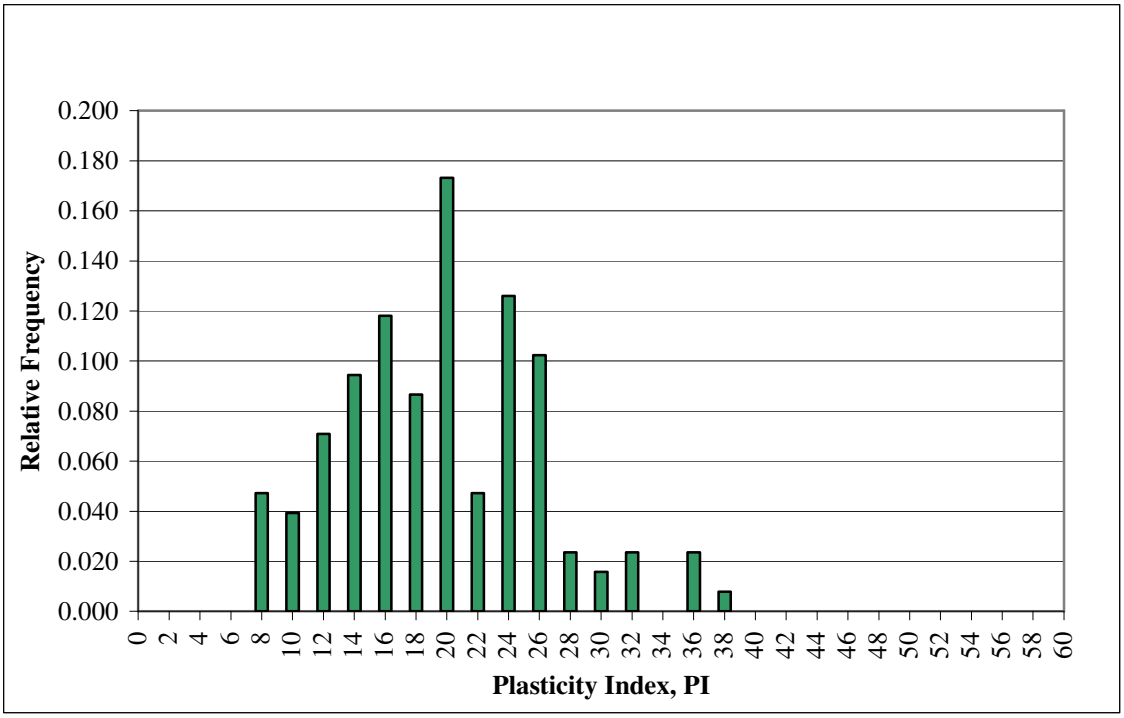

Figure D.6 Relative Frequency Histogram of Sample C Plasticity Index

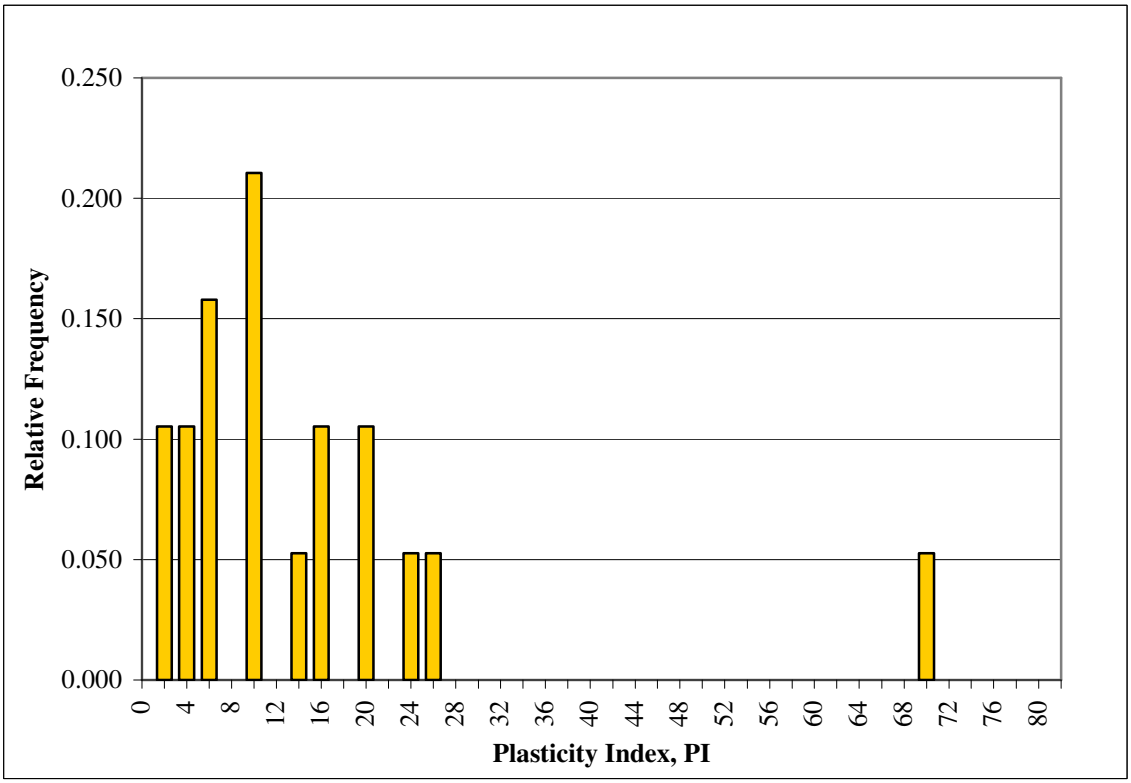

Figure D.7 Relative Frequency Histogram of Sample D Plasticity Index

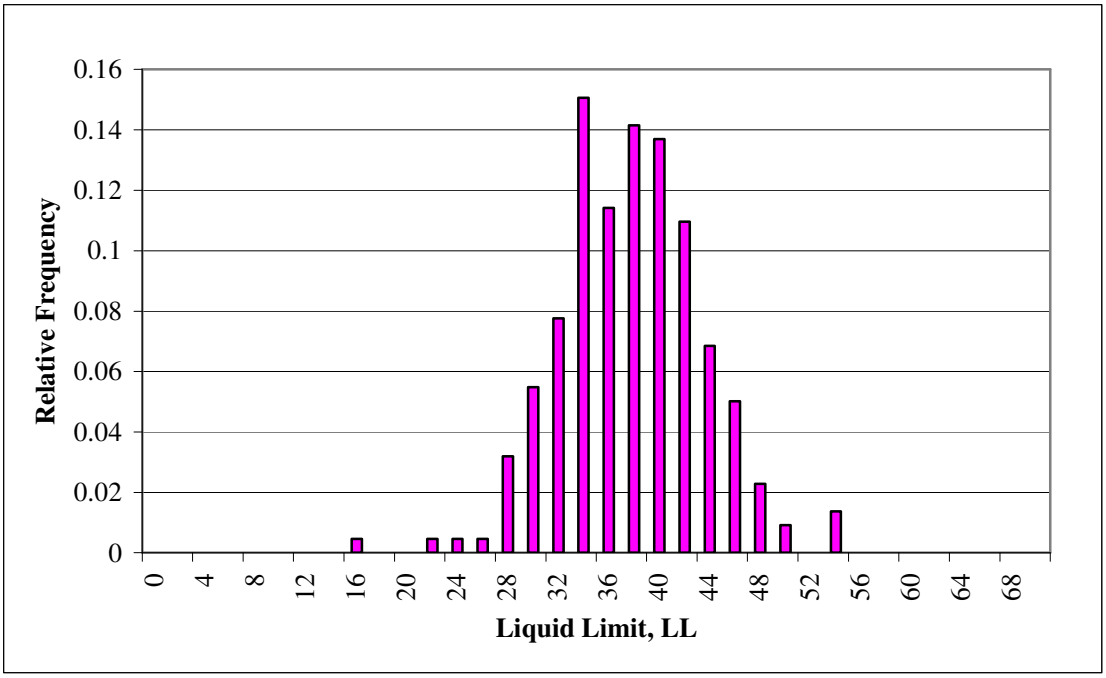

Figure D.8 Relative Frequency Histogram of Sample E Plasticity Index

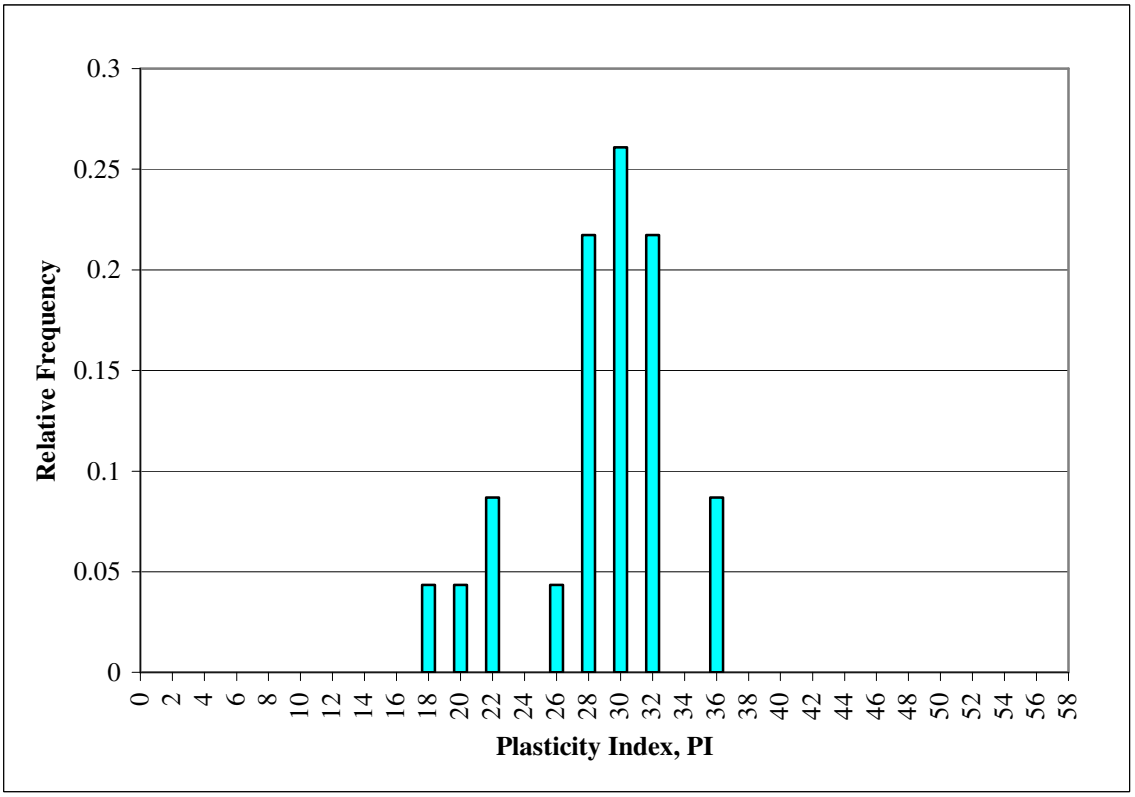

Figure D.9 Relative Frequency Histogram of Sample F Plasticity Index

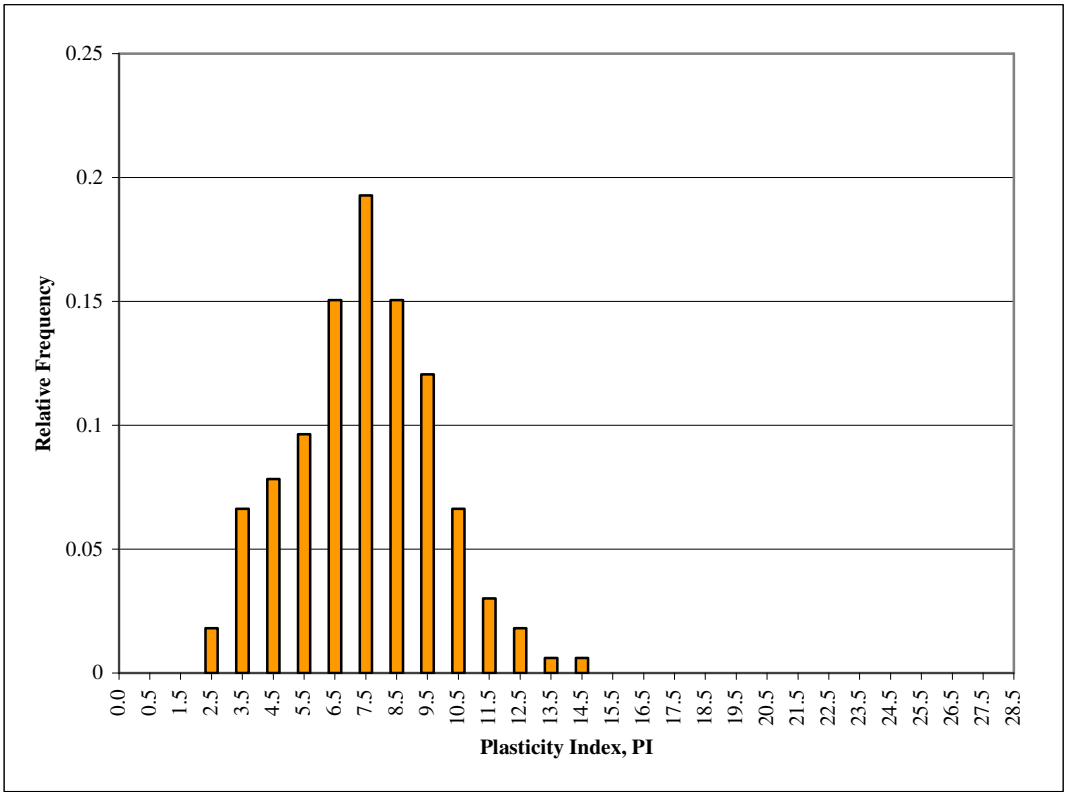

Figure D.10 Relative Frequency Histogram of Sample G Plasticity Index

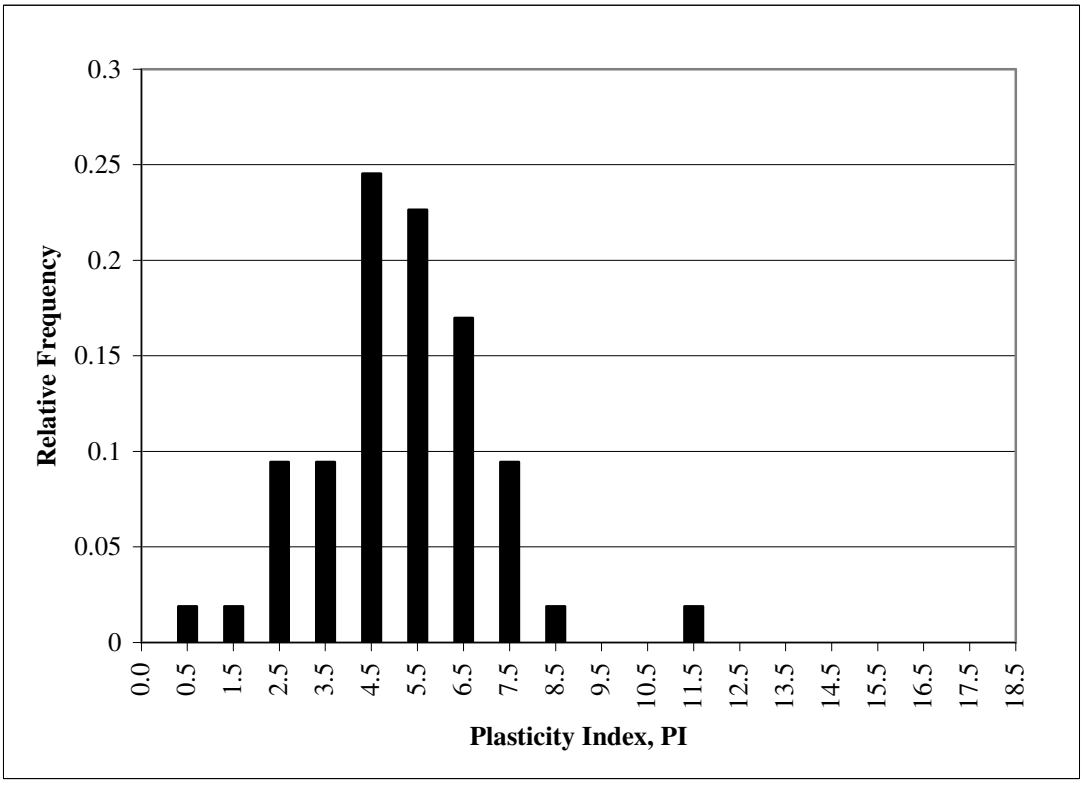

Figure D.11 Relative Frequency Histogram of Sample H Plasticity Index

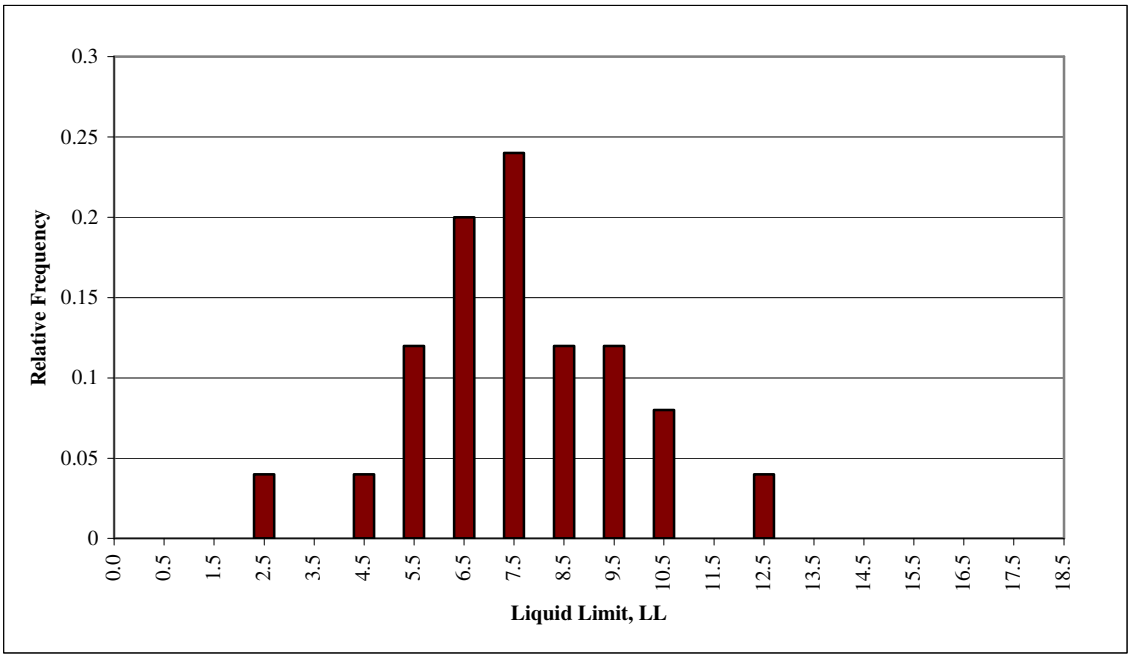

Figure D.12 Relative Frequency Histogram of Sample I Plasticity Index

Appendix E

Z-Score Plots, Youden Diagrams and Relative Frequency Histograms for Linear Shrinkage

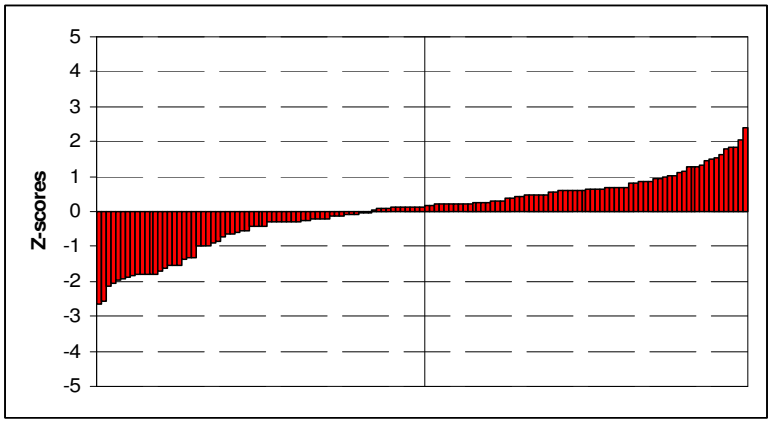

(a)

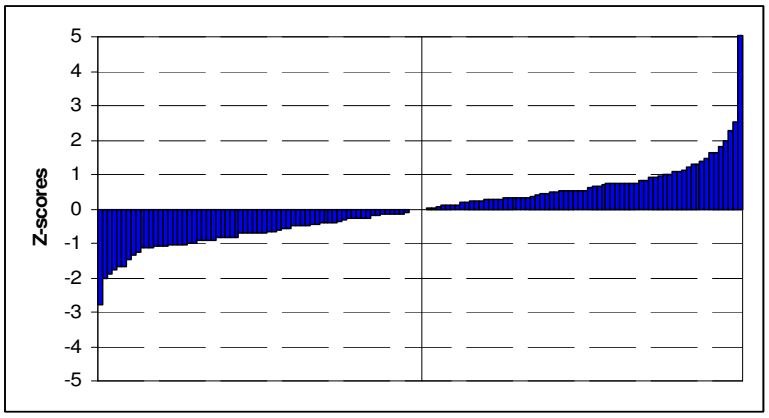

(b)

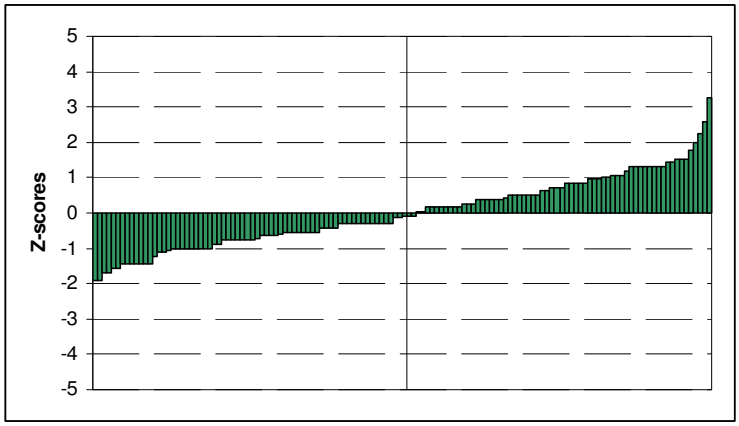

(c)

Figure E.1 Standardised Z-Scores for the Linear Shrinkage (a) Sample A, (b) Sample B and (c) Sample C

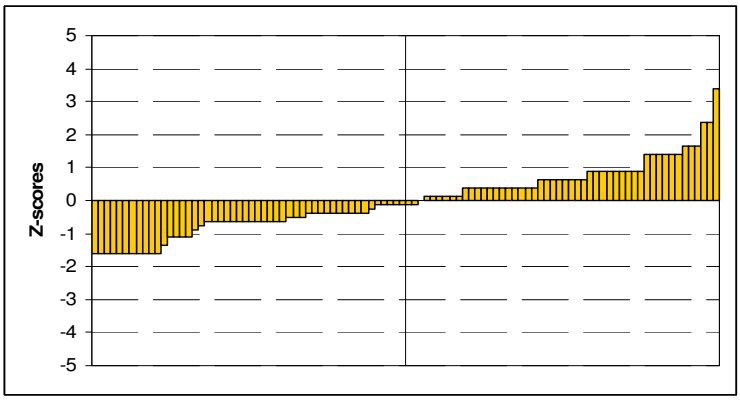

(a)

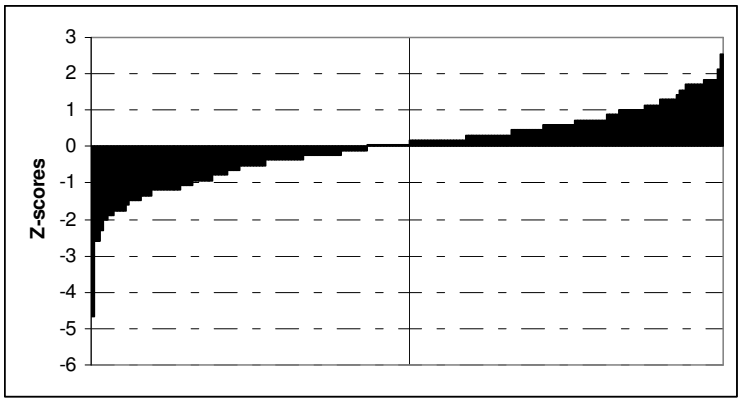

(b)

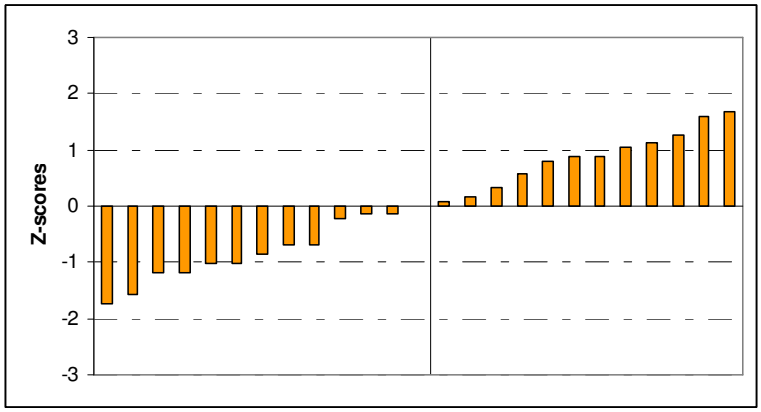

(c)

Figure E.2 Standardised Z-Scores for the Linear Shrinkage of (a) Sample D, (b) Sample E and (c) Sample F

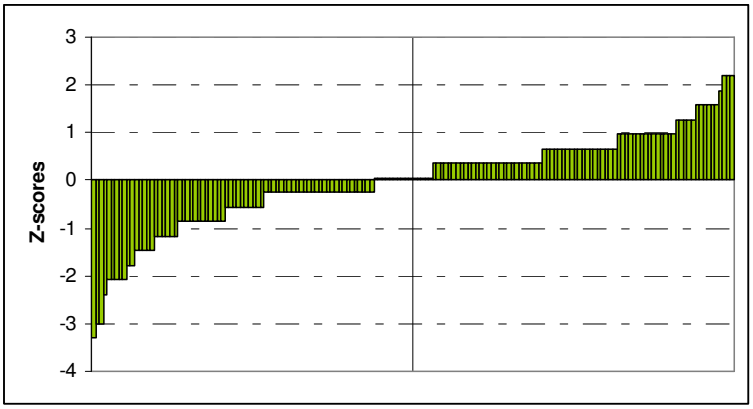

(a)

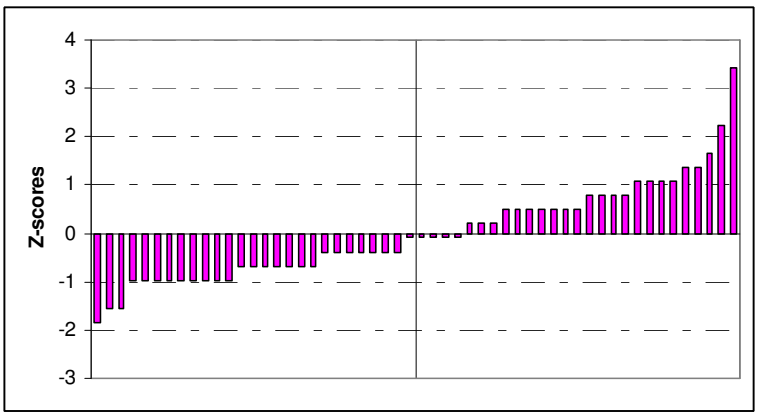

(b)

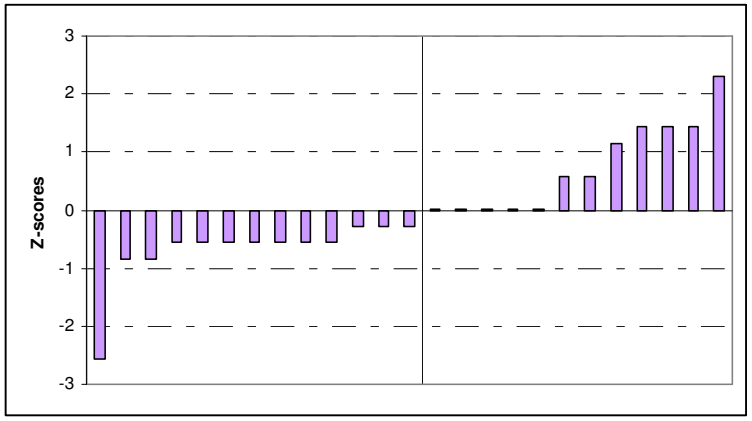

(c)

Figure E.3 Standardised Z-Scores for the Linear Shrinkage of (a) Sample G, (b) Sample H and (c) Sample I

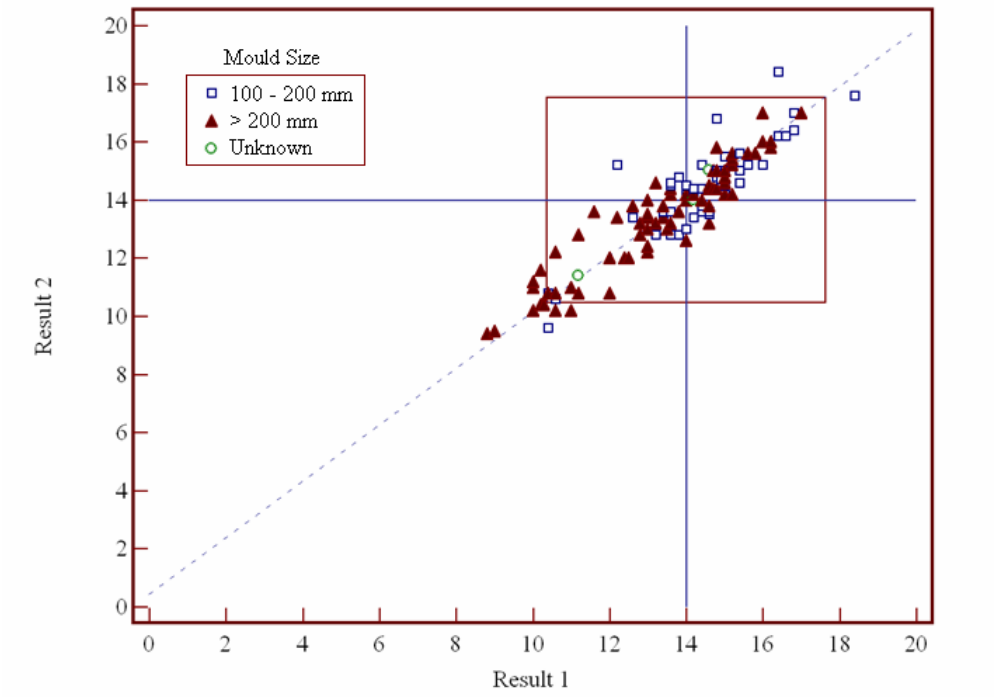

(a)

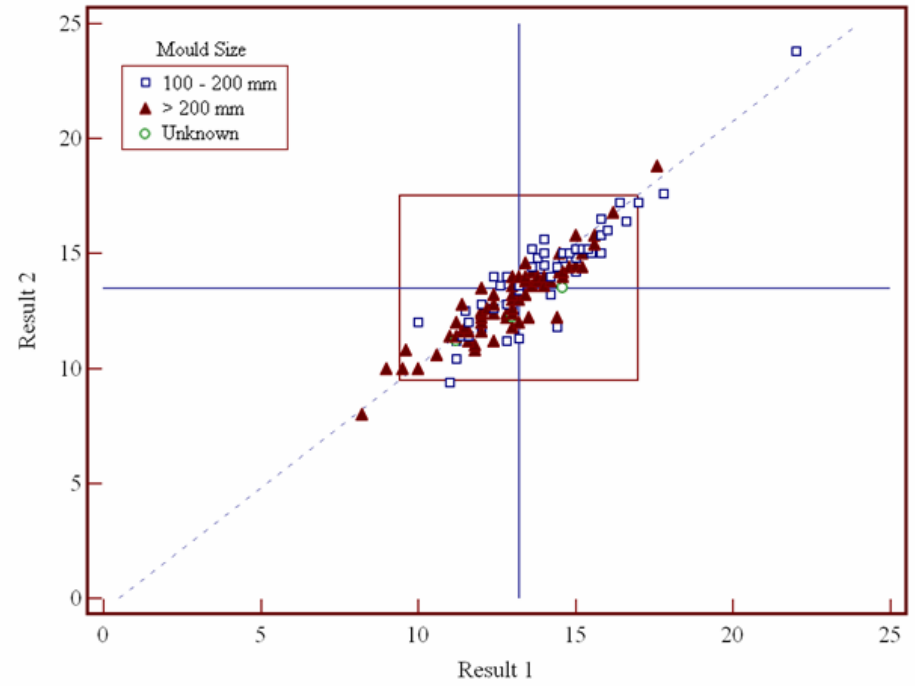

(b)

Figure E.4 Youden Plots for the Measured Linear Shrinkage of (a) Sample A and (b) Sample B

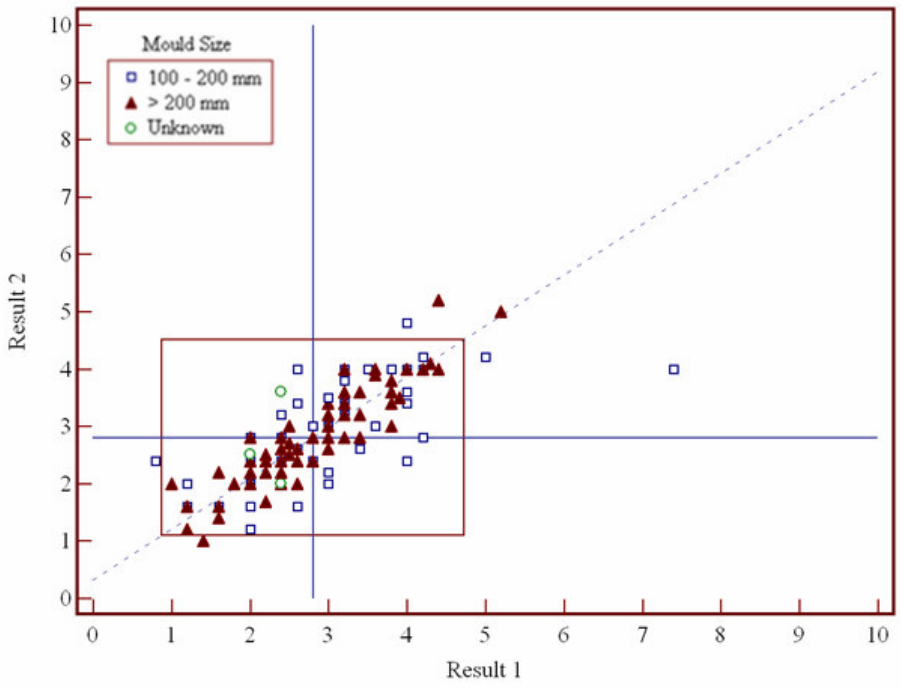

(a)

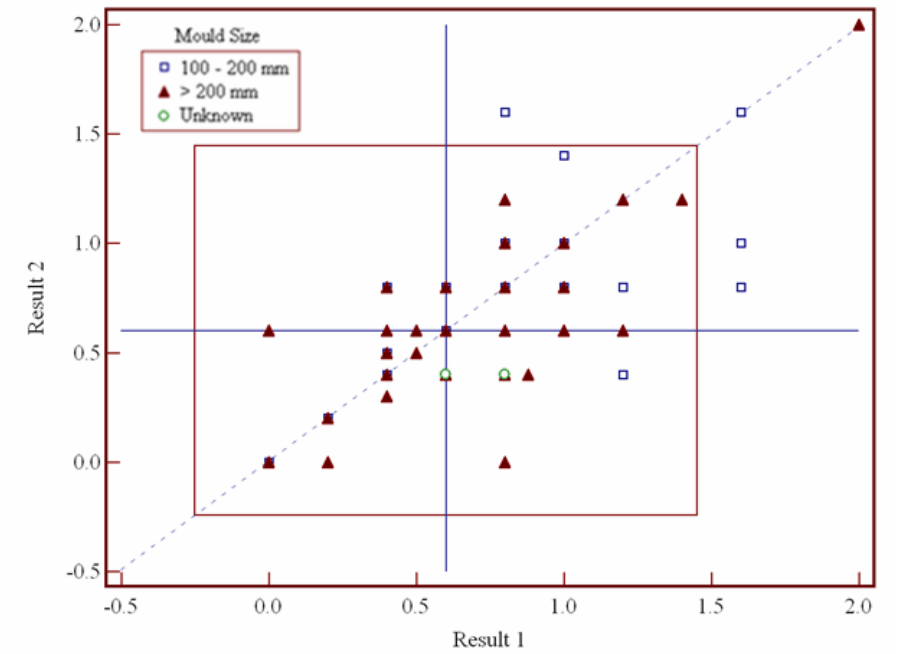

(b)

Figure E.5 Youden Plots for the Measured Linear Shrinkage of (a) Sample C and (b) Sample D

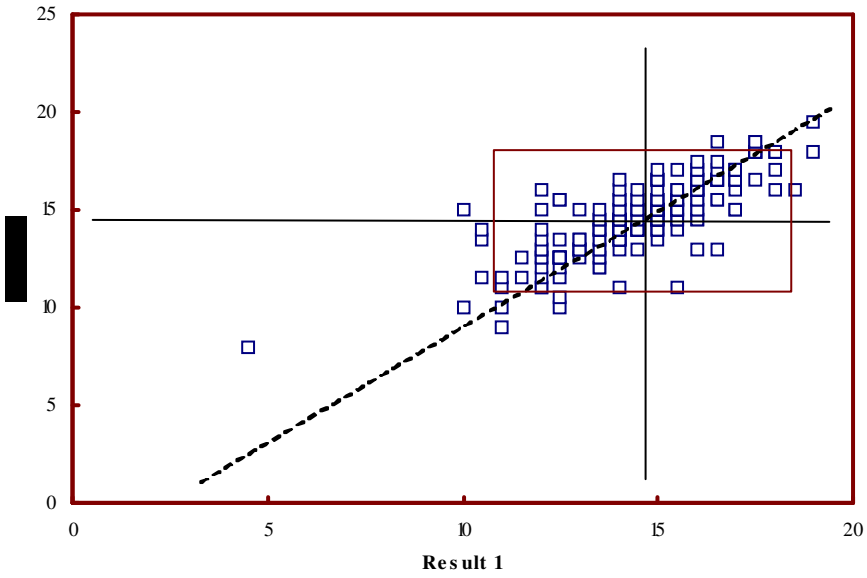

(a)

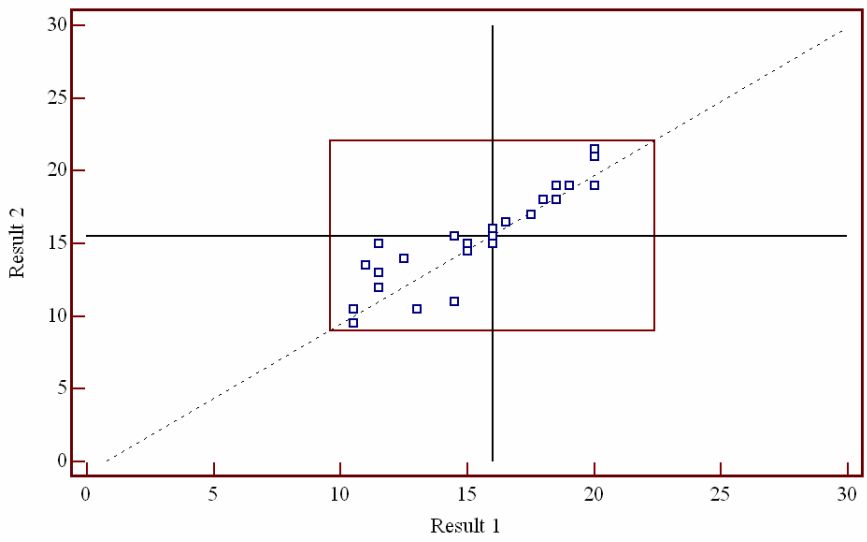

(b)

Figure E.6 Youden Plots for the Measured Linear Shrinkage of (e) Sample E and (f) Sample F

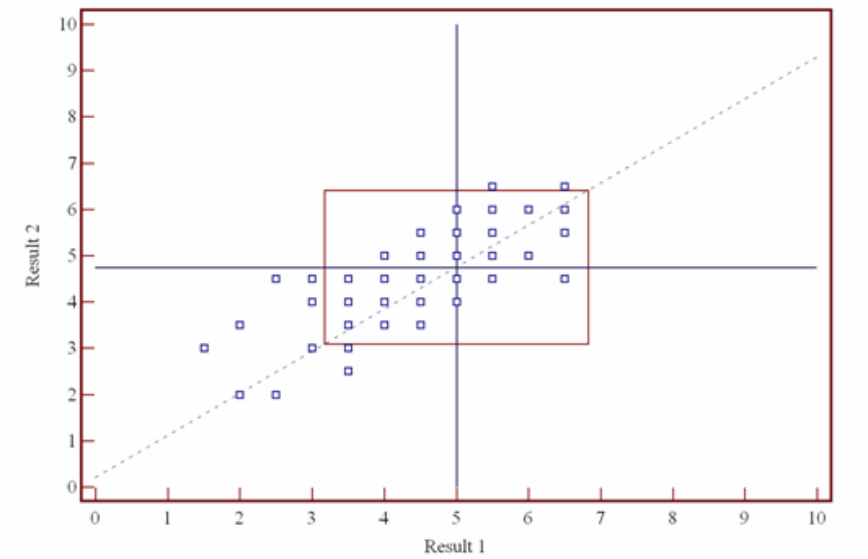

(a)

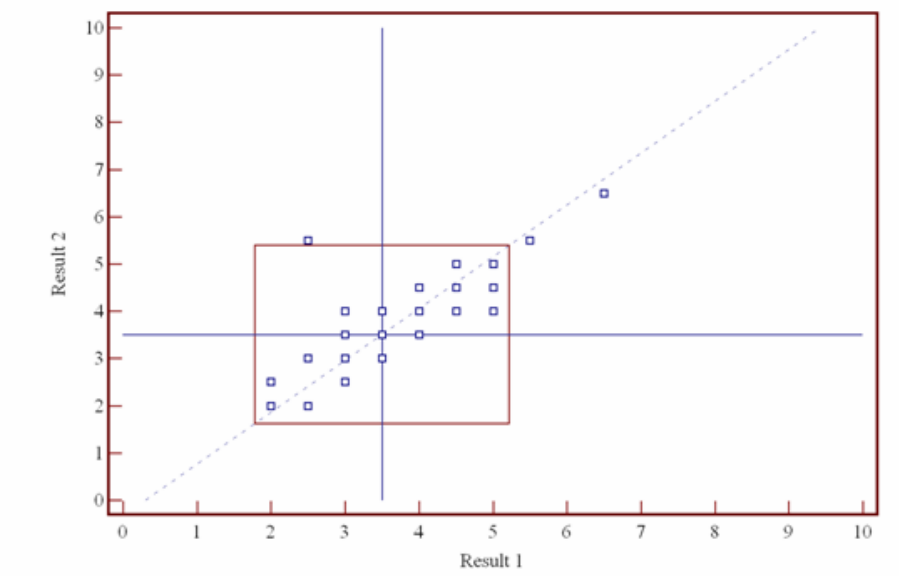

(b)

Figure E.7 Youden Plots for the Measured Linear Shrinkage of (a) Sample G and (b) Sample H

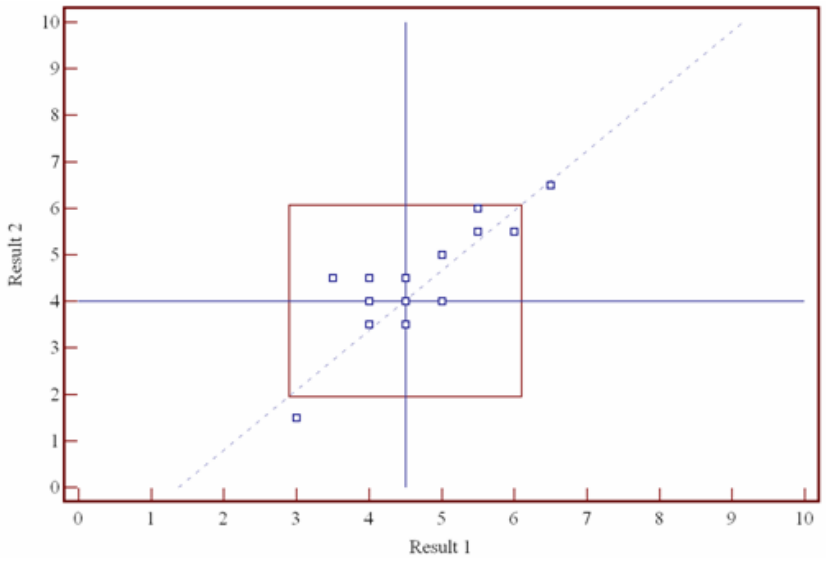

Figure E.8 Youden Plot for the Measured Linear Shrinkage of Sample I

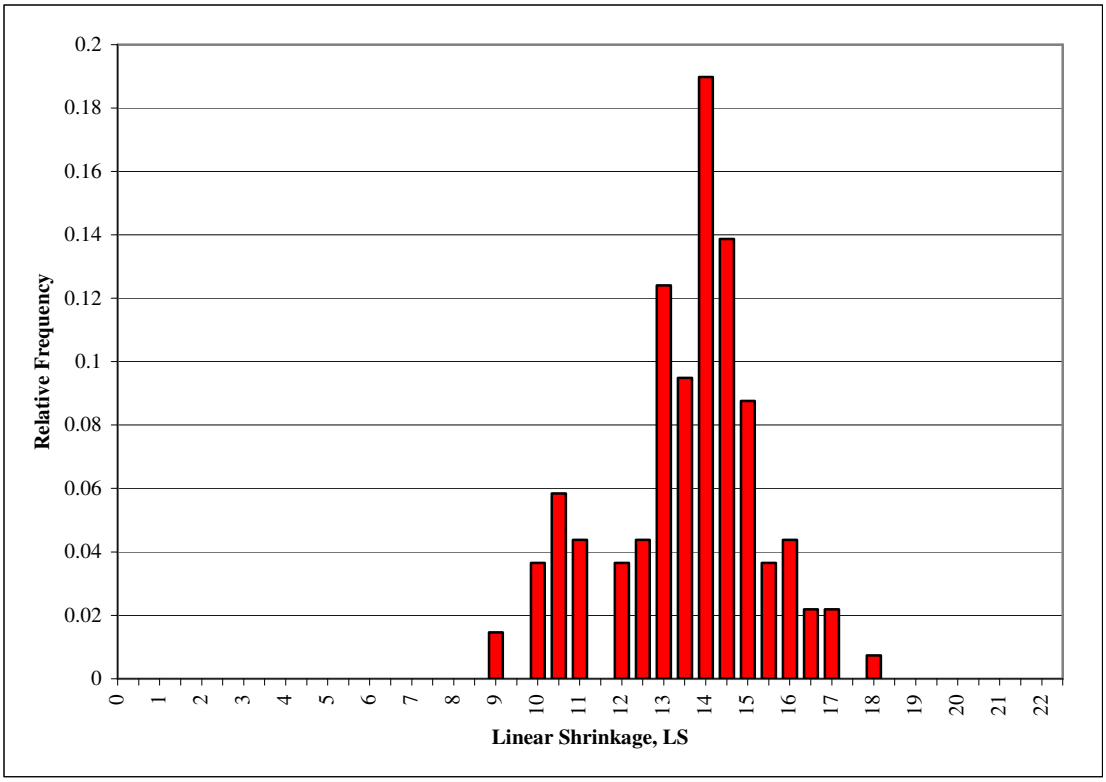

Figure E.9 Relative Frequency Histogram of Sample A Linear Shrinkage

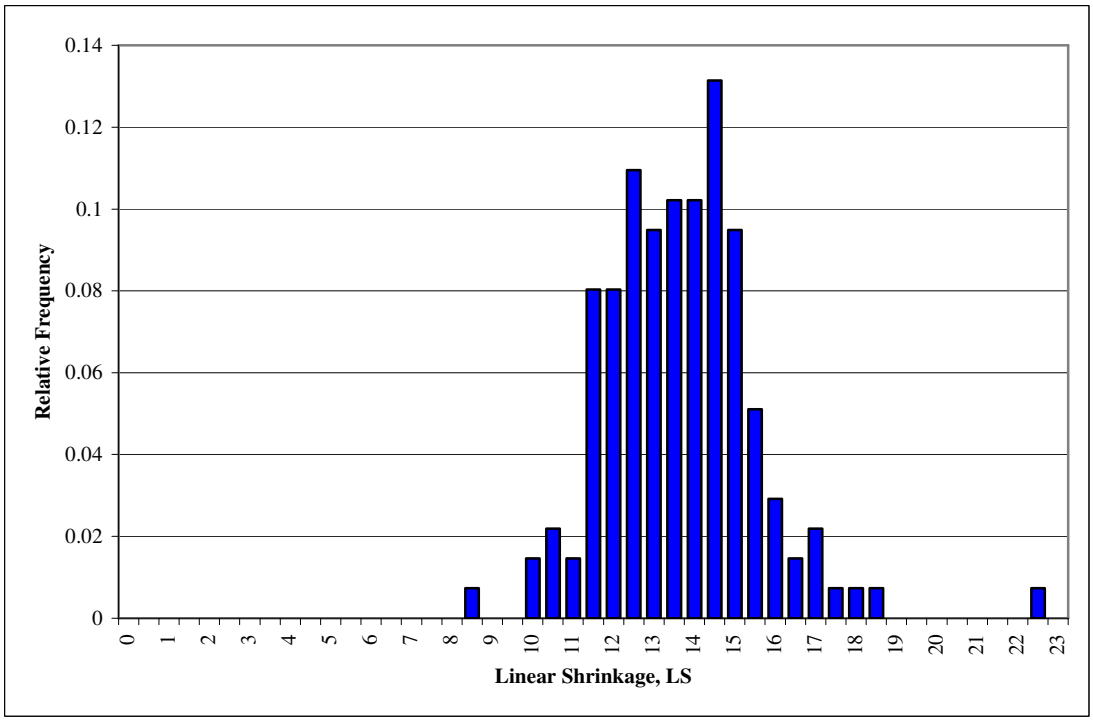

Figure E.10 Relative Frequency Histogram and of Sample B Linear Shrinkage

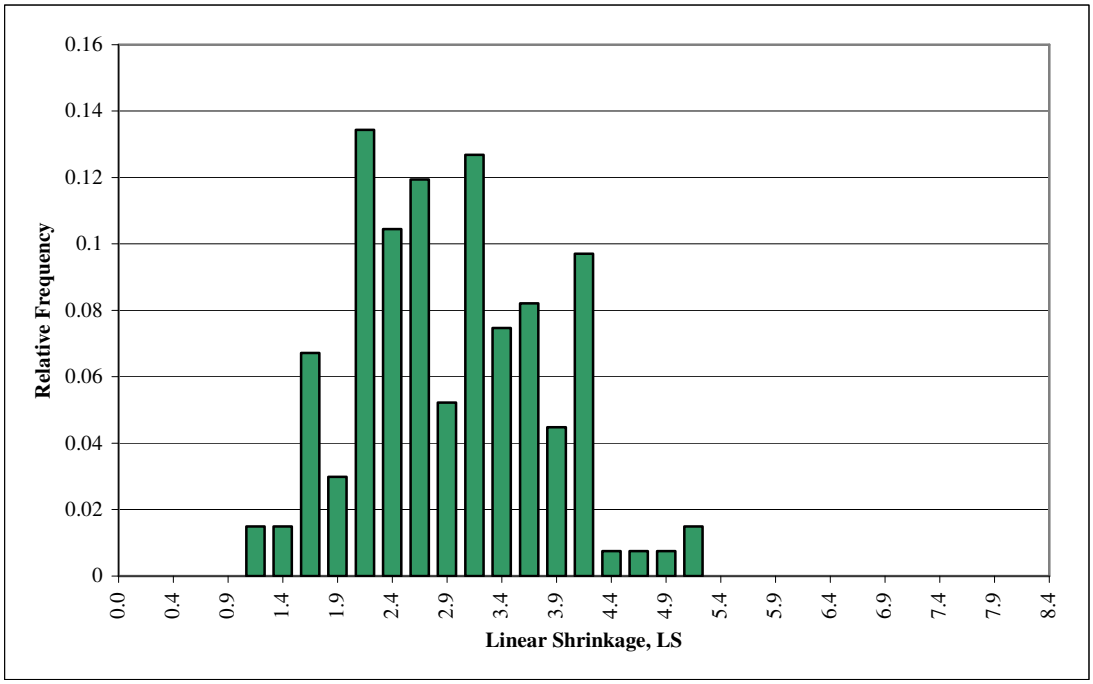

Figure E.11 Relative Frequency Histogram of Sample C Linear Shrinkage

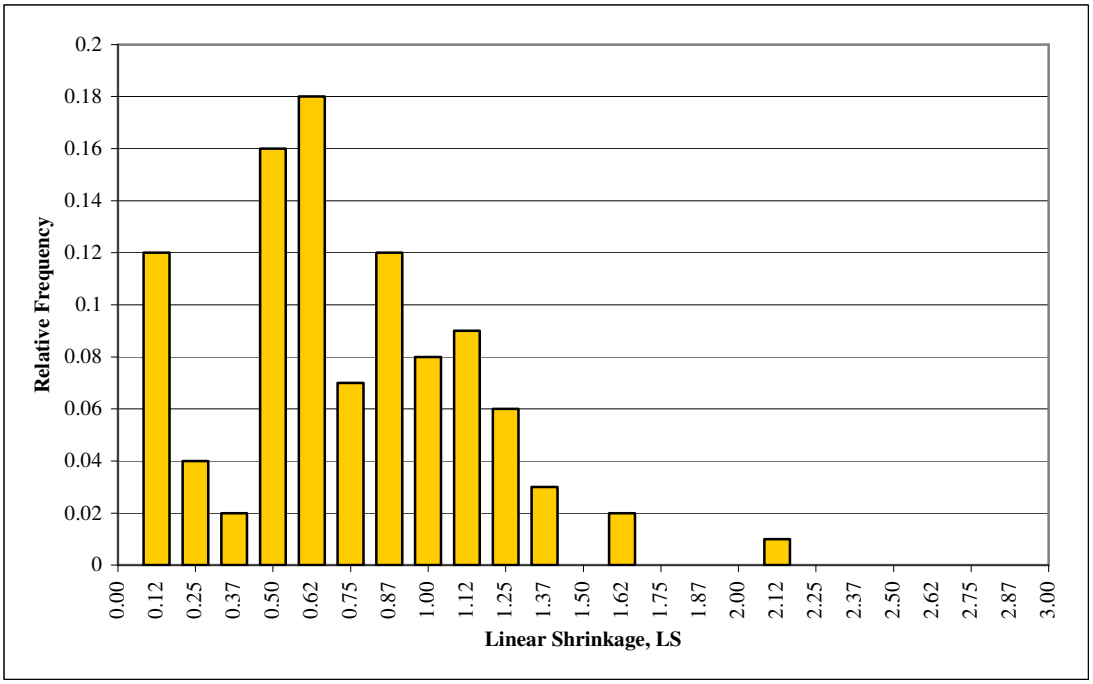

Figure E.12 Relative Frequency Histogram of Sample D Linear Shrinkage

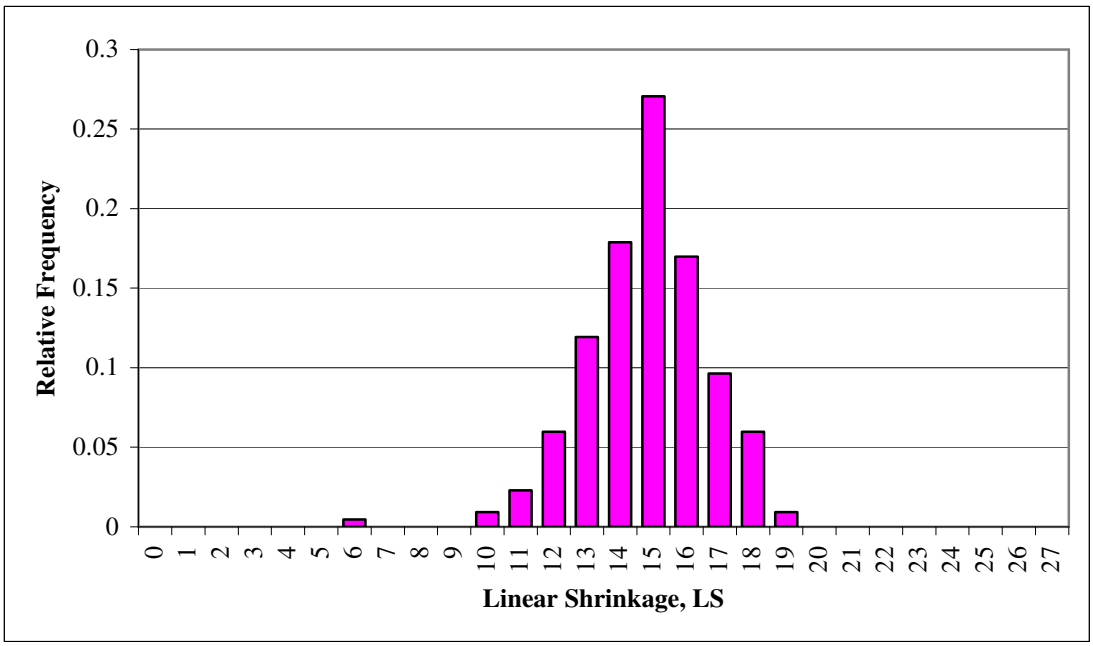

Figure E.13 Relative Frequency Histogram of Sample E Linear Shrinkage

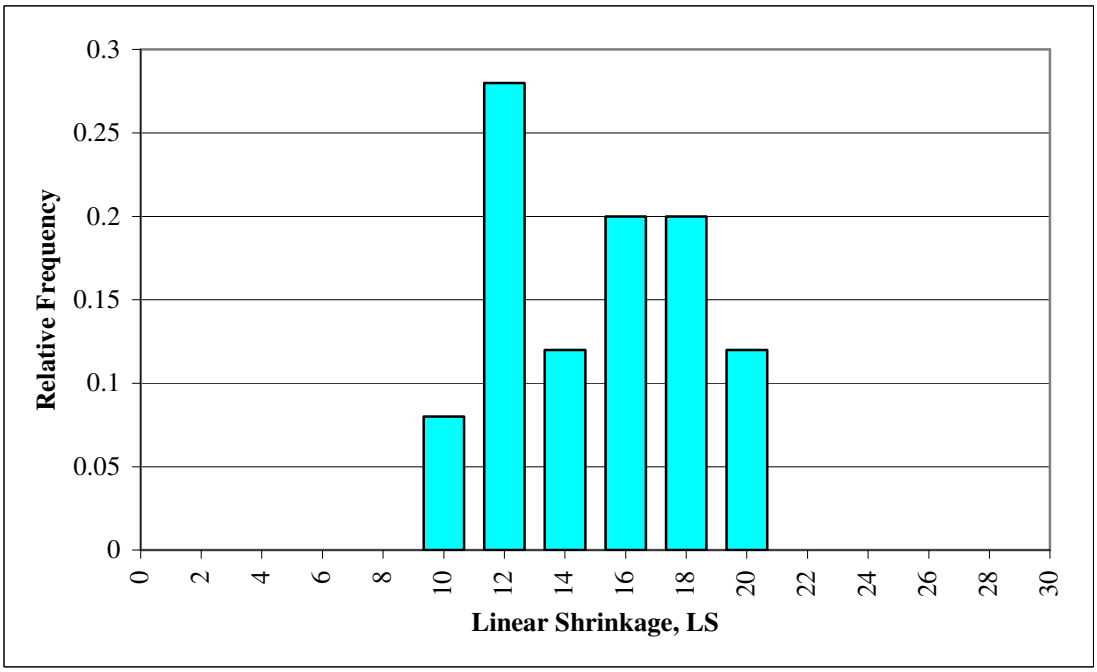

Figure E.14 Relative Frequency Histogram of Sample F Linear Shrinkage

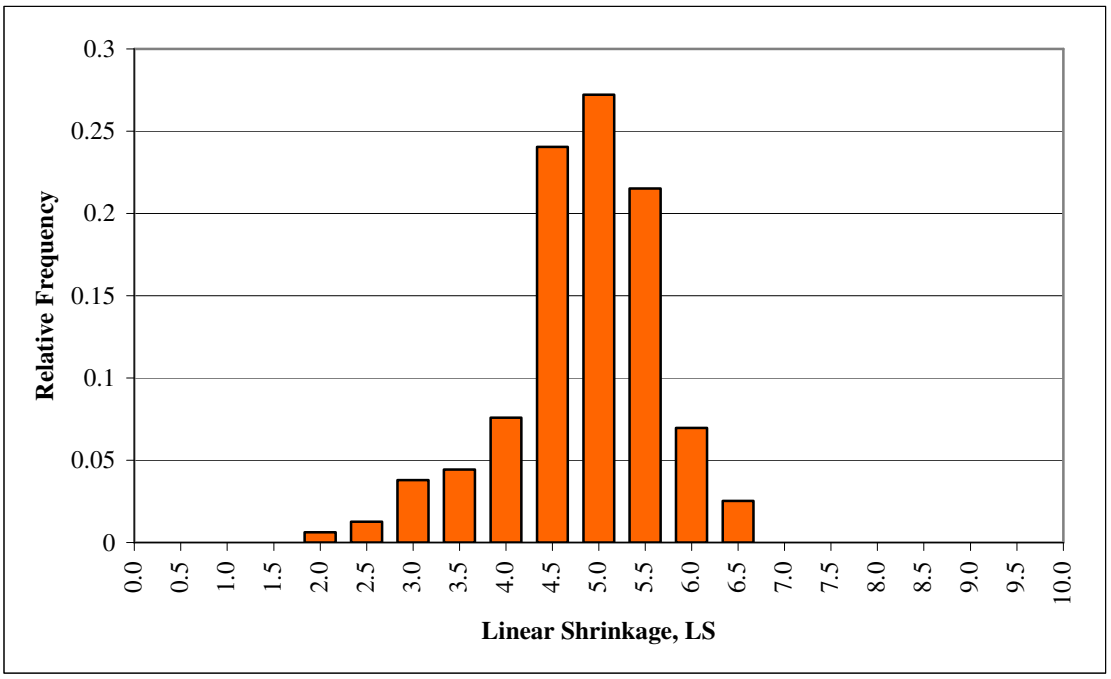

Figure E.15 Relative Frequency Histogram of Sample G Linear Shrinkage

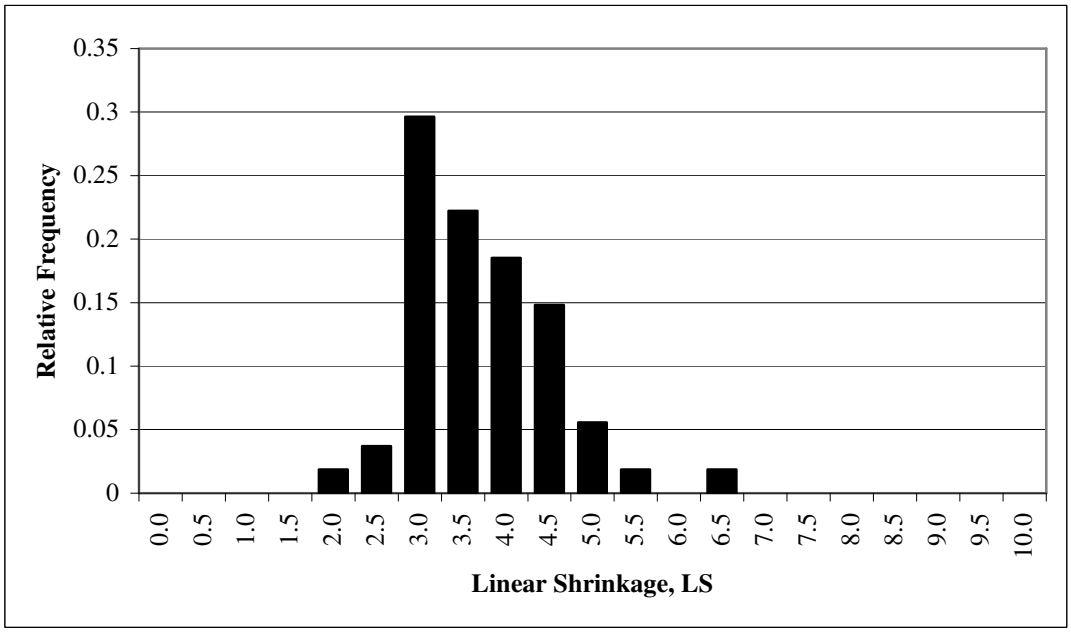

Figure E.16 Relative Frequency Histogram of Sample H Linear Shrinkage

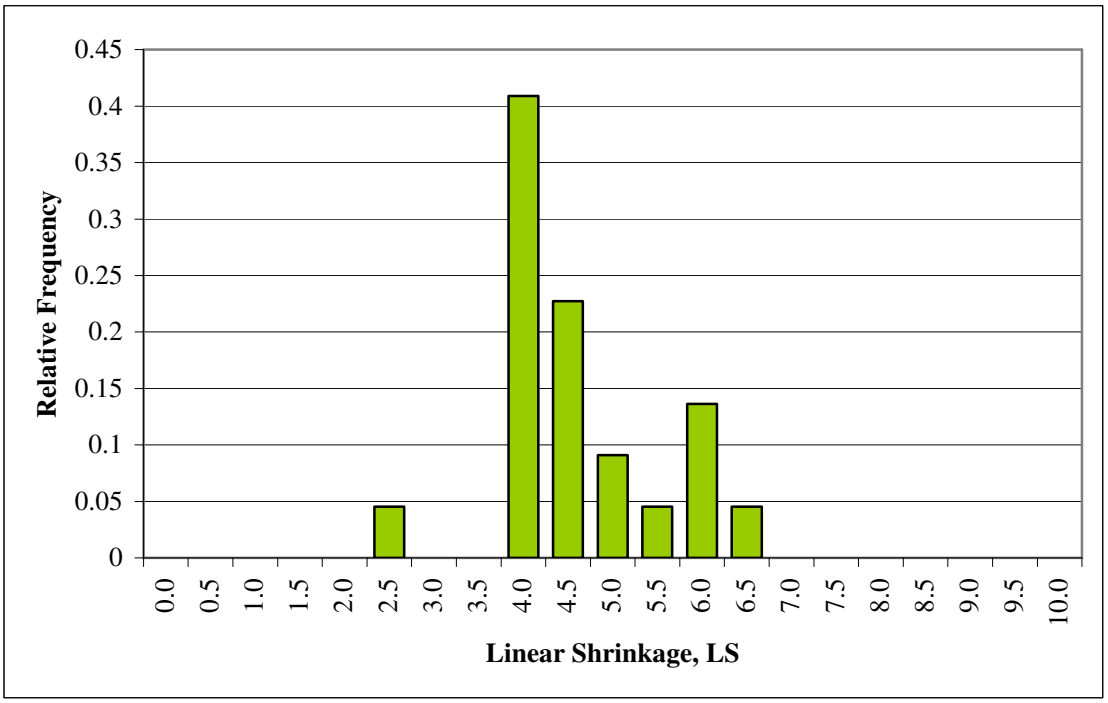

Figure E.17 Relative Frequency Histogram of Sample I Linear Shrinkage

Appendix F

Harr's (1977) Gamma Function Table

Table F.1 Harr's (1977) Gamma Function Table

N	$\Gamma(N)$	N	$\Gamma(N)$	N	$\Gamma(N)$	N	$\Gamma(N)$
1.00	1.000 00	1.25	0.906 40	1.50	0.886 23	1.75	0.919 06
1.01	0.994 33	1.26	0.904 40	1.51	0.886 59	1.76	0.921 37
1.02	0.988 84	1.27	0.902 50	1.52	0.887 04	1.77	0.923 76
1.03	0.983 55	1.28	0.900 72	1.53	0.887 57	1.78	0.926 23
1.04	0.978 44	1.29	0.899 04	1.54	0.888 18	1.79	0.928 77
1.05	0.973 50	1.30	0.897 47	1.55	0.888 87	1.80	0.931 38
1.06	0.968 74	1.31	0.896 00	1.56	0.889 64	1.81	0.934 08
1.07	0.964 15	1.32	0.894 64	1.57	0.890 49	1.82	0.936 85
1.08	0.959 73	1.33	0.893 38	1.58	0.891 42	1.83	0.939 69
1.09	0.955 46	1.34	0.892 22	1.59	0.892 43	1.84	0.942 61
1.10	0.951 35	1.35	0.891 15	1.60	0.893 52	1.85	0.945 61
1.11	0.947 40	1.36	0.890 18	1.61	0.894 68	1.86	0.948 69
1.12	0.943 59	1.37	0.889 31	1.62	0.895 92	1.87	0.951 84
1.13	0.939 93	1.38	0.888 54	1.63	0.897 24	1.88	0.955 07
1.14	0.936 42	1.39	0.887 85	1.64	0.898 64	1.89	0.958 38
1.15	0.933 04	1.40	0.887 26	1.65	0.900 12	1.90	0.961 77
1.16	0.929 80	1.41	0.886 76	1.66	0.901 67	1.91	0.965 23
1.17	0.926 70	1.42	0.886 36	1.67	0.903 30	1.92	0.968 77
1.18	0.923 73	1.43	0.886 04	1.68	0.905 00	1.93	0.972 40
1.19	0.920 89	1.44	0.885 81	1.69	0.906 78	1.94	0.976 10
1.20	0.918 17	1.45	0.885 66	1.70	0.908 64	1.95	0.979 88
1.21	0.915 58	1.46	0.885 60	1.71	0.910 57	1.96	0.983 74
1.22	0.913 11	1.47	0.885 63	1.72	0.912 58	1.97	0.987 68
1.23	0.910 75	1.48	0.885 75	1.73	0.914 67	1.98	0.991 71
1.24	0.908 52	1.49	0.885 95	1.74	0.916 83	1.99	0.995 81
						2.00	1.000 00

Appendix G

Index Properties for Sites A, B, C and Davis (1999) Data

Table G.1 Index Properties for Sites, A, B, C and Davis (1999) Data

Location	Sample No.	Depth (m)	BH No.	LL	PL	PI	LS	LI
Site A	1V_TB	0.5	BH1	74.4	24.3	50.1		
	1H_TB*	0.5	BH1	74.4	24.3	50.1		0.735
	2H_TB*	0.5	BH1	74.4	24.3	50.1		0.713
	2V_TB	0.5	BH1	74.4	24.3	50.1		0.752
Site B	JCU2_L2	2.7	BH38	32.5	27.2	5.3		0.698
	JCU2_L3	5.7	BH38	30.3	24.5	5.8		1.154
	JCU2_L4	13.2	BH38	74.4	24.29	50.11		0.742
	JCU2_L5	17.7	BH38	66	26.4	39.6		0.782
	JCU2_L6	20.7	BH38	62.2	30	32.2		0.287
	JCU2_L7	23.7	BH38	39	19.3	19.7		0.285
Site C	GS90/501A	0.7	BH24A	24	18.8	5.2		8.192
	GS90/501B	1.15	BH24B	24	18.8	5.2		3.308
	GS90/498A	1.7	BH23C	49	14	35		1.286
	GS90/449	1.7	BH9A	47.4	23.4	24		0.958
	GS90/404B	2.45	BH12C	76	26.6	49.4		1.947
	GS90/630	2.17	BH47B	78.6	33.4	45.2		2.204
	GS90/564B	2.2	BH27C	130	31	99		0.860
	GS90/489	4.2	BH22J	77.8	32.4	45.4		
	GS91/012	2.3	BH29C	77.8	29.8	48		2.017
	GS90/627A	2.45	BH46F	80.2	35	45.2		2.195
	GS90/631	2.92	BH47C	75	32.4	42.6		1.864
	GS90/549	1.7	BH9A	23	12	11		0.900

Table G.1 (Cont'd) Index Properties for Sites, A, B, C and Davis (1999) Data

Location	Sample No.	Depth (m)	BH No.	LL	PL	PI	LS	LI
Site A	1V_TB	0.5	BH1	74.4	24.3	50.1		
	1H_TB*	0.5	BH1	74.4	24.3	50.1		0.735
	2H_TB*	0.5	BH1	74.4	24.3	50.1		0.713
	2V_TB	0.5	BH1	74.4	24.3	50.1		0.752
Site B	JCU2_L2	2.7	BH38	32.5	27.2	5.3		0.698
	JCU2_L3	5.7	BH38	30.3	24.5	5.8		1.154
	JCU2_L4	13.2	BH38	74.4	24.29	50.11		0.742
	JCU2_L5	17.7	BH38	66	26.4	39.6		0.782
	JCU2_L6	20.7	BH38	62.2	30	32.2		0.287
	JCU2_L7	23.7	BH38	39	19.3	19.7		0.285
Site C	GS90/501 A	0.7	BH24A	24	18.8	5.2		8.192
	GS90/501 B	1.15	BH24B	24	18.8	5.2		3.308
	GS90/498 A	1.7	BH23C	49	14	35		1.286
	GS90/449	1.7	BH9A	47.4	23.4	24		0.958
	GS90/404 B	2.45	BH12C	76	26.6	49.4		1.947
	GS90/630	2.17	BH47B	78.6	33.4	45.2		2.204
	GS90/564 B	2.2	BH27C	130	31	99		0.860
	GS90/489	4.2	BH22J	77.8	32.4	45.4		
	GS91/012	2.3	BH29C	77.8	29.8	48		2.017
	GS90/627 A	2.45	BH46F	80.2	35	45.2		2.195
	GS90/631	2.92	BH47C	75	32.4	42.6		1.864
	GS90/549	1.7	BH9A	23	12	11		0.900

Table G.1 (Cont'd) Index Properties for Sites, A, B, C and Davis (1999) Data

Location	Sample No.	Depth (m)	BH No.	LL	PL	PI	LS	LI
Davis (1999) Data	2			70.1	30.8	39.3	16	1.522
	3			69.3	38.8	30.5	15	1.102
	49			70.1	30.8	39.3	16	1.522
	50			69.3	38.8	30.5	15	0.793
	51			75	40	35	16	0.229
	52			75	40	35	16	0.597
	53			59.6	30.3	29.3	14	1.355
	54			59.6	30.3	29.3	14	1.116
	55			75	40	35	16	0.229
	56			59.6	30.3	29.3	14	1.188
	57			75	40	35	16	0.283
	58			69.3	38.8	30.5	15	1.102
	59			59.6	30.3	29.3	14	1.355
	60			75	40	35	16	0.597
	61			70.1	30.8	39.3	16	1.522
	62			46	24	22	11	1.509
	63			69	33	36	13	0.844
	64			70	35	35	17.5	0.960
	65			67	28	39	15.5	0.792
	66			59	28	31	14	1.490
	67			59	28	31	14	0.958
	90			27	21	6	3.5	8.450
	91			39	28.4	10.6	8.5	3.057
	92			58.8	28.6	30.2	14.5	1.603
	93			43.2	24.8	18.4	12	3.109
	94			39	28.4	10.6	8.5	4.755
	95			58.8	28.6	30.2	14.5	1.272
	96			58.8	28.6	30.2	14.5	2.652
	97			58.8	28.6	30.2	14.5	2.391
	98			31.2	19.8	11.4	9	3.939
	99			70	35	35	17.5	1.069
	100			46	24	22	11	3.027
	103			51.8	26.6	25.2	17.5	1.687
	104			57.6	28.6	29	11	2.138
	107			57.6	28.6	29		2.097
	109			52.8	23	29.8		1.584
	110			57.6	28.6	29		1.417

Appendix H

Specific Gravity Values for Sites A, B, C and Davis (1999) Data

Table H.1 Specific Gravity Values for Sites, A, B, C and Davis (1999) Data

Source	BH No.	Depth (m)	Specific Gravity, G_s
Site A	1	0.5	2.68
Site B	BH38	2.5	2.7
	BH28	4	2.73
	BH43	4	2.7
	BH38	5.5	2.71
	BH33	7	2.72
	BH43	10	2.75
	BH38	13	2.52
	BH43	16	2.75
	BH38	17.5	2.59
	BH38	20.5	2.62
	BH43	23.5	2.73
	BH38	23.5	2.42
	BH43	26.5	2.69
	BH43	29.5	2.75
Site C	46A	0	2.528
	19A	0	2.56
	20A	0.2	2.584
	46B	0.4	2.41
	25A	0.5	2.558
	44A	0.75	2.592
	45A	0.75	2.568
	46C	0.8	2.43
	19B	0.8	2.45
	23B	1	2.62
	20B	1	2.49
	53A	1.29	2.682
	24C	1.4	2.636
	23C	1.5	2.53
	44B	1.5	2.608

Table H.1 (Cont'd) Specific Gravity Values for Sites, A, B, C and Davis (1999) Data

Source	BH No.	Depth (m)	Specific Gravity, G_s
Site C	45B	1.5	2.684
	5AD	1.5	2.546
	9A	1.5	2.54
	11B	1.5	2.578
	9AE	1.6	2.592
	13BC	1.6	2.572
	19C	1.6	2.452
	47B	1.97	2.532
	20C	1.8	2.458
	27C	2	2.57
	53B	2.04	2.562
	52B	2.05	2.572
	29C	2	2.546
	29C	2	2.559
	12C	2.25	2.49
	44C	2.25	2.634
	45C	2.25	2.598
	22E	2.3	2.598
	5AF	2.3	2.58
	19D	2.4	2.582
	46F	2.65	2.56
	47C	2.72	2.618
	47C	2.72	2.514
	53C	2.79	2.194
	20D	2.6	2.412
	16D	3	2.542
	44D	3	2.574
	13BE	3.2	2.548
	19E	3.2	2.514
	47D	3.47	2.518
	47D	3.47	2.527
	44E	3.5	2.574

Table H.1 (Cont'd) Specific Gravity Values for Sites, A, B, C and Davis (1999) Data

Source	BH No.	Depth (m)	Specific Gravity, G_s
Site C	20E	3.4	2.434
	29E	3.5	2.526
	12E	3.75	2.572
	45E	3.75	2.59
	22J	4	2.546
	22J	4	2.609
	27G	4	2.35
	44F	4	2.626
	19F	4	2.464
	47E	4.22	2.632
	20F	4.2	2.532
	29F	4.3	2.626
	11F	4.5	2.626
	45F	4.5	2.638
	47F	4.97	2.588
	47F	4.97	2.565
	19G	4.8	2.478
	20G	5	2.636
	13D	5.25	2.526
	47G	5.72	2.564
	19H	5.6	2.482
	37D	5.9	2.564
	20H	5.8	2.486
	11H	6	2.632
	22L	6.1	2.6
	47H	6.47	2.644
	20J	6.6	2.462
	22M	6.8	2.55
	27L	7	2.644
	20K	7.4	2.428
	20L	8.2	2.458
	22P	8.4	2.624
	22P	8.4	2.52

Table H.1 (Cont'd) Specific Gravity Values for Sites, A, B, C and Davis (1999) Data

Source	BH No.	Depth (m)	Specific Gravity, G_s
	20M	9	2.482
Site C	4N	9.25	2.418
	20N	9.8	2.458
	4U	15	2.658

Appendix I

Consolidation Parameter Values for Sites A, B, C and Davis (1999) Data

Table I.1 Consolidation Parameter Values for Sites, A, B, C and Davis (1999) Data

Source	Sample ID.	Depth (m)	C_c	C_r	Coefficient of Consolidation, c_v (cm/s)			
					OC Clay		*NC Clay*	
					Min	*Max*	*Min*	*Max*
Site A	BH1	0.5	0.012	0.001	9.462E-04	3.356E-03	2.445E-04	6.922E-04
	BH1	0.5	0.012	0.001	8.159E-04	3.356E-03	5.479E-04	2.670E-03
	BH1	0.5	0.001	0.0003	8.863E-04	1.491E-03	5.143E-04	9.364E-04
	BH1	0.5	0.001	0.0004	1.944E-04	6.713E-03	4.877E-04	1.224E-03
Site B	BH38	2.7	0.177	0.017	2.390E-06	8.400E-02	2.390E-06	2.300E-02
	BH28	4	0.343	0.050	1.200E-03	5.000E-02	1.700E-03	5.000E-02
	BH43	4	0.245	0.022	3.400E-04	2.000E-02	3.500E-04	1.600E-02
	BH38	5.7	0.127	0.019	9.000E-04	5.600E-03	3.400E-03	-
	BH33	7	0.297	0.027	1.000E-03	1.640E-02	3.000E-04	4.000E-03
	BH43	10	0.549	0.081	2.000E-04	4.600E-02	1.000E-04	1.100E-03
	BH11	10.2	0.566	0.091	1.000E-04	9.000E-04	1.000E-04	4.600E-02
	BH26	10.2	0.249	0.013	2.400E-03	8.000E-03	2.000E-03	2.000E-04
	BH38	13.2	0.605	0.083	3.000E-04	6.000E-04	2.000E-04	2.400E-03
	BH26	13.2	0.561	0.076	1.000E-04	7.000E-04	1.000E-04	3.000E-04
	BH43	16	0.710	0.125	1.000E-04	2.500E-03	1.000E-04	4.000E-04
	BH11	16.2	0.804	0.156	0.000E+00	1.300E-03	-	1.100E-03
	BH26	16.2	1.052	0.140	1.000E-04	1.300E-03	-	-
	BH38	17.7	0.751	0.097	2.000E-04	1.200E-03	1.000E-04	9.000E-04
	BH26	19.2	0.700	0.109	1.000E-04	1.200E-03	1.000E-04	-
	BH11	19.2	0.930	0.186	0.000E+00	3.000E-04	1.000E-04	-
	BH38	20.7	0.261	0.036	3.000E-04	6.500E-03	5.000E-04	1.300E-03
	BH26	22.2	0.902	0.125	1.000E-04	1.500E-03	-	-
	BH43	23.5	0.644	0.096	1.000E-04	1.780E-02	-	-
	BH38	23.7	0.149	0.024	3.300E-03	1.120E-02	2.500E-02	7.420E-02
	BH26	25.2	0.784	0.145	1.000E-04	7.000E-04	-	-
	BH43	26.5	0.779	0.129	1.000E-04	1.430E-02	-	-
	BH26	28.2	0.516	0.069	3.000E-04	2.000E-03	-	-
	BH43	29.5	0.432	0.058	2.000E-04	1.720E-02	-	-
	BH26	31.2	0.485	0.044	3.000E-04	2.400E-03	-	-
Site C	BH24A	0.7	0.138	0.053	4.452E-03	-	8.403E-04	2.156E-03
	BH24B	1.15	0.138	0.053	4.452E-03	-	8.403E-04	2.156E-03
	BH45A	0.95	0.283	0.077	2.806E-03	4.925E-03	5.930E-04	2.806E-03
	BH19C	1.2	0.527	0.075	2.026E-04	8.990E-04	1.465E-04	3.152E-04
	BH24B	1.2	0.687	-	3.399E-03	8.017E-03	1.896E-04	8.130E-04
	BH9AD	1.7	0.213	0.043	2.641E-03	6.770E-03	7.610E-04	1.709E-03
	BH25C	1.5	0.408	0.084	-	4.883E-03	1.269E-03	1.333E-03
	BH22C	1.6	0.505	0.033	3.012E-04	3.900E-04	2.860E-04	4.198E-04
	BH11B	1.75	1.511	0.209	9.989E-05	9.545E-04	4.376E-05	6.596E-05
	BH23C	1.7	0.522	0.149	3.171E-05	4.439E-05	1.046E-04	2.568E-04
	BH23C	1.7	0.522	0.149	3.171E-05	4.439E-05	1.046E-04	2.568E-04
	BH26B	1.7	1.090	0.067	4.883E-04	7.705E-04	6.881E-05	7.991E-05
	BH45B	1.7	1.835	0.093	9.069E-04	5.920E-03	8.974E-05	2.568E-04
	BH9A	1.7	0.213	0.043	2.641E-03	7.452E-04	7.610E-04	1.709E-03
	BH12C	2.45	1.184	0.083	4.585E-04	1.006E-03	7.071E-05	1.696E-04
	BH12C	2.45	1.184	0.083	4.585E-04	1.006E-03	7.071E-05	1.696E-04
	BH46E	1.8	0.696	0.084	1.440E-04	2.822E-04	2.188E-05	1.319E-04
	BH47B	2.17	1.196	0.091	6.501E-05	3.076E-04	8.974E-05	1.024E-04
	BH27C	2.2	1.449	0.141	7.610E-05	4.186E-04	6.342E-05	7.927E-05
	BH19B	1.2	0.527	0.075	2.026E-04	8.990E-04	1.465E-04	3.152E-04
	BH20C	2.2	1.038	0.149	2.029E-05	5.749E-04	1.078E-05	7.705E-05
	BH20D	3	1.243	0.097	8.879E-06	1.113E-04	7.610E-06	1.015E-04
	BH20E	3.8	0.955	0.123	2.315E-05	4.709E-04	8.562E-06	1.050E-04

Table I.1 (Cont'd) Consolidation Parameter Values for Sites, A, B, C and Davis (1999) Data

Source	Sample ID.	Depth (m)	C_c	C_r	Coefficient of Consolidation, c_v			
					OC Clay		*NC Clay*	
					Min	*Max*	*Min*	*Max*
Site C	BH20E	3.8	0.984	0.130	5.359E-05	1.426E-03	7.547E-05	9.037E-05
	BH20E	3.8	0.727	0.142	4.661E-05	6.659E-05	5.486E-05	7.420E-05
	BH22E	2.5	1.842	0.034	1.224E-04	4.300E-03	8.657E-05	2.454E-04
	BH22E	2.5	1.842	0.034	1.224E-04	4.300E-03	8.657E-05	2.454E-04
	BH25F	2.5	0.980	0.025	7.610E-05	4.186E-04	6.342E-05	7.927E-05
	BH22J	4.2	1.425	0.075	1.354E-04	8.952E-04	6.786E-05	7.737E-05
	BH29C	2.3	1.241	0.108	9.925E-05	2.638E-04	7.801E-05	8.847E-05
	BH29C	2.3	1.241	0.108	9.925E-05	2.638E-04	7.801E-05	8.847E-05
	BH30E	3.9	0.797	0.091	5.232E-05	3.434E-04	7.801E-05	8.752E-05
	BH45C	2.45	0.769	0.162	4.091E-04	5.882E-03	1.008E-04	4.091E-04
	BH45D	3.2	1.792	0.143	4.785E-04	7.154E-03	4.661E-05	6.342E-05
	BH46F	2.45	1.959	0.036	3.390E-04	1.259E-03	5.454E-05	5.898E-05
	BH46F	2.45	1.959	0.036	3.390E-04	1.260E-03	5.454E-05	5.898E-05
	BH46G	2.85	1.552	0.085	1.566E-04	8.958E-04	5.327E-05	7.579E-05
	BH47C	2.92	1.050	0.075	7.610E-05	6.634E-03	6.659E-05	8.879E-05
	BH47F	5.17	0.121	0.041	9.037E-05	1.547E-04	1.154E-04	1.265E-04
	BH47F	5.17	0.121	0.027	9.037E-05	1.547E-04	1.154E-04	1.265E-04
	BH9A	1.7	0.213	0.043	1.046E-04	6.770E-03	7.610E-04	1.709E-03
	BH37D	6.1	0.866	0.118	5.200E-05	1.483E-03	6.469E-05	9.259E-05
	BH20J	7	1.155	0.108	4.503E-05	4.902E-04	4.756E-05	5.137E-05
	BH22M	7	0.593	0.081	5.961E-05	7.740E-04	5.264E-05	8.879E-05
	BH20K	7.8	0.754	0.100	1.671E-04	7.401E-04	5.993E-05	1.211E-04
	BH20L	8.6	0.569	0.116	3.773E-05	1.059E-04	2.981E-05	5.866E-05
	BH22P	8.6	0.568	0.050	1.855E-04	5.552E-04	7.040E-05	9.164E-05
	BH4N	9.475	0.338	0.053	1.294E-03	2.007E-03	3.295E-04	1.176E-03
Davis (1999) Data	2	2	-	-	2.500E-03	7.000E-03	5.000E-04	2.500E-03
	3	3	1.110	0.211	3.500E-04	3.500E-03	4.000E-04	3.500E-04
	9	9	0.789	0.066	2.000E-03	4.000E-03	4.000E-03	2.000E-03
	33	33	0.071	0.033	1.410E-04	1.420E-04	2.390E-04	1.420E-04
	34	34	0.127	0.058	6.500E-04	8.300E-04	1.100E-03	8.300E-04
	35	35	0.692	0.070	5.000E-04	7.200E-04	3.500E-04	5.000E-04
	36	36	0.270	0.138	8.300E-04	5.600E-03	2.100E-04	8.300E-04
	37	37	0.449	0.042	5.000E-04	7.200E-04	3.500E-04	5.000E-04
	38	38	0.270	0.138	8.300E-04	5.600E-03	2.100E-04	8.300E-04
	39	39	0.449	0.042	3.000E-04	3.200E-04	9.100E-06	3.000E-04
	41	41	0.824	0.241	1.500E-03	3.900E-03	1.500E-03	3.900E-03
	42	42	0.143	-	1.000E-04	9.300E-04	6.400E-06	1.000E-04
	43	43	0.166	0.084	2.200E-03	4.400E-03	5.600E-06	4.400E-03
	44	44	0.210	0.057	7.500E-05	1.600E-03	4.900E-06	7.500E-05
	45	45	0.983	0.205	4.900E-04	6.500E-04	1.500E-03	4.900E-04
	46	46	0.202	0.078	2.000E-04	4.100E-04	3.900E-05	2.000E-04
	47	47	0.174	0.063	2.300E-04	3.100E-04	1.100E-04	2.300E-04
	48	48	1.338	0.428	4.300E-05	1.300E-03	1.900E-06	4.300E-05
	49	49	1.417	0.270	9.900E-04	6.500E-03	5.300E-04	9.000E-04
	50	50	1.163	0.454	6.500E-04	2.500E-03	4.000E-04	6.500E-04
	51	51	0.637	0.365	3.000E-03	5.000E-03	8.400E-04	3.000E-03
	52	52	0.549	0.066	5.200E-04	1.100E-03	3.100E-04	5.200E-04
	53	53	0.817	0.165	2.000E-04	7.100E-04	1.000E-04	2.000E-04
	54	54	0.994	0.260	9.200E-04	2.800E-03	6.900E-04	9.200E-04
	55	55	0.637	0.353	2.800E-03	5.700E-03	8.300E-04	2.800E-03
	56	56	0.604	0.050	6.800E-03	8.100E-03	5.700E-04	6.800E-03

Table I.1 (Cont'd) Consolidation Parameter Values for Sites, A, B, C and Davis (1999) Data

Source	Sample ID.	Depth (m)	C_c	C_r	Coefficient of Consolidation, c_v			
					OC Clay		*NC Clay*	
					Min	*Max*	*Min*	*Max*
Davis (1999) Data	57	57	0.804	0.066	1.500E-03	5.000E-03	8.100E-04	1.000E-03
	58	58	0.349	0.103	3.800E-03	7.100E-03	6.500E-04	3.800E-03
	59	59	0.830	0.302	2.800E-04	8.300E-04	1.000E-04	2.800E-04
	60	60	0.787	0.249	6.400E-04	7.300E-04	5.500E-04	6.400E-04
	61	61	0.787	0.197	2.000E-03	5.000E-03	5.600E-04	2.000E-03
	62	62	1.163	0.454	1.800E-03	7.100E-03	7.400E-03	1.800E-03
	63	63	0.676	0.036	4.500E-03	6.000E-04	4.000E-04	2.000E-03
	64	64	0.761	0.131	1.700E-04	6.000E-04	5.300E-05	1.700E-04
	65	65	0.765	0.136	3.500E-04	1.000E-03	6.700E-06	3.500E-04
	66	66	0.689	0.091	3.100E-03	7.900E-03	6.000E-04	3.100E-03
	67	67	0.787	0.136	2.200E-03	3.300E-03	6.400E-04	2.200E-03
	90	90	0.596	0.085	2.000E-04	8.000E-04	9.000E-05	2.000E-04
	91	91	0.601	0.093	5.500E-04	1.800E-05	2.500E-03	5.500E-04
	92	92	0.382	0.038	4.000E-04	2.900E-03	7.000E-05	4.000E-04
	93	93	0.684	0.093	2.400E-04	2.100E-03	8.000E-05	2.400E-04
	94	94	0.669	0.087	4.500E-04	2.000E-03	1.100E-05	4.500E-04
	95	95	0.642	0.103	1.000E-04	2.000E-03	5.700E-05	1.000E-04
	96	96	0.693	0.121	2.100E-04	2.300E-03	2.900E-05	2.100E-04
	97	97	0.762	0.150	1.600E-04	2.200E-03	6.000E-05	1.600E-04
	98	98	0.669	0.121	1.000E-04	2.300E-03	2.600E-04	1.000E-04
	99	99	0.470	0.071	2.100E-03	3.600E-03	3.500E-04	2.100E-03
	100	100	0.755	0.106	1.900E-03	6.600E-03	5.000E-04	1.900E-03
	101	101	1.106	0.123	3.100E-04	4.900E-04	5.600E-05	3.100E-04
	102	102	0.615	0.054	1.200E-04	9.000E-04	6.100E-05	1.200E-04
	103	103	0.889	0.154	2.000E-04	3.300E-04	1.300E-04	2.000E-04
	104	104	0.659	0.073	3.000E-04	1.400E-03	1.000E-04	3.000E-04
	105	105	1.562	0.237	3.000E-04	1.400E-03	4.400E-05	3.000E-04
	106	106	0.847	0.063	8.600E-04	1.800E-03	4.300E-04	8.600E-04
	107	107	0.358	0.147	3.200E-04	1.600E-03	7.000E-05	3.200E-04
	108	108	1.092	0.125	2.000E-04	7.900E-04	7.000E-05	2.000E-04
	109	109	0.810	0.100	2.500E-04	8.900E-04	5.700E-05	2.500E-04
	110	110	0.725	0.105	6.000E-05	4.500E-05	1.300E-04	6.000E-05
	111	111	0.468	0.072	2.400E-04	2.300E-03	1.400E-04	2.400E-04
	112	112	1.113	0.123	2.000E-04	4.200E-04	2.600E-04	2.000E-04
	113	113	0.347	0.033	3.800E-04	8.100E-04	1.800E-04	3.800E-04
	114	114	0.724	0.033	8.000E-04	4.600E-03	1.700E-04	8.000E-04
	115	115	0.871	0.154	5.500E-04	2.200E-03	2.200E-04	5.500E-04

Appendix J

Secondary Compression Values for Sites A, B, C and Davis (1999) Data

Table J.1 Secondary Compression Values for Sites, A, B, C and Davis (1999) Data

Source	Sample ID.	Depth (m)	C_α
Site B	BH38	2.7	0.001
	BH38	5.7	0.001
	BH38	13.2	0.023
	BH38	17.7	0.007
	BH38	20.7	0.005
	BH38	23.7	0.002
	BH43	4	0.004
	BH43	10	0.011
	BH43	16	0.021
	BH43	23.5	0.006
	BH43	26.5	0.005
	BH43	29.5	0.015
	BH11B	1.75	0.073
	BH12C	2.45	0.008
	BH12C	2.45	0.008
	BH20E	3.8	0.080
	BH20E	3.8	0.045
Site C	BH24A	0.7	0.004
	BH24B	1.15	0.004
	BH26B	1.7	0.0005
	BH45A	0.95	0.0028
	BH45B	1.7	0.0009
	BH45C	2.45	0.0004
	BH45D	3.2	0.0005
	BH46E	1.8	0.0001
	BH46F	2.45	0.0003
	BH46F	2.45	0.0003
	BH9A	1.7	0.0026
Davis (1999) Data	90		0.0002
	91		0.0006
	92		0.0004
	93		0.0002

Table J.1 (Cont'd) Secondary Compression Values for Sites, A, B, C and Davis (1999) Data

Source	Sample ID.	Depth (m)	C_α
Davis (1999) Data	95		0.0001
	96		0.0002
	102		0.0001
	103		0.0002
	104		0.0003
	105		0.0003
	106		0.0009
	107		0.0003
	108		0.0002
	109		0.0003
	110		0.0001
	111		0.0002
	112		0.0002
	113		0.0004
	114		0.0008
	115		0.0006

Appendix K

Validation Calculations forLateral Displacement Solutions

Calculations used for validation of these approximate solutions are summarised below. The primary trapezoid was considered as the only source contributing to the lateral displacements induced at Point A. However, with respect to Point B, both the primary and secondary trapezoids were regarded to factor into the lateral displacements which were induced.

Assumed values:

a = 17 m

B = 22 m

L_x = 0 m (at embankment toe)

H= 16 m

h = 2.85 m

Calculations

Influence Depth, z_{inf}:

To check whether or not the clay layer could be assumed as infinite, the influence depth z_{inf} was evaluated.

$$\frac{z_{inf}}{B} = 1.6 - 0.7\nu$$

$$= 1.6 - (0.7)(0.5)$$

$$= 1.6 - 0.35$$

$$= 1.25$$

Thus, the influence depth was equivalent to 1.25*base width of the primary trapezoid.

$$Z_{inf} = (1.25)(22)$$

$$= 27.5 \text{ metres}$$

Z_{inf} > H $\therefore$ correction factors for finite layer depths need to be applied to all further calculations

For Point A:

L_x = 0 m (at embankment toe)
h = 16 m
H = 2.85 m

Main embankment (primary trapezoid) was assumed to be the only contributor to lateral displacements for Point A.

a/B = 0.773
L_x/B = 0

Maximum Lateral Displacement, $\delta_{at,max}$:

$$\therefore \Phi_1 = 0.067 (L_x/B)^2 - 0.475 (L_x/B) + 3.249$$
$$= 0.067 (0)^2 - 0.475 (0) + 3.249$$
$$= 3.249$$

$$\therefore \Phi_2 = 0.88\left(\frac{H}{5B}\right)^{-0.44}$$
$$= 0.88\left(\frac{16}{110}\right)^{-0.44}$$
$$= 2.055$$

Undrained Poisson's Ratio, ν = 0.5

$$\therefore I_{peak} = \left[0.030\left(\frac{a}{B}\right)+0.032\right]e^{\Phi_1 \nu}$$

$$= [0.030*(0.773)+0.032]e^{(3.249)(0.5)}$$

$$= [0.0552]e^{1.626}$$

$$= 0.265$$

$$\text{Thus, } \delta_{lat,\max} = \Phi_2 \frac{qBI_{peak}}{E_{foundation}}$$

$$= (2.055)\left[\frac{(2039*2.85*9.81)(22)(0.265)}{1.048x10^7}\right]$$

$$= 0.0652 \text{ m}$$

$$= 65.2 \text{ mm}$$

Depth of Maximum Displacement, z_{max} :

$$\Phi_3 = 0.056\left(\frac{L_x}{B}\right)+1.0$$

$$= (0.056)(0) + 1.0$$

$$= 1.0$$

$$\frac{z_{\max}}{B} = \Phi_3(0.68\nu - 0.545)$$

$$= (1.0)((0.68)(0.5)-0.545)$$

$$= -0.196$$

$$\therefore z_{\max} = 22* - 0.196$$

$$= - 4.31 \text{ m (below ground level)}$$

For Point B:

As previously shown for Point A, the calculated influence depth is greater than the single clay layer thickness, and correction factors for finite depth layers must be applied for all further calculations.

Both the main embankment and berm were considered to contribute to the lateral displacement at this point. Thus, in calculating the magnitude of maximum lateral displacement for Point B, contributions from each of the separate trapezoids were calculated Due to an overlap of these two trapezoids, the contributions of a third trapezoid were required to be calculated, and subtracted from the sum of the first two.

With respect to the depth at which this maximum lateral displacement occurs, the main embankment section was considered as the determinant embankment geometry, and thus, calculations were only undertaken for the primary trapezoid.

Maximum Lateral Displacement, $\delta_{at,max}$:

Main Embankment Contribution:

Assumed values:

a = 17 m

B = 22 m

L_x = 6.5 m

H= 16 m

h = 2.85 m

$(a/B)_{T1}$ = 0.773

$(L_x/B)_{T1} = \frac{6.5}{22}$

= 0.295

$\therefore \Phi_{1,T1}$ = 0.067 $(L_x/B)^2$ - 0.475 (L_x/B) + 3.249

$= 0.067\ (6.5/22)^2 - 0.475\ (6.5/22) + 3.249$

$= 3.115$

$$\therefore \Phi_{2,T1} = 0.88\left(\frac{H}{5B}\right)^{-0.44}$$

$$= 0.88\left(\frac{16}{110}\right)^{-0.44}$$

$= 2.055$

Undrained Poisson's Ratio, $\nu = 0.5$

$$\therefore I_{peak,T1} = \left[\left[0.030\left(\frac{a}{B}\right)+0.032\right]e^{\Phi_1 \nu}\right]_{T1}$$

$$= \left[0.030*(0.773)+0.032\right]e^{(3.115)(0.5)}$$

$$= \left[0.0552\right]e^{1.558}$$

$= 0.262$

$$\delta_{lat,\max,T1} = \left[\Phi_2 \frac{qBI_{peak}}{E_{foundation}}\right]_{T1}$$

$$= (2.055)\left[\frac{(2039*2.85*9.81)(22)(0.262)}{1.048x10^7}\right]$$

$= 0.0645$ m

$= 64.5$ mm

Thus, displacement caused by primary trapezoid is 64.5 mm.

Berm Contribution:

Assumed values:

a = 33 m

B = 35 m

L_x = 0 m

H= 16 m

h = 1.0 m

$(a/B)_{T2}$ = 0. 943

$(L_x/B)_{T2} = \frac{0}{35}$

= 0

$\therefore \Phi_{1,T2}$ = 0.067 (0)^2 - 0.475 (0) + 3.249

= 3.249

$\therefore \Phi_{2,T2} = 0.88\left(\frac{H}{5B}\right)^{-0.44}$

$= 0.88\left(\frac{16}{175}\right)^{-0.44}$

= 2.520

Undrained Poisson's Ratio, ν = 0.5

$\therefore I_{peak,T2} = \left[\left[0.030\left(\frac{a}{B}\right)+0.032\right]e^{\Phi_1 \nu}\right]_{T2}$

$= [0.030*(0.943)+0.032]e^{(3.249)(0.5)}$

$= [0.0603]e^{1.626}$

= 0.307

$\delta_{lat,\max,T2} = \left[\Phi_2 \frac{qBI_{peak}}{E_{foundation}}\right]_{T2}$

$= (2.520)\left[\frac{(2039*1.0*9.81)(35)(0.307)}{1.048x10^7}\right]$

= 0.0517 m

= 51.7 mm

Thus, displacement caused by the berm is 51.7 mm.

Overlapped Area Contribution:

Assumed values:

a = 20 m

B = 22 m

H= 16 m

h = 1.0 m

$(a/B)_{overlap}$ = 0.909

$(L_x/B)_{T2}$ = 0

$\therefore \Phi_{1,overlap}$ = $0.067\ (0)^2 - 0.475\ (0) + 3.249$

= 3.249

$$\therefore \Phi_{2,overlap} = 0.88\left(\frac{H}{5B}\right)^{-0.44}$$

$$= 0.88\left(\frac{16}{110}\right)^{-0.44}$$

= 2.055

Weighted Poisson's Ratio, ν = 0. 5

$$\therefore I_{peak,overlap} = \left[\left[0.030\left(\frac{a}{B}\right)+0.032\right]e^{\Phi_1 \nu}\right]_{overlap}$$

$$= \left[0.030*(0.909)+0.032\right]e^{(3.249)(0.5)}$$

$$= \left[0.0593\right]e^{1.626}$$

$= 0.301$

$$\delta_{lat,\max,overlap} = (2.055)\left[\frac{(2039*1.0*9.81)(22)(0.301)}{1.048x10^7}\right]$$

$= 0.0260$ m

$= 26.0$ mm

Thus, displacement caused by the overlap is 26.0 mm.

$\therefore$ The overall maximum lateral displacement is:

$$\delta_{lat,\max} = \delta_{lat,\max,T1} + \delta_{lat,\max,T2} - \delta_{lat,\max,overlap}$$

$= 64.5 + 51.7 - 26.0$

$= 90.2$ mm

Depth of Maximum Displacement, z_{max} :

$$\Phi_3 = 0.056\left(\frac{L_x}{B}\right) + 1.0$$

$$= (0.056)\left(\frac{6.5}{22}\right) + 1.0$$

$= 1.017$

$$\frac{z_{\max}}{B} = \Phi_3(0.68\nu - 0.545)$$

$$= (1.017)((0.68)(0.5) - 0.545)$$

$= -0.208$

$\therefore z_{\max} = 22* - 0.208$

$= -4.59$ m (below ground level)